

TRABAJO FINAL DE MÁSTER



TÍTULO

**THM MODELLING OF DEPOSITION TUNNEL IN
ONKALO PROJECT**

AUTOR

ERDEM TOPRAK

TUTOR

SEBASTIA OLIVELLA

ESPECIALIDAD

GEOTECHNICAL ENGINEERING

FECHA

January 2013



**Dept. d'Enginyeria del Terreny, Cartogràfica i Geofísica
E.T.S. Enginyers de Camins, Canals i Ports**

UNIVERSITAT POLITÈCNICA DE CATALUNYA



Abstract

This thesis is concerned with preliminary analyses of coupled Thermo-Hydro-Mechanical (THM) processes in the ONKALO Project. It is a project of Finland and it will be the final disposal repository of nuclear waste. The Code_Bright finite-element software program is used in performing the modelling and calculations. The objective of the thesis was to analyse important design parameters of the project.

The time required to reach full saturation for the buffer, the maximum temperature reached in buffer, deformations at the buffer-backfill interface and the stress-deformation balance in interaction between buffer and backfill also buffer and backfill homogenization are the critical design criteria.

A fundamental issue was determining corresponding thermal boundary conditions for the modelling task. The main reason for this is that the boundaries can not be extended to a distance that the thermal problem would require. Temperature on the boundaries considered in this study depends on the initial canister power, the fuel power decay characteristic and rock thermal properties.

With regard to the hydraulic analyses, the time required to achieve full saturation is sensitive to vapour diffusion and heat transport, intrinsic permeability and initial suction. Sensitivity studies have been undertaken to determine the reliability of the used parameters.

Modelling of the buffer-backfill interface is an essential element in tunnel backfill design. The aim of the calculations is to reveal deformations at this interface whose behaviour is important in connection with swelling of the buffer.

The modelling was carried out under axisymmetric conditions, with the Barcelona Basic Model (BBM) being used to model performance of the bentonite buffer and backfill soil materials.

Acknowledgments

I wish to thank, first and foremost my Professor Sebastian Olivella. This thesis would not have been possible without his guidance and persistent help. Also I would like to thank for providing funding for the thesis from Finnish companies of Posiva Oy and B+ Tech Oy.

In addition, thanks for Nadia Mokni and Xavier Pintado for the helps during the preparation of the thesis.

I would like to thank my parents who have given me the opportunity of an education from the best institutions and support throughout my life.

Abstract.....	2
Acknowledgments	3
1. INTRODUCTION	6
2. PROPERTIES OF MATERIALS.....	11
2.1. Host Rock	11
2.2. Buffer.....	12
2.3. Backfill	15
2.4 Pellets	17
2.5. Canister.....	19
3. PART I - THERMAL CALCULATIONS	22
3.1- Introduction	23
3.2. Geometry of Canister Area.....	25
3.3. Thermal Properties Of Materials	28
3.4. Canister Power.....	30
3.5. Reference Model.....	33
3.6. Thermal Conditions	34
3.7. Comparative Analyses.....	35
3.7.1 Effect of Tunnel and Canister Spacing.....	35
3.7.2 Effect of Boundary Distance	37
3.8. Proposed Model.....	42
3.9. Conclusions for Thermal Calculations	45
4. MODELLING OF BUFFER MATERIAL BY MEANS OF OEDOMETER AND INFILTRATION TESTS.....	46
4.1. Introduction	46
4.2. Oedometer Tests	48
4.2.1 Experimental results	48
4.2.2 Model geometry and initial conditions.....	54
4.2.3. Modelling results of tests 100212c_oedometer and 101222a_oedometer....	55
4.2.4. Modelling results of test 100212a_oedometer	56
4-3. Infiltration Test.....	62
4.4. Concluding Remarks For Modelling Of Laboratory Test	71
5. THM ANALYSIS FOR DEPOSITION HOLE	73
5.1. Introduction	74
5.2. Base case THM analyses	80
5.3. Sensitivity analyses	98
5.3.1 Comparison of evolution of temperature.....	100
5.3.2 Comparison of the evolution of liquid pressure	105
5.3.3 Comparison of the evolution of total mean stress	110
5.3.4 Comparison of the evolution of effective mean stress	115
5.3.5 Comparison of the evolution of porosity.....	120
5.3.9 Comparison of the evolution of vertical displacements	140
5.4. Conclusions for THM modelling of deposition hole.....	145
6. GAP EFFECT ON THM ANALYSIS	147
6.1. Introduction	148
6.2. Geometrical and Physical Properties of the Problem	150

6.2.1 Gap Properties	151
6.3. Initial and Boundary Conditions	154
6.4. THM Analysis Including Gap Effect	156
6.4.1. Model A - Permeability of rock 10^{-18} m^2	157
6.4.2. Model B - Permeability of rock 10^{-19} m^2	164
6.4.3. Model C Permeability of rock 10^{-19} m^2 (without gap).....	170
6.4.4. Comparison of the results of 3 Models.....	176
6.5. Model with Final Mesh and Geometry.....	180
7. CONCLUSIONS	190
Annex I. Description of basic THM formulation	191
AI.1. General features of computer code.....	191
AI.2. Some features important to THM modeling of repositories.....	191
AI.3. Mathematical representation of mechanical processes	191
AI.3.1 Equations of motion	191
AI. 3.2 Mechanical Constitutive models	192
AI-4. Mathematical representation of fluid flow processes.	194
AI.5. Mathematical representation of heat transfer processes.....	194
AI.6. Some special features of the code	195
AI.6.1 Retention curve.....	195
AI.6.2 Molecular Diffusion	196
AI. 6.3 Mechanical Dispersion.....	196
References	198

1. INTRODUCTION

Posiva Oy has been preparing a project for the storage of final disposal of spent nuclear fuel in the crystalline bedrock of Finland. Preparations for nuclear waste management were started already in the 1970s when the first power plants were still under construction. In 1983, the Finnish Government confirmed a target schedule for nuclear waste management, in which the construction of the disposal facility was scheduled for the 2010s and the start of actual final disposal for the year 2020. The site for the repository has been chosen on the basis of site investigations. In 1999 preliminary investigations were finished for four sites. Olkiluoto island in Eurajoki was proposed as the primary site for the repository.

Olkiluoto is a large island (about 10 km²) in the Baltic sea coast and separated from the mainland by a narrow strait. Figure 1-1 shows a detailed map of Olkiluoto island. There is a nuclear power plant with two reactors in operation and a third one under construction and a fourth in planning stage also VML repository for low and intermediate waste are located in the western part of island. The final repository for the spent nuclear fuel is under construction and located in the central and eastern part of the island. The project name for the final repository is ONKALO that is an acronym based on the Finnish language expression for Olkiluoto Rock Characterization for Final Disposal. The word “Onkalo” also means cave in Finnish.

The final repository is planned to be consisted of a system of exploratory tunnels that can extend to a depth of 460 m.

The infrastructure of the site is almost completed. The concrete walls of the tunnel entrance, the washing hall, the fuel distribution station and the asphaltting of the machine field and roads are completed. The site office has been built, the site perimeter has been fenced and site surveillance has been organized.

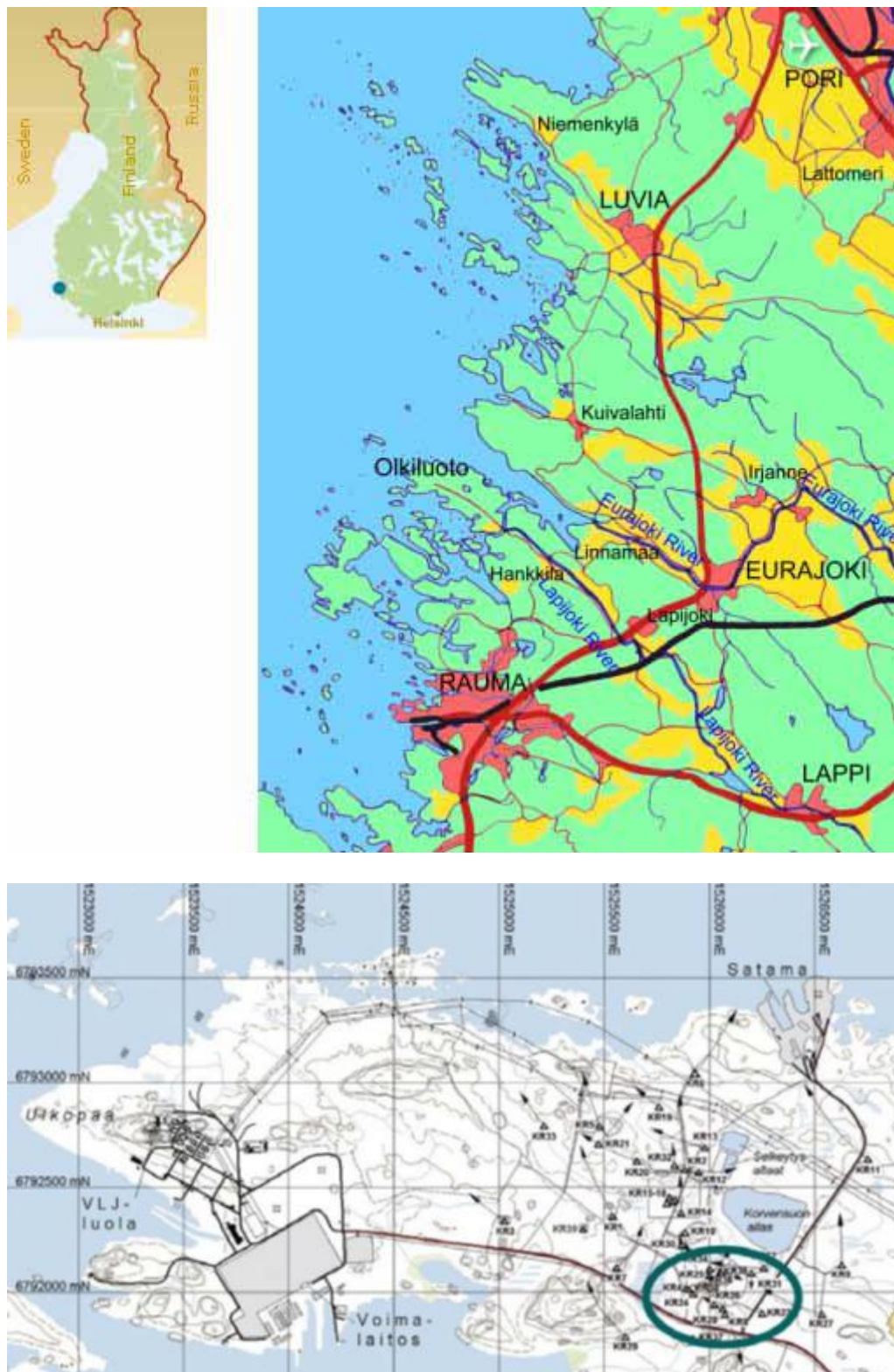


Figure 1-1. Map of Olkiluoto site. Location of ONKALO is marked together with the location of deep investigation boreholes

The ONKALO will be a part of the final repository, which will consist of tunnels excavated at a depth of approximately 460 m and located at approximately 25 m from each other. The spent fuel will be encapsulated in final disposal canisters made of cast iron, enclosed in a copper shell. These canisters will be placed in holes drilled at the bottom of the repository tunnels and surrounded with bentonite clay, which not only prevents direct groundwater flow to the surface of the canister, but also protects the canister against minor bedrock movements. After placement of the canisters, the tunnel will be backfilled with a mixture of bentonite and crushed rock.

Figure 1-2 shows the typical geologic disposal system which involves both natural and engineered barriers. These barriers are used to isolate the spent fuel so that it can never harm the organic environment also it can not be accessible to people. The depth of several hundreds of meters also guarantees sufficient protection against the influence of any future ice ages. The disposal system will be protected by bedrock against external influence. The bedrock also will create mechanically and chemically stable conditions in the repository and restrict the amount of water that can come into contact with the engineered barriers.

As is shown in the Figure 1-2 the repository will consist of disposal tunnels excavated in the bedrock and connected by transport tunnels. The spent fuel is sealed in canisters at the encapsulation plant of the final disposal facility. The canisters are embedded into holes drilled in the tunnel floor and surrounded with bentonite clay. Bentonite is natural clay that swells strongly as it absorbs water. The layer of compacted bentonite separates the canisters from nearby processes in the bedrock. The clay not only prevents groundwater from flowing directly onto the canister surface, but also protects the canister against small movements of the bedrock. After the last canisters have been disposed of in the final repository, the encapsulation plant is decommissioned, the tunnels filled with a suitable backfilling material and the access routes sealed. The final facility requires no monitoring after it has been closed.

Figure 1-3 shows the actual situation of the project. Excavation of tunnels is under progress. It is planned that in one panel there are 30 tunnel pairs and each tunnel pair has 50 canisters. Totally there are 1500 canisters. Disposing rate is 45 canisters per year. It takes 34 years to dispose all the canisters to one panel.

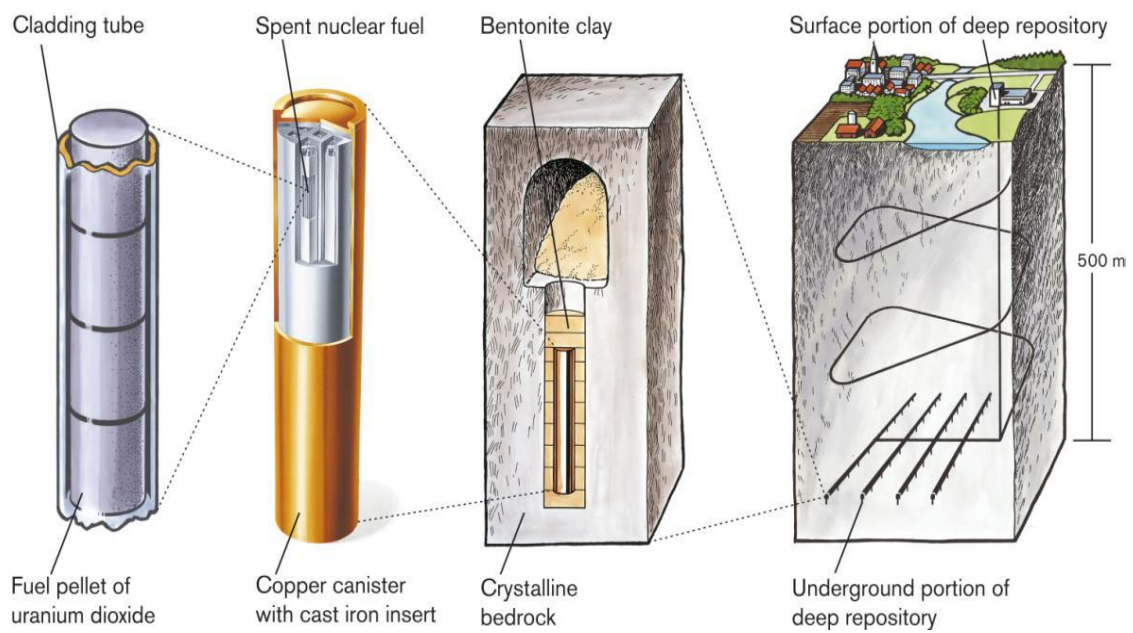
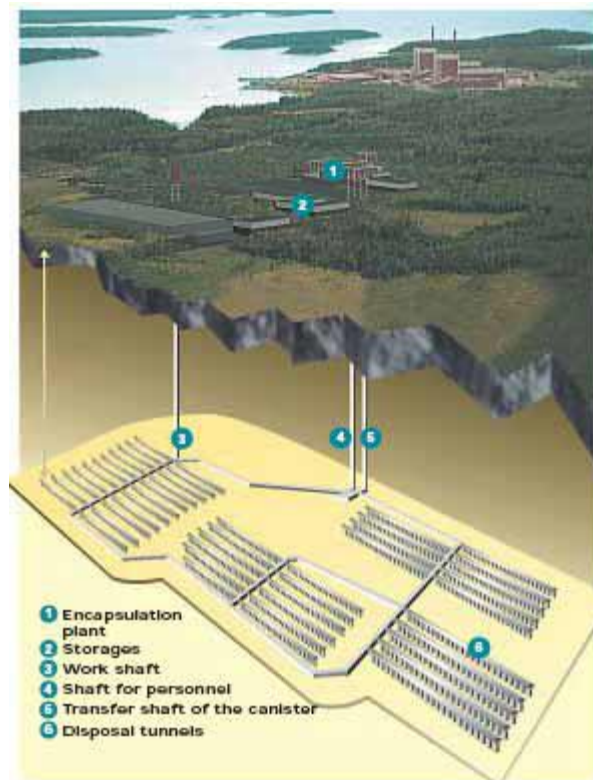


Figure 1-2. A possible design of the final disposal facility planned to be constructed at the Olkiluoto site.

A deposition hole subjected in this thesis is consisted of bedrock, buffer, backfill, pellets, canister and air gap between canister and buffer. Detailed geometry of the deposition hole is given in Part I Thermal Calculations (see Figure 3-3). THM modeling of these elements have been performed by the aid of laboratory experiments and information supplied by the POSIVA researches.

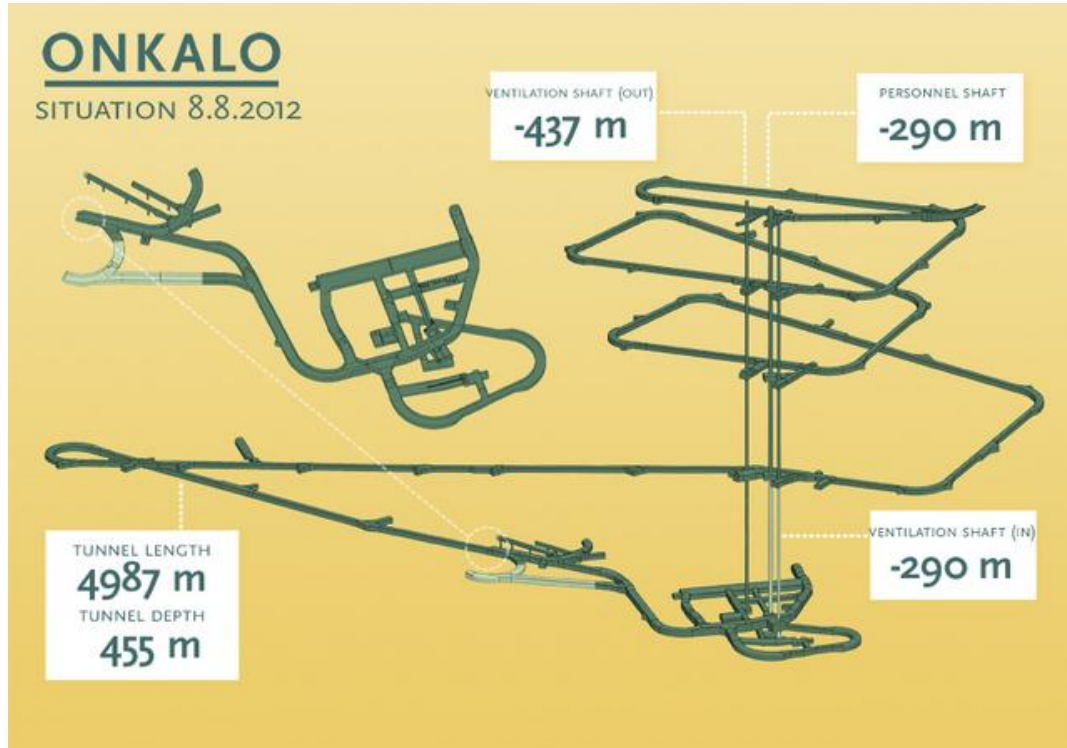


Figure 1-3. Actual excavation situation of ONKALO

The reached maximum temperature in buffer, required time for saturation of buffer, homogenization of buffer and backfill also displacements occurred at the interface of buffer and backfill are the main interest of this thesis because evolution of these factors are the main safety requirements of the project.

Characteristic of materials, thermal calculations and modeling, laboratory test simulations and finally THM evolution of deposition hole including gap is studied.

2. PROPERTIES OF MATERIALS

In this section, mainly the safety requirements of materials composing deposition hole are studied. Main characteristics of host rock, buffer, backfill, pellets and canister is summarized.

2.1. Host Rock

The bedrock protects the disposal system against external influence such as restricting the amount of water that can come into contact with the engineered barriers. It creates mechanically and chemically stable conditions in the repository. Safety function indicators and associated criteria for the host rock are summarized in Table 1-1.

Table 1-1. Safety function indicators and criteria for the host rock

Safety function	indicator	Criterion Rationale
Minimum ionic strength	Total divalent cation concentration $> 10^{-3}$ M	Avoid buffer erosion
Limited salinity	(expressed in terms of total dissolved solids, TDS) [NaCl] < 100 g/l	Avoid detrimental effects, in particular on swelling pressure of buffer
Limited concentration of detrimental agents for buffer, distance block and canister	Applies to HS ⁻ , K ⁺ and Fe(II) /Fe(III). The lower the better (no quantitative criterion)	Avoid canister corrosion by sulphide, avoid illitisation (K ⁺) and chloritisation (Fe) of buffer
Limited rock shear at canister / distance block locations in deposition drift	< 10 cm	Avoid canister failure due to rock shear in deposition drift

The safety functions of the host rock can be listed as:

- Isolate the spent fuel from the biosphere.
- Provide appropriate and predictable mechanical, geochemical and hydrogeological conditions for the engineered barriers.

- Protect them from potentially detrimental processes taking place above and near the ground surface, and limit and retard the inflow to and release of harmful substances from the repository.

In this study, chemical processes are not considered. Bed rock is handled in terms of thermo-hydro-mechanical concept.

2.2. Buffer

The buffer material has been planned to use in ONKALO project is MX-80 bentonite. Several laboratory experiments have been performed to validate MX-80 performance as a buffer material. In this section main characteristic of buffer is explained.

The main requirements of the buffer can be splitted into two functions; requirements for 'isolation' and those requirements for 'retardation'. The isolation functions are as follows:

- envelop the canister for a long period of time - 'remain in the deposition cavity'
- bear the canister in the deposition hole
- prevent groundwater flow
- dissipate heat from the canister
- resist chemical transformation for a long time
- protect the canister by comprising a plastic protection against rock movements.

Retardation functions can be listed as:

- prevent flow of groundwater and thereby retard transport of radionuclides
- resist chemical alteration for a long time
- permit generated gas to escape
- filter colloids.

The requirements of a buffer as summarized in Table 1-2 and Table 1-3 include providing a favorable environment for maintaining the isolation of the waste canister and acts as a protective layer between the canister and rock with respect to the mechanical and chemical forces.

Table 1-2. Safety function indicators and criteria for buffer

Function	Properties
canister envelopment	swelling pressure; shear strength; resistance to alteration
bear canister in central position	swelling pressure; shear strength;
prevent groundwater flow	hydraulic conductivity; porosity
heat dissipation	thermal conductivity
resist chemical transformation	chemical composition; hydraulic conductivity
non-compromisation of canister and rock functions	chemical composition; swelling capacity; hydraulic conductivity
protect canister from rock movements	swelling capacity; rheological properties; shear strength
prevent groundwater flow	hydraulic conductivity; porosity
resist chemical transformation	chemical composition; hydraulic conductivity
canister envelopment	swelling pressure; shear strength; resistance to alteration
allow gas escape	water content; hydraulic conductivity; porosity; diffusion properties
filter colloids	pore volume

This thesis mainly concentrated on the thermo-hydro-mechanical forces which have been considered by to affect the performance of the bentonite buffer. In this thesis computational modeling of bentonite behavior has progressed by means of laboratory test performed by B+Tech Oy. Mechanical behavior of bentonite has been investigated by term of re-saturation, swelling, elasticity, plasticity, failure and friction.

Table 1-3. General requirement for buffer material

Function	Criterion	Rationale
Bulk hydraulic conductivity	$k^{Buffer} < 10^{-12}$ m/s	Limit mass transport to a diffusion dominated process
Swelling pressure	> 1 MPa	Ensure tightness, self sealing
Maximum temperature	$T^{Buffer} < 100^{\circ}\text{C}$	Ensure that the buffer will retain its favorable properties in the long term
Minimum temperature	$T^{Buffer} > -4^{\circ}\text{C}$	Avoid freezing
Swelling pressure around entire canister	> 0.2 MPa	Avoid canister sinking
Buffer saturated density around entire canister	$> 1,650$ kg/m ³	Prevent colloid transport through buffer
Buffer density around entire canister	$< 2,050$ kg/m ³	Ensure protection of canister against

Many of the processes which control the mechanical properties of the bentonite buffer are coupled processes. Main mechanical requirements can be listed as:

- Prevent the canister from sinking.
- Protect the canister from shear deformation.
- Resist fracture under expected repository conditions.
- Enable fractures which may form to heal rapidly.
- Flow and swell to infill gaps remaining after emplacement.
- Generate a microstructure which will limit the permeability of the system.

2.3. Backfill

Friedland-clay is a candidate as backfill material in this project. However, investigations and laboratory experiments are still going on to find the most appropriate material that will use in the deposition hole. In this thesis Friedland-clay was selected as a backfill material and modeled through laboratory tests performed on this material.

In backfilling concept, it is planning to mix natural clay with crushed rock (30:70). The most important geotechnical properties for the backfill are hydraulic conductivity, swelling ability and compressibility and also the material should be easy to handle and compact.

The main advantages of using natural clays as backfill materials are their naturally low hydraulic conductivity, high specific surface area and in some cases swelling ability. The possible disadvantages of natural clays as backfilling material can be compressibility, sensitivity to water content during emplacement and sensitivity to salt content of the groundwater in the expected repository conditions.

Requirements for the backfill in general can be summarized as:

- The backfill should be sufficiently incompressible in order to prohibit upward expansion of the buffer so that the density and other desired properties of the buffer remain unchanged.
- The backfill should have low hydraulic conductivity and there should not be boundary flow between the backfill and the rock surrounding the tunnel to restrict advection of water transportation of radionuclides along the tunnel.
- The backfill should contribute keeping the tunnels mechanically stable.
- The backfill should not have any significantly harmful effect on the other barriers in the repository.
- The backfill should maintain its performance under the expected repository conditions for a time range determined in the safety analysis.

Table 1.4 summarized safety functions and criteria for backfill. These safety criteria are adopted to this study from SKB and POSIVA reports.

Table 1.4 *Safety function indicators and criteria for backfill*

Performance target	Applicable time window	Rationale
<p>Backfill shall limit the water flow so that transport is diffusion dominated.</p> <p>Hydraulic conductivity $< 10^{-10}$ m/s.</p>	<p>After the target state has been reached, up to one hundred thousand years at least.</p>	<p>Backfill should contribute to favorable conditions for the buffer and canister and limit radionuclide transport in case of canister failure. A sufficiently low hydraulic conductivity is required to avoid significant advective transport along the tunnel and any essential change in bedrock hydrology.</p>
<p>Backfill shall ensure a tight contact with the rock wall.</p> <p>Swelling pressure > 200 kPa.</p>	<p>After the target state has been reached, up to one hundred thousand years at least</p>	<p>Backfill should contribute to favorable conditions for the buffer and canister and to the mechanical stability of the deposition tunnels and near-field rock.</p>
<p>Backfill materials should have a sufficiently low compressibility</p>	<p>After the target state has been reached, up to one hundred thousand years at least</p>	<p>Backfill should contribute to favorable conditions for the buffer and canister and limit radionuclide transport in case of canister failure. The backfill should be able to limit the expansion of the buffer. It should keep the buffer in place so that the density requirements of the buffer are met.</p>

2.4 Pellets

In the deposition tunnel pellets are planned to locate between buffer and rock. Investigations and laboratory test has been performed to find out the most suitable pellet material for the project. In this study, pellets are modeled by the information supplied by B+TECH. Pellets can be produced using two basic techniques; firstly by squeezing through a mould (Extrusion) and secondly by roller pressing. These two techniques are commonly used in industry to produce compacted pellets of various materials and have been demonstrated to be viable for production of bentonite materials. Figure 1.4 shows different sizes of pellets proposed for use in filling the space between the backfill blocks and the rock are expected to represent a potentially significant proportion of the tunnel cross-section. Pellets materials required amount of swelling minerals, smectite composition, other minerals intentionally added, stray materials. Specifications for pellet material:

- Dry density and water content of individual pellets.
- Granule size or range of sizes.



Figure 1-4. Examples of bentonite pellets used in repository sealing studies

It is expected that pellet will have a volume of 10–20% of the excavation volume associated with tunneling. It is also anticipated that the pre-compacted backfill blocks will swell and compress the pellet materials. As a result of that backfill block/pellet material in the tunnel should meet the performance requirements of the backfill. However, in this thesis backfill is considered as a homogenous material and pellets are only considered between buffer and rock. Detailed information is given in subsequent chapters.

In many respects it can be said that the pellet component is a simple filler of the space between the buffer blocks and the rock. It does not permit a significant density loss of buffer. The pellets also provide short-term mechanical and hydraulic protection to the blocks by means of minimizing the potential for their mechanical disruption due to localized water inflow and providing for a more uniform wetting than would otherwise occur. The pellet materials also provide protection of erosional redistribution of buffer blocks that might otherwise occur during water inflow.

2.5. Canister

The canister consists of two main components: the integral insert structure of nodular cast graphite iron and the copper over pack. Figure 1.5 shows the general features of canister.

The main safety function of the canister is to ensure a prolonged period of complete containment of radionuclides. As long as its copper shell is not breached, a canister will provide complete containment of radionuclides. Therefore, the spent fuel will interact with the environment only by means of heat generation and low-level gamma and neutron radiation penetrating through the canister walls. This safety function depends firstly on the mechanical strength of the canister insert and the corrosion resistance of the copper surrounding it.

The basic design requirements of the canister for nuclear waste disposal can be listed as:

- The canister must not be penetrated by corrosion during the first 100 000 years after disposal.
- The minimum cooling time of the assemblies should be 20 years.
- Canister voids should prevent water filling.
- The surface temperature shall not be more than + 100 °C to guarantee the chemical stability of the surrounding bentonite.
- The canister must be designed to resist the loads caused by disposal at a depth of 300 to 700 m, which requires an evenly distributed load of 7 MPa hydrostatic pressures from ground water and 10 MPa pressure of bentonite swelling pressure.
- The canister should have a sufficient strength in non-symmetric bentonite swelling conditions or in a case of additional hydrostatic load caused by 3 kilometers of ice during a glaciation.
- The strength of the copper over pack is checked for handling and operational loads and the tolerance of the gap between the copper over pack and the iron insert is limited in such a way that the plastic or creep strain in copper will be less than 5 % in case the copper over pack is pressed against insert.

These main design requirements of canister are adopted by POSIVA and SKB reports.



Figure 1-5. Disposal canister for the spent fuel from the Loviisa 1–2 (VVER-440), Olkiluoto 1–2 (BWR) and Olkiluoto 3 (EPR) reactors (from left to right). All versions of the canister have the same outer diameter of 1.050 m. The heights are 3.6 m, 4.8 m, and 5.25 m (from left to right). (Raiko 2005a)

Table 1.5 shows the general safety functions for canister design. In the current reference design, the canisters have a design lifetime of at least 100,000 years. The canisters are designed to maintain their collectivity taking into account the processes and events that take place in the repository over period of 100,000 years. Extreme conditions will give rise to earlier canister failures, and these possibilities must be considered in connection with safety assessment. If the copper shell is breached, then a canister is considered to have failed, even though it may continue to offer some resistance to the ingress of water and the release of radionuclides for a significant period thereafter.

Table 1.5 Safety function indicators and criteria for the canister

Safety function	indicator	Criterion Rationale
Minimum copper thickness	> 0 mm	Zero copper thickness anywhere on the copper surface would allow relatively rapid water ingress to the canister interior and radionuclide release
Isostatic pressure on canister	< pressure for isostatic collapse (varies between canisters, but probability of collapse at 44 MPa is vanishingly small)	An isostatic pressure on the canister greater than 44 MPa would imply a more significant possibility of failure due to isostatic collapse
Shear stress on canister limit	< rupture	A shear stress on the canister greater than the rupture limit would imply failure due to rupture

In this thesis, the heat flow from canister was main interest. In chapter 3, thermal calculations for the canister are detailed.

3. PART I - THERMAL CALCULATIONS

In this chapter, it has been concentrated on thermal analysis of the deposition tunnel. A 2D-axisymmetric solution for thermal analyses of a single canister has been performed. Having an appropriate boundary condition for the boundaries was a main interest of this chapter. The material properties considered in this chapter are based on investigations and Posiva reports.

In this chapter firstly it is described the geometry of the tunnel and canister area and an appropriate geometry for 2D-modelling is proposed. Secondly, it has been handled residual power calculation of disposed canister and residual heat due to decay of radioactive products.

Although the maximum temperature permitted in the canister surface under disposal conditions is 100°C, as indicated by Ikonen (2005), the maximum permitted bentonite temperature is set to 90°C. This permits an additional safety margin which covers uncertainties in thermal parameters, heterogeneities and other uncertainties. It has been considered 2D-modelling and so the temperature on the canister surface can be limited by increasing the tunnel spacing and the canister spacing. The pre-cooling time of canister (fuel age) also influences the maximum temperature achieved for a given geometry. Another problem discussed is the distance from the canister to the upper and lower boundaries where a thermal boundary condition should be imposed.

The program CODE_BRIGHT (Olivella et al, 1996) is used to perform comparative analysis to reach a proposed model. A thermal calculation which gives realistic temperatures is a previous step to carry out THM calculations for which it is convenient to consider a relatively reduced domain in order to avoid excessive number of elements or high different size between the elements in the buffer and the ones in the rock far away from the disposal drift.

Despite the fact that gaps between buffer and canister and as well as canister emplacement on the repository have importance for the thermal results, they have not been analysed in this chapter. Gap modelling is given in subsequent chapters.

3.1- Introduction

The main objective of this part of the thesis is to describe the thermal behaviour of a single canister and propose a 2D-modelling for thermal solutions which will be used later for THM calculations. Figure 3-1 shows the principal lay-out of the repository system.

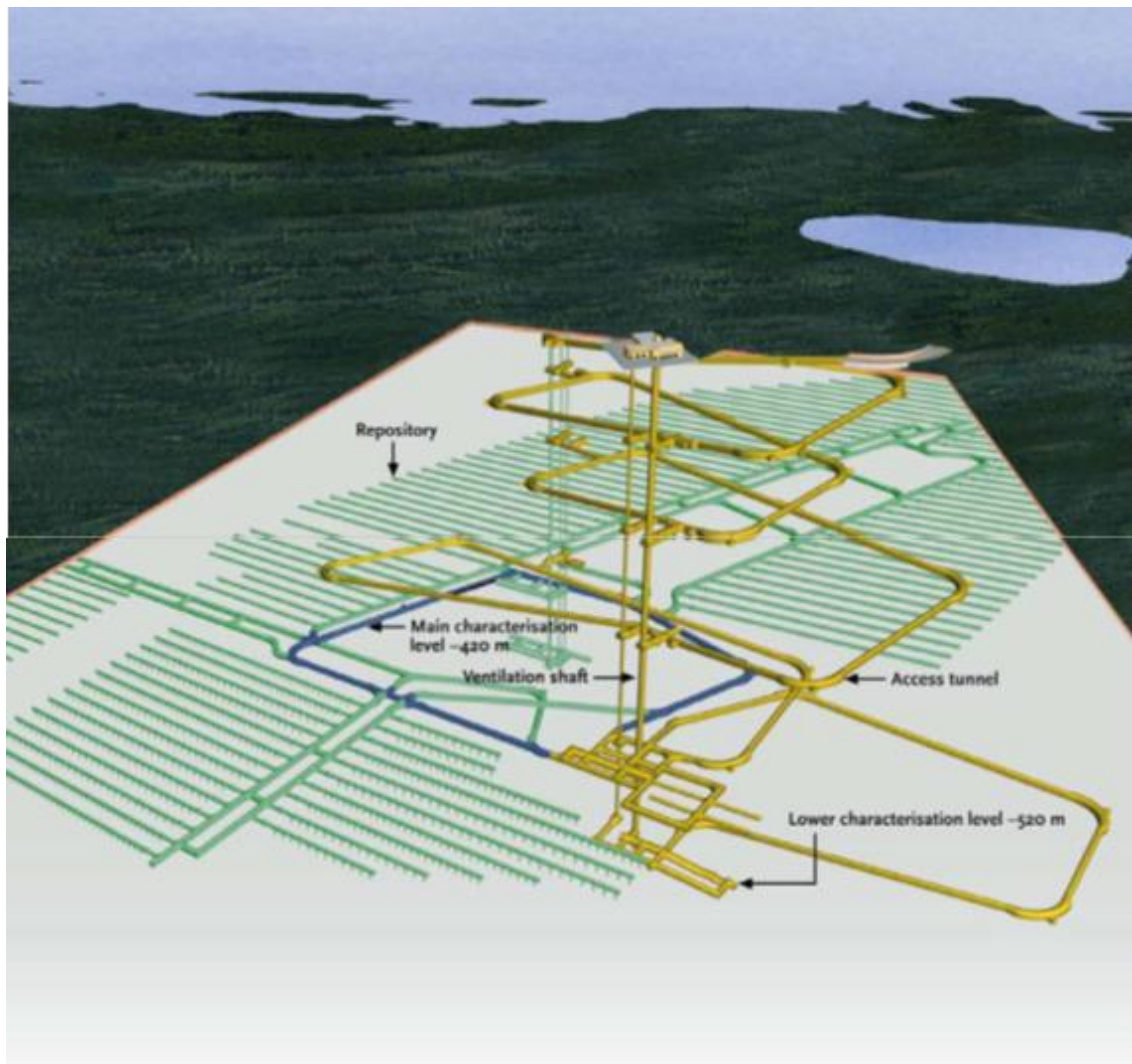


Figure 3-1. Layout of Spent Nuclear Final Disposal Facility

From Ikonen (2005) it is known that the repository is at a depth of 400 m and the initial ambient rock temperature is $+10.5^{\circ}\text{C}$.

In order to perform thermal analyses of the modelled area it has been used the finite element program CODE BRIGHT. In this part of the thesis, backfill, rock and a single canister which is surrounded by buffer have been modelled in terms of thermal analysis.

The spacing of canisters and tunnels should be as small as possible to minimise the repository area. It has been considered an axisymmetric geometry taking into account tunnel and canister spacing separately.

A power of 1700 W for each canister is considered as a reference value from Ikonen (2005) and received project data. A decay of heat canister power is considered to represent the decrease of activity. It has been involved an exponential function with different parameters corresponding to four intervals.

A 1700 W of canister power, 25 m of tunnel spacing and 11 m of canister spacing and constant temperature of 10.5 °C are selected as parameters for a the reference model. As it is shown in Figure 3-2 there is two alternative disposal conditions of the spent fuel. In one of them the canisters are disposed in a horizontal position in the horizontal tunnels. In the alternative disposal method, the canisters are emplaced vertically in boreholes excavated in horizontal tunnels. The two methods have some common specifications such as the use of buffer and backfill material, the first surrounding the canister and the second to fill the horizontal drift.

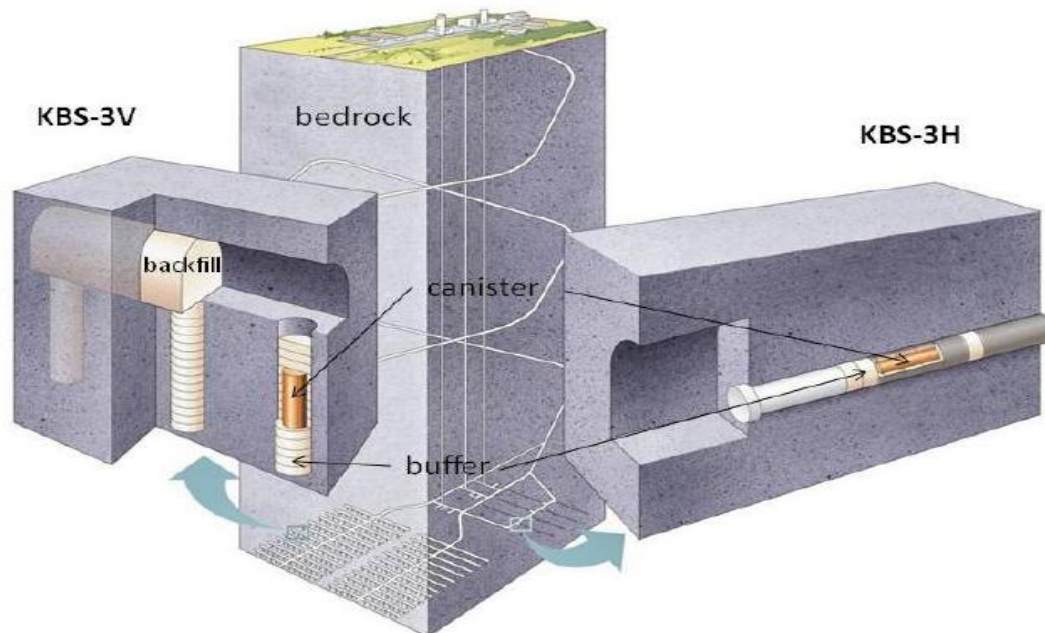


Figure 3-2. The KBS-3V (left) and KBS-3H (right) alternative realizations of the KBS-3 spent fuel disposal method (modified from Posiva 2009a)

3.2. Geometry of Canister Area

Figure 3-3 shows the dimensions and layout of the disposal hole and tunnel as well as the general geometry which has been drawn using GID, including the considered materials. In the thermal analyses included in this report, for the BWR fuel canister the height of the canister has been set to 4.8 m and the external diameter has been set to 1.05 m. Buffer blocks height is 1.2 and 0.8 m respectively and the backfilled tunnel has a height of 4.4 m.

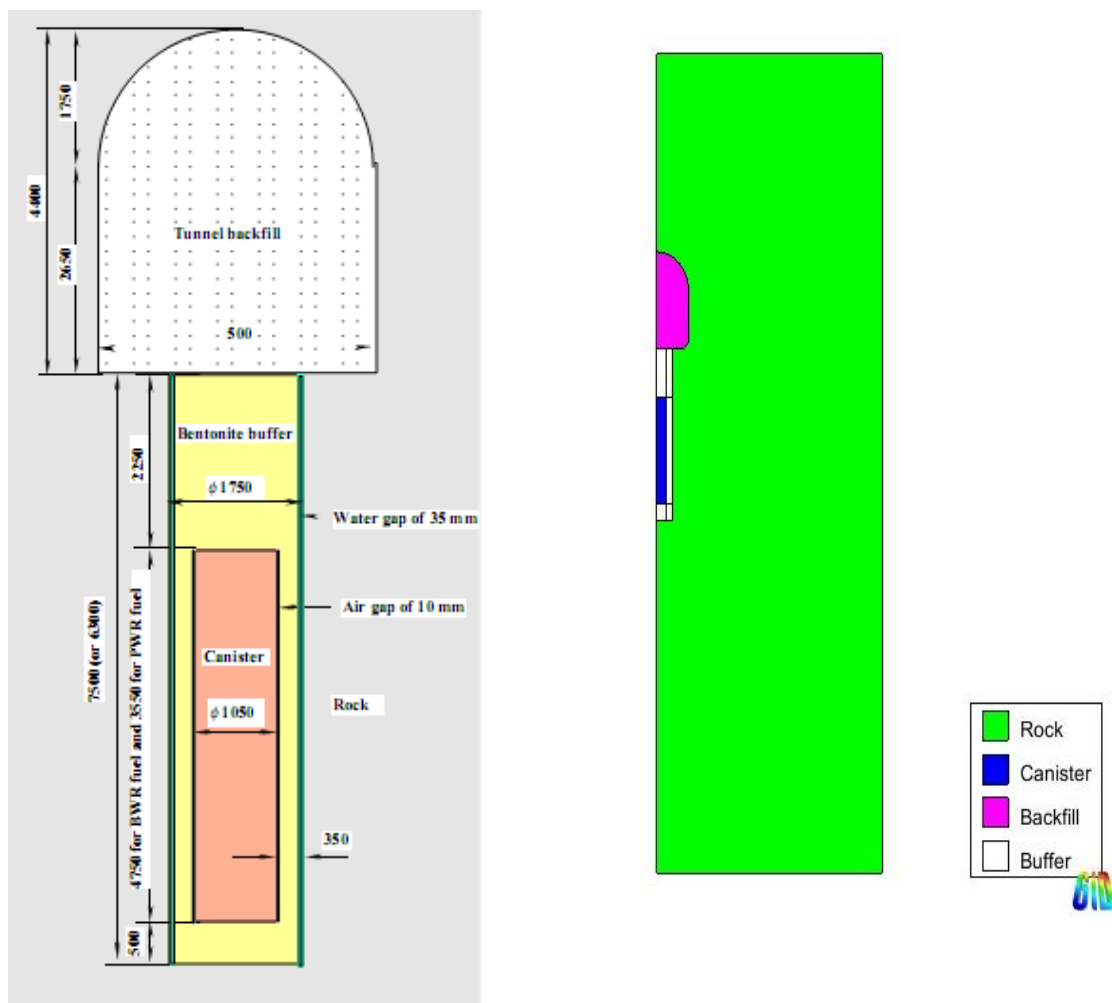


Figure 3-3. Dimensions (cm) of final disposal hole and tunnel

Despite the gaps between materials that may play a role in the thermal analysis neither air gap between canister and bentonite nor water gap between bentonite and bedrock are not taken into account in this chapter. These will be considered in the coupled analyses.

As a reference scheme of Posiva, it has been proposed that a reasonable canister and tunnel spacing is 11 m and 25 m, respectively (Figure 3-4). If a 2D modelling under axisymmetric conditions is considered, an equivalent radius is required. The axisymmetric model implies the same spacing in both directions. The same volume between tunnel and canister is considered. This is achieved with a value of 8.3 m for the equivalent radius (diameter 16.6 m) to be considered for the axisymmetric model. As it has been mentioned before, spacing between adjacent canisters and adjacent tunnels are fundamental parameters on the maximum design temperature of 100°C.

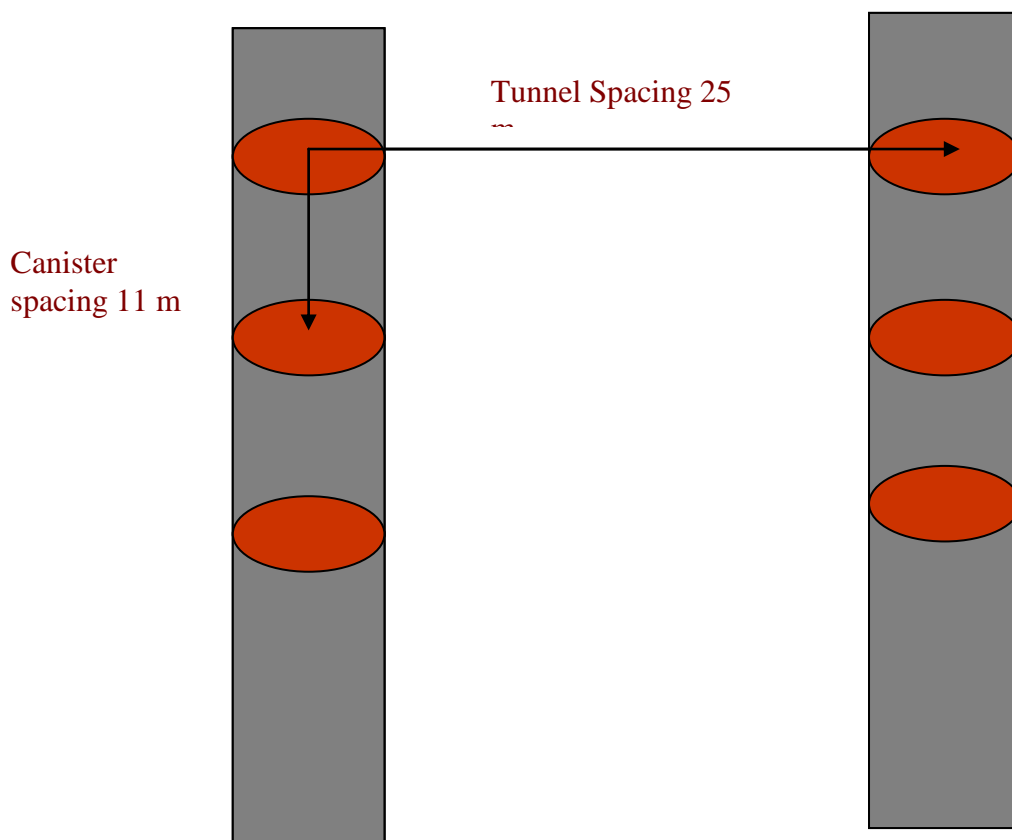


Figure 3-4. Schematics of tunnel and canister spacing

Figure 3-5 shows the respective situation for adjacent tunnel and canisters. The appropriate geometry where the tunnel and canister spacing have an equivalent radius of 8.3 m is determined as reference model equivalent spacing.

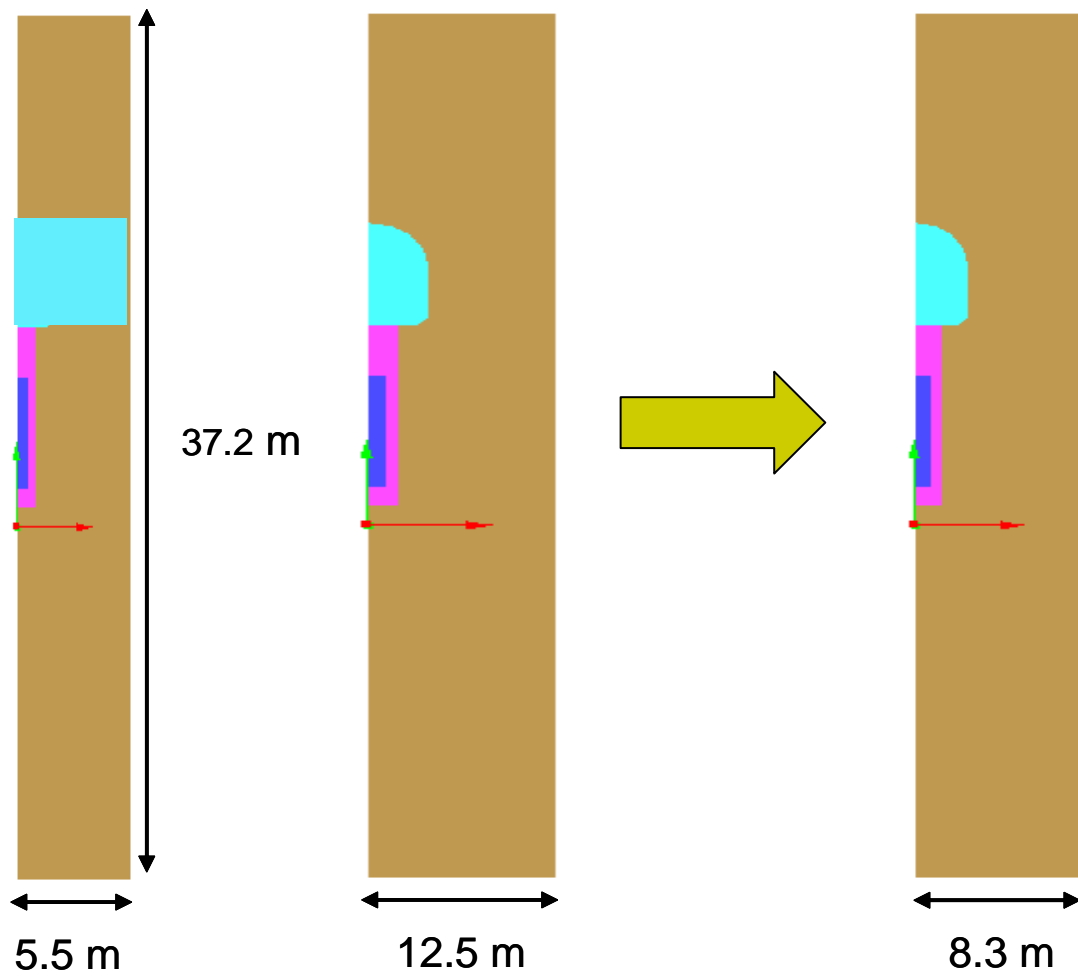


Figure 3-5. Schematics of tunnel and canister spacing. The view with 5.5 m width shows the tunnel longitudinally while the view with 12.5 m width shows the cross section of the tunnel. The axisymmetric approximation implies an axisymmetric cavity.

3.3. Thermal Properties Of Materials

Figure 3-6 and 3-7 show a scheme of the repository and the main components of the canister. The thermal model needs only thermal properties of the four components considered in the model.

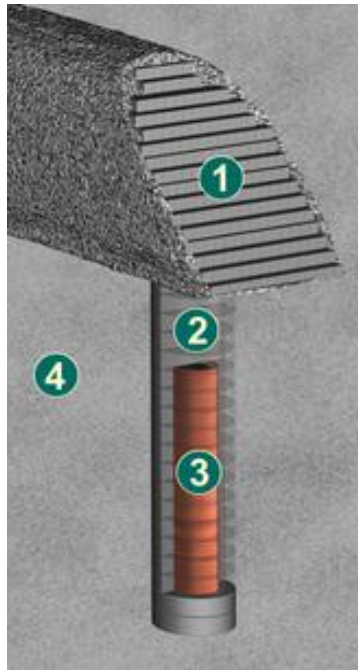


Figure 3-6. Materials in deposition tunnel

The main materials considered are represented in figure 3-6 which are:

- 1- The backfill of the drift
- 2- The buffer made of bentonite
- 3- The canister
- 4- The bedrock or host rock

In this chapter, the material data considered are based on Posiva reports. As it will be explained in the table 3.1, the buffer and backfill have some common specifications.

For the thermal analysis, only the thermal conductivity (λ), the specific heat (c_s) and the density (ρ_{nat}) are the parameters for the materials. The dry density can be calculated as a function of solid density and porosity. Table 3-1 summarizes the thermal properties of these materials.

Table 3-1. Thermal properties of materials

Materials	Thermal Properties				
	Solid density (kg/m ³)	Porosity	Natural density (kg/m ³)	Specific Heat (J/kgK)	Thermal Conductivity (W/mK)
Rock	2749	0.02	2749	784	2.61
Canister	7800	0.01	7847	450	390
Backfill	2780	0.4604	1720	1208	0.544
Bentonite	2780	0.438	1830	1287	0.906

Despite the fact that, there have been proposals on backfill material alternatives such as mixture of bentonite and ballast, friedland-clay etc, in this chapter the specifications supplied by Posiva for backfill have been considered. The canister is assumed with a high thermal conductivity associated with the copper.

3.4. Canister Power

Regarding the canister power evolution, there are two main parameters playing a fundamental role which are the residual power at the time of deposition and decay rate. The work by Hökmark and Fäith (2009) is taken into account as a reference for the calculation of the power and the decay heat rate.

Following the work by Clay Technology, the power as a function of time belonged to an individual canister can be expressed as:

$$P(t) = P(0) \sum_{i=1}^7 a_i \exp(-t / t_i) \quad (3-1)$$

In this expression $P(0)$ is the canister power at the time of deposition and a_i, t_i are parameters related to time. Table 3-2 shows two parameter sets from SKB power data. A burn-up of 38M Wd/kgU is used as a reference. The coefficients given in Table 3-2 are valid for an initial power of 1837.3 W (in the case of 30 year old fuel) and an initial power of 1545.3 W (in case of 40 year old fuel).

Table 3-2. Parameters for the exponential expression (equation 3.1)

i	t_i (years)	a_i (30 years)	a_i (40 years)
1	20	0.070	0.049
2	50	0.713	0.696
3	200	-0.051	-0.059
4	500	0.231	0.271
5	2000	0.024	0.027
6	5000	-0.009	-0.010
7	20000	0.022	0.026

For 30 year old fuel $P(0) = 1837.3$ W. For 40 year old fuel $P(0) = 1545.3$ W
The presently performed work is targeting a 1700 W of initial power at the time of deposition. The power for different times is shown in Table 3-3.

Table 3-3. Canister power data corresponding a 1700 W of power at the time of deposition

Years	Power (W)		
	30 year old fuel	40 year old fuel	Interpolated
0	1700	1700	1700
60	725	751	726
100	502	533	514
200	320	347	316
1000	105	105	101

As Code_Bright uses single exponential functions to represent the power as a function of time, the heat power is approximated in this way. The parameters that have been adjusted are shown in Table 3-4. The two power functions are sufficiently similar as shown in Figure 3-8. The temperature obtained from thermal calculations based on a large model (described later) is shown in Figure 3-7 and 3-8. The evolution of power displayed in Figure 3-7 will be considered in the modelling. It is a function defined in 4 intervals and uses the parameters shown in Table 3-4.

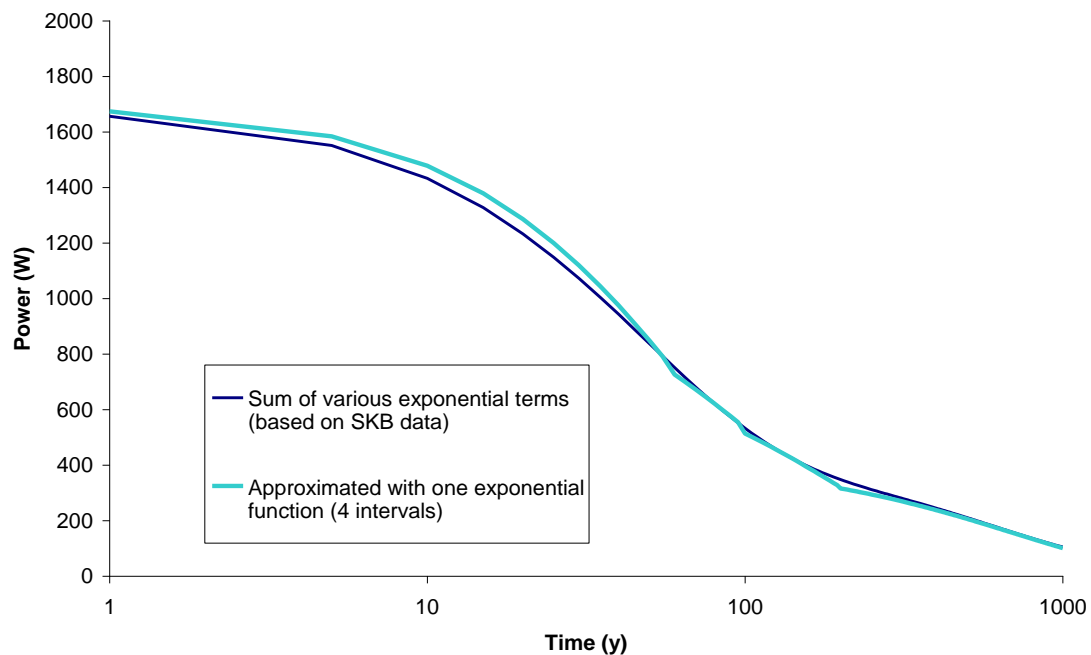


Figure 3- 7. Power of canister as a function of time using different approximations

Table 3-4. Point source heat flow and decay of heat flow corresponding to three individual injected heat source point on the canister surface.

Intervals	Source Heat flow (J/s)	Decay of heat flow (1/s)
0-60	566	4.4×10^{-10}
60-100	385	2.45×10^{-10}
100-200	275	1.5×10^{-10}
200-1000	140	4.51×10^{-11}

Figure 3-9 show the temperature evolution for a model with an equivalent tunnel and canister spacing of 8.3 m and a top and bottom boundary sufficiently far from the drift. In the subsequent section of thermal analysis proposed model will be explained.

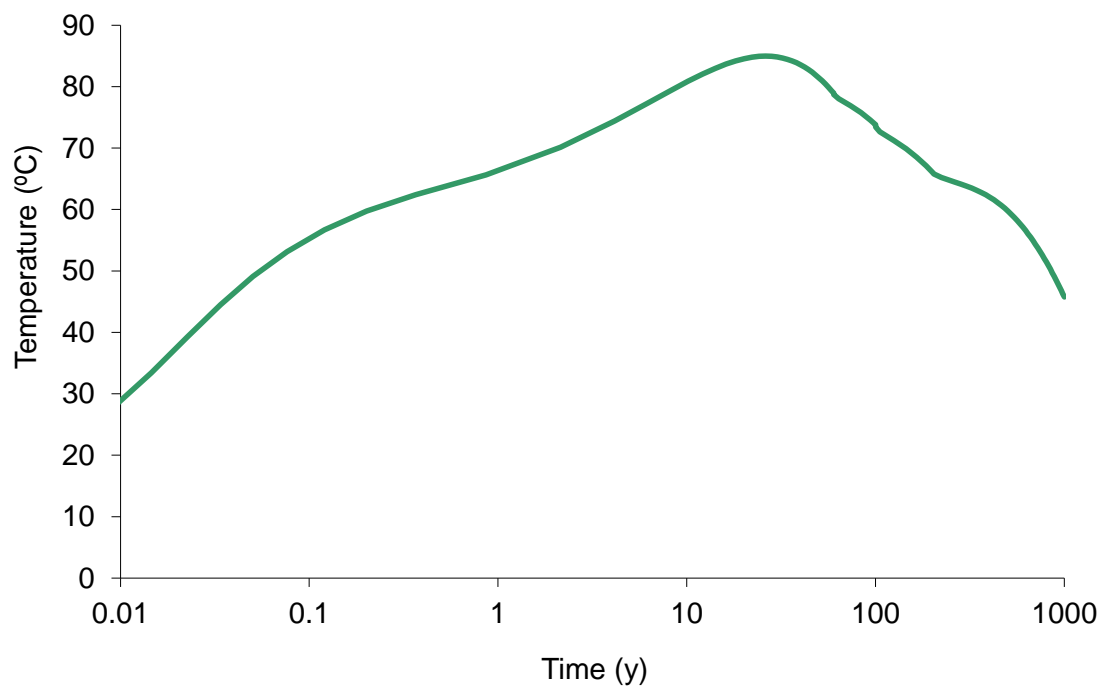


Figure 3-8. Temperature evolution of the proposed model

3.5. Reference Model

A reference model is defined in this chapter to carry out comparative thermal analyses. The reference model will be compared with other cases.

The reference model is defined with a radius of 8.3 m, (equivalent to 11 m of canister spacing and 25 m of tunnel spacing), three single heat source points on the canister surface to simulate inflow heat from canister, 1700 W of heat power at the time of deposition, with decay rate as defined in Table 3-4 and constant temperature on the top and bottom boundaries (Figure 3-9). As the thermal conductivity of the canister is very high, the temperature distribution is practically uniform within the area representing the canister.

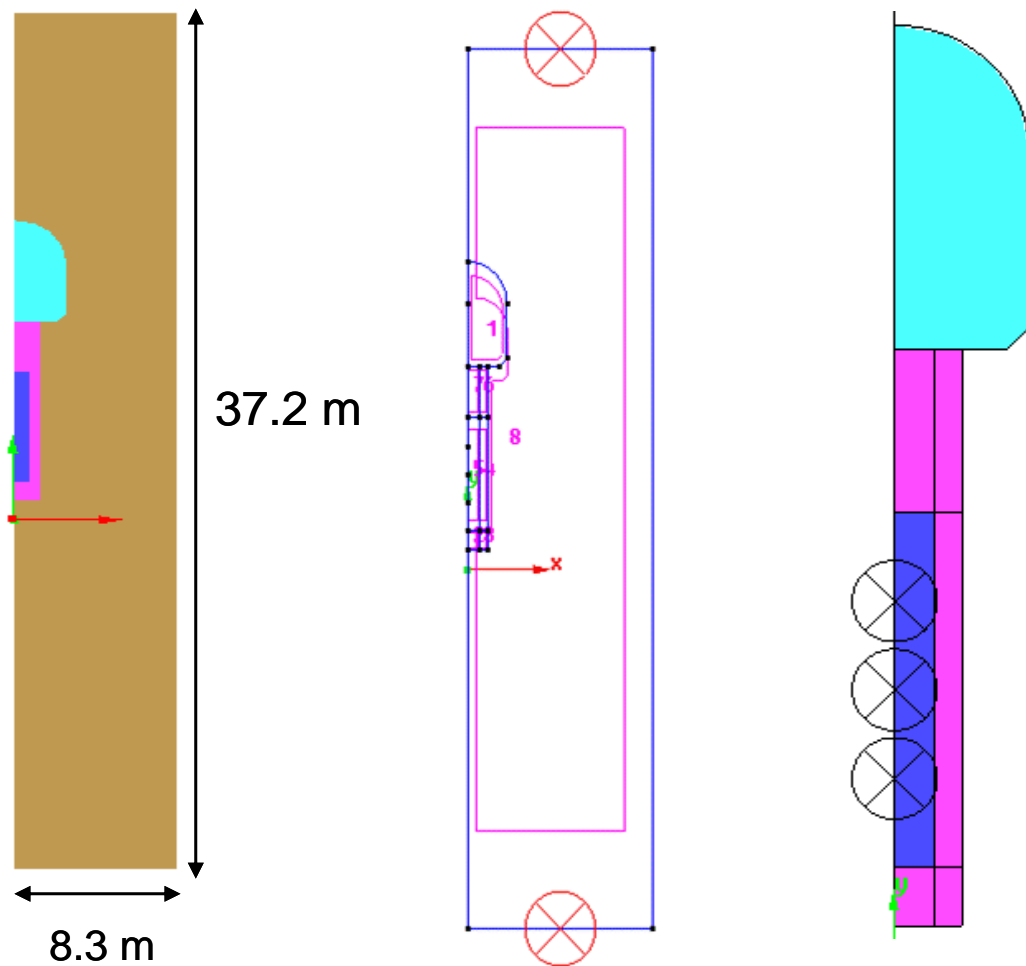


Figure 3-9. General geometry, boundary conditions and canister heat flow conditions of the reference model

3.6. Thermal Conditions

There have been taken into account three conditions to simulate thermal behaviour of a single canister which are:

- a) Initial surface temperature condition (10.5 C)
- b) Boundary flow rate conditions (constant temperature)
- c) Heat flow from canister (power decreasing with time)

As the initial temperature of the rock is +10.5°C, this temperature is assigned as a boundary condition on the top and bottom boundaries of the rock in the case of the reference model. The heat inflow from the canister takes into account the decay due to the degradation of the spent fuel.

There are two ways of defining heat flow from canister area, one of them using a compound line source by specifying canister surface as a volumetric heat flux source the other is known as injecting some point heat sources on the canister surface. The power J (J/s) is the point source of heat flow at some points in the canister, P is the canister power (W) and N_p is the number of points:

$$J = J_o \exp(-\lambda t) \quad (3.2)$$

As the power is injected in the canister at some individual points, the power

$$J_o = P_o / N_p \quad (3.3)$$

In order to compute conductive heat flux Fourier's law is used:

$$\mathbf{i}_c = -\lambda \nabla T \quad (3.4)$$

where λ is the equivalent thermal conductivity and it can be calculated using a geometric mean approximation using the values of dry and saturated thermal conductivities:

$$\lambda = \lambda_{sat}^{S_l} \lambda_{dry}^{(1-S_l)} \quad (3-5)$$

where λ_{sat} and λ_{dry} are the thermal conductivities of soil in saturated and dry conditions respectively and S_l the degree of saturation.

3.7. Comparative Analyses

Calculations have been performed with the 2D axi-symmetric model of one single canister to reach a proposed model which has realistic thermal behaviour. Different parameters have been taken into consideration, these are:

- Effect of tunnel and canister spacing
- Effect of boundary distance

All of these effects are need to be handled carefully. Comparative analyses have been performed by the CODE_BRIGHT (Olivella et al., 1996) program which has been developed for a variety of geo-mechanical analyses.

3.7.1 Effect of Tunnel and Canister Spacing

It is important to have a spacing of canisters and tunnels as small as posible in order to minimise the repository area. Thermal analyses have been performed using 2D axisymmetric longitudinal section.

Basically it has been carried out a study to highlight the effect of spacing on the temperature. In Figure 12 “TCS” refers to tunnel and canister spacing. The values of 25 m and 11 m of tunnel and canister spacing are considered.

It is obvious from the calculations that bigger spacing gives lower temperatures around the canister. Figure 3-10 and Figure 3-11 show the evolution of temperature.

The temperature evolution shows a very rapid decay and this is motivated by the constant temperature imposed on the boundary. From these models it seems that the spacing of 11 m could accomplish the requirement of maximum temperature below 100 °C. However, as it will be shown in the next section, the distance between the boundaries plays also an important role in the achieved maximum temperatures.

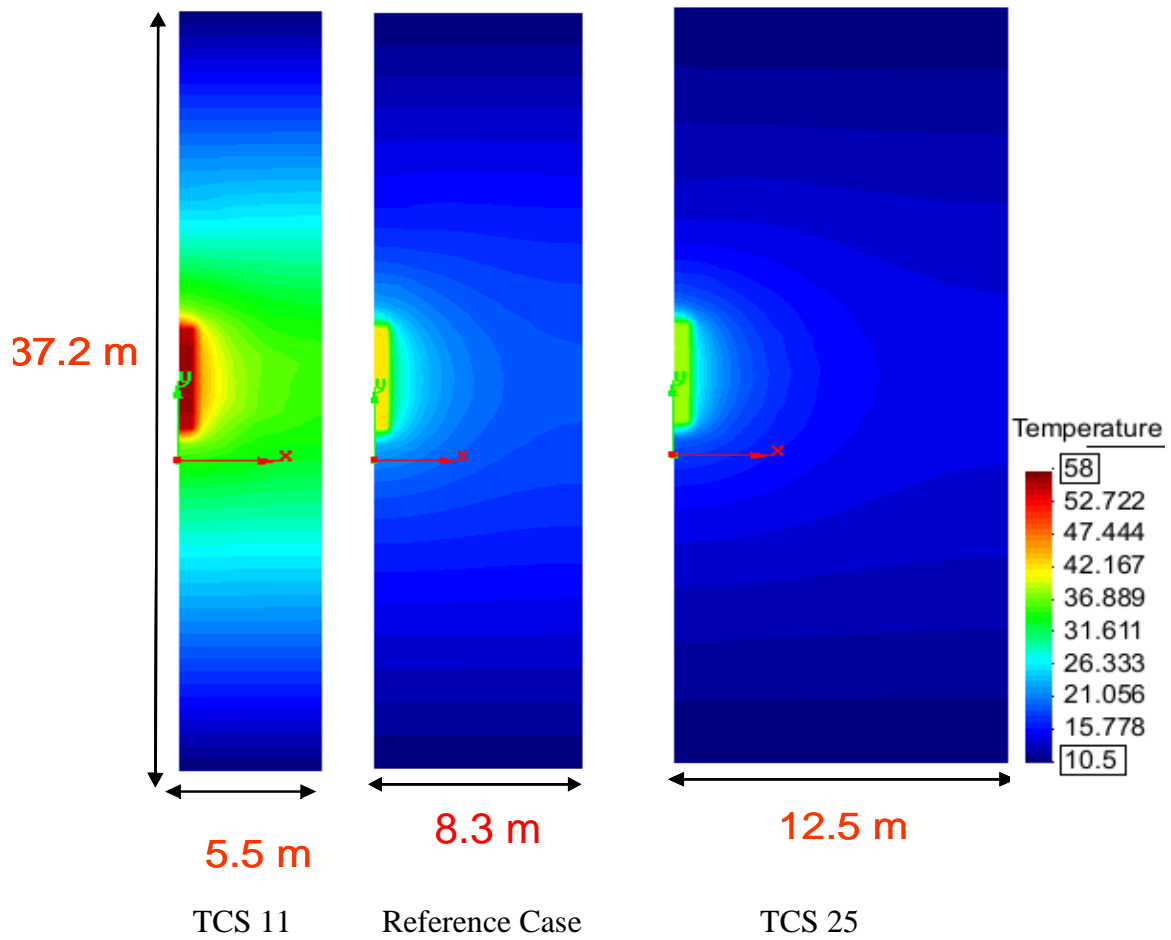


Figure 3-10. Temperature (°C) distribution of different models after 60 years depending of tunnel and canister spacing

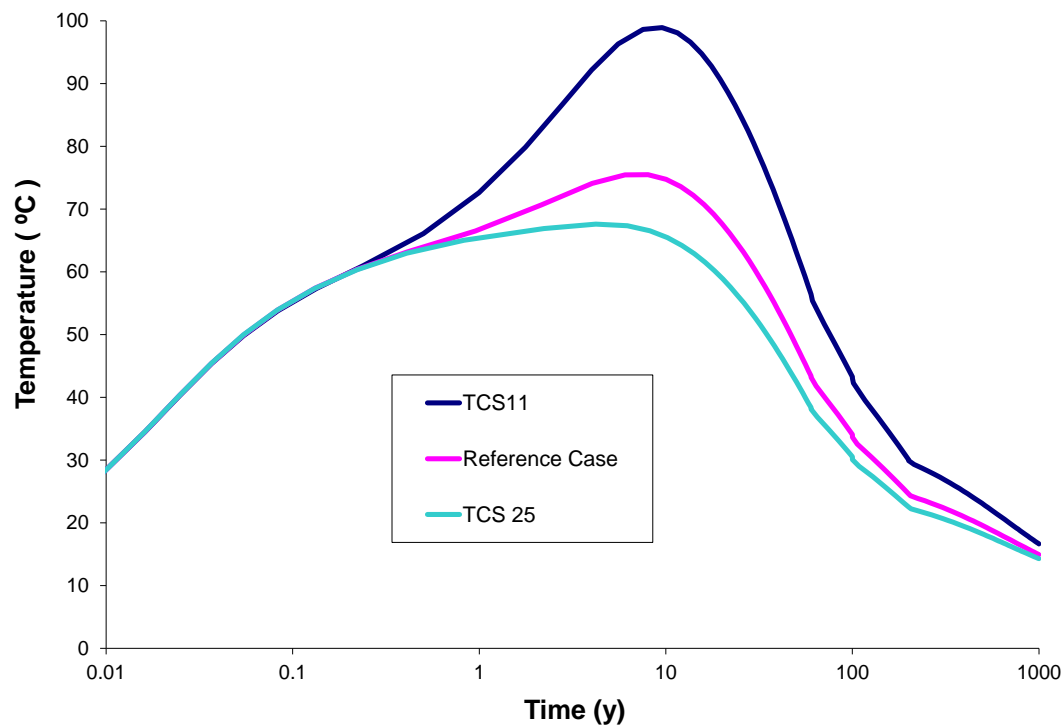


Figure 3-11. Temperature evolution of single canister relating different equivalent spacing

3.7.2 Effect of Boundary Distance

To perform THM calculations in a favourable way, the domain should not be too large. Domain proposed in the reference model (37.2 m) will be used later for THM calculations. However, the top and bottom boundaries of this model are too close so boundaries can not have constant temperature. In order to find an appropriate boundary condition for the top and bottom boundaries, thermal analysis has been performed in larger geometries. The model is enlarged considering boundaries which are at distances 10 and 20 times bigger than the reference model. Table 3-4 summarises the geometry of the cases studied.

Table 3-4. Effect of boundary distance on the achieved maximum temperatures

Models	Lenght of free rock (m)		Maximum temperature on canister surface
	Backfill to Upper Boundary	Buffer to Lower Boundary	
Reference model	9 m	16 m	78
Factor 10	90 m	160 m	85
Factor 20	180 m	320	85

Figures 3-12 and 3-13 show the distribution of temperatures for the different geometries after 200 days of canister emplacement. Figure 3-14 shows the evolution of temperature on the canister surface. The maximum temperature is same for the Factor 10 and Factor 20 models and remains below 90 °C but the so called reference model has lower maximum temperature. It can be seen that in a limited domain, dissipation of heat takes place so that proposing constant temperature at the boundaries are not realistic and it causes to underestimation of temperature in the considered domain as it is depicted in Figure 3.12. It is obvious that after a certain factor, the maximum temperature in the canister is not affected by the boundary distance. The boundries of the 20 times larger model can be proposed as the most realistic case because the deposition hole will have a depth of 400 m.

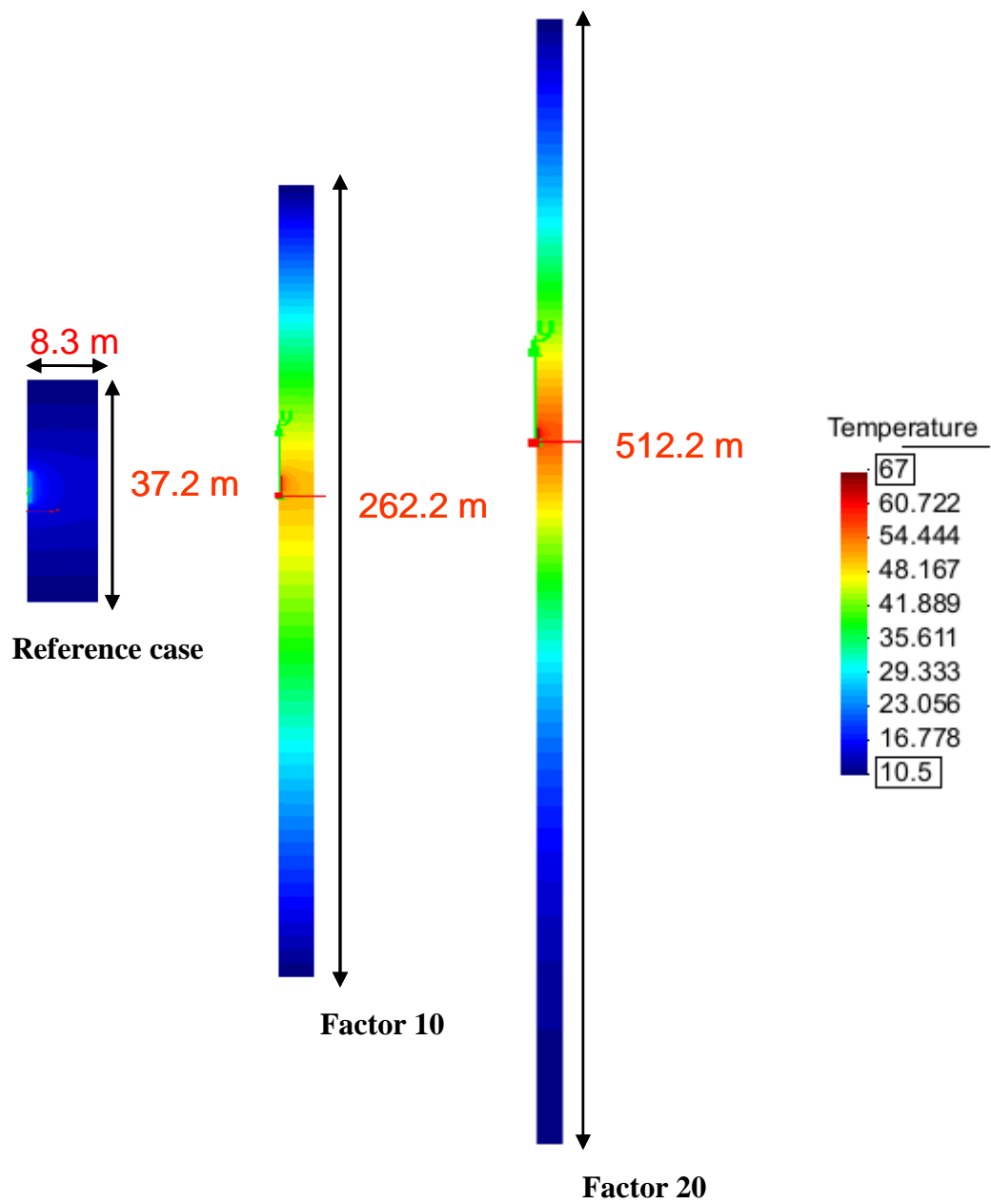


Figure 3-12. Temperature (°C) distribution in the canister, buffer and backfill after 200 years for the three models.

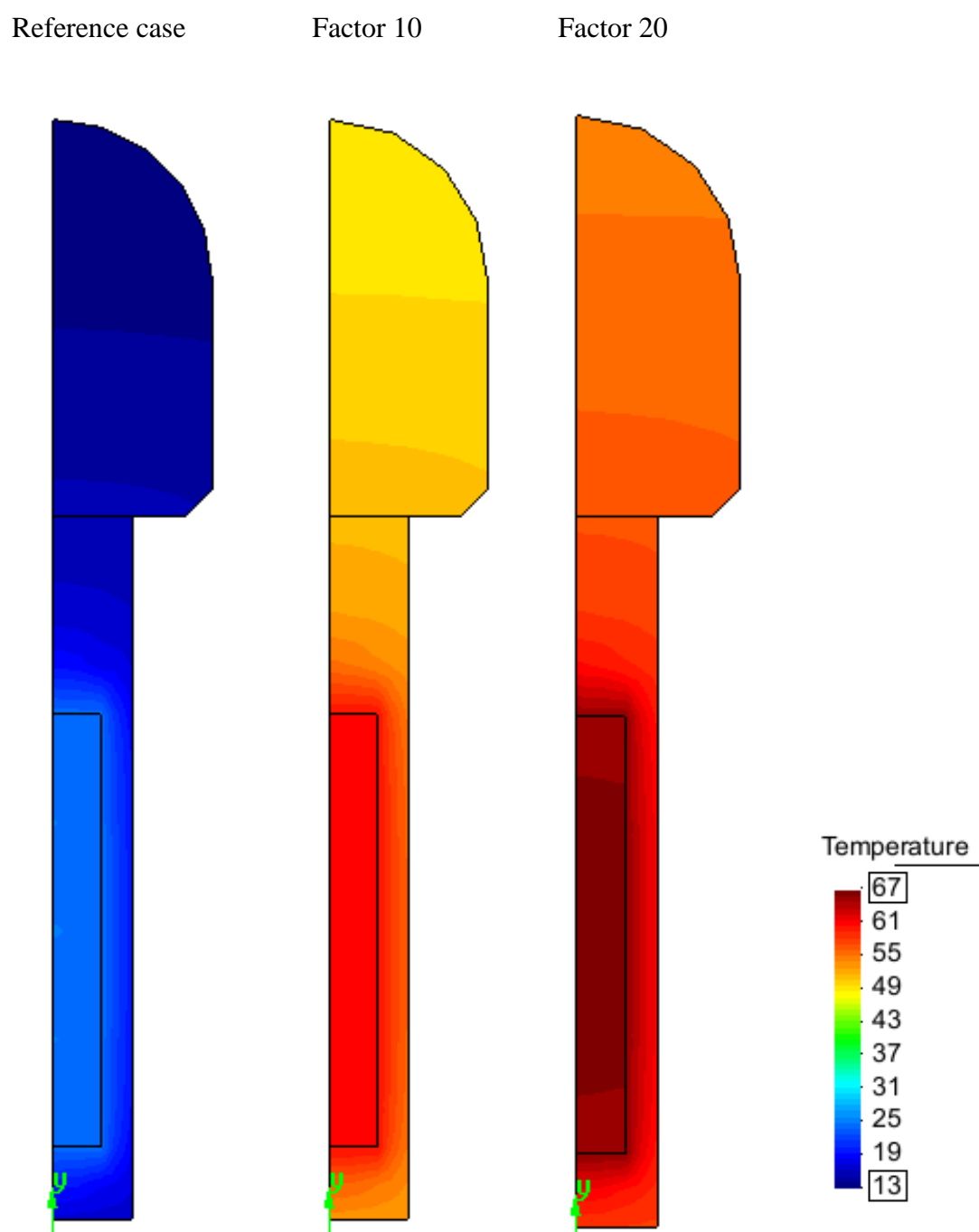


Figure 3-13. Temperature (°C) distribution in the canister, buffer and backfill after 200 years for the three models.

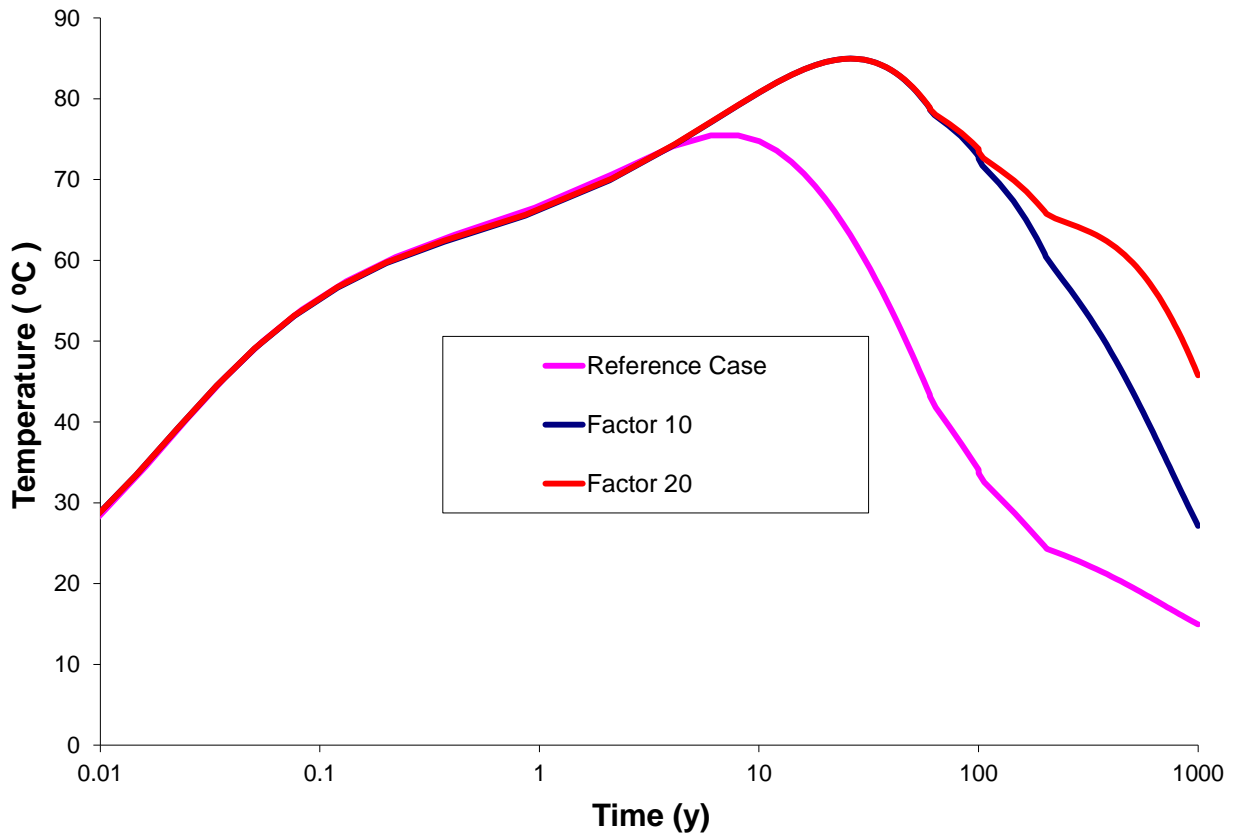


Figure 3-14. Temperature evolution of canister surface as a factor of distance from canister to boundaries.

It is clear that, all three models meet the safety requirement for the maximum temperature on the canister surface. However, temperature evolution of Factor 20 is more realistic. In all three models temperature increases sharply but in models Factor 10 and 20 it does not decrease vigorously. As reference model has a limited domain and constant temperature on the boundaries, heat dissipation takes place and causing underestimated temperatures. Therefore, a proposed model has to be defined and it must have relevant thermal boundary condition which is presented in subsequent section.

3.8. Proposed Model

To overcome the problem of heat dissipation in limited domain, which causes to underestimation of temperature achieved in the concerned domain, a model that has relevant thermal boundary condition have to be proposed. It has been shown that constant temperature of 10.5 °C is far away to simulate realistic temperature in the domain because there is excessively heat outflow through these boundaries.

There are two ways to deal with this problem. One of them is to use an analytical solution and the other one is the numerical solution. In this thesis, numerical solution has been used by means of imposing a variable temperature on the boundary which corresponds to model Factor 20 that has a 20 times large domain compares to reference model. The temperature evolution at the corresponding distance of the model Factor 20 is imposed for the boundaries of the reference model.

Figure 3-15 shows the temperature distribution at 200 years for the reference case, the enlarged case (Factor 20) and the proposed model. The proposed model is obtained by prescribing the temperature values of enlarged model at the corresponding distance. This means that less heat flux takes place on the top and bottom boundaries because the gradient is smaller.

Finally, Figure 3-16 shows the evolution of canister surface temperature for the reference model and for the proposed model. It is clear that the domain with a close boundary gives realistic temperatures only if the special boundary condition is implied.

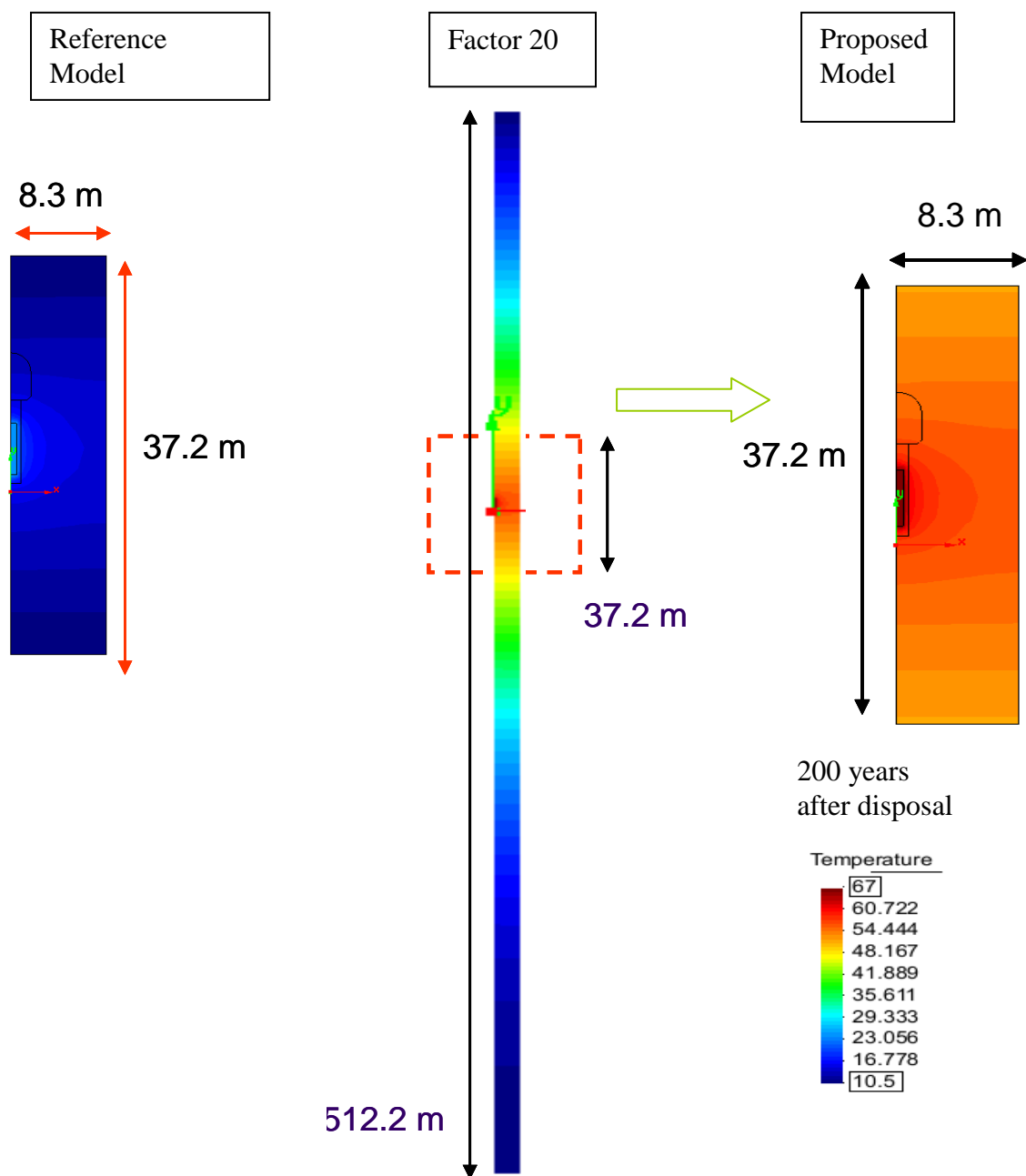


Figure 3-15. Temperatures (°C) after 200 years of disposal for the reference model (left), x20 model (centre) and proposed model (right).

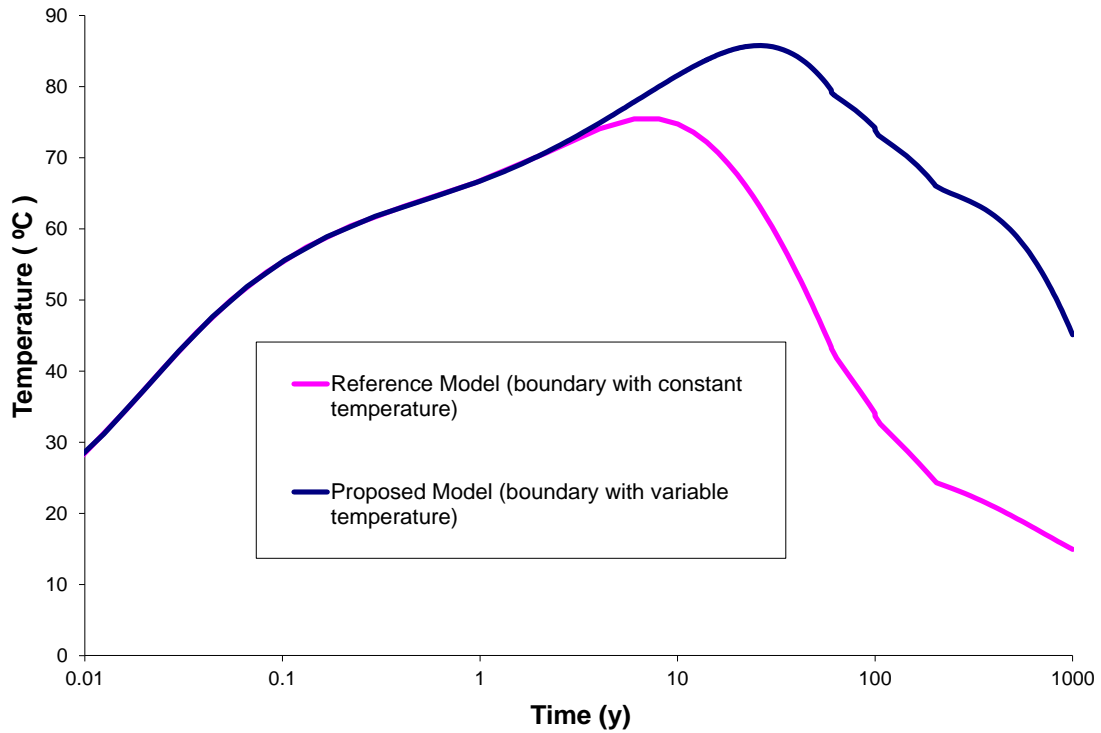


Figure 3-16. Temperature evolution of reference and proposed model

It is shown that reference model underestimates the temperatures achieved in the domain. By means of proposed model that have variable temperature on the boundaries, it can be possible to simulate realistic temperature in a limited domain. These boundary conditions also will have importance in THM calculations that will be explained in subsequent chapters.

3.9. Conclusions for Thermal Calculations

The main objective of this part of the thesis was to study the main effects on the reached maximum temperature on the canister surface. The study consisted of specification of material properties and performing analysis by taking into account different impacts.

It has been shown that tunnel and canister spacing, initial canister power and decay characteristic and also thermal boundary conditions have an importance on the reached maximum temperature in the domain. Therefore comparative analyses are held to validate the performance of proposed model.

A 1700 W of canister power, 25 m of tunnel spacing and 11 m of canister spacing and variable temperature on the boundaries are the reached modelling parameters to perform THM calculations.

It has been demonstrated that in the proposed model that does not cause heat dissipation from boundaries and has an equivalent radius combining tunnel and canister spacing, achieved maximum temperature on the canister surface remains below 90 °C and meets thermal safety requirement for buffer.

After reaching suitable power function, decay characteristic and geometry in terms of adjacent tunnel and canister spacing and also the relevant thermal boundary condition, it can be passed to THM calculations safely.

4. MODELLING OF BUFFER MATERIAL BY MEANS OF OEDOMETER AND INFILTRATION TESTS

It is known that various types of bentonite have been investigated in many countries as buffer materials in high-level radioactive waste disposal concepts. In Finland, MX-80 bentonite is considered one of the best candidates to be used as buffer material for the construction of the multiple barrier disposal site for spent nuclear fuel repository. In order to investigate the hydro-mechanical behavior of MX80 bentonite, a series of laboratory tests have been started up by B+TECH. Two types of tests have been performed: oedometer tests and infiltration tests. These tests have been modelled using the finite element code Code_Bright. The Barcelona Basic Model (BBM) (Alonso *et al.*, 1990) has been used to model the mechanical constitutive behaviour of the material.

4.1. Introduction

The multiple barrier concept is envisaged in most of the proposed schemes for underground disposal of radioactive wastes. The concept invokes a series of barriers, both engineered and natural, between the high level radioactive waste canister and the surface. In almost all countries with a high-level radioactive waste management program, Bentonite, in the form of dry compacted blocks will be used as a buffer material.

In Finland, Olkiluoto was chosen as final disposal site of spent nuclear fuel. One element of the site investigations conducted at Olkiluoto is the excavation of the underground rock characterization facility (ONKALO) that will be extended to the final disposal depth. One of the methods that are studied for the final placement of the radioactive waste considers the vertical deposition of the copper canisters in holes lined with bentonite clay. The tunnel will then be sealed with compressed clay blocks in pellets. Figure 4.1 shows a schematic representation of the deposition holes.

The long term performance of the repository as a whole (canister, buffer, host rock, backfill, pellets and gaps), and in particular, that of the bentonite buffer is of great importance. MX-80 bentonite, is considered one of the best candidates to be used as buffer material, due to its physical and chemical properties which is explained in previous chapters.

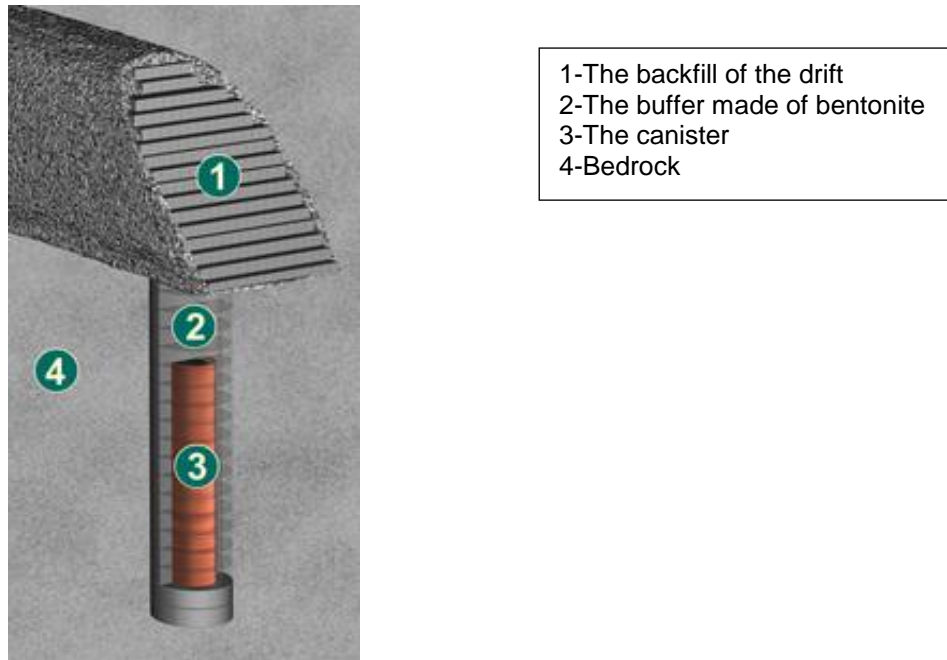


Figure 4-1. Scheme of the repository

Understanding the thermo-hydro-mechanical behavior of bentonite buffer (MX-80 bentonite) is one of the objectives in this chapter. An experimental program has been set up to get insight into the material behaviour. The set of tests that have been performed consists of oedometer and infiltration tests.

In order to analyse the hydro-mechanical behaviour of MX80 bentonite, the above mentioned tests are modelled using the finite element code Code_Bright. The Barcelona Basic Model (BBM) (Alonso et *al.*, 1990) has been used to model the mechanical constitutive behaviour of the material. The purpose of this work is to determine and calibrate BBM parameters of MX80 bentonite clay according to the available tests data.

4.2. Oedometer Tests

As mentioned above, two types of tests have been performed on compacted samples (i) oedometer tests under humidity controlled conditions and (ii) an infiltration test.

In this section the experimental and modelling results of the oedometer tests performed on three samples of MX80 bentonite will be described.

4.2.1 Experimental results

In order to characterize the effect of suction on compressibility of MX-80 bentonite, three oedometer tests under controlled humidity conditions, considering different stress paths, have been carried out. The experimental set-up is shown in Figure 4-2.

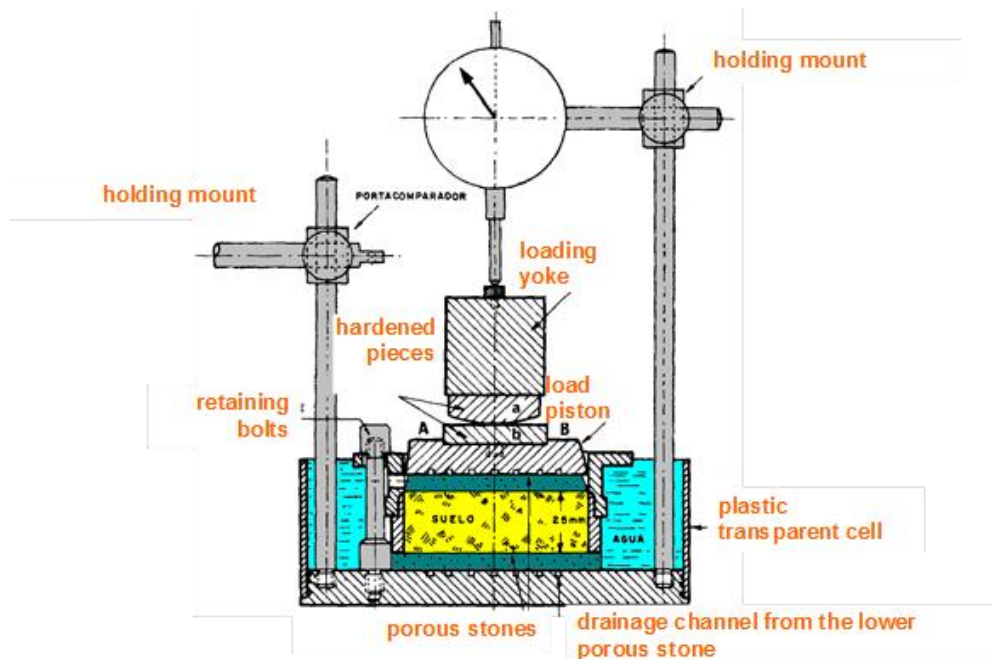


Figure 4-2. Oedometer test cell

The samples (50 mm diameter and 19.05 mm high) were compacted at a dry density around 16 kN/m^3 and at constant water content around 6%. Table 4-1 completes the information of the initial conditions of the three tested samples.

Table 4-1. Initial properties of MX80 bentonite sample
(Oedometer tests)

	100212c_oedometer (Test/Sample A)	101222a_oedometer (Test/Sample B)	100212a_oedometer (Test/Sample C)
Solid Density (kN/m ³)	16	15.9	16
Water content (%)	6.04	5.98	6.04
Porosity (-)	0.375	0.375	0.375
Initial suction(MPa)	153	219	153

**A, B and C is a notation for this report.*

The tested samples were subjected to different suction and stress paths. Once compacted the samples were placed in the oedometer cell and the following steps were followed

For samples A and B (100212c_oedometer and 101222a_oedometer):

- Wetting path at a low vertical stress: the specimens were inundated to reach saturated condition, that is, zero suction. For both cases the swelling deformation were measured.
- Loading-unloading at constant suction $s=0$ MPa (saturated conditions). The pre and post yield compressibility parameters for changes in vertical stress, as well as the yield stress, were determined for each suction level.

For sample C (100212a_oedometer):

- Loading-unloading at constant suction $s=153$ MPa (dry conditions).

Different constant loading steps were applied on the samples. Each loading step was applied instantaneously and maintained for some time. For each test different loading-unloading steps were considered. The vertical displacement for each loading step was recorded as a function of time. However, consolidation effects are not simulated and therefore the time evolution of deformations is not discussed here. Table 4-2 summarizes the different suction conditions and loading/unloading steps for each test.

Table 4-2. Suction and loading-unloading conditions in the tests

100212c_oedometer (Test A)		101222a_oedometer (Test B)		100212a_oedometer (Test C)	
Vertical Load (MPa)	Suction (MPa)	Vertical load (MPa)	Suction (MPa)	Vertical Load (MPa)	Suction (MPa)
0.23	153	0.196	219	0.392	153
0.23	0	0.196	0	0.73	153
0.39	0	0.476	0	1.6	153
0.95	0	1.877	0	3.2	153
2.63	0	3.559	0	6.6	153
4.88	0	5.240	0	3.2	153
2.63	0	1.597	0	1.6	153
0.95	0	0.476	0	0.84	153
		0.196	0		
		1.877	0		
		4.119	0		
		1.877	0		

The coupled hydro-mechanical response of the MX80 bentonite samples subjected to the hydraulic and stress paths described previously are depicted in Figures 4-3 to 4-6. Figure 4-3 shows the measured vertical stress-strain relationship for the three tested specimens. As mentioned previously, samples A and B (100212c_oedometer and 101222a_oedometer) were initially inundated and allowed to swell at a constant axial stress. For sample A (100212c_oedometer) hydrated under $\sigma_v = 0.23$ MPa, a swelling deformation around 0.4 is measured. Afterwards, the sample was subjected to a loading up to 4.88 MPa followed by unloading up to 0.95 MPa. Sample B, hydrated under $\sigma_v = 0.196$ MPa shows lower swelling (0.2) as compared to sample A. In this case after loading up to 5.24 MPa, the sample was unloaded up to 0.196 MPa and then subjected to an additional loading/unloading cycle where the maximum vertical stress reached 4.119 MPa.

The post-yield compressibility parameter $\lambda(s) = \frac{\partial e}{\partial \ln(\sigma_v)}$ for the case of sample A and for the case of sample B is rather similar. The elastic compressibility parameter $\kappa(s) = \frac{\partial e}{\partial \ln(\sigma_v)}$ is also similar between samples A and B.

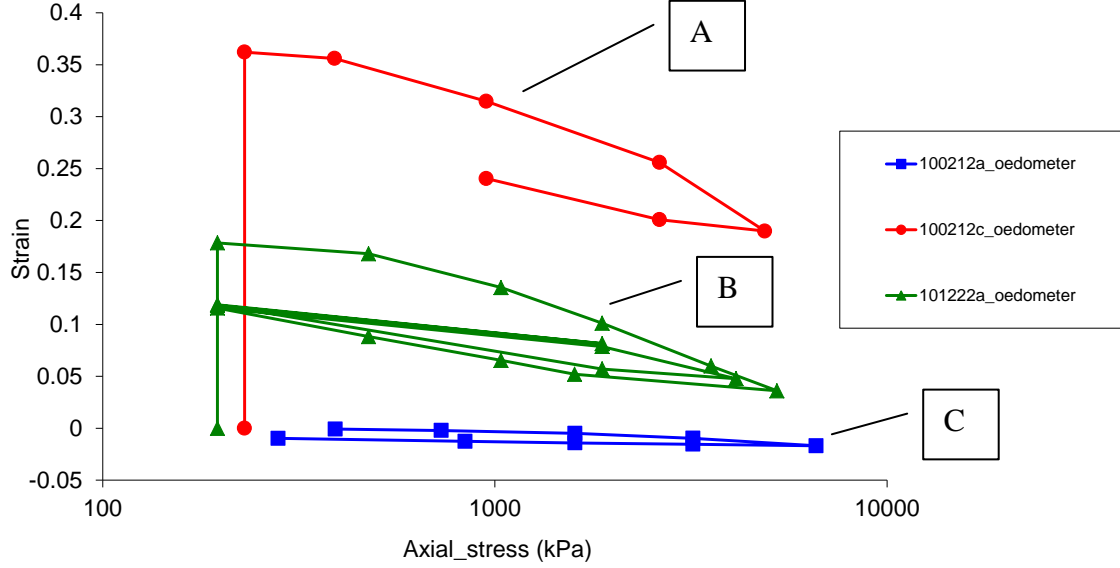


Figure 4-3. Axial stress_strain relationship for the three tested samples.

Sample C (100212a_oedometer) tested under dry conditions ($s=153$ MPa) shows a quite different behaviour. In this case the sample was loaded up to 4.88MPa. In spite of this high vertical stress, the sample showed little deformation (0.009). The slope $\lambda(s)$ of the normal compression line showed a significant drop when suction was reduced to zero. The normal compression line for zero suction (saturated conditions) fell considerably below the normal compression line for $s=153$ MPa. This variation of $\lambda(s)$ is consistent with the proposals of Alonso et al. (1990) who proposed a monotonic decrease of $\lambda(s)$ with increasing suction so that the normal compression line for different values of suction diverged with increasing the vertical net stress.

Plots in the conventional stress path $p:q$ and $\sigma_v: \sigma_h$ planes are depicted in Figures 4-4 and 4-5. In Figure 4-4 the mean effective stress (p) is calculated as $p = (\sigma_1 + 2\sigma_3)/3$ and the deviatoric stress (q) is calculated as $q = |\sigma_1 - \sigma_3|$ where σ_1 and σ_3 are principal

stresses. The results of the oedometer tests in terms of radial stress versus axial stress are displayed in Figure 4-5. When suction is reduced under constant axial stress (samples A and B) the material experiences a swelling tendency resulting in a sharp increase of the radial stresses.

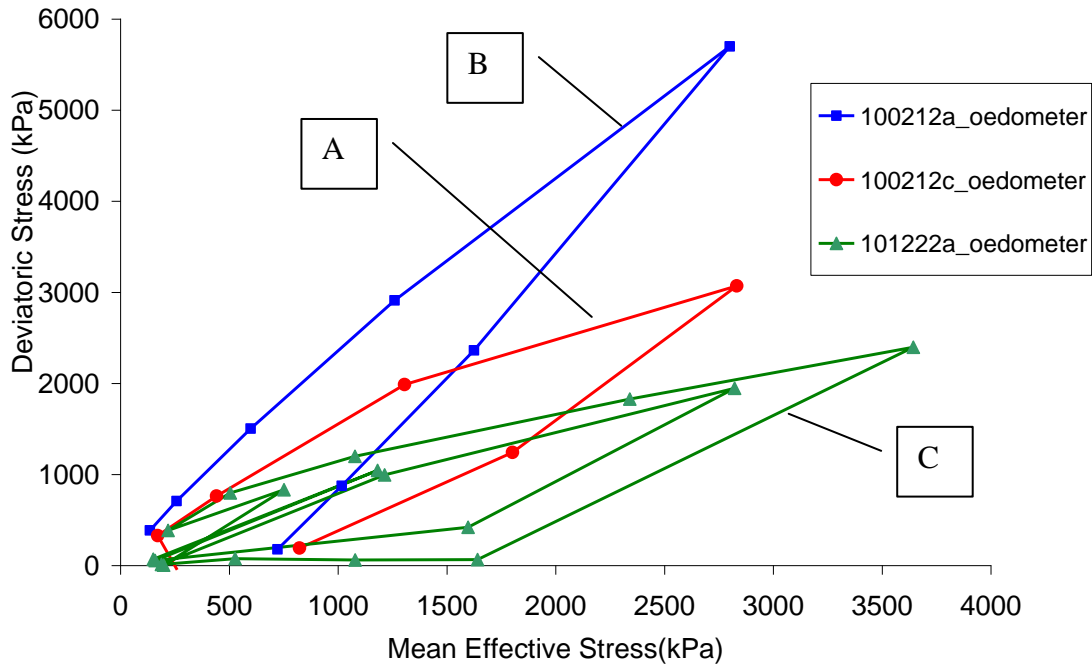


Figure 4-4. Plots in the conventional stress path p:q

Radial stress is given as increments. Another important parameter that can be deduced from the oedometer tests results is the lateral earth pressure coefficient K_0 calculated as $K_0 = \sigma'_h / \sigma'_v$. Figure 4-6 shows the data plotted in form of K_0 against σ_v for the three tested samples. For samples A and B (100222a_oedometer and 100212c_oedometer) swelling under constant axial stress provokes a sharp increase of the horizontal stresses causing an increase of lateral earth pressure coefficient ($K_0 > 1$). Therefore by the end of the hydration phase both samples were over-consolidated. During unloading, axial stress decreases faster than horizontal stress and consequently an increase of K_0 is observed. For samples A and C (100212c_oedometer and 100212a_oedometer) K_0 at the end of the test reaches a value of 0.8 and 0.65 respectively.

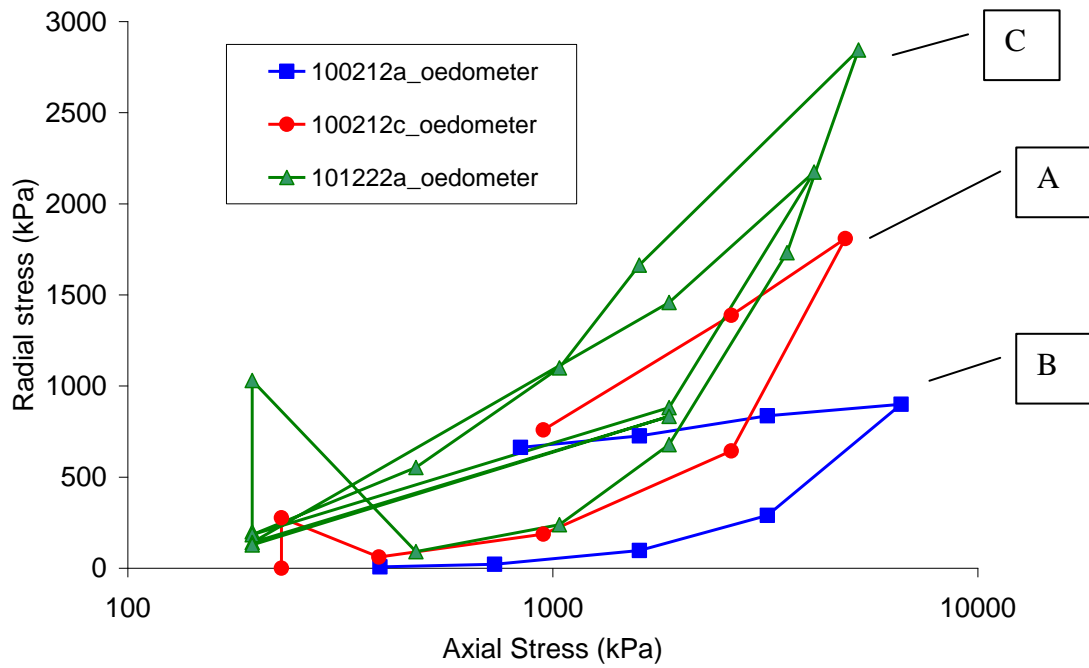


Figure 4-5. Axial stress_radial stress relationship for the three tested samples.

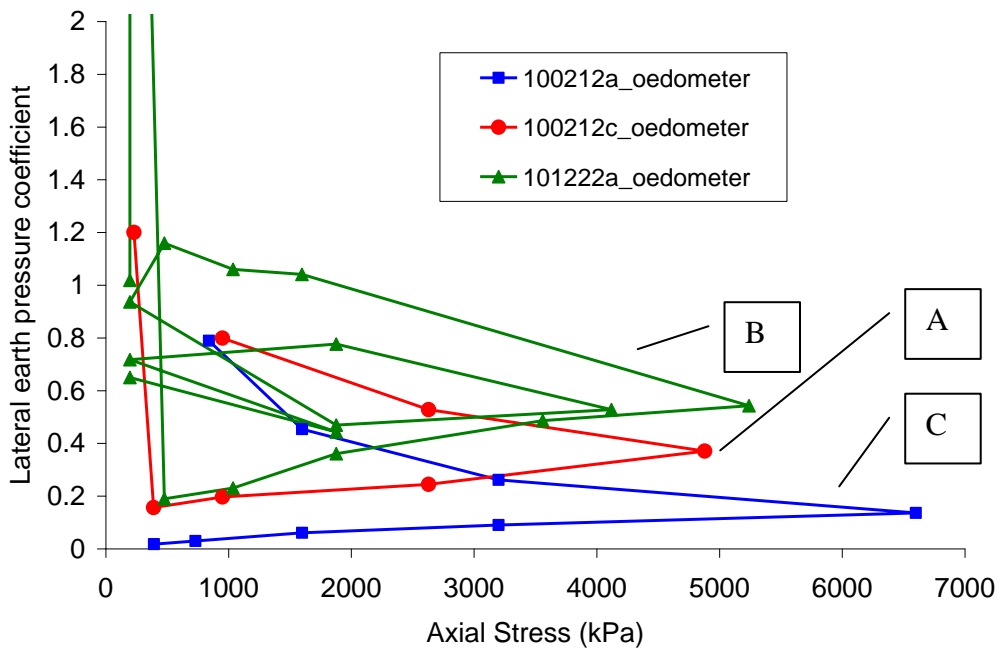


Figure 4-6. Comparison of tests results represented in terms of lateral earth pressure coefficient versus axial stress.

4.2.2 Model geometry and initial conditions

In order to analyse the hydro-mechanical behaviour of MX80 bentonite, the above mentioned tests are modelled using the finite element code Code_Bright. Figure 4-7 shows the model geometry together with the applied boundary conditions. Along the vertical boundaries of the domain, horizontal displacements are restricted to represent the oedometric conditions. Along the horizontal upper boundary a constant axial stress is imposed. Several time intervals were considered in the simulation and for each one the imposed vertical stress was varied to simulate the loading/unloading steps followed in the experiments. As mentioned in the previous section, the oedometer tests were performed under controlled humidity conditions. For two tests (100212c_oedometer and 101222a_oedometer) the samples were hydrated to reach zero suction and for one test (100212a_oedometer) the suction were maintained constant ($s=153$ MPa). To simulate this, hydraulic boundary conditions was imposed on the top and on bottom boundaries.

The Barcelona Basic Model (BBM) has been used to model the mechanical constitutive behaviour of the material. A brief description of the model equations and of the parameters is included in Appendix I.

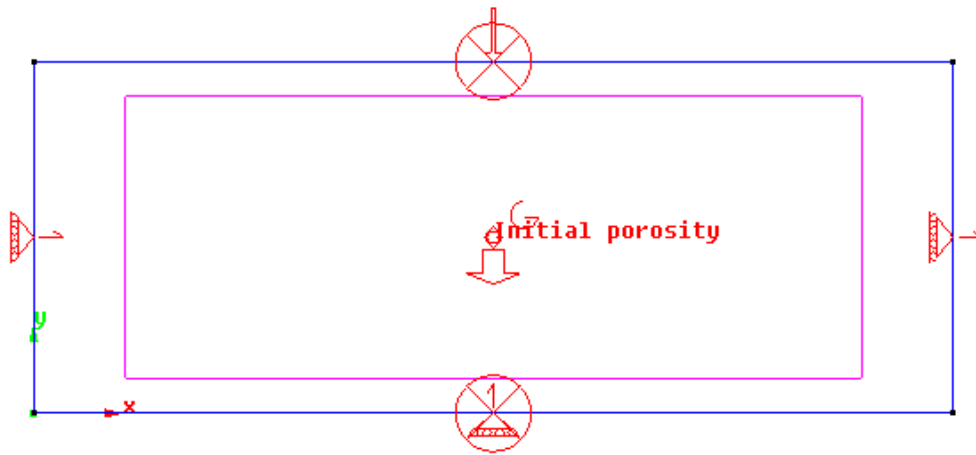


Figure 4-7. Model geometry and boundary conditions

4.2.3. Modelling results of tests 100212c_oedometer (A) and 101222a_oedometer (B)

Table 4-3 shows the parameters of the BBM model for MX80 bentonite used for the calibration of the two tests (100212c_oedometer and 101222a_oedometer). The table includes the values of non-linear elasticity and elasto-plasticity parameters. The parameters have been calibrated to simulate the experiment performed with sample A (100212c_oedometer) (see Table 4-2 for suction and stress paths). The same parameters were used to simulate the experimental results of sample B (101222a_oedometer).

Table 4-3. BBM parameters for tests 100212c_oedometer and 101222a_oedometer

Parameters	Symbols	Units	Values
Poisson's ratio	ν (-)	-	0.35
Parameters for elastic volumetric compressibility against mean stress change	κ_{i0}	-	0.05
	α_i	-	-0.003
Parameters for elastic volumetric compressibility against suction change	κ_{s0}	-	0.25
	α_{sp}	-	-0.145
Elasto-plastic volumetric compressibility	$\lambda(0)$	-	0.15
Parameters to define LC yield curve	r	MPa ⁻¹	0.8
	β		0.02
Reference stress	p^c	MPa	0.01
Initial porosity	ϕ_0		0.375
Preconsolidations stress	p_o^*	MPa	0.75
Strength parameter	M	-	1.07

Figures 4-8 a and b show the vertical stress-strain and the vertical stress-void ratio relationships for 100212c_oedometer and 101222a_oedometer tests respectively. The plots show comparisons between the experimental data and the numerical simulations. For both tests, the modeled results fit quite well with the experimental data (taking into account that the model parameters have been calibrated with 100212c_oedometer). The model predicts well the swelling deformations that occur during the wetting phase. The calculated swelling deformations for 100212c_oedometer (0.3) are in the same order of magnitude as the measured value (0.4). For experiment 101222a_oedometer, the swelling is over predicted by the model. The sharp increase of the lateral stresses observed during swelling under constant axial stress is also quite well captured by the model (Figure 4-9). The model does not predict very well the variation of the lateral

stresses that occurs during loading/unloading phase (Figure 4-9). These discrepancies could be attributed to uncertainties that occurred during the experiment, as it is difficult to measure lateral stresses in an oedometer.

Figure 4-10 shows test 100212c_oedometer plotted in form of K_0 against σ_v . The plots show that swelling under constant axial stress causes an increase of lateral earth pressure coefficient ($K_0 > 1$). Therefore by the end of the hydration phase the sample was over-consolidated. During unloading, axial stress decreases faster than horizontal stress and consequently an increase of K_0 is observed.

4.2.4. Modelling results of test 100212a_oedometer (C)

As described in Section 4-1, in this test the sample were tested under nearly dry conditions. In fact, suction was maintained constant and equal to 153 MPa during the loading/ unloading phase. Sample C (100212a_oedometer) tested under dry conditions ($s=153$ MPa) shows a quite different behaviour. In this case the sample was loaded up to 4.88MPa. In spite of this high vertical stress, the sample showed little deformation (0.009). Table 4-4 shows the parameters of the BBM model used for the calibration of this test (100212a_oedometer). In this case, the calibrated elastic parameters were 10 times lower than those obtained for calibration of tests 100212c_oedometer and 101222a_oedometer. For the properties considered, the model reproduced quite well the experimental results in terms loading/unloading induced deformations (Figure 4-11).

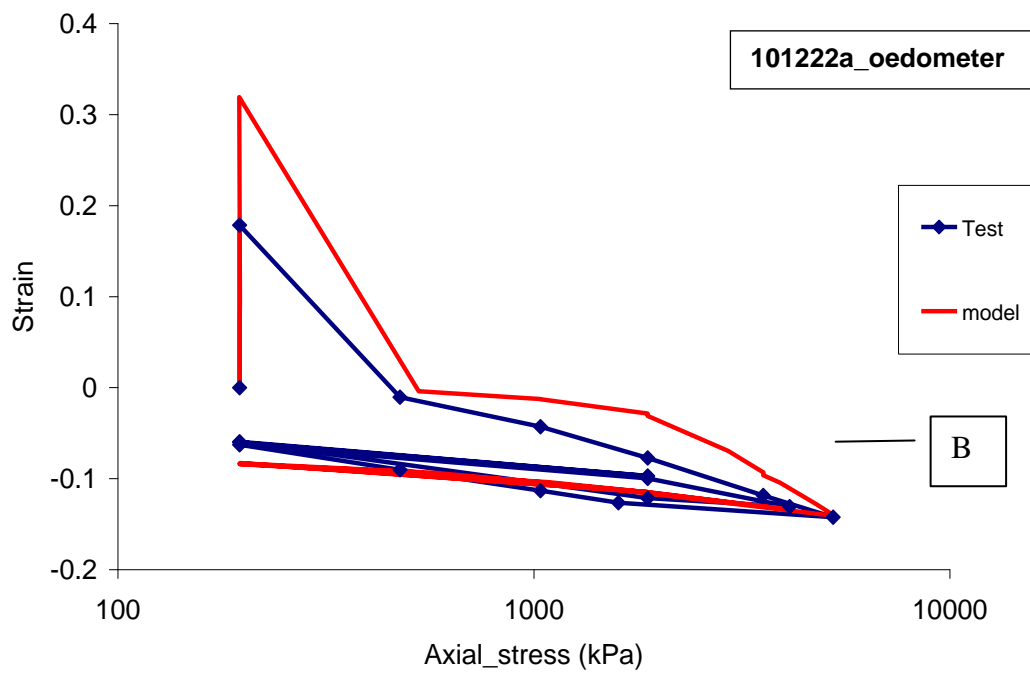
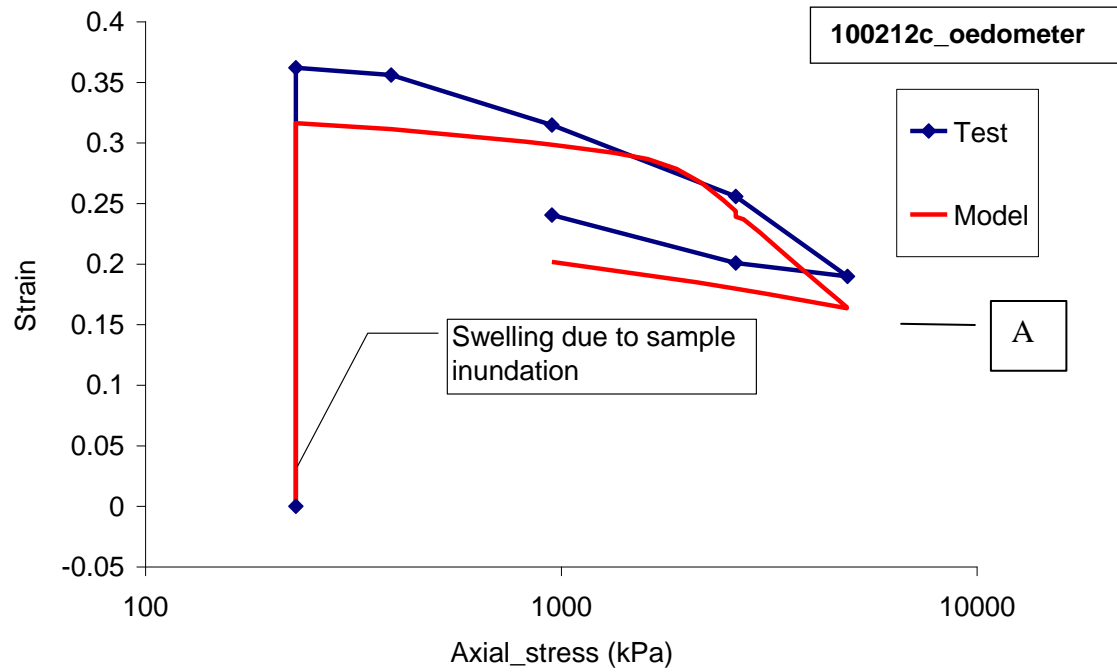


Figure 4-8. Modelling and experimental results.

Axial stress_strain relationship for 100212c_oedometer (A)

Axial stress_strain relationship for 101222a_oedometer (B)

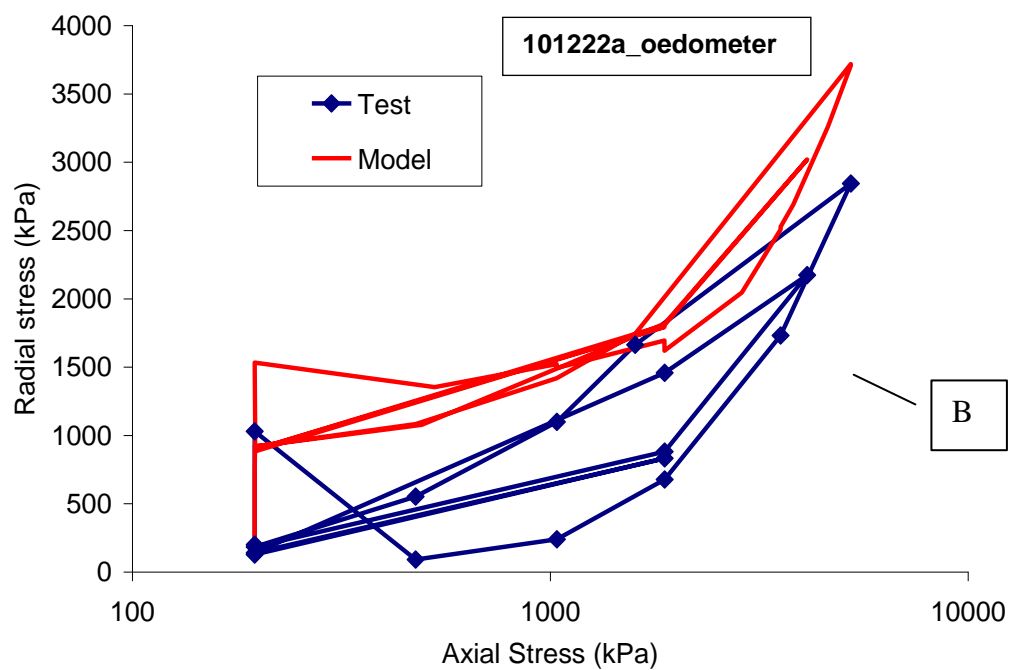
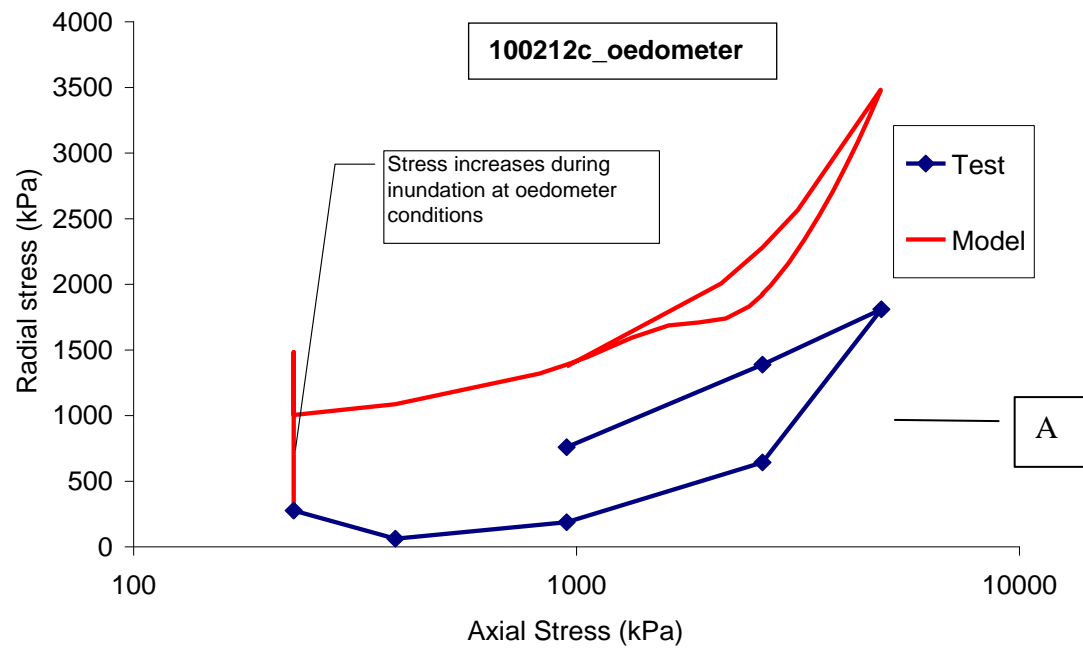


Figure 4-9. Axial stress_radial stress relationship for 100212c_oedometer (A) and 101222a_oedometer (B)

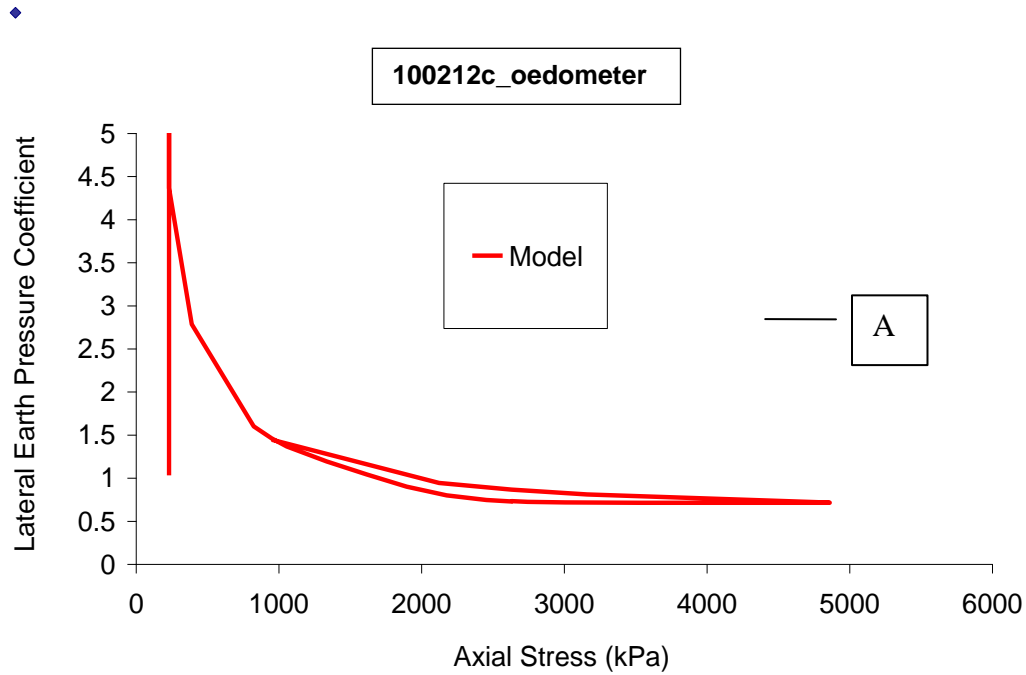


Figure 4-10. 100212c_oedometer (A) represented in terms of lateral earth pressure coefficient versus axial stress.

Table 4- 4. Material parameters for test 100212a_oedometer

Parameters	Symbols	Units	Values
Poisson's ratio	ν (-)	-	0.2
Parameters for elastic volumetric compressibility against mean stress change	κ_{i0}	-	0.005
	α_i	-	-0.003
Parameters for elastic volumetric compressibility against suction change	κ_{s0}	-	0.025
	α_{sp}	-	-0.145
Elasto-plastic volumetric compressibility	$\lambda(0)$	-	0.02
Parameters to define LC yield curve	r	MPa ⁻¹	0.7
	β		0.02
Reference stress	p^c	MPa	0.1
Initial porosity	ϕ_0		0.375
Preconsolidation stress	P_o^*	MPa	0.75
Strength parameter	M	-	1.07

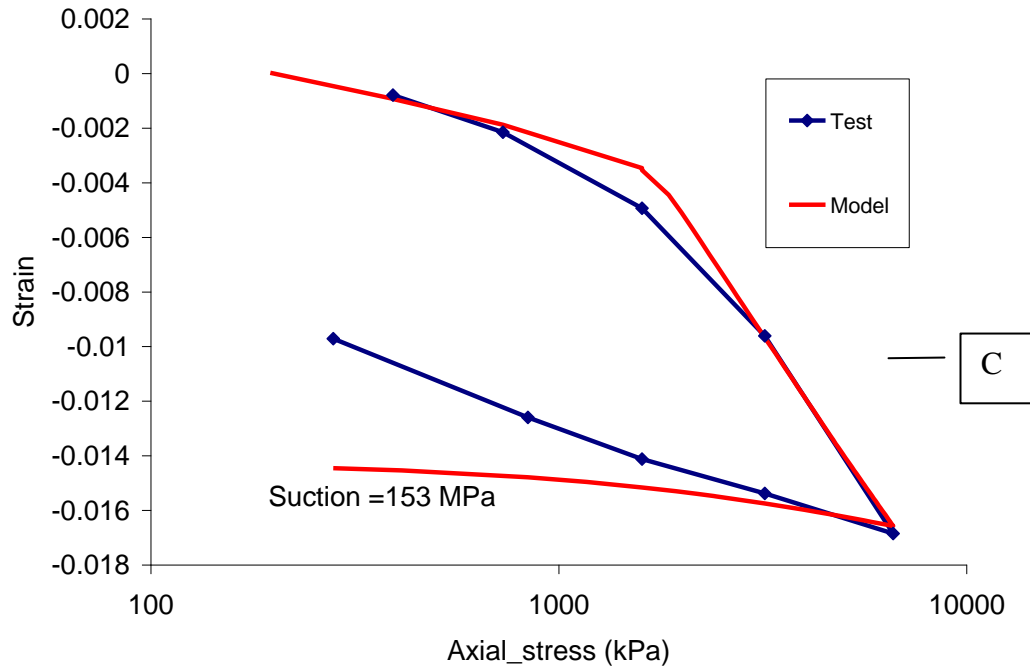


Figure 4-11. Calculated and measured strain during the loading/unloading phase

Figure 4-12 shows the modeling results in term of K_θ versus σ_v . In Figure 4-13 the stress path in $p: q$ plane is shown. Some differences are observed between the model and the experimental results.

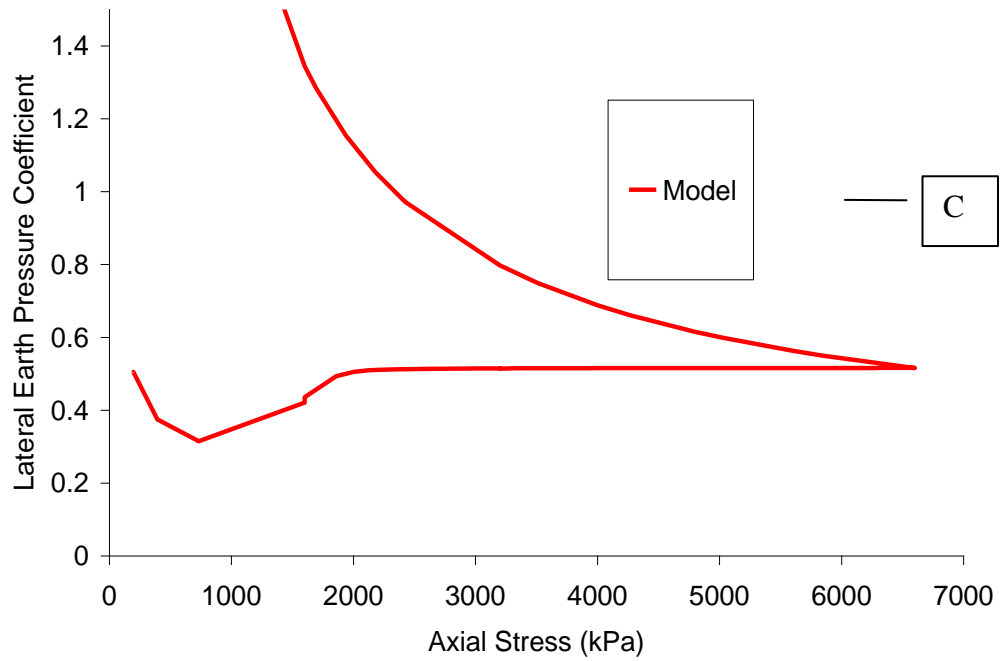


Figure 4-12. Model lateral earth pressure coefficient

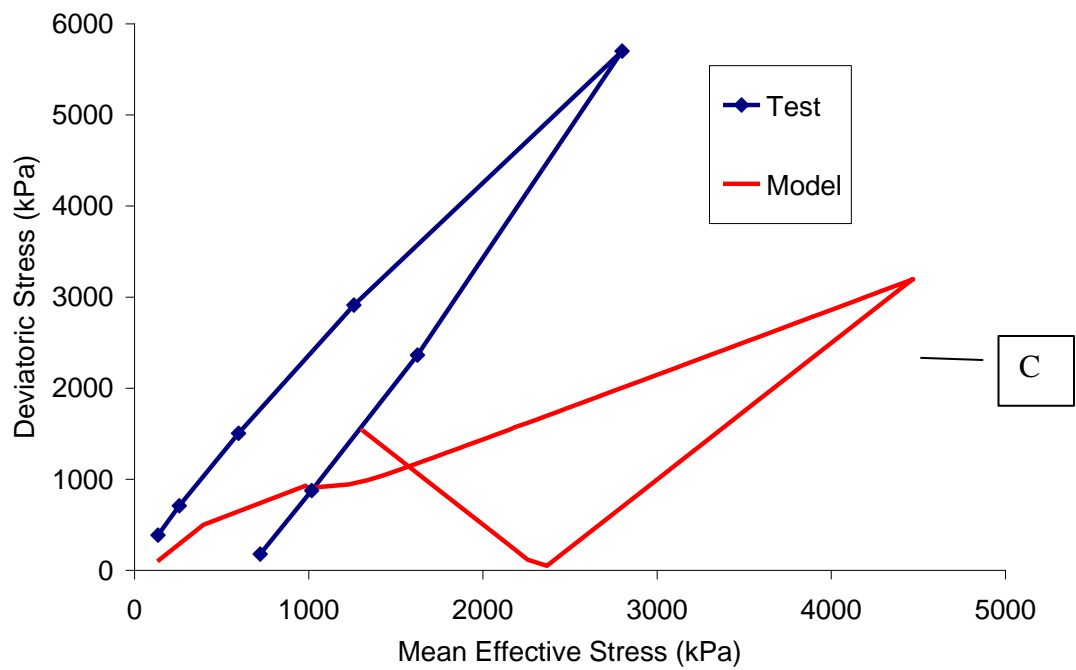


Figure 4-13. Mean effective stress versus deviatoric stress. Experimental and modelling results

4-3. Infiltration Test

In order to explore the behaviour of bentonite buffer upon hydration under confined conditions, an infiltration test was performed on MX80 bentonite. The samples were compacted at a dry density $\gamma_d = 17 \text{ kN/m}^3$ and at constant water content $w = 5.33\%$. Table 4-5 completes the information of the initial conditions of the tested sample.

Table 4-5. Initial properties of MX80 bentonite sample
(Infiltration test)

Dry density (kN/m^3)	17
Water Content (%)	5.33
Degree of saturation (%)	23.34
Porosity	0.375
Intrinsic permeability (m^2)	5.59×10^{-21}
Initial suction (MPa)	243

A schematic drawing of the infiltration test cell is presented in Figure 4-14. The lower face of the sample is maintained in contact with a porous stone. The hydration inlets are connected to a standard pressure/volume controller which is a water pressure source and volume change gauge. Water is then collected into a reservoir.

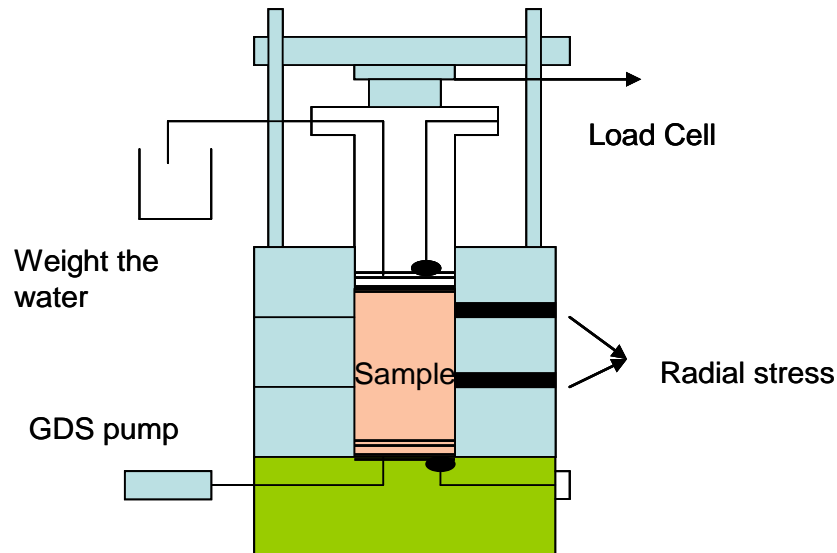


Figure 4-14. Scheme of infiltration test device

4.3.1 Modelling results

The infiltration test is modelled using the finite element code Code_Bright. Figure 4-15 shows the model geometry together with the applied boundary conditions. The test is performed under confined conditions. Along the vertical and horizontal boundaries of the domain, displacements are restricted. Water inflow, is allowed at lower boundary of the domain.

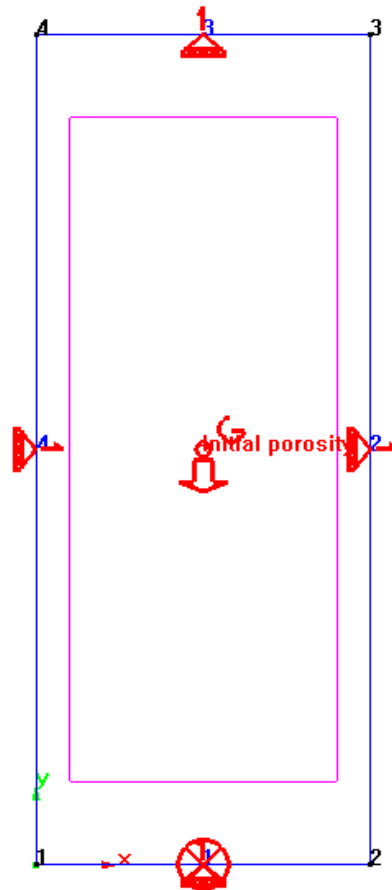


Figure 4-15. Model geometry and boundary conditions

The Barcelona Basic Model (BBM) (Alonso *et al.*, 1990) has been used to model the mechanical constitutive behaviour of the material. The same model parameters as for the simulation of tests 100212c_oedometer and 101222a_oedometer were used (Table 4-3) except for the pre-consolidation pressure which was set to 12 MPa (value corresponding to the fabrication pressure).

Figure 4-16 shows the time evolution of water pressure within the simulated sample. As mentioned previously, the initial suction the sample is $s=243$ MPa. Water is then driven by advection into the sample because of the gradient of suction existing between the water filling partially the soil and the external reservoir (Figure 4-17). As a consequence there is dissipation of the negative pore pressure prevailing initially into the sample pores (Figure 4-16).

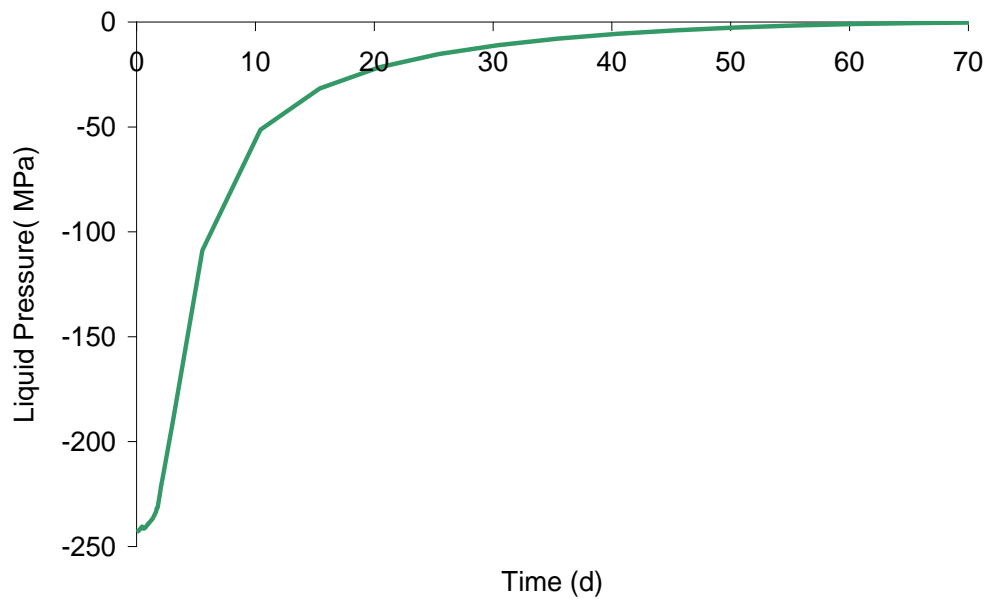


Figure 4-16. Liquid pressure evolution (centre of the sample)

The inflow of water into the sample induces the swelling of the material. Since the infiltration test is performed under confined conditions (constant volume) an increase of the total stresses into the sample is observed. Figure 4-18 shows the evolution with time of the calculated and measured stresses into three representative points (at the top, base and at the center of the sample). The modeling results are in the range of the measurements.

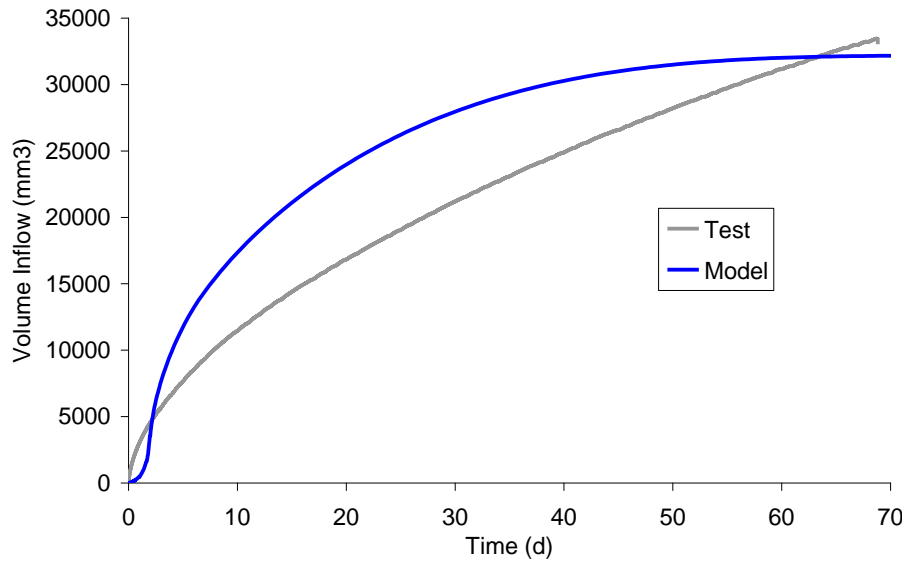


Figure 4-17. Comparison of volume inflow

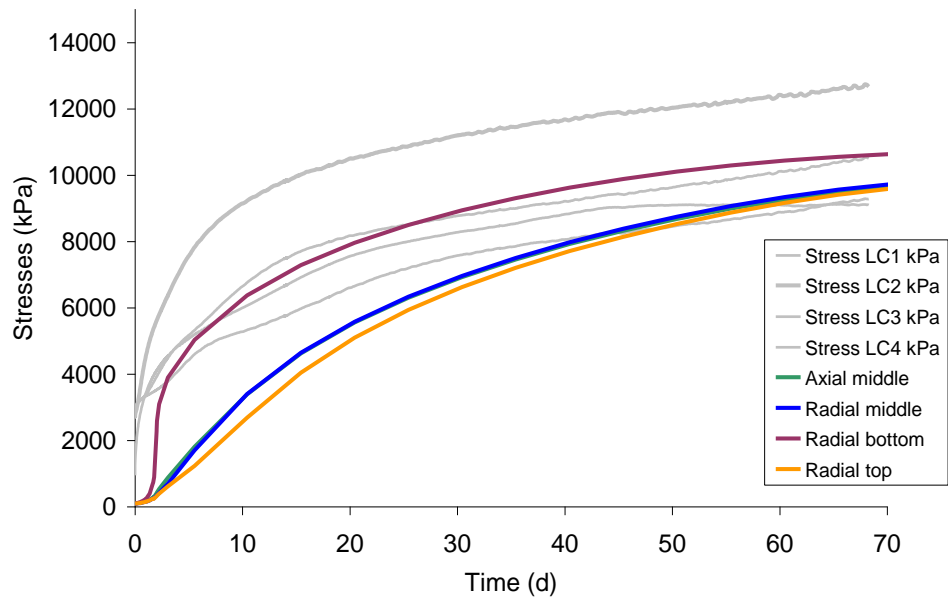


Figure 4-18. Comparison of stresses

Figure 4-19 shows the evolution of the porosity at two selected points. At the bottom of the sample the inflow of water causes the wetted layers to swell. As a result, porosity increases at the layers near to the hydration surface. Simultaneously, since the test is performed under constant volume conditions, compressed upper layers inducing a decrease of porosity at this related zone as it is depicted in Figure 4-19.

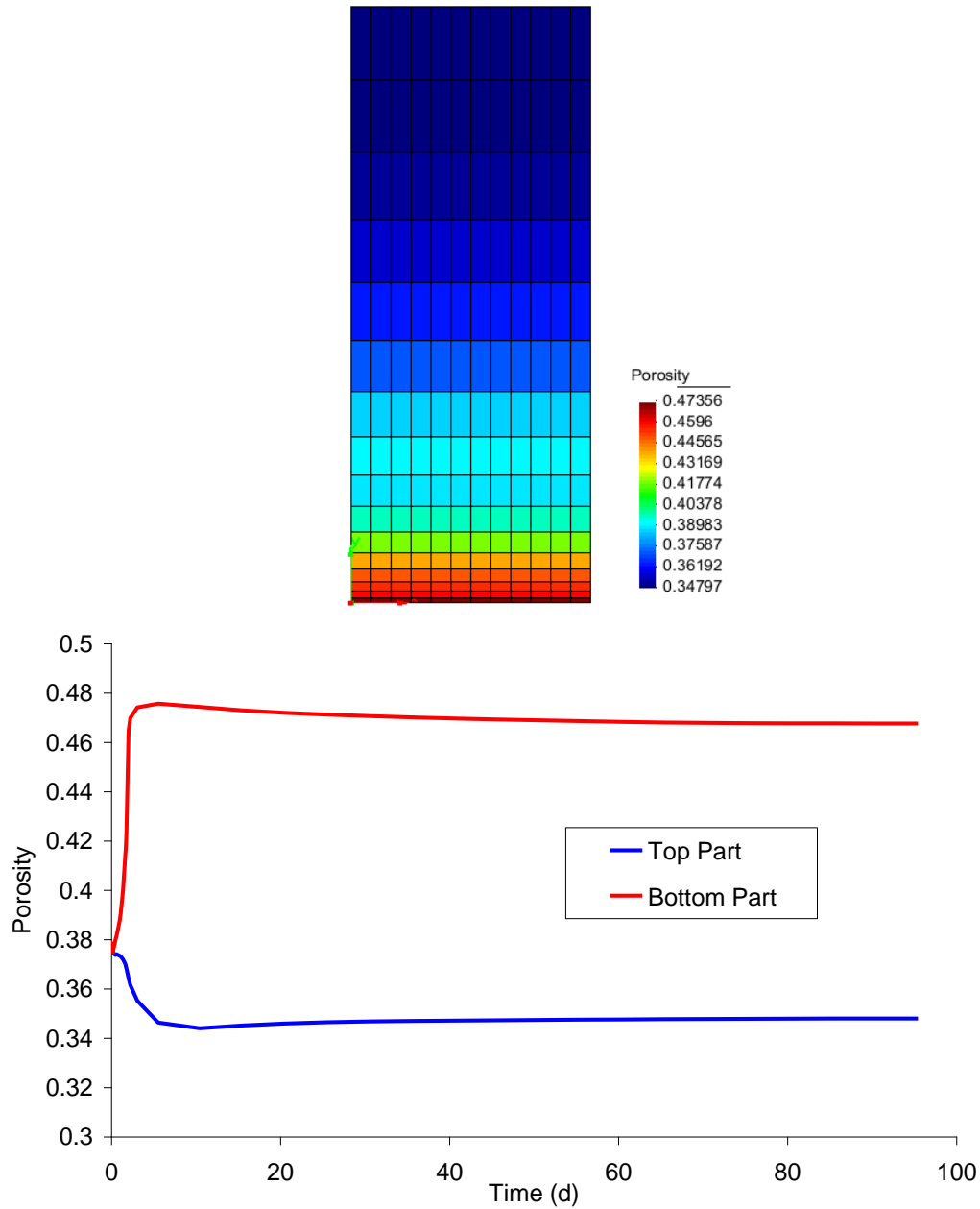


Figure 4-19. Porosity evolution at different points of the sample

The porosity profiles obtained after 0.1, 1, 10, and 100 days are displayed in Figure 4-20. The maximum porosity is obtained near the hydration surface. The maximum peak is followed by a continuous and pronounced decrease of the porosity when progressing in the depth of the sample (upper layers). Permeability k has been considered as a function of porosity. Profiles of intrinsic permeability after 0.1, 1, 10, and 100 days are presented in Figure 4-21. The plots show that permeability increases and reaches a maximum near to the hydration surface. After 100 days, porosity increases and reaches

a maximum value of 0.48 at the bottom layers and decreases to a value of 0.34 at the upper layers (Figure 4-20). For the same period, the permeability varies between $5 \times 10^{-21} \text{ m}^2$ and $\sim 1 \times 10^{-21} \text{ m}^2$ when progressing deeper in the sample (Figure 4-21).

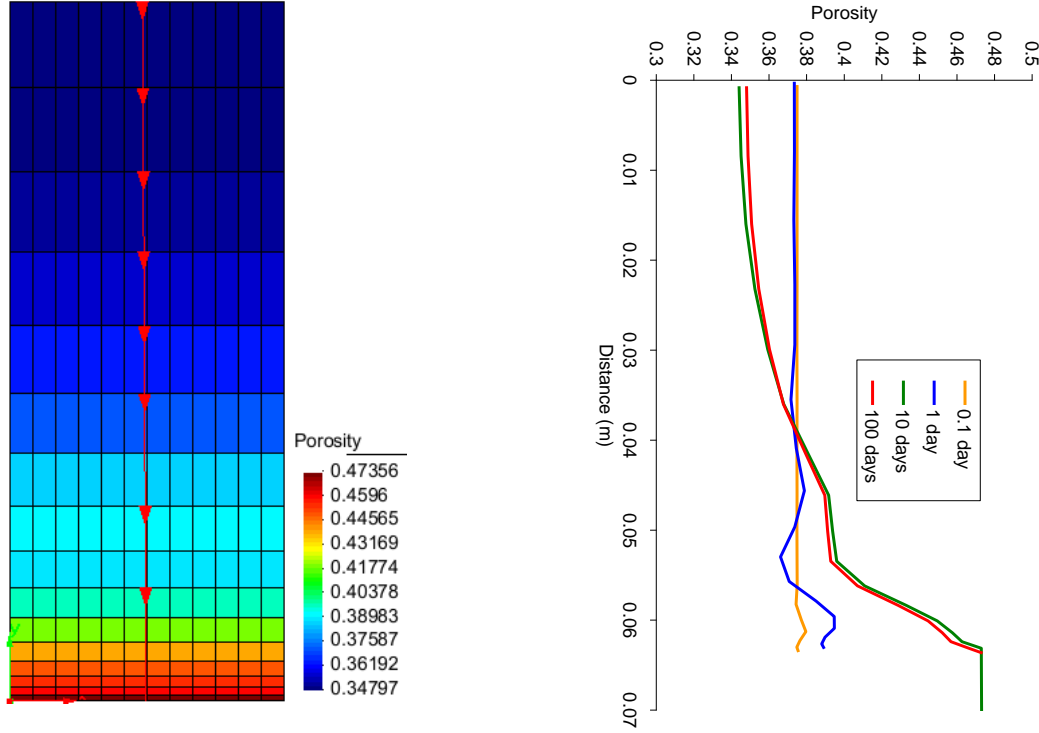


Figure 4-20. Profiles of porosity

As for all unsaturated materials, hydraulic conductivity is also strongly dependent on the degree of saturation. The relative permeability of the liquid phase (k_{rl}) is given by

$$k_{rl} = A S_e^\lambda; \quad S_e = \frac{S_l - S_{rl}}{S_{ls} - S_{lr}} \quad (1)$$

Where A is a constant, degree and λ is power S_e is the effective degree of saturation. Profiles of relative permeability at several times are shown in Figure 4-22. Initially water is driven into the sample to dissipate the gradient of suction existing between the sample and the external reservoir. As a consequence the degree of saturation of the hydrated layers starts increasing. At early times, a small increase of k_r takes place at the outer most layers. As the hydration progresses in the front, degree of saturation increases and results in an increase of k_r .

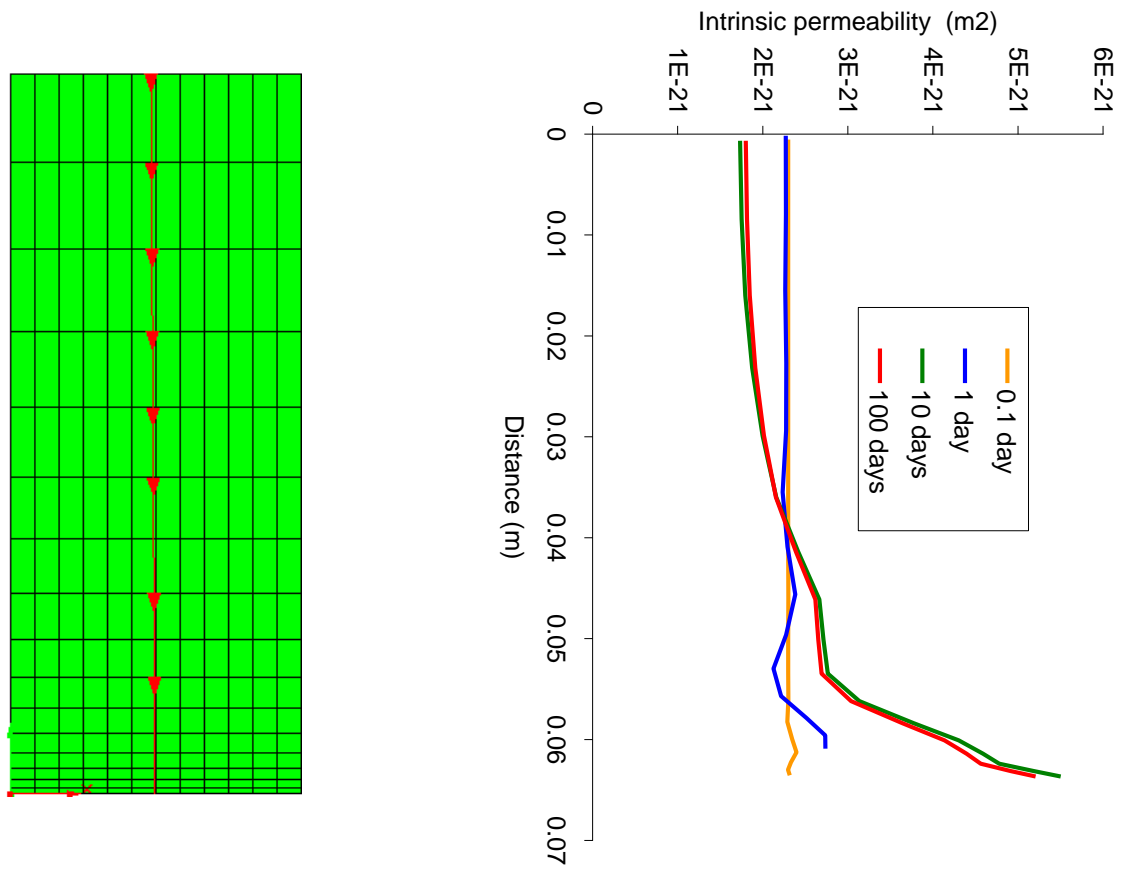


Figure 4-21. Profiles of intrinsic permeability

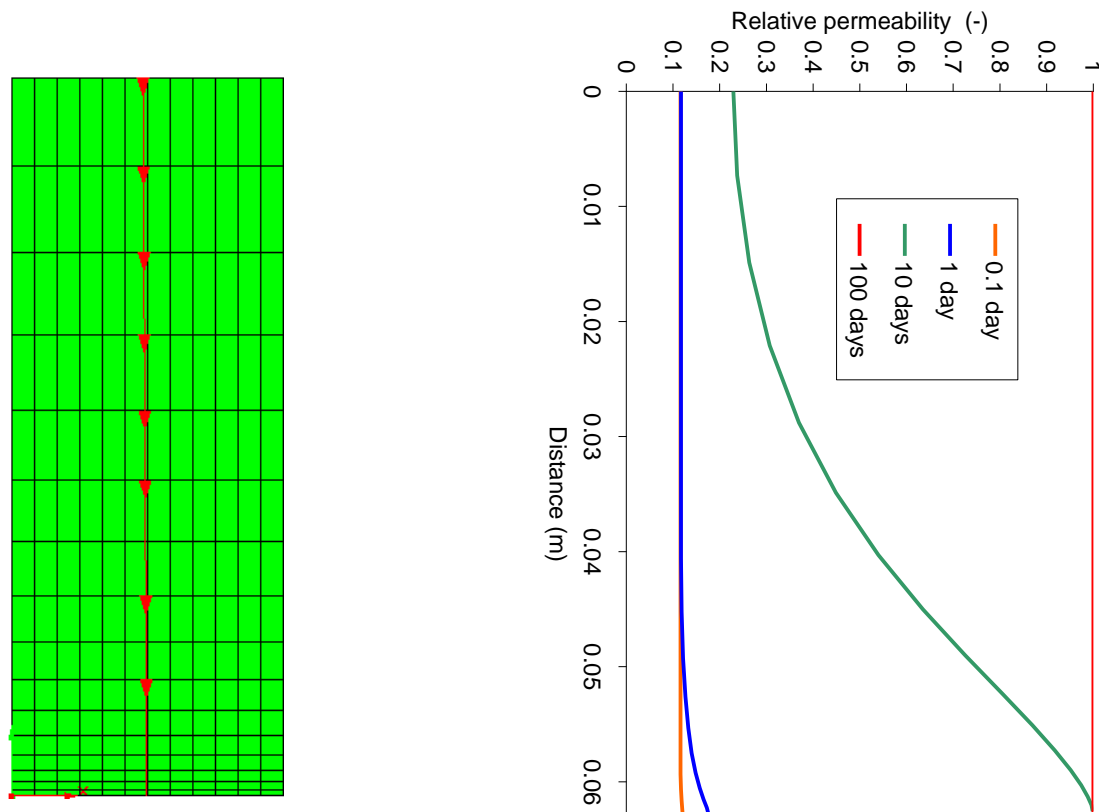


Figure 4-22. Profiles of relative permeability

Figure 4-23 shows some variables of the simulation at the end of the test period. As it is shown, mean effective stress reaches to 10 MPa, at the moment the sample is fully saturated. Radial and axial stresses reach 10 MPa as well, so the stress state is nearly isotropic. Overall it can be said that the entrance of water provokes an increase of the porosity and a decrease of the dry density in the sections closer to the hydration surface due to the swelling of the clay. In contrast, at sections far from the hydration point are compressed.

It is clear that modeling tasks for infiltration test are achieved by using the calibrated BBM parameters. The obtained results from the model have a strong analogy with the test results.

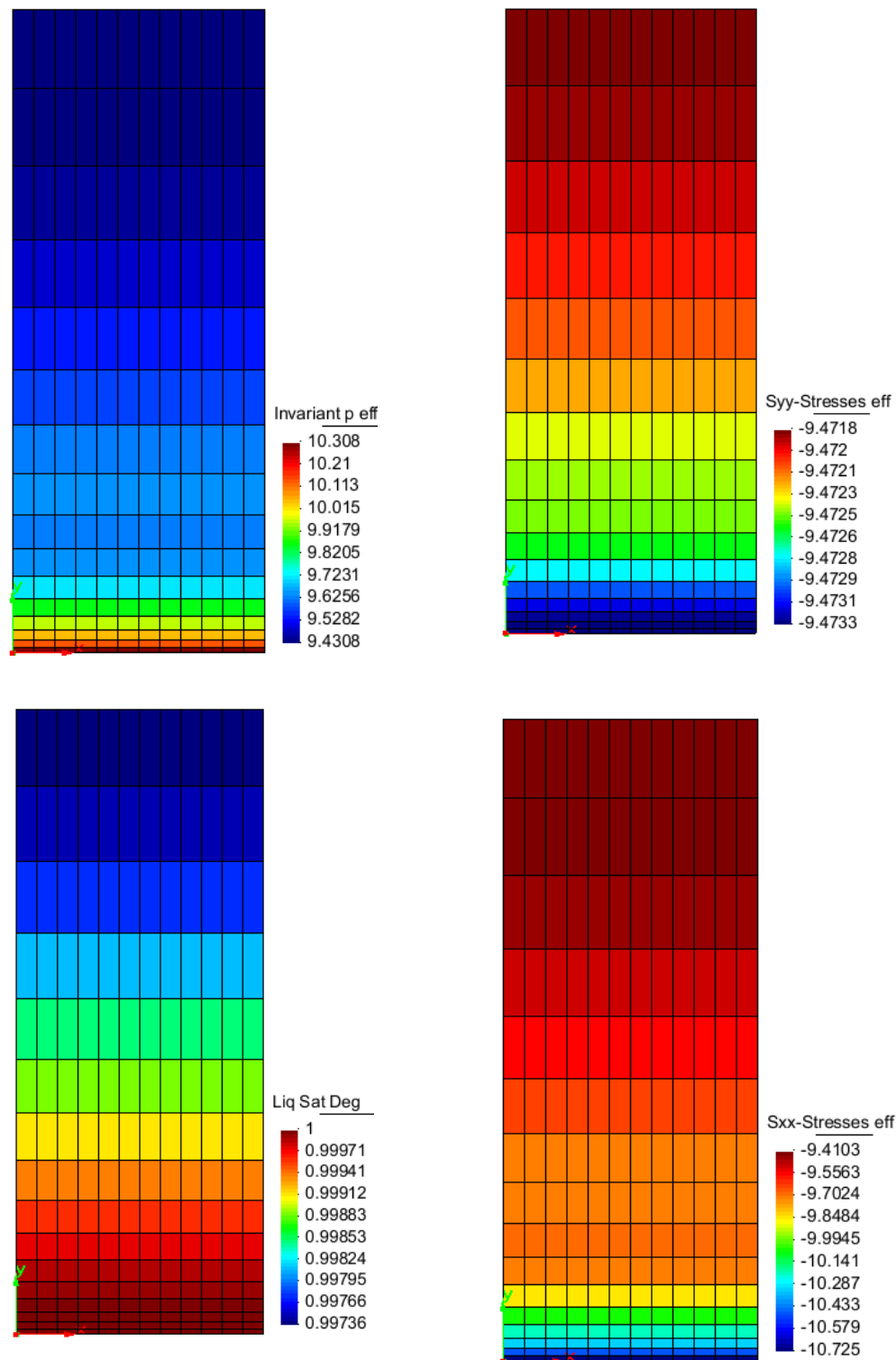


Figure 4-23. Generated stresses (MPa) and degree of saturation at the end of the test .

4.4. Concluding Remarks For Modelling Of Laboratory Test

In this chapter of the thesis experimental and numerical results on the hydro-mechanical behaviour of MX80 bentonite have been presented. Three oedometer tests and an infiltration test have been done by B+Tech. These tests have been modelled using the finite element code Code_Bright. The Barcelona Basic Model (BBM) has been used to model the mechanical constitutive behaviour of the material. The parameters have been calibrated according to 100212c_oedometer test data. The same parameters were used for the simulation of 101222a_oedometer test and of the infiltration test. Reasonably good estimates of the evolution of the deformation for the two oedometer tests have been obtained as well as of the evolution of stresses in the infiltration test (constant volume). Table 4-6 summarizes the parameters of the BBM model for MX80 bentonite. The table compares the calibrated parameter and the parameters for MX80 and FEBEX for BBM found in the literature.

Table 4-6. Elastic and elastoplastic parameters of MX80 bentonite calibrated.
Comparison to BBM parameters of FEBEX bentonite

Parameters	Symbols	Units	MX80 (this report)	MX80 (*)	FEBEX (**)
Poisson's ratio	ν (-)	-	0.35	0.2	0.4
Parameters for elastic compressibility against mean stress change	κ_{i0}	-	0.05	0.06	0.05
	α_i	-	-0.003	-	-0.003
Parameters for elastic volumetric compressibility against suction change	κ_{s0}	-	0.25	0.3	0.25
	α_{sp}	-	-0.145	-	-0.161
	α_{ss}		0	-	0
	p_{ref}	MPa	0.01	0.01	0.01
Elasto-plastic volumetric compressibility	$\lambda(0)$	-	0.15	0.15	0.9
Parameters to define LC yield curve	r	MPa ⁻¹	0.8	0.925	0.75
	β		0.02	0.05	0.03
Reference stress	p^c	MPa	0.01	0.2	0.5
Slope of critical state	M	-	1.07	1	1
Parameter for the plastic potential	α	-	0.53	1	0.53
Initial pre-consolidation stress for saturated conditions	po^*	MPa	12	3	12
Initial void ratio	e_0	-	0.6	0.579	0.63

These parameters will be used to perform thermo-hydro-mechanical modeling of the in situ repository disposal site.

(*) MX80 “Mechanical modelling of MX80 – Quick tools for BBM parameter analysis”
O. Kristenson, M. Akesson. Clay Technology.

(**) FEBEX “2010 Code_Bright Course Tutorial_VII_THM_Mockup_test

5. THM ANALYSIS FOR DEPOSITION HOLE

This chapter concerns preliminary analyses of coupled Thermo-Hydro-Mechanical (THM) processes in the POSIVA ONKALO Project. The Code_Bright finite-element software program is used in performing the modelling calculations. The objective was to study a number of fundamental design parameters.

The time required for the buffer to reach full saturation, the maximum temperature reached in canisters, deformations in the buffer-backfill interface and the stress-deformation balance in interaction between buffer and backfill are the critical design criteria.

A fundamental issue was determining corresponding thermal boundary conditions for the modelling task. The main reason for this is that the boundaries cannot be extended to a distance that the thermal problem would require. As discussed in Chapter III Thermal Analysis, the temperature on the boundaries considered in this study depends on the initial canister power, the fuel power decay characteristic and rock thermal properties.

With regard to the hydraulic analyses, the time required to achieve full saturation is sensitive to vapour diffusion and heat transport, intrinsic permeability and initial suction. A sensitivity study is undertaken to determine the reliability of the Reference case and how it corresponds to actual conditions.

Modelling of the buffer-backfill interface is an essential element in tunnel backfill design. The aim of the calculations is to reveal deformations at this interface whose behaviour is important in connection with swelling of the buffer.

The modelling was carried out under axisymmetric conditions, with the Barcelona Basic Model (BBM) being used to model performance of the bentonite buffer and backfill soil materials. Annex I contains a description of the formulae used in CODE_BRIGHT.

5.1. Introduction

Planning and investigating of the Olkiluoto site for use as a repository for spent fuel elements from Finnish nuclear power stations is currently in progress. The repository consists of a series of tunnels and deposition holes located deep in the bedrock. The canisters containing spent fuel will be surrounded by bentonite buffer rings. The modelling geometry and mesh are shown in Figure 5-2.

MX80 bentonite will be used as the buffer material providing a protective and isolating barrier between the canisters and the surrounding host rock. Specific properties of this buffer material include low permeability to minimise the advective transport of radionuclides, stress-deformation properties that allow for reasonably large rock movements without harmful loads being transferred to the canister, and the capacity to swell in order to fill any gaps that remaining after canister emplacement.

Friedland clay is considered to be one of the candidates best suited for use as backfill material to meet the long-term performance requirements set for backfilling disposal tunnels in the repository. Current plans envisage 60-80% of the total volume of deposition tunnels being backfilled with pre-compacted blocks of Friedland clay and the remaining space being backfilled with bentonite pellets. One of the most important requirements for a deposition tunnel is that the backfill should be so stiff that when it is compressed as the buffer swells, the buffer density should not decrease significantly. Low hydraulic conductivity, high specific surface area and, in some cases, swelling ability are other necessary characteristics of backfill material.

One essential functional requirement for a deposition tunnel is the maximum temperature achieved. Even though the maximum canister temperature permitted during disposal is 100°C, Ikonen (2005) states that the maximum permitted canister temperature should be 90°C to provide an additional safety margin covering uncertainties in thermal conditions, heterogeneities and other unknowns. This subject is discussed in Chapter III.

In the initial conditions, the buffer will not be fully saturated because of the manufacturing and transportation processes. Estimation of the time required for hydration is therefore important. In its initial unsaturated condition, the buffer will not transfer heat efficiently and relatively-high canister temperatures will be the result. Saturation of the buffer is an important issue.

Another important concept is the mechanical behaviour of the interaction between buffer and backfill. The stress – deformation balance at this interface is one of the critical design considerations.

Table 5-1. BBM parameters used for the buffer and backfill

Parameters	Symbols	Units	Buffer (MX80)	Backfill (*)
Poisson's ratio	ν (-)	-	0.35	0.35
Parameters for elastic compressibility against mean stress change	κ_{i0}	-	0.05	0.05
	α_i	-	-0.003	-0.003
Parameters for elastic volumetric compressibility against suction change	κ_{s0}	-	0.25	0.025
	α_{sp}	-	-0.145	-0.145
	α_{ss}		0	0
	p_{ref}	MPa	0.01	0.01
Elasto-plastic volumetric compressibility	$\lambda(0)$	-	0.15	0.3
Parameters to define LC yield curve	r	MPa ⁻¹	0.8	0.8
	β		0.02	0.02
Reference stress	p^c	MPa	0.01	0.01
Slope of critical state	M	-	1.07	1.07
Parameter for the plastic potential	α	-	0.53	0.53
Initial pre-consolidation stress for saturated conditions	po^*	MPa	12	0.5
Initial void ratio	e_0	-	0.6	0.6

The BBM parameters used for the buffer and backfill are shown in Table 5-1. These parameters have been obtained from simulated laboratory tests. The calibration process and a comparison of model predictions against the experimental results can be found in Chapter IV. These parameters were calibrated by modelling the oedometer and infiltration tests carried out by POSIVA.

There are differences between the buffer and backfill material properties in the BBM material model. Firstly, the elasto-plastic volumetric compressibility $\lambda(0)$ which is obtained in the oedometer test on Friedland clay carried out by SKB has a value of 0.3. Another parameter that is different is the initial pre-consolidation stress for saturated conditions which is set to 0.5 MPa for the reference case. A comparative study has been performed where the backfill pre-consolidation stress has a value of 2 MPa. Finally, the swelling potential has been reduced by a factor of 10. Figure 5-1 shows predicted main processes at the canister scale during the early post-closure period (unsaturated conditions).

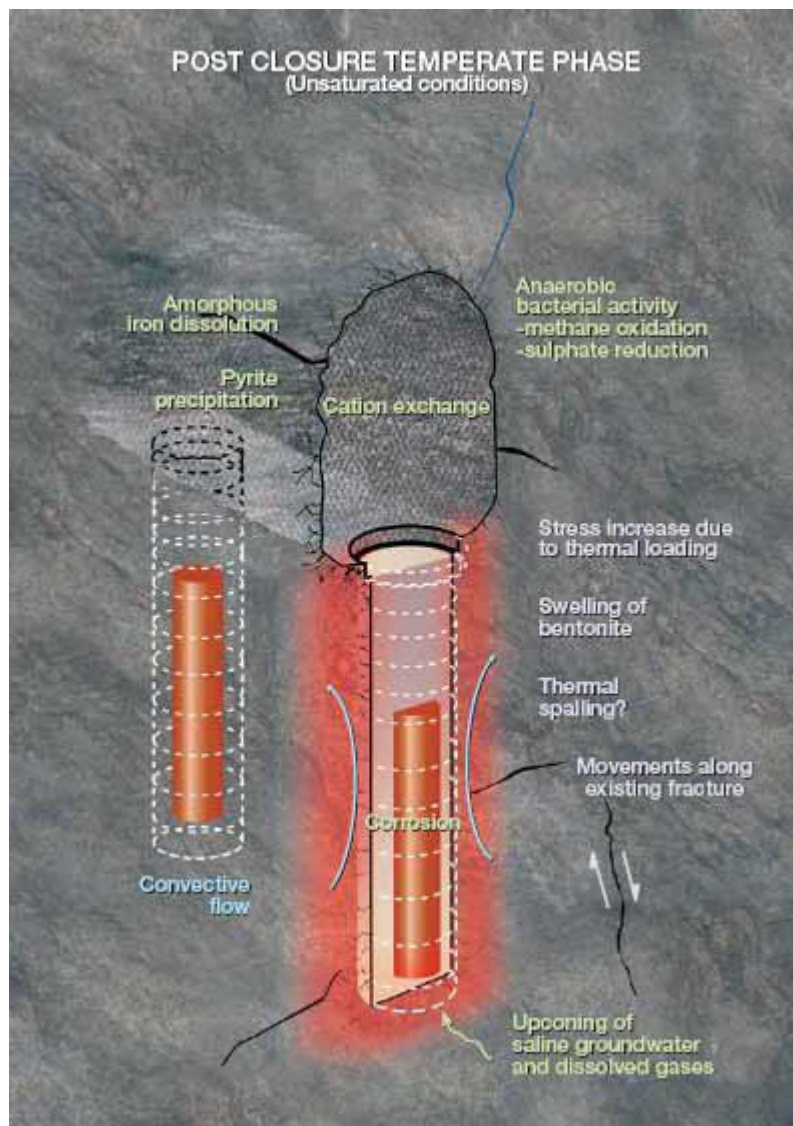


Figure 5.1 Main processes in the canister near field after closure of the repository unsaturated conditions.

These are the main conditions expected and possible variations during this period. It has been anticipated complex couplings among the thermo-hydro-mechanical and chemical processes occurring after the repository is closed. However, chemical process is not included in this thesis.

It is expected that the rock temperature will gradually increase and reach its maximum value within the first hundred years after closure. Rock movements along existing fractures continue as the rock adapts to the thermal load from the canister and to the swelling pressure from the backfilling and the buffer.

The mechanical load to the canister increases since groundwater pressure reaches its equilibrium pressure (4-5 MPa) at the same time the buffer begins to swell. Uneven buffer swelling during the unsaturated period might cause additional mechanical loads to the canister so deformation of the copper shell.

Canister corrosion continues during the early post-closure period via general corrosion as long as oxygen is present. Corrosion rates slow down when oxygen is consumed and the environment becomes reducing. “Even during the one million year overall assessment period, expected corrosion of the canister for an assumed temperate climate would cause corrosion depths of the order of a few millimetres (SKB 2006a).”

However, canister corrosion is not a subject of this thesis.

After a certain period of time the system evolves to a quasi-steady state in which thermal, hydraulic, mechanical and chemical conditions at the repository depth are subject to much slower changes. The buffer and the backfill are expected to be saturated in this period and so they will be more efficient. In this period, the convective flow caused by thermal gradients will disappear. Swelling pressure of the bentonite and residual stress relaxation might cause changes of the rock stress field in this period.

Table 5-2. Hydraulic and phase properties of materials in the buffer, backfill and rock

	Buffer	Backfill	Rock
Solid phase density γ_s (kg/m ³)	2779	2781	2749
Intrinsic permeability k (m ²)	5.59e-21	1.0e-18	1.0e-17
Initial porosity ϕ (-)	0.37	0.368	0.02
Initial suction(MPa)	-41	-40.2	-

Rock was modelled as a linear elastic material with a Young's Modulus, E , of 6300 MPa and a Poisson's ratio, ν , of 0.25. Thermal parameters for these three materials are given in Chapter III.

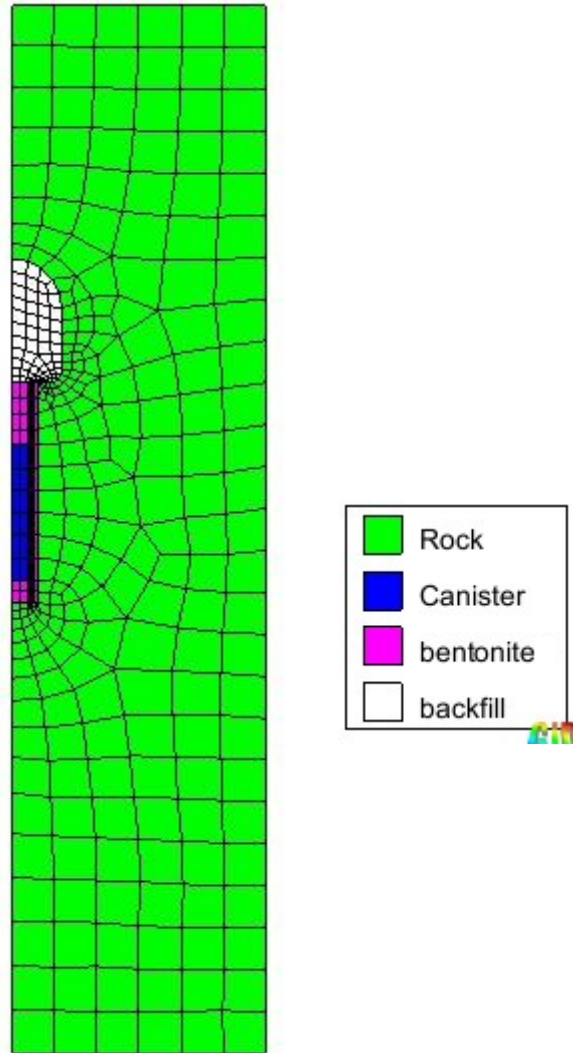


Figure 5-2. The axisymmetric domain, mesh and materials under consideration

In the models presented in this study, four materials are used in the deep geological disposal of high-level nuclear waste in a final repository. Figure 5-2 shows these four materials. In the geometry shown in Figure 5-2, the buffer is considered to be a homogenous material and neither the gap between canister and the buffer nor the gap between the buffer and rock are taken into account. The stages of the excavation process have been shown in the Figure 5-3.

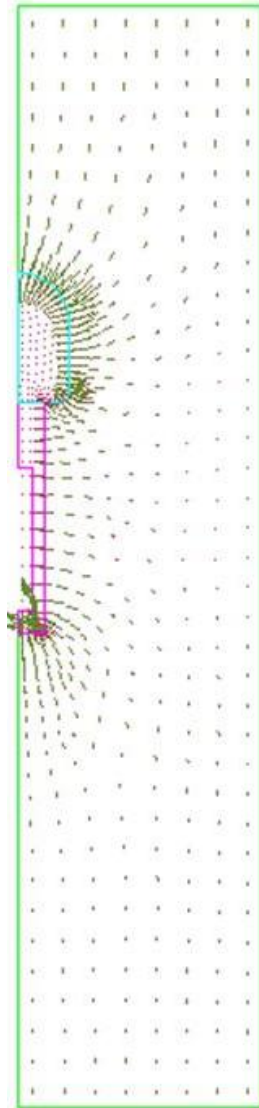


Figure 5-3. Excavation process

The rock in contact with the buffer and backfill is considered to be at atmospheric pressure and saturated before the buffer and backfill materials are placed. The atmospheric pressure condition for the excavation wall is removed as the different materials (buffer, canister and then backfill) are installed.

5.2. Base case THM analyses

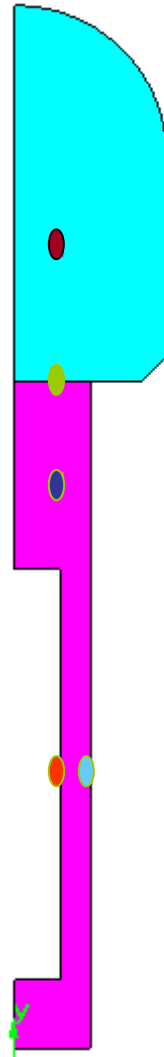







Figure 5-4. Representative points used for materials

	Backfill
	Backfill-buffer interface
	Buffer
	Canister-buffer interface
	Buffer-rock interface

For plotting purposes in the THM analyses, five representative points are used. Figure 5-4 shows their position. As already indicated, the parameters used in the reference case are given in Table 5-1 and Table 5-2.

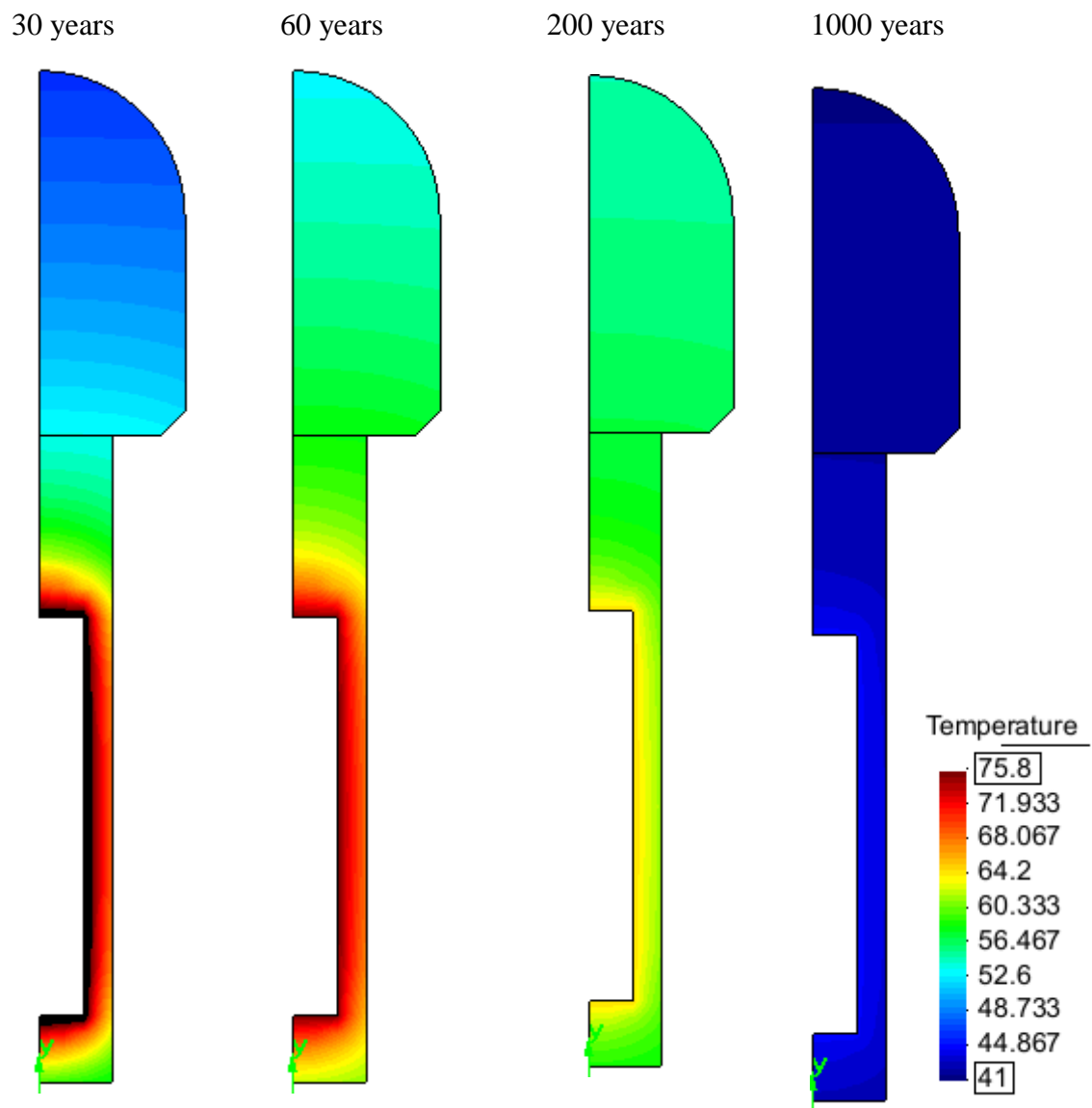


Figure 5-5. Temperature (°C) changes in the buffer and backfill materials

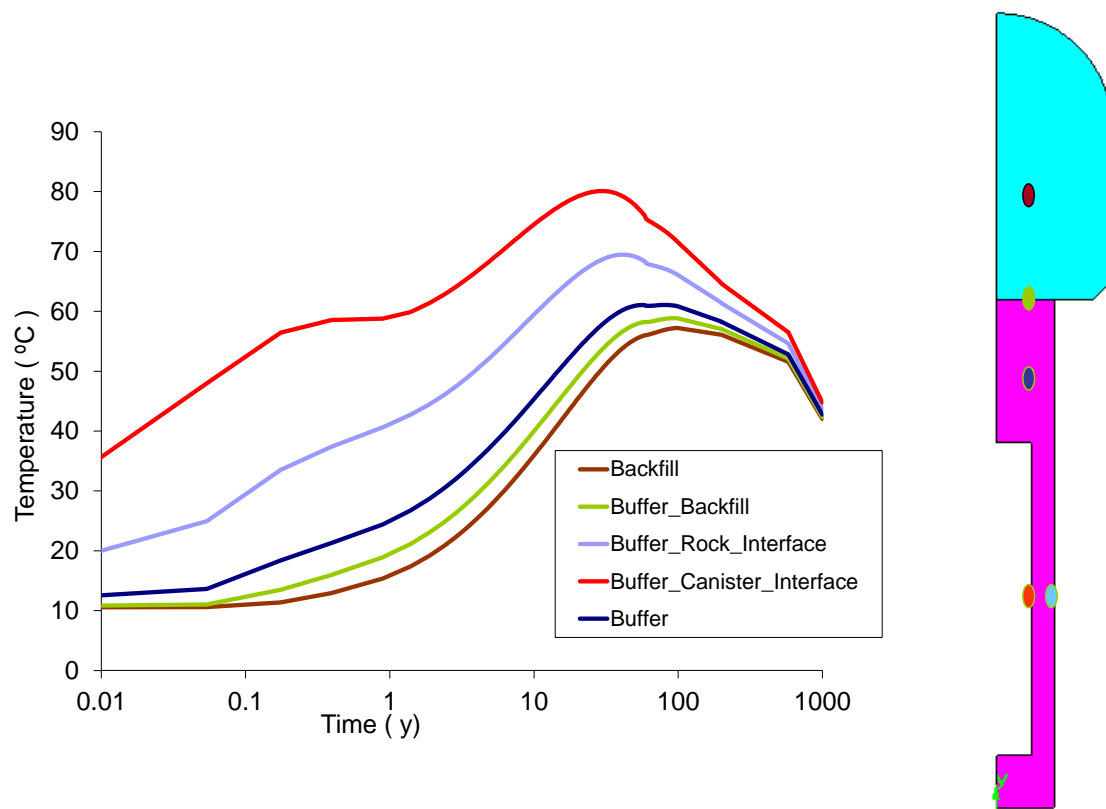


Figure 5-6. Temperature evolution at the five representative points.

In the ONKALO Project, the maximum allowable calculated canister temperature and a fundamental parameter in planning, dimensioning and operating the repository is set as 90°C. While the primary factor influencing this temperature is the canister power at disposal, the distances between adjacent tunnels and to neighbouring canisters also play a vital role. A detailed explanation of the thermal analyses is given in Chapter III .

Figure 5-6 shows that the maximum temperature of 80°C is reached at the buffer-canister interface after 30 years. After 1000 years, the model reaches a stable condition with both materials at the same temperature, approximately 42°C.

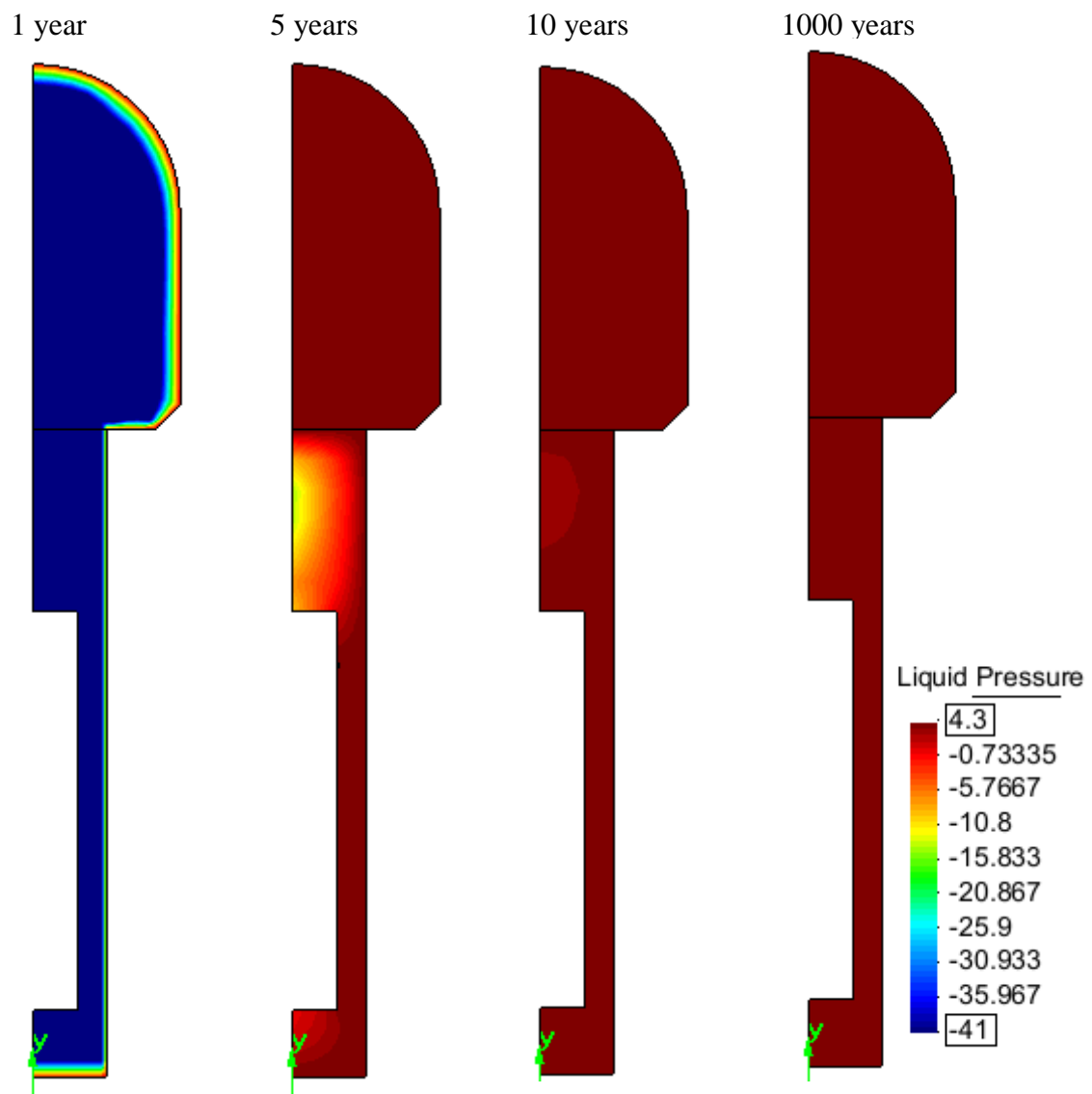


Figure 5-7. Liquid pressure (MPa) changes in the buffer and backfill materials.

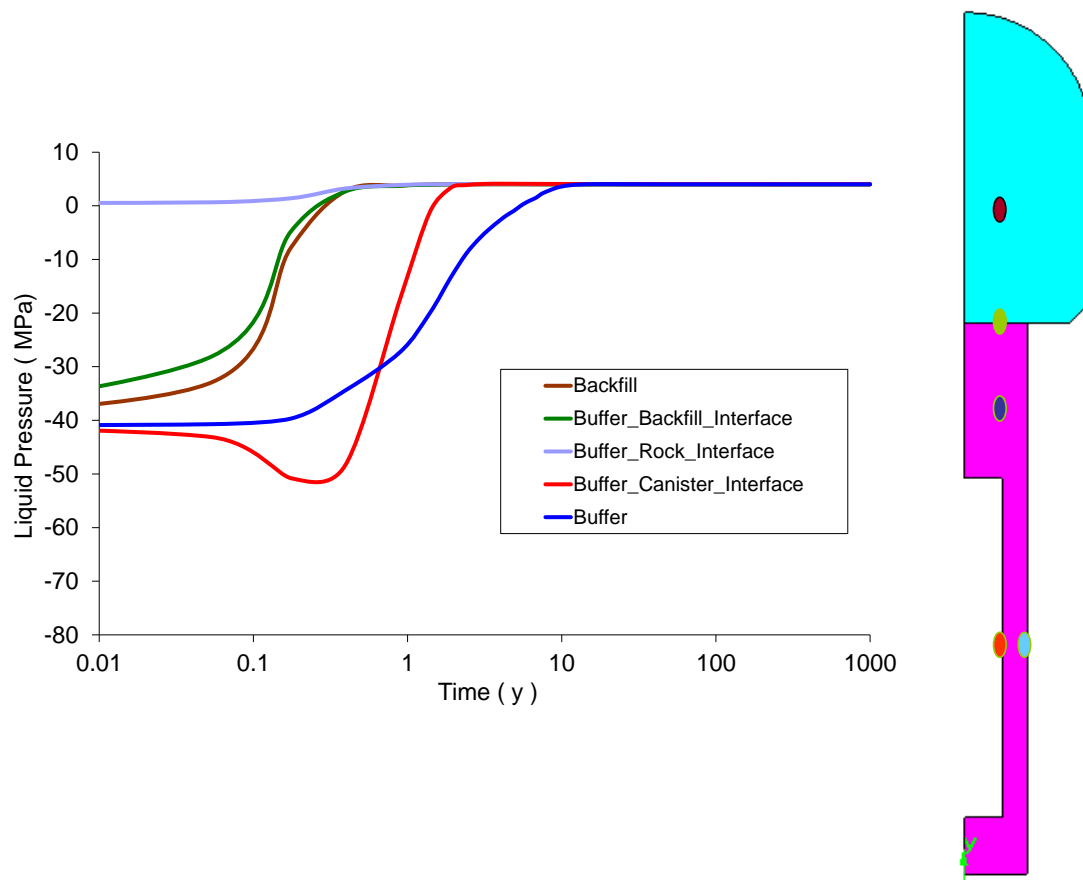


Figure 5-8. Evolution of liquid pressure at the five representative points.

Liquid pressure is affected by heating, with a strong decrease near the canister as water is evaporated. Figure 5-7 indicates that the buffer will be almost fully saturated after 10 years.

The evolution of liquid pressure shown in Figure 5-8 shows drying of the buffer adjacent to the canister as heat is being generated. The representative point closest to the canister has the highest suction. At the buffer-canister interface the liquid pressure drops to -50 MPa after one year and its evolution follows a different trend line. In the backfill, liquid pressure increases with time and reaches a steady-state condition in three years. This suction behaviour has an important influence on the time required for the buffer and backfill to become fully saturated.

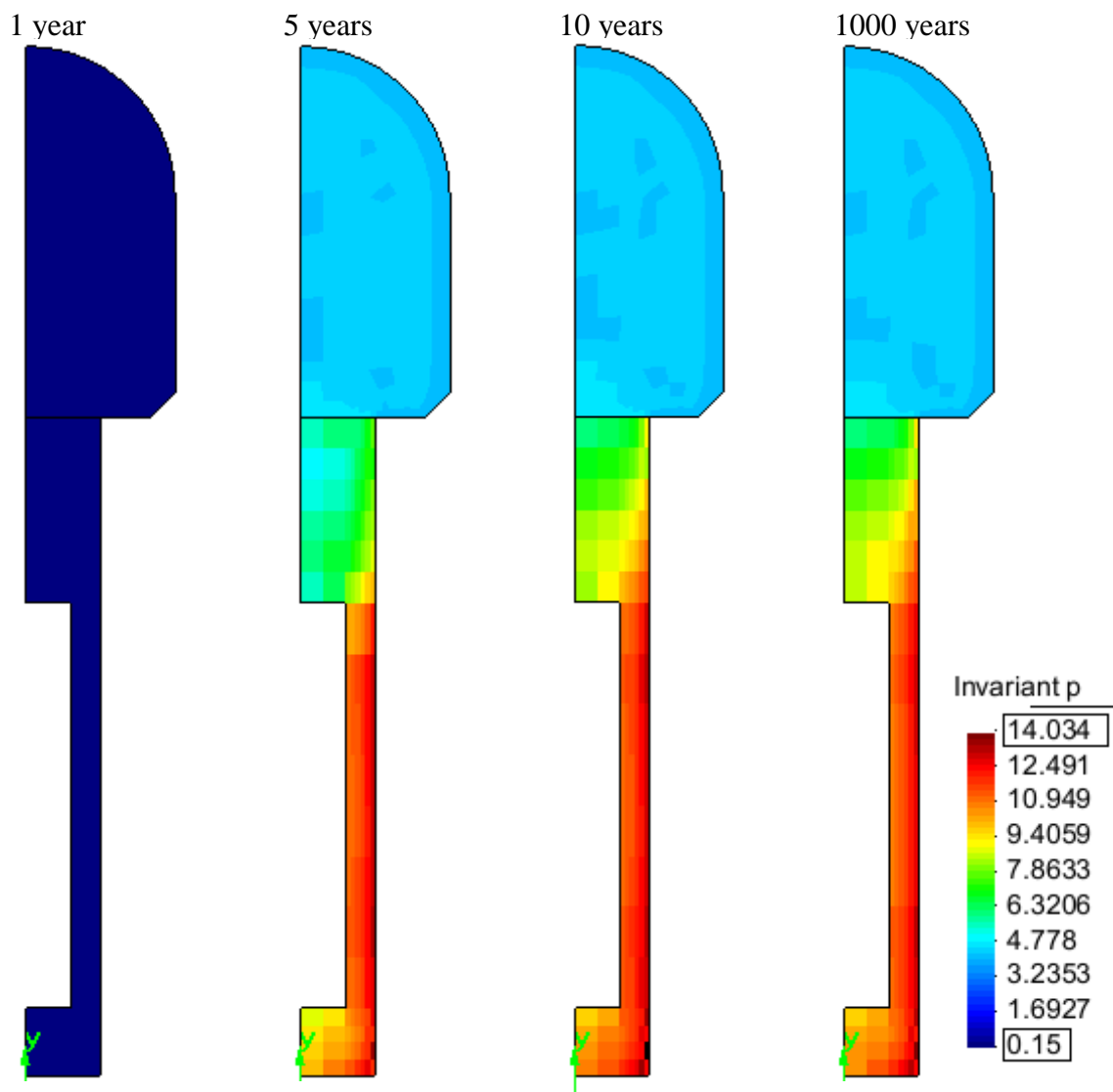


Figure 5-9. Changes in total mean stress (MPa) in the buffer and backfill

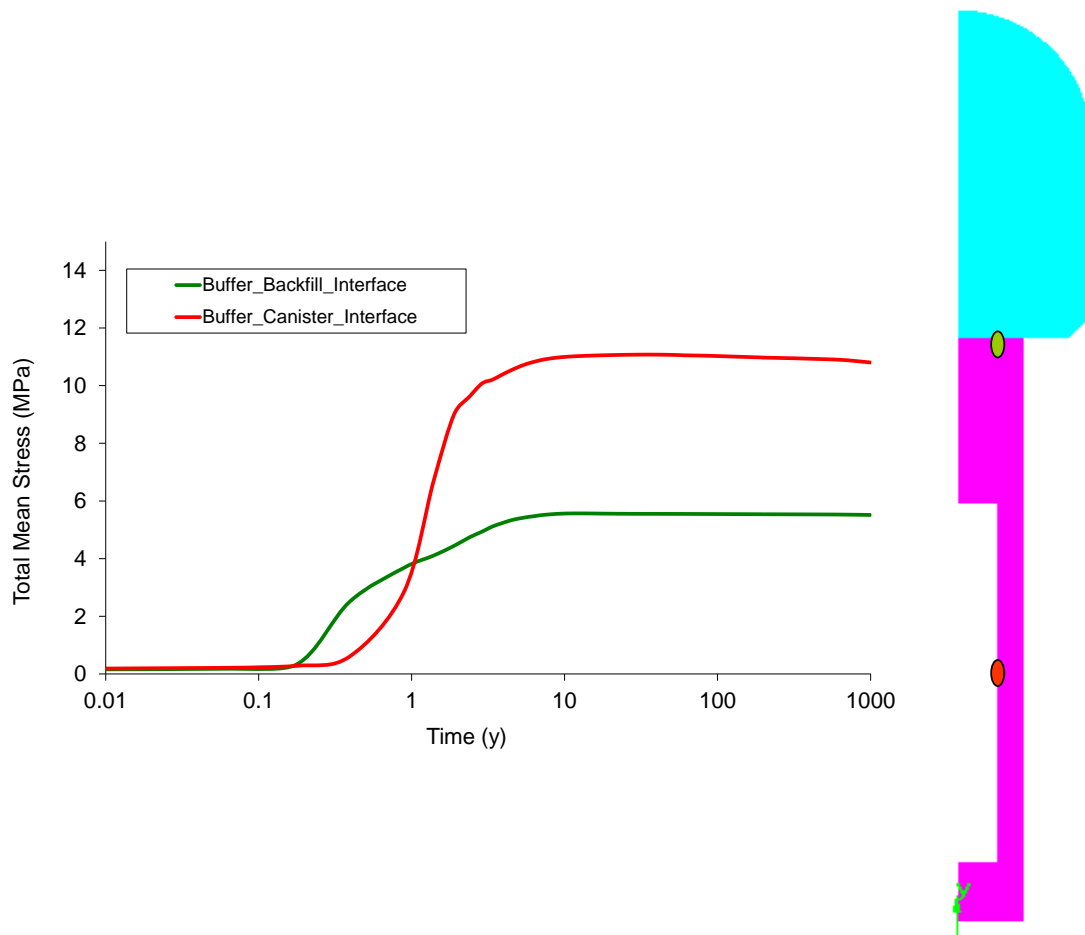


Figure 5-10. Evolution of total mean stress at two representative points

One of the objectives in this study was to identify the dominant forces on the buffer and backfill materials and their values. One of the main design requirements is that the backfill should hold the buffer material in place, preventing a significant loss of density through upwards swelling. As the backfill is compressible and has a lower swelling pressure than the buffer material, some upwards swelling is expected. Stresses generated in the buffer and backfill materials have a role to play in this connection.

Total mean stress increases over time and reaches 10 MPa at the buffer-canister interface. As shown in Figure 5-10, the model calculations indicate that total mean stress becomes stable after a period of time and then remains constant.

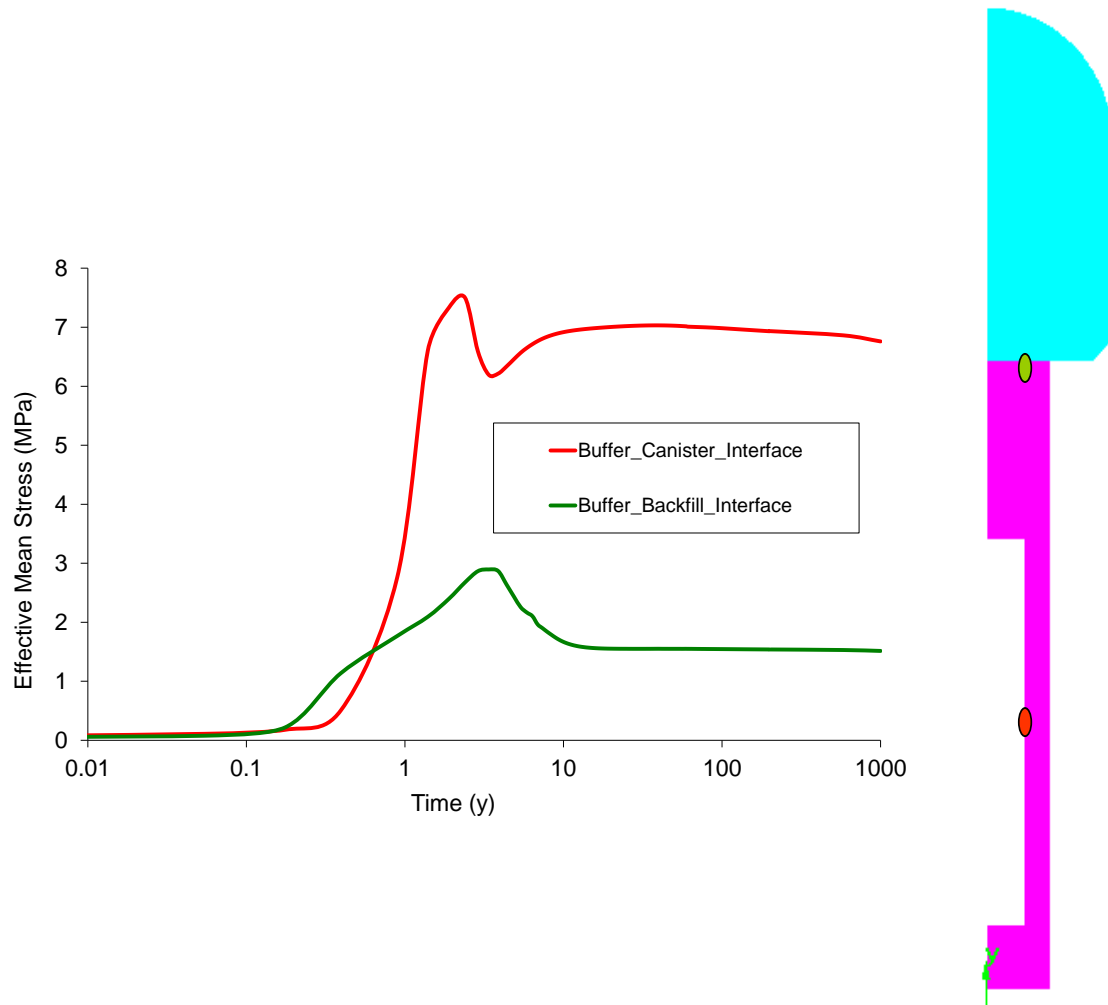


Figure 5-11. Evolution of effective mean stress at two representative points

The buffer load capacity and the rate at which a canister will sink through the buffer material to the base of a deposition hole is a mechanical case that needs to be handled. Resistance to canister sinking is also one of the buffer requirements to be assessed. The time required for full saturation of the buffer material gives an indication of the time when full swelling pressure will occur. Swelling pressure is an important property in this connection and the effective mean stress ratio is therefore a critical modelling parameter.

Effective mean stresses initially increase due to hydration of the swelling materials. At the buffer-canister interface, the effective mean stress reaches 8 MPa and then starts to fall. It becomes constant after a period of time.

As the bentonite in the buffer expands due to hydration, it compresses the backfill in the deposition tunnel. Bentonite swells as a result of absorbing water during the saturation process and this is expected to fill voids in the buffer material. The long-term performance of the buffer will therefore be critically affected by both the amount of swelling and the speed at which it takes place. Swelling of the buffer material is primarily controlled by the hydraulic conductivity of the rock. One of the main reasons for using bentonite as buffer material in a final repository is the material's low hydraulic conductivity.

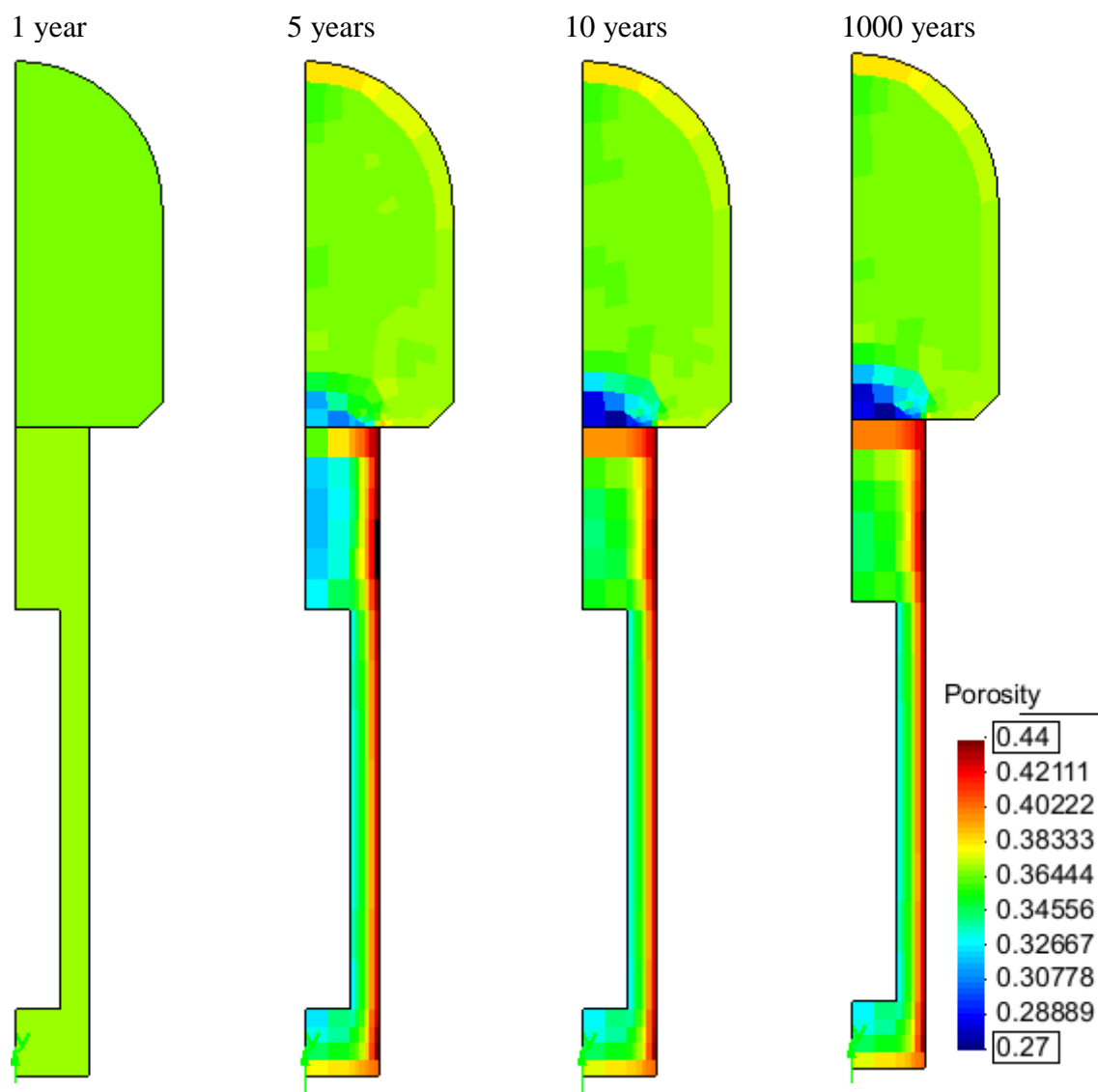


Figure 5-12. Changes in porosity levels in the buffer and backfill materials

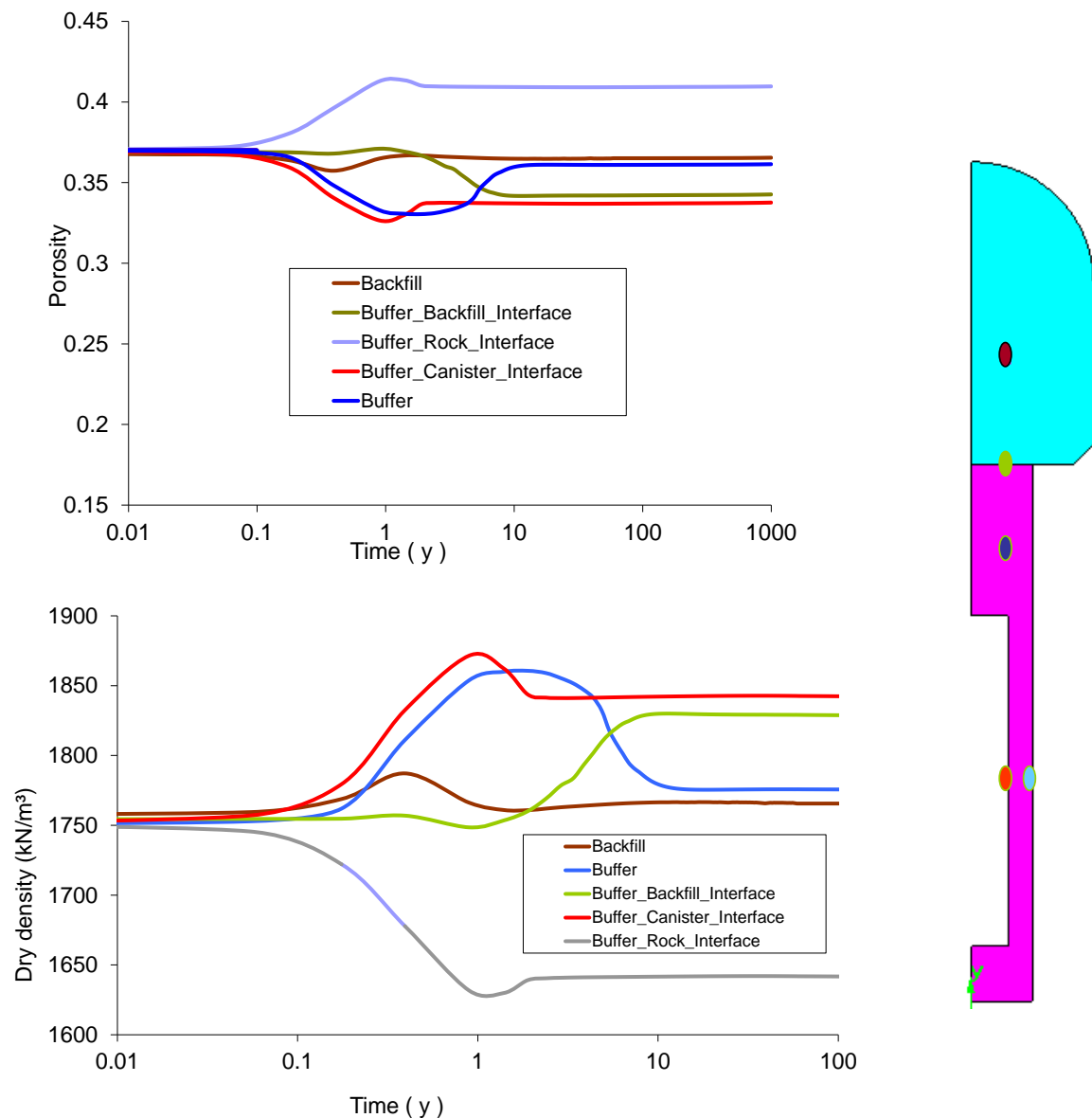


Figure 5-13. Evolution of porosity and dry density at five representative points

When a canister is placed in a deposition, drying will take place in the buffer space as result of heating by the canister. Evaporation of water caused by heat from the canister will induce a reduction in porosity next to the canister. At the rock wall, hydration and a porosity increase will occur. Dry density changes accordingly to porosity changes.

A high buffer density creates a high swelling pressure and makes the bentonite more resistant to deformation. On the other hand, bentonite of lower density could result in canister sinkage. Buffer density is therefore an important design parameter. One of the most important requirements for a deposition tunnel is that the backfill should be stiff enough to prevent a significant decrease in buffer density even when it is compressed by

the swelling of buffer material. Figure 5-13 shows that the modelling results indicate good agreement with this backfill requirement.

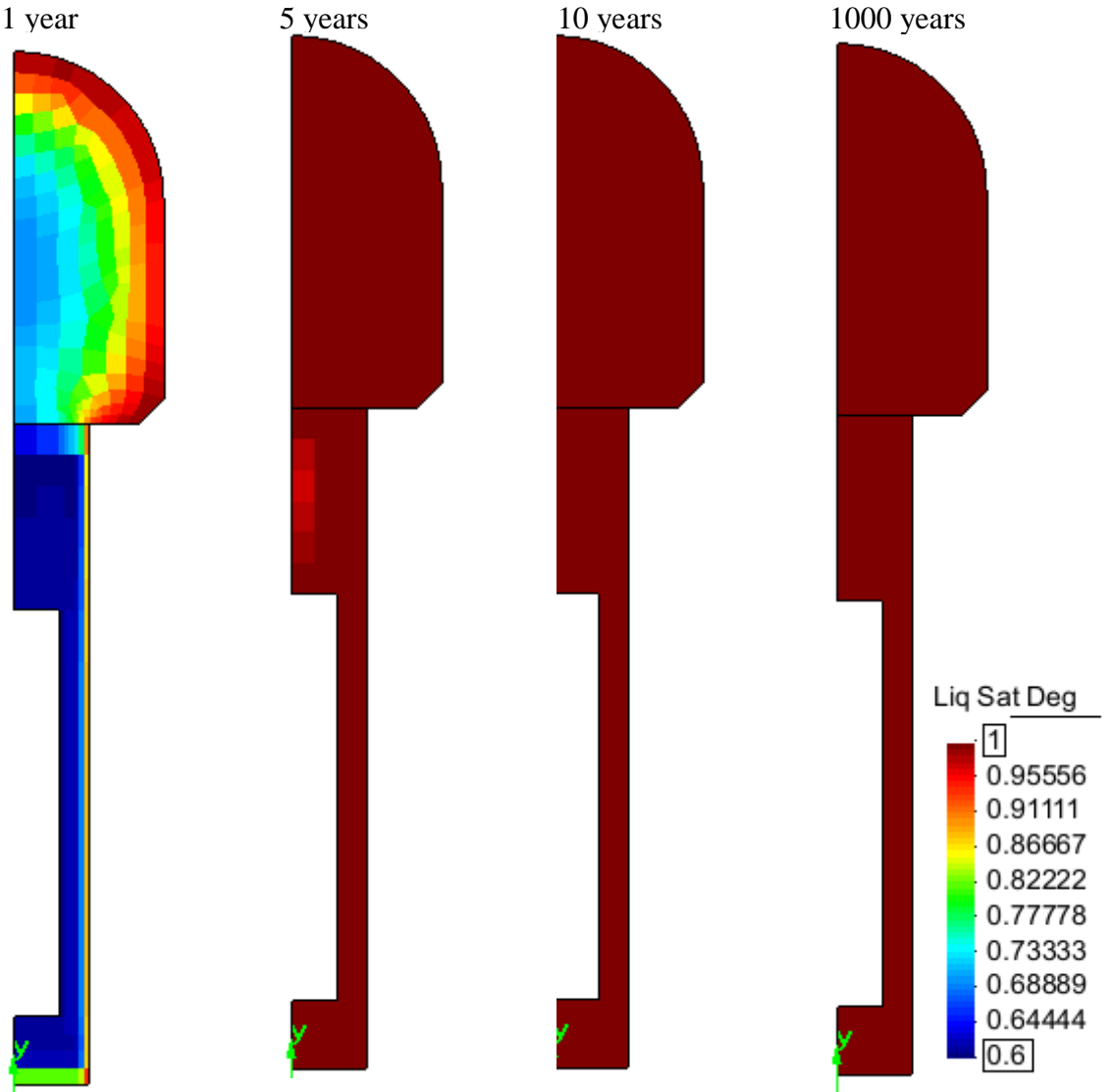


Figure 5-14. Future degree of saturation of buffer and backfill materials.

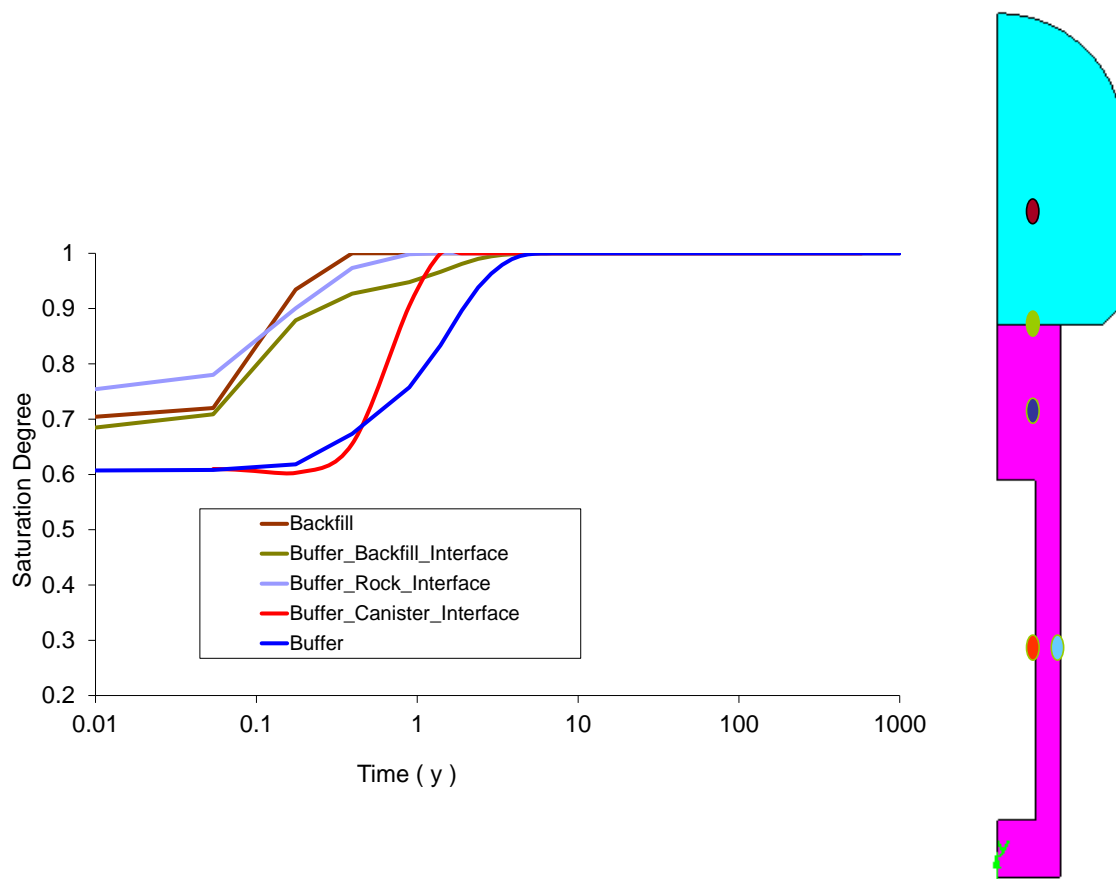


Figure 5-15. Evolution of degree of saturation for the five representative points

Manufacturing and engineering constraints mean that buffer material is placed in the repository in a compacted, unsaturated state. This in turn means that the intrinsic properties of the bentonite will only provide an effective buffer when it has become saturated. The unsaturated period also affects the performance of buffer long after it has become saturated. The time required to achieve full buffer saturation is therefore very important in the modelling process.

Temperature has a significant influence on saturation of the materials in the model. Intrinsic permeability and vapour diffusion rates also play an important role in the time required to achieve full saturation. As the rock permeability is high, saturation of the buffer and backfill will take place in approximately five years.

The buffer space between the rock wall and the canister will be saturated 4-5 years after deposition of the canister. The maximum buffer temperature will be reached after 30

years, long after the buffer is fully saturated. Figure 5-15 shows desaturation of the buffer material close to the canister surface.

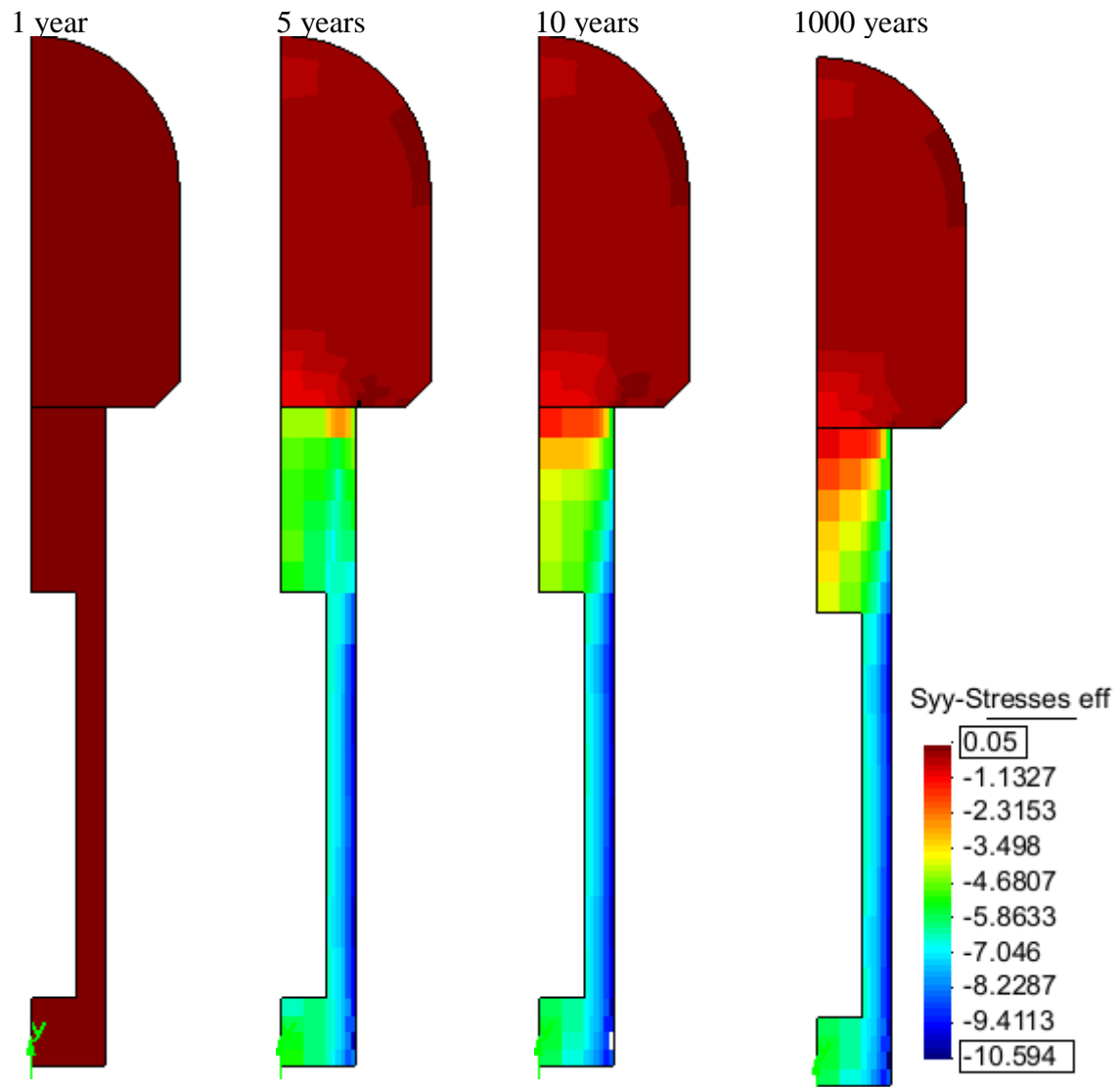


Figure 5-16. Future axial effective stress (MPa) in buffer and backfill materials

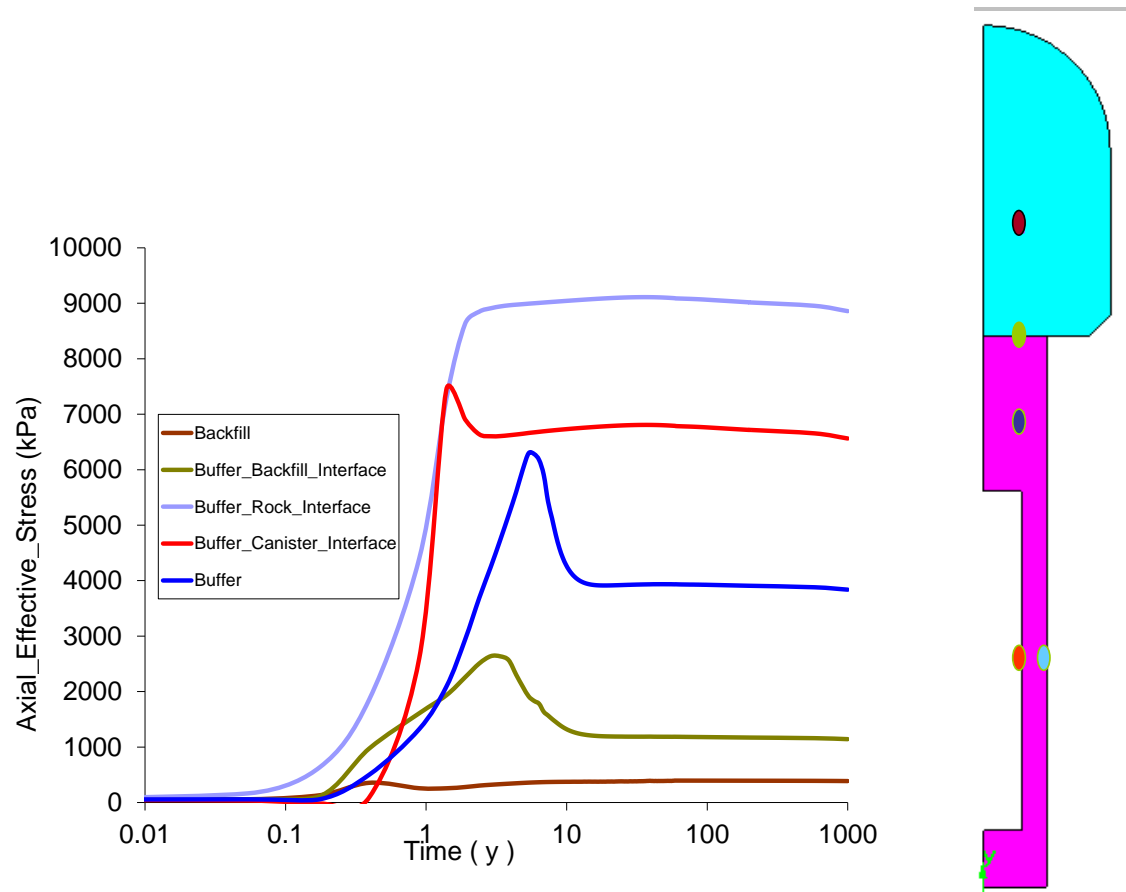


Figure 5-17. Evolution of axial effective stress for five representative points

The stress-deformation balance at the buffer and backfill interface is one of the most important parameters in repository design. A fundamental functional parameter for the deposition tunnel is backfill stiffness. Even though the buffer material swells and compresses the backfill that holds it in place, the density of the buffer must not suffer a significant reduction. The degree of saturation of both the buffer and backfill has a role to play in the balance between stress and displacement at the buffer-backfill interface.

The axial effective stress increases initially as a result of several effects, then falls to a constant level. At the buffer-canister interface it reaches a level of 6 MPa.

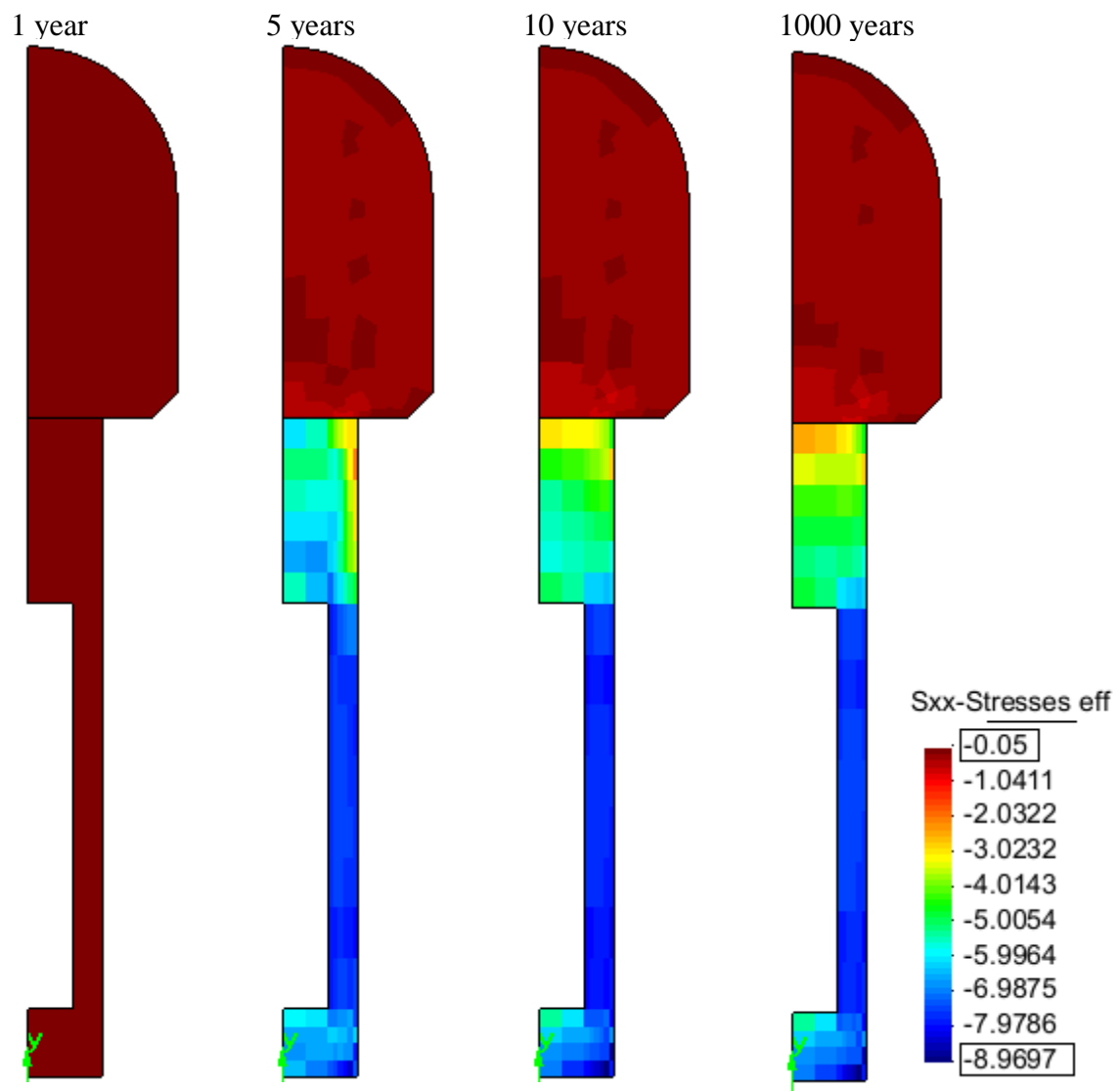


Figure 5-18. Future radial effective stress (MPa) in buffer and backfill materials

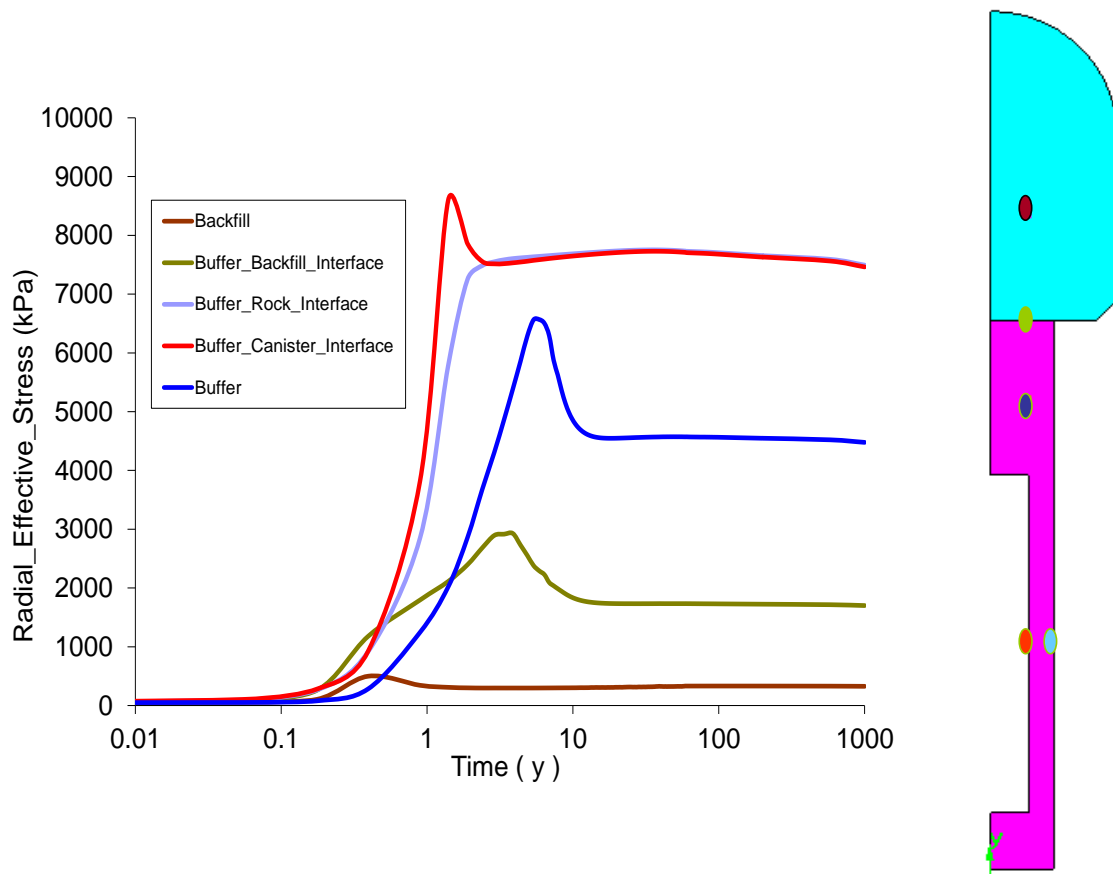


Figure 5-19. Evolution of radial effective stress at the five representative points

One of the objectives of this study was to achieve an understanding of the mechanical response of the bentonite buffer in the repository. Figure 5-19 indicates the radial stress situation at different times in the future.

Radial effective stress develops in a similar manner to axial stress, decreasing after a period of time and becoming stable. The maximum radial stress generated on the buffer is 9 MPa, but this falls somewhat in the longer term and the maximum stable value is of the order of 8 MPa.

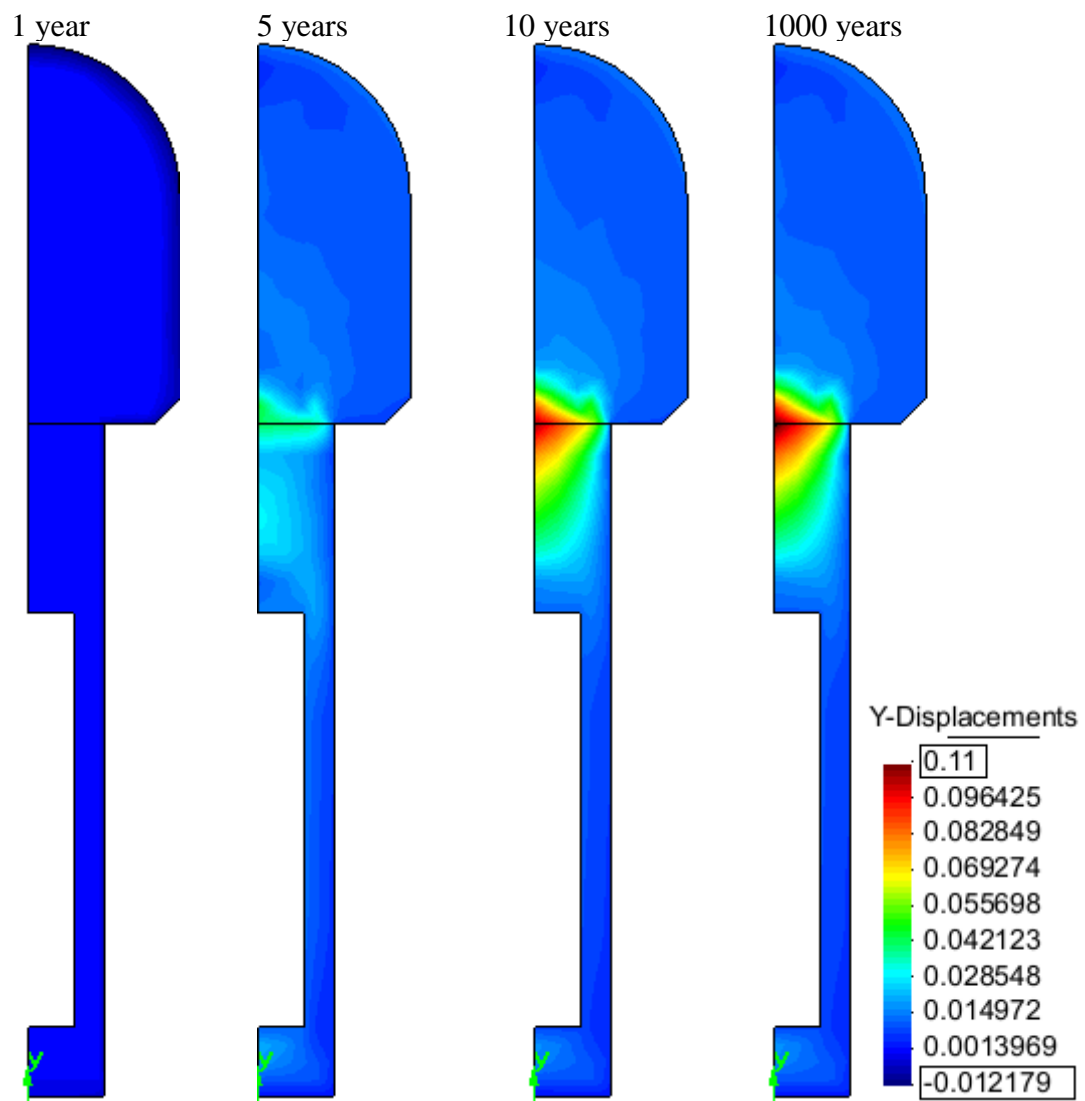


Figure 5-20. Future vertical displacement (m) of buffer and backfill materials

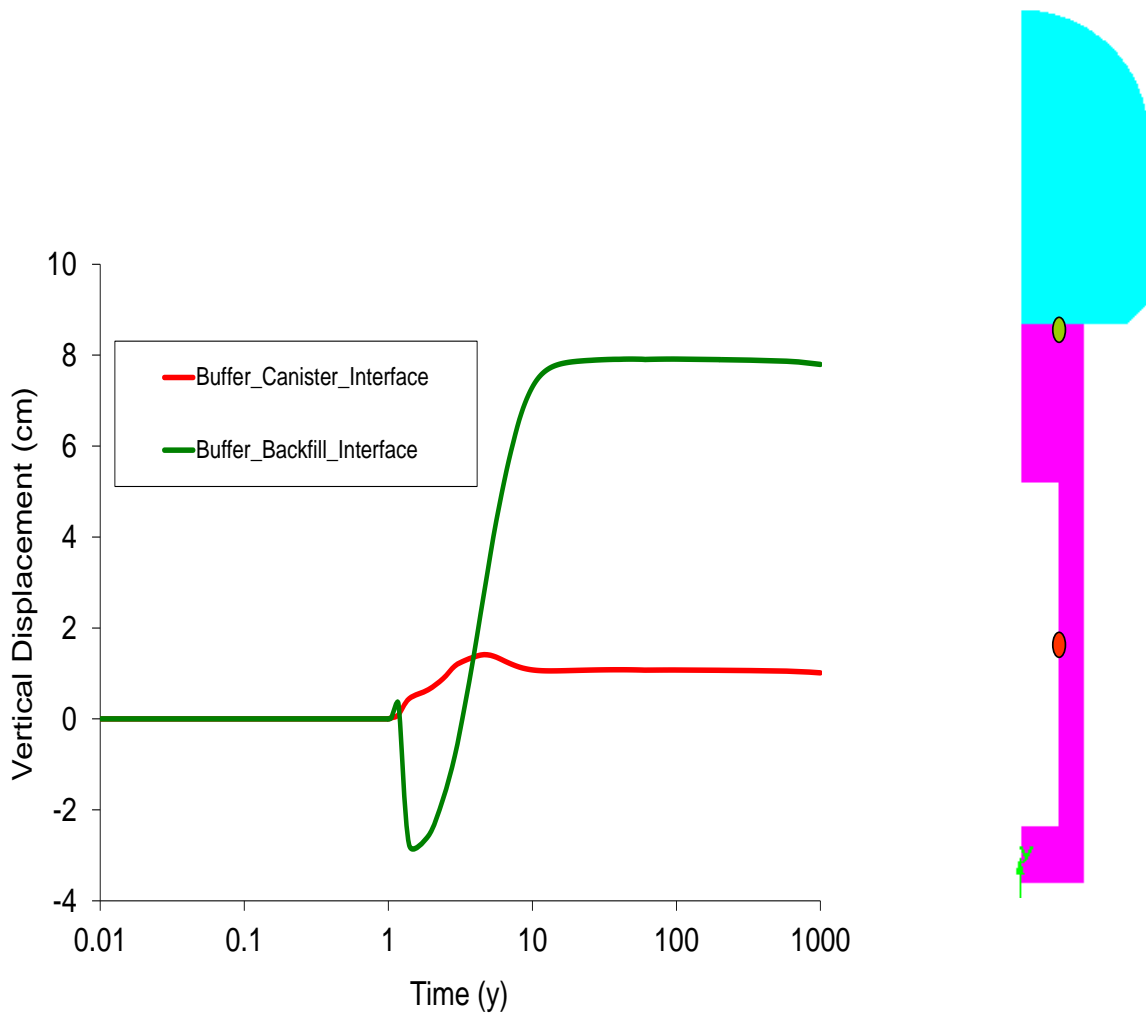


Figure 5-21. Evolution of vertical displacement for two representative points

Figure 5-20 shows the distribution of vertical displacement. Displacements are considered to be a critical element in the design of the ONKALO Project. Figure 5-20 and Figure 5-21 both indicate that the bentonite-backfill interface moves upwards as the bentonite buffer swells.

As buffer drying takes place during the initial phases, the backfill will move down to some extent because of contraction. When swelling takes place, the buffer material begins to move up and compress the backfill. The final vertical displacement of the buffer-backfill interface is approximately 8 cm.

5.3. Sensitivity analyses

A series of sensitivity calculations to understand the effect of different parameters on model performance have been carried out. While the time required for full saturation of the bentonite buffer mainly depends on the hydrological conditions around deposition holes, it is also connected with the bentonite material model.

The first step in these sensitivity analyses was to choose parameters for the buffer material model which give a better understanding of bentonite hydration in repository deposition holes. The second step was to consider the mechanical aspects: the backfill pre-consolidation pressure is increased to generate stiffer conditions through better compaction, with the aim of determining its effect on the results obtained. (The cases and parameters are summarised in Table 5-3.

Liquid flux and vapour flux control saturation of the buffer. Relevant formulae are given below, and the liquid and vapour flux parameters are varied when performing the sensitivity analyses.

The Darcy flux q is given by:

$$\mathbf{q}_\alpha = -\frac{\mathbf{k}k_{r\alpha}}{\mu_\alpha}(\nabla P_\alpha - \rho_\alpha \mathbf{g}) \quad 5.1$$

where viscosity, density and relative permeability are defined in other laws

For the relative permeability, a generalized power law is assumed:

$$k_{rl} = AS_e^\lambda \quad 5.2$$

In which λ is the power.

The intrinsic permeability is a function of porosity:

$$\mathbf{k} = \mathbf{k}_o \frac{\phi^3}{(1-\phi)^2} \frac{(1-\phi_o)^2}{\phi_o^3} \quad 5.3$$

ϕ_o : reference porosity
 \mathbf{k}_o : intrinsic permeability for matrix ϕ_o

The diffusive vapour flux is driven by the vapour mass:

$$\mathbf{i}_\alpha^i = -(\tau \phi \rho_\alpha S_\alpha D_m^i \mathbf{I}) \nabla \omega_\alpha^i \quad 5.4$$

Where τ is the tortuosity factor.

Table 5-3. Parameters employed in the sensitivity analyses

Models	Parameters			
	Intrinsic Permeability of Rock (k)	Power in the relative permeability law (λ)	Coefficient of tortuosity for molecular diffusion (τ)	Pre-consolidation pressure of backfill (p_0^*)
Reference case	1e-17 m ²	3	0.4	0.5 Mpa
Case A	1e-17 m ²	6	0.4	0.5 Mpa
Case B	1e-18 m ²	3	0.4	0.5 Mpa
Case C	1e-17 m ²	3	0.8	0.5 Mpa
Case D	1e-18 m ²	6	0.8	0.5 Mpa
Case E	1e-17 m ²	3	0.4	2 Mpa

The intrinsic permeability of the rock, power in the relative permeability law (λ), the coefficient of tortuosity (τ) corresponding to the buffer material and the pre-consolidation pressure of the backfill (p_0^*) have all been considered in the sensitivity analyses.

5.3.1 Comparison of evolution of temperature

Figures 5-22 to 5-26 show that both the maximum temperature reached and temperature behaviour do not differ greatly between the reference case and the other cases. The hottest point in buffer material which is in contact with a canister has a temperature of 80°C. It can be seen that the maximum buffer temperature is not affected by incomplete buffer saturation in the initial stages.

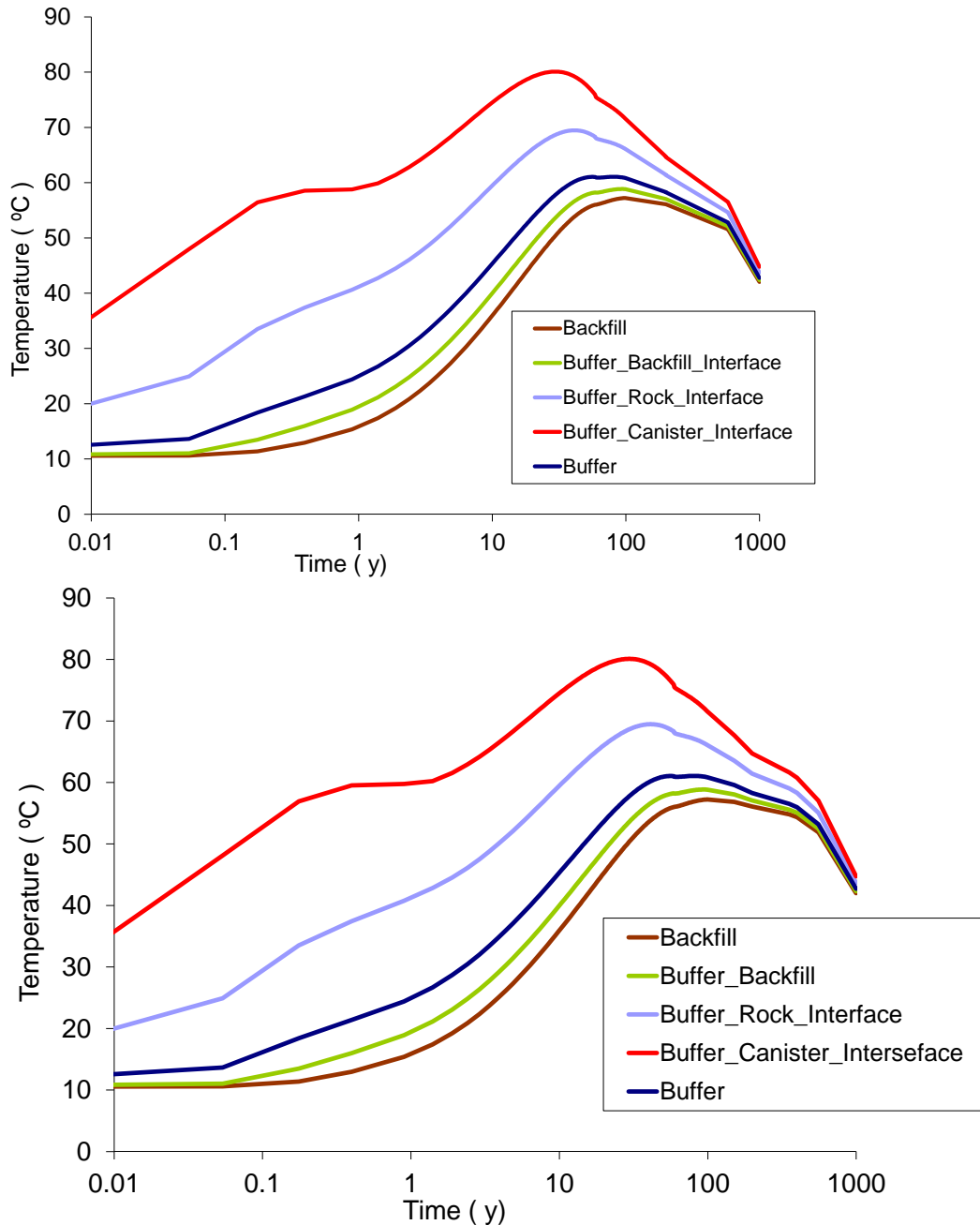


Figure 5-22. Evolution of temperature (Reference case above, Case A below)

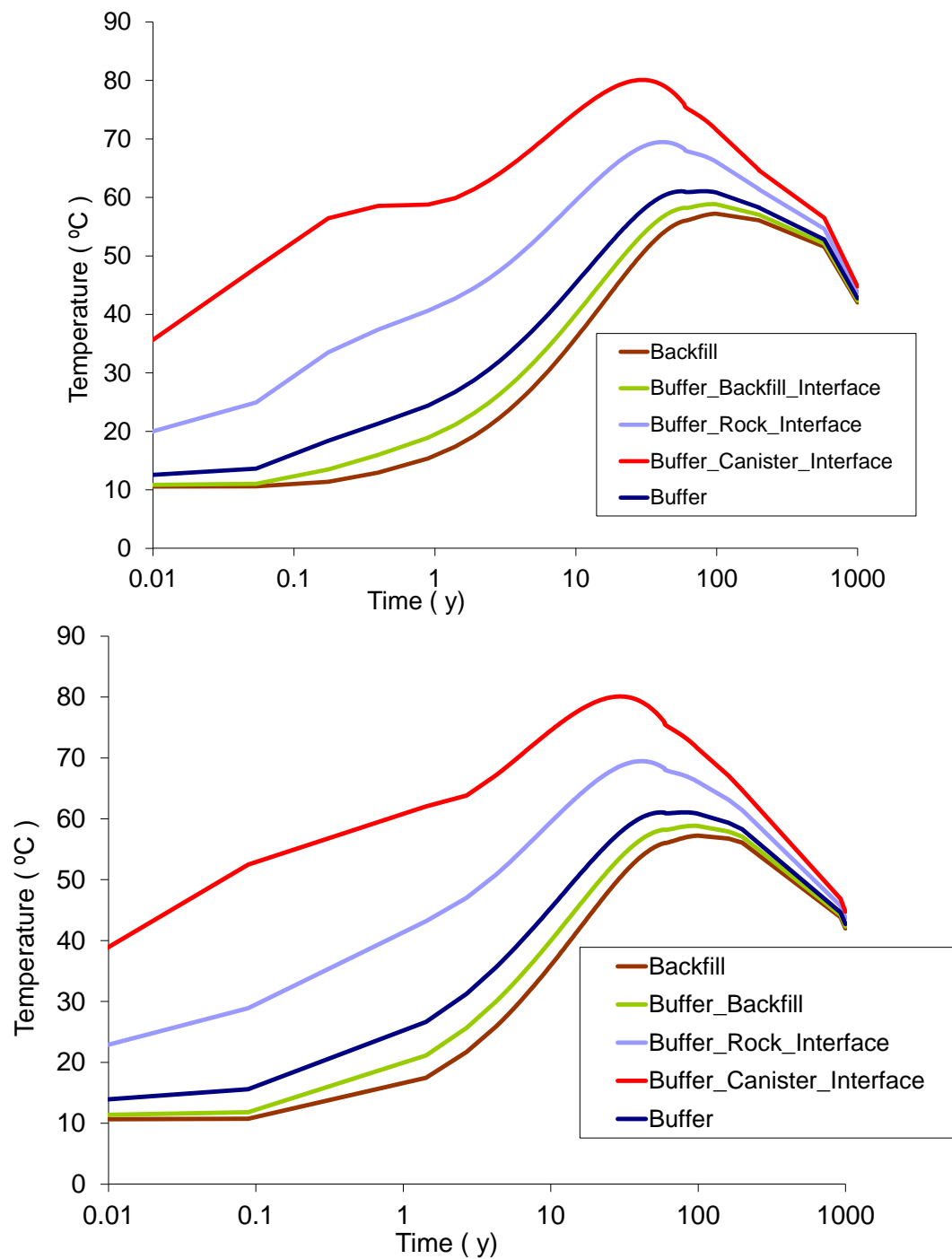


Figure 5-23. Evolution of temperature (Reference case above, Case B below)

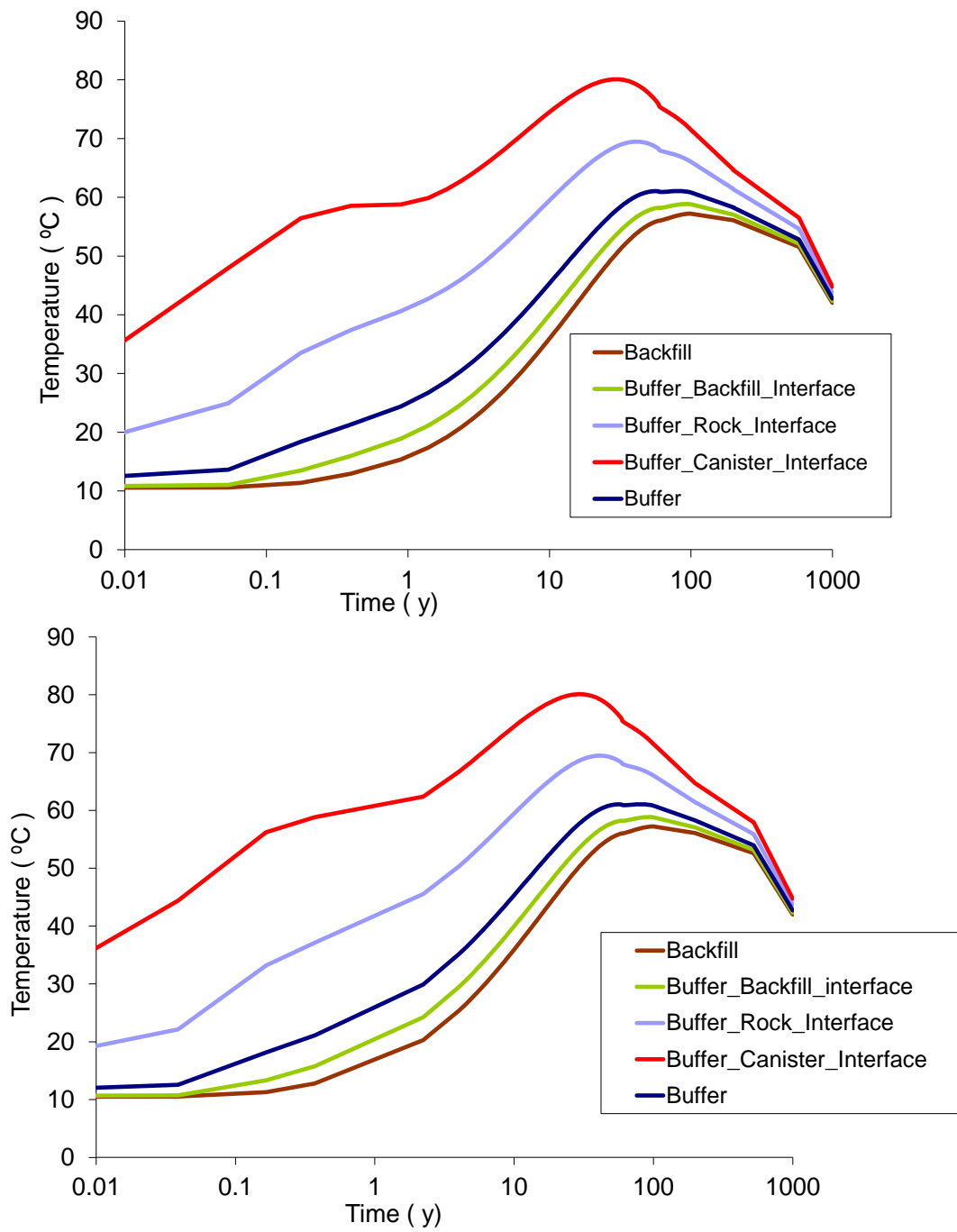


Figure 5-24. Evolution of temperature (Reference case above, Case C below)

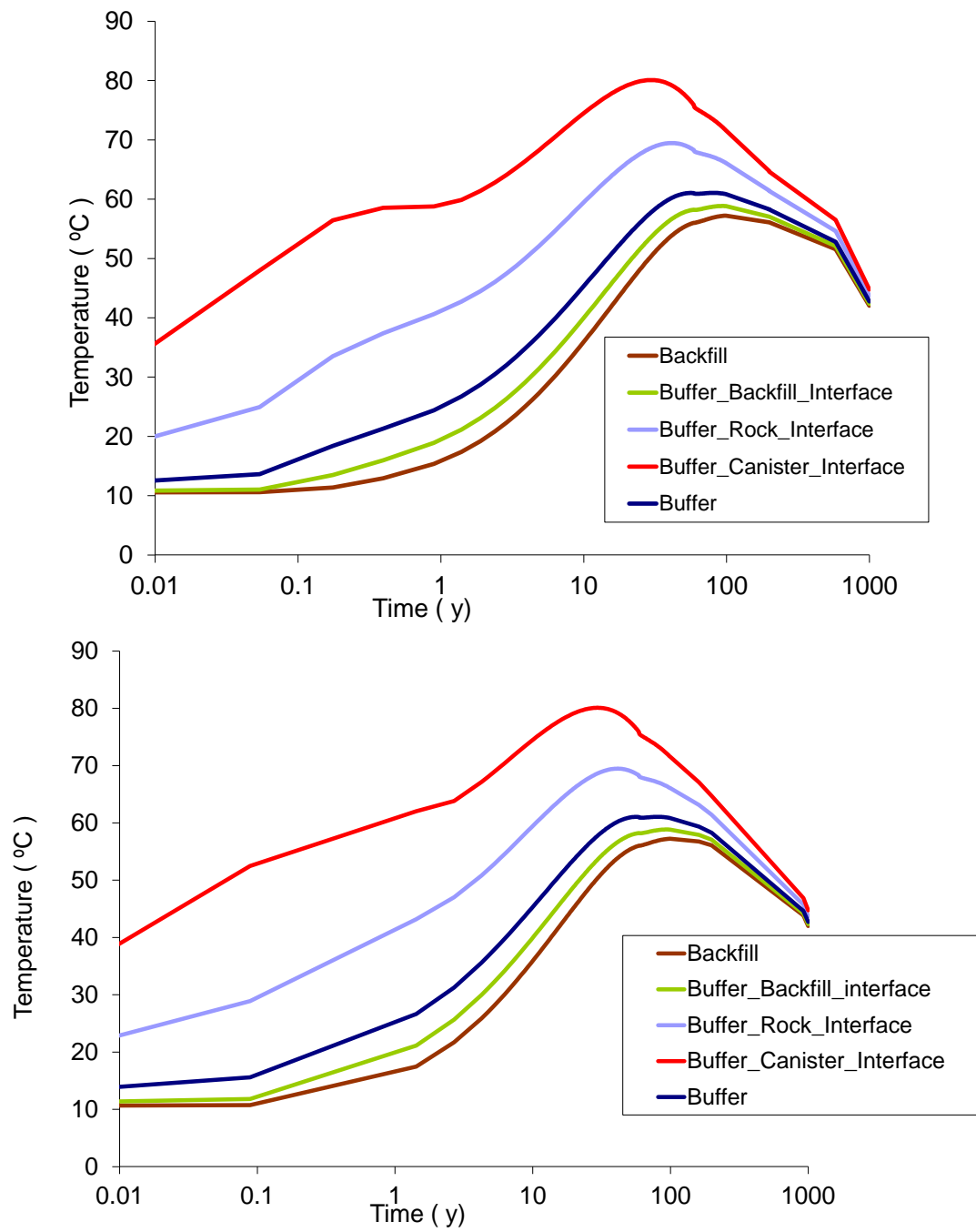


Figure 5-25. Evolution of temperature (Reference case above, Case D below)

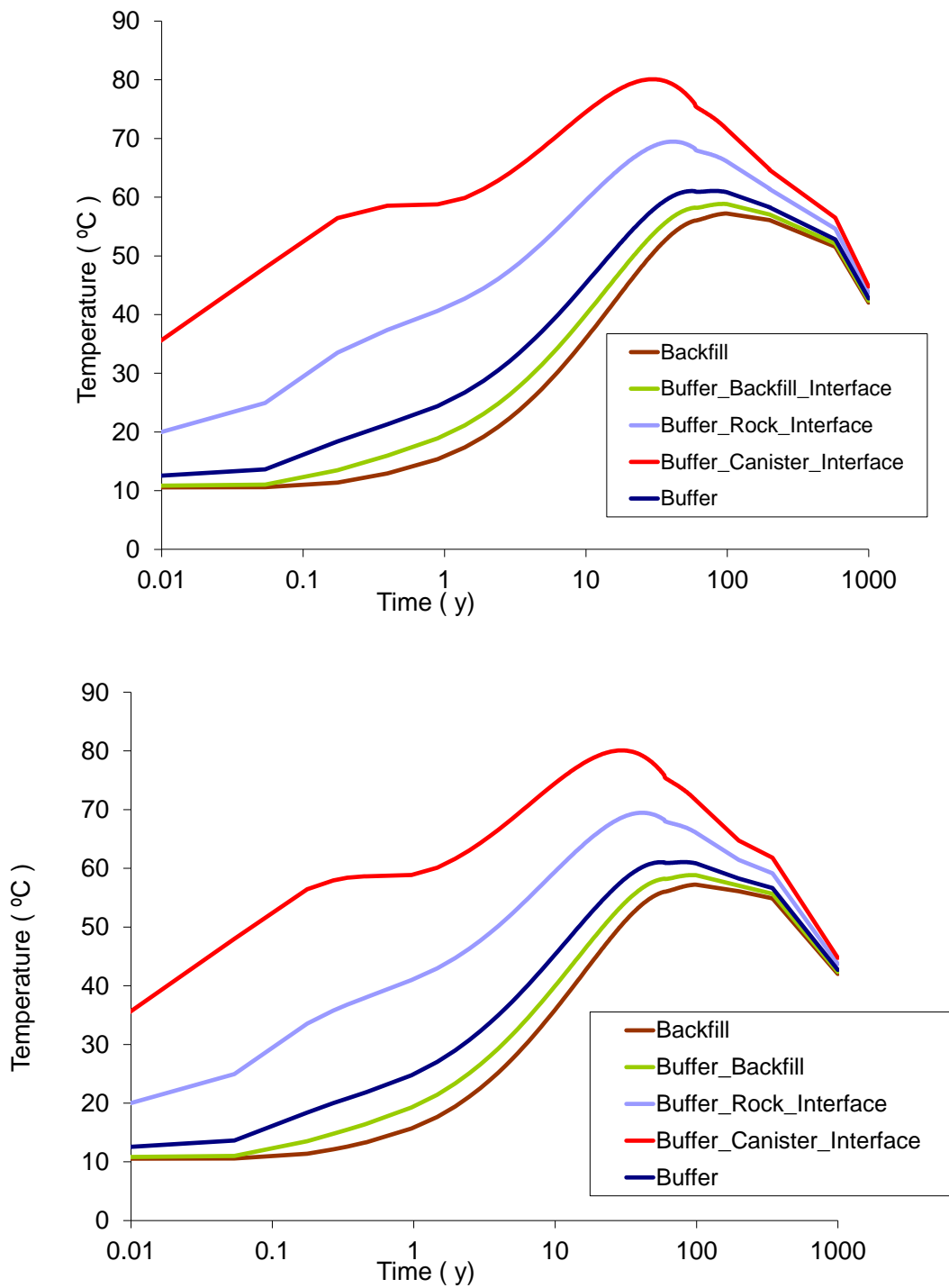


Figure 5-26. Evolution of temperature (Reference case above, Case E below)

5.3.2 Comparison of the evolution of liquid pressure

Liquid pressure is an essential aspect of hydration. The figures 5-27 to 5-31 show how its behaviour depends on changes in permeability and vapour diffusivity. In general terms, Case B and Case D exhibit similar trends because the same value for intrinsic permeability is employed. Although the coefficient of tortuosity for molecular diffusion (τ) and power in the relative permeability law (λ) do not have a great influence on the time required for full saturation of the buffer, they affect the value of liquid pressure achieved close to the canister.

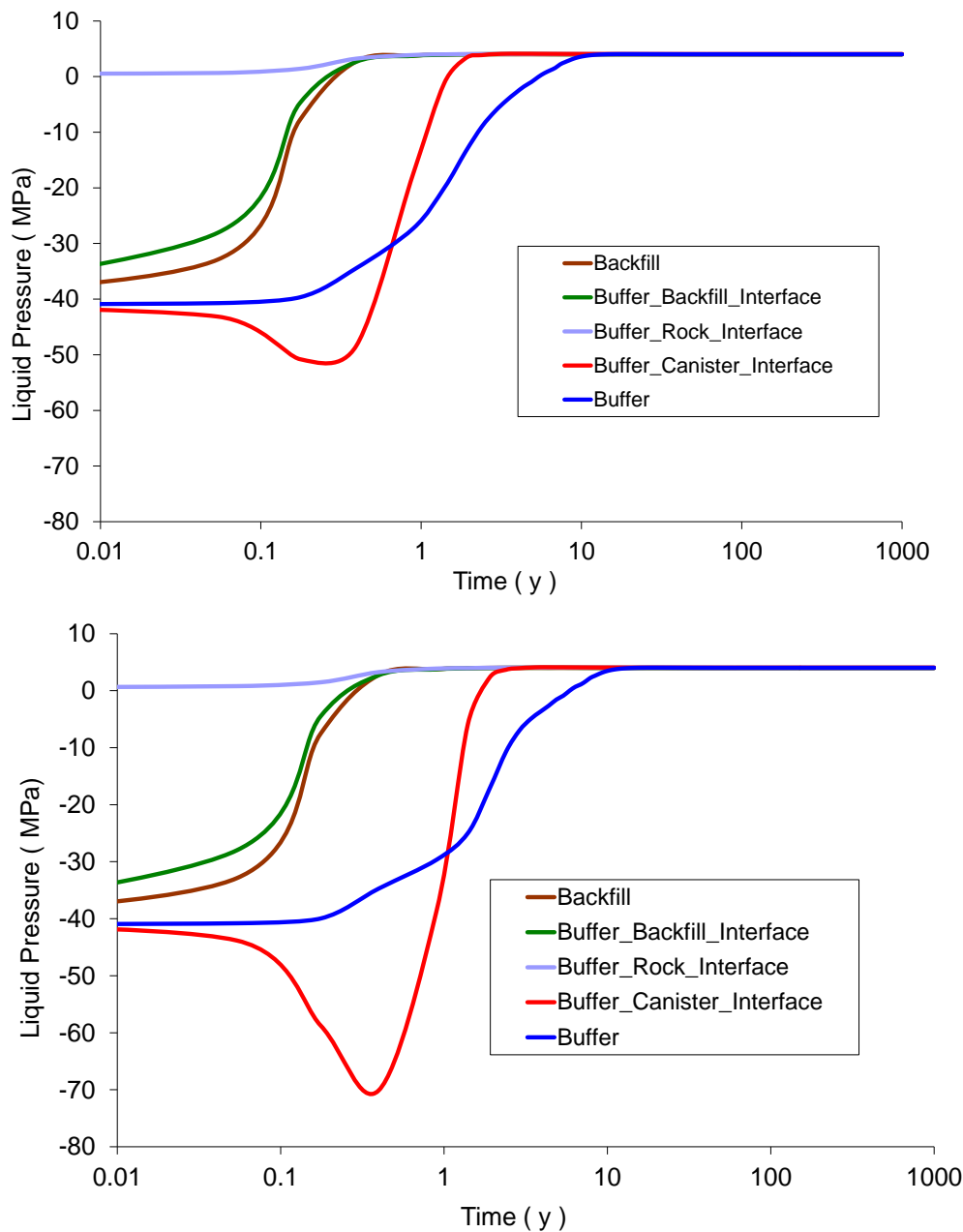


Figure 5-27. Evolution of liquid pressure (Reference case above, Case A below)

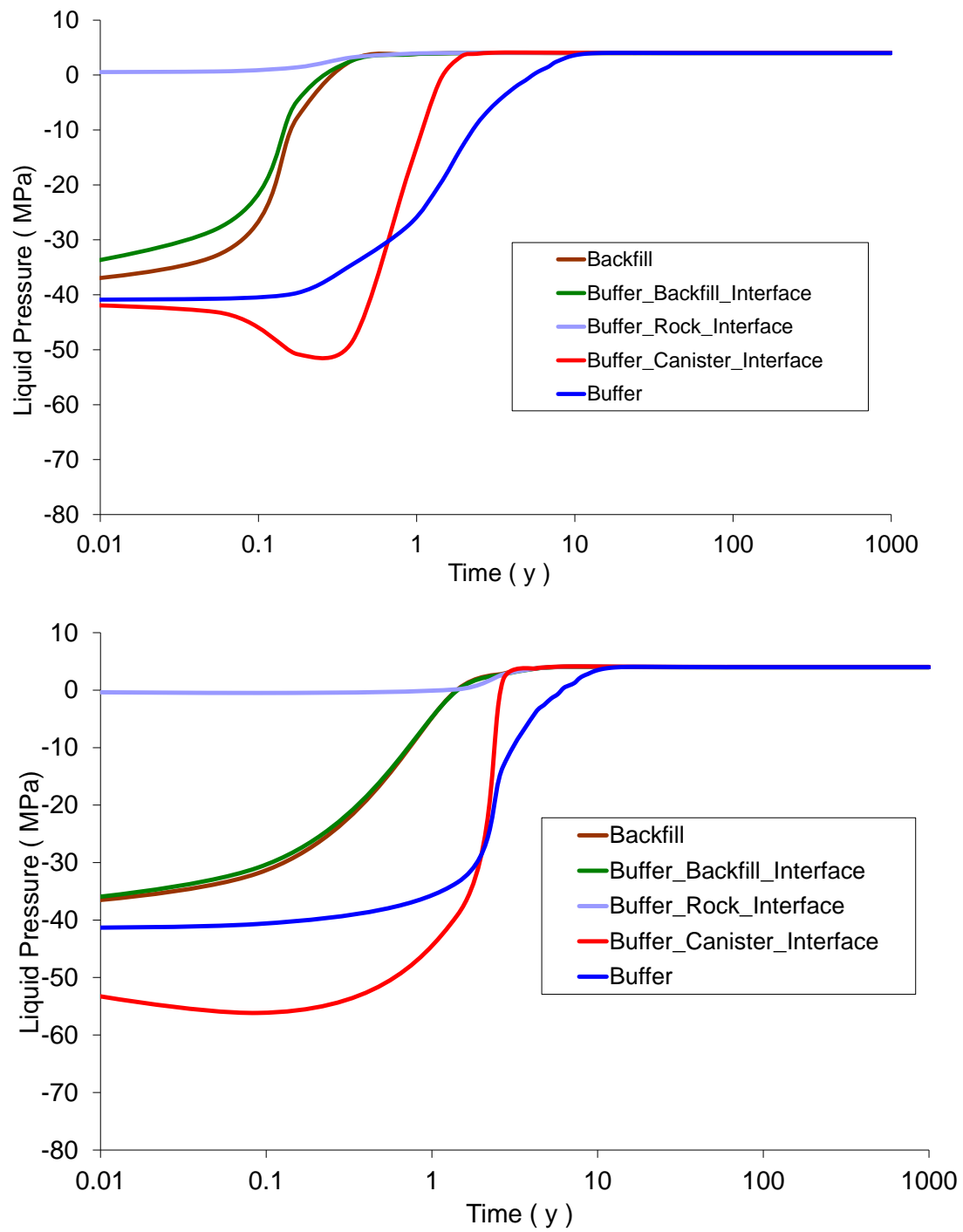


Figure 5-28. Evolution of liquid pressure (Reference case above, Case B below)

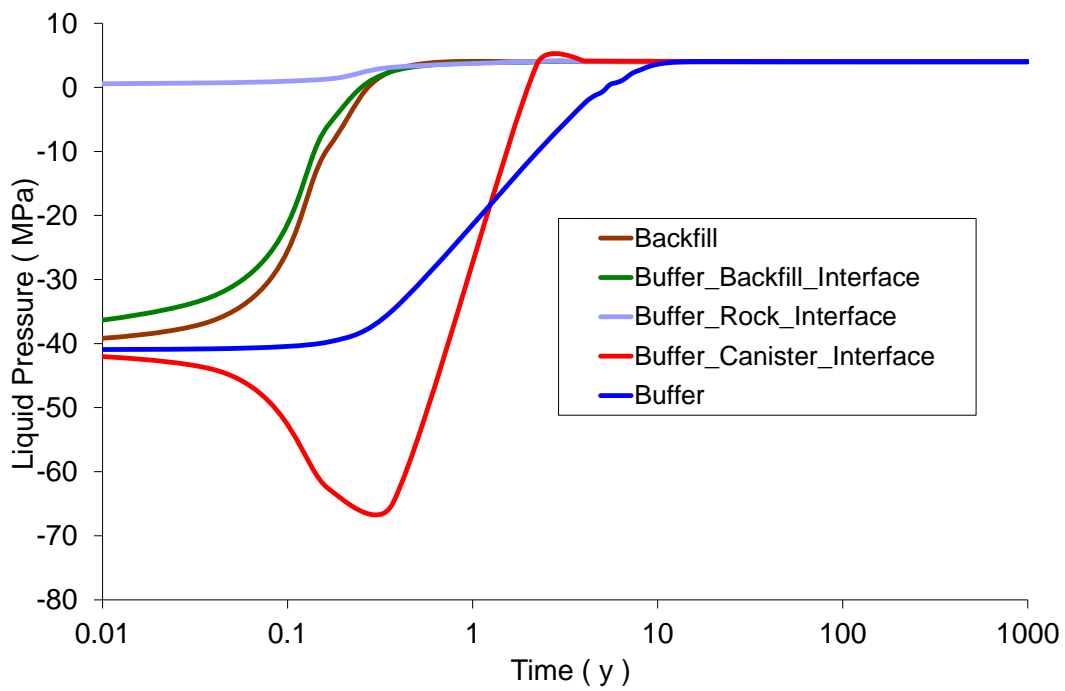
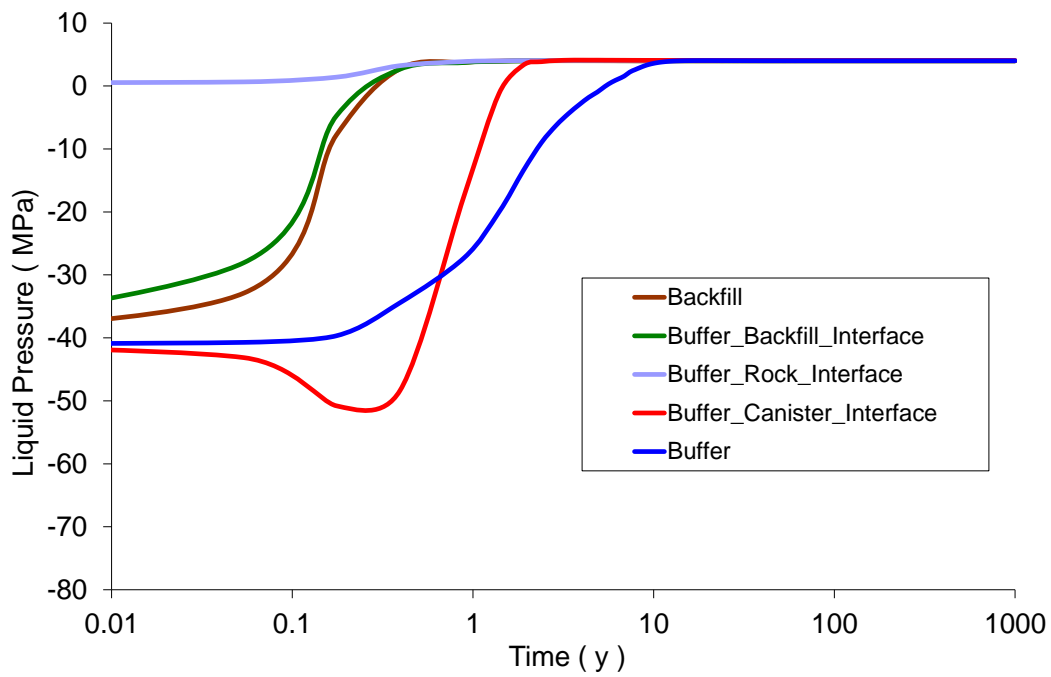


Figure 5-29. Evolution of liquid pressure (Reference case above, Case C below)

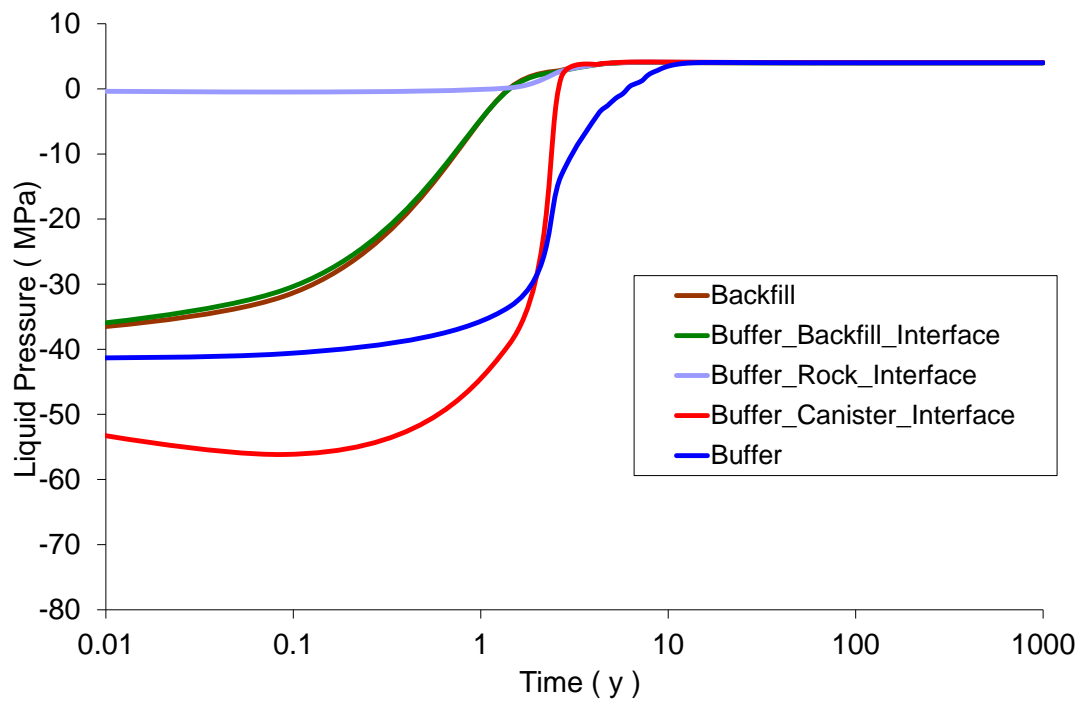
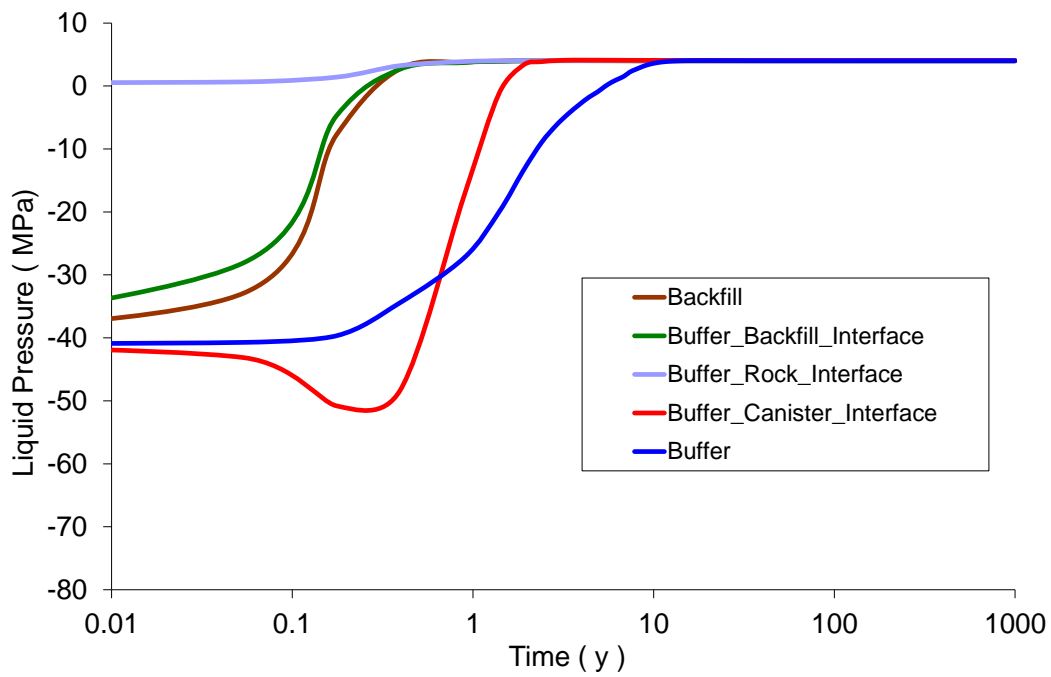


Figure 5-30. Evolution of liquid pressure (Reference case above, Case D below)

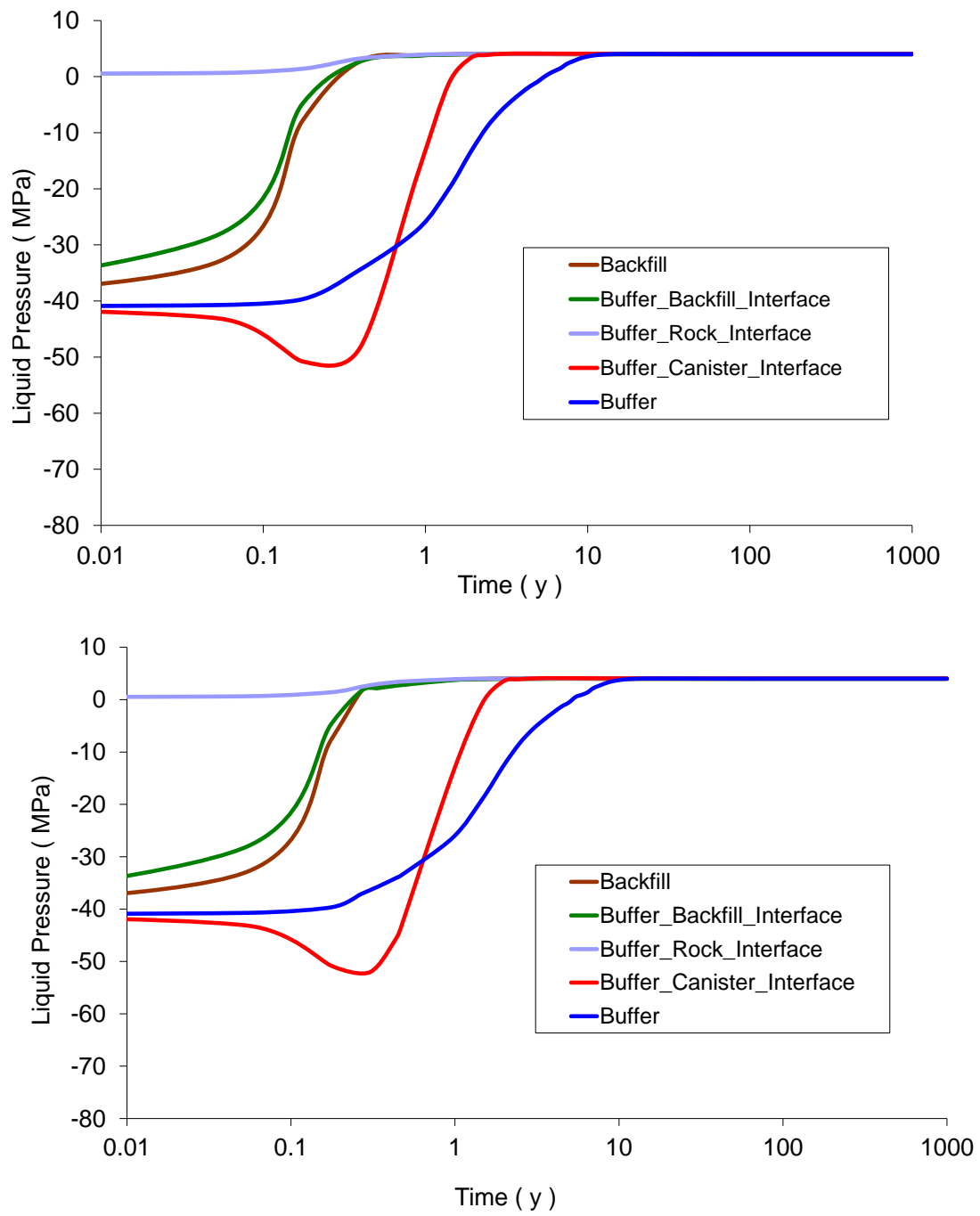


Figure 5-31. Evolution of liquid pressure (Reference case above, Case E below)

5.3.3 Comparison of the evolution of total mean stress

From a mechanical viewpoint, the total mean stresses that will develop on the buffer material are important and need to be analysed. Even though there are some small differences in the transient response between the Base case, Case B and Case D, the maximum value of stress achieved is almost the same in all cases as it is shown Figure 5-32 to Figure 5-36.

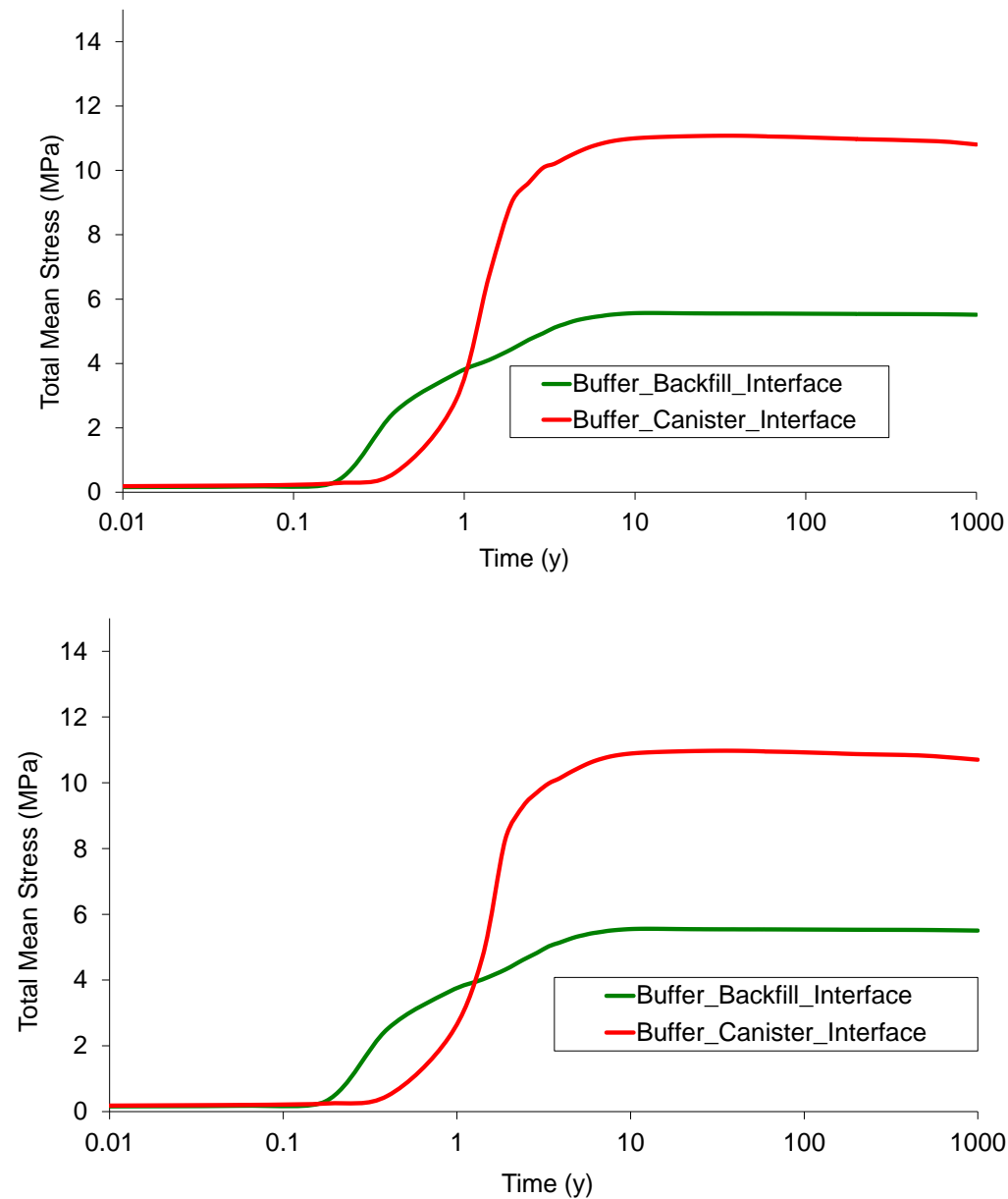


Figure 5-32. Evolution of total mean stress (Reference case above, Case A below)

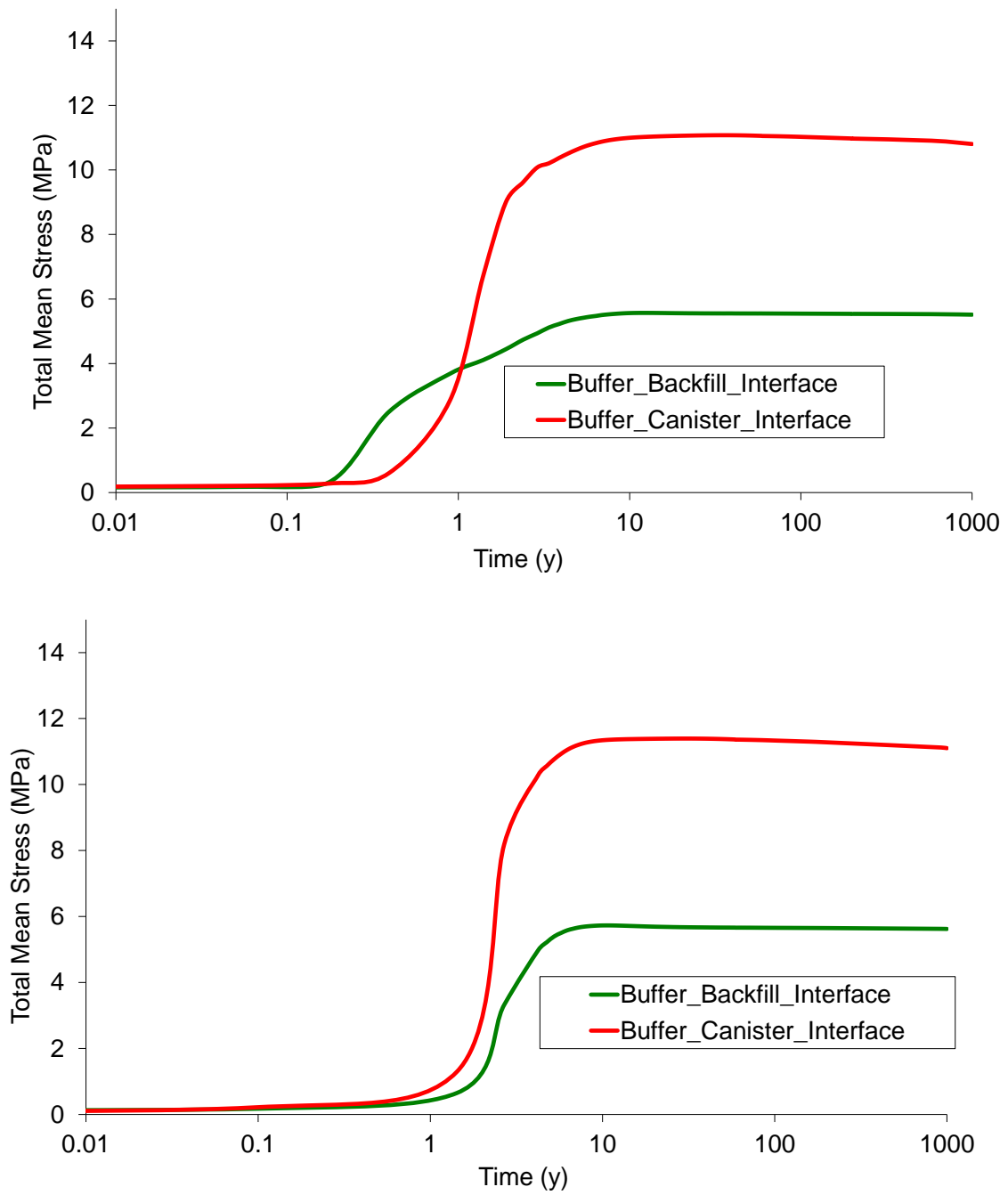


Figure 5-33. Evolution of total mean stress (Reference case above, Case B below)

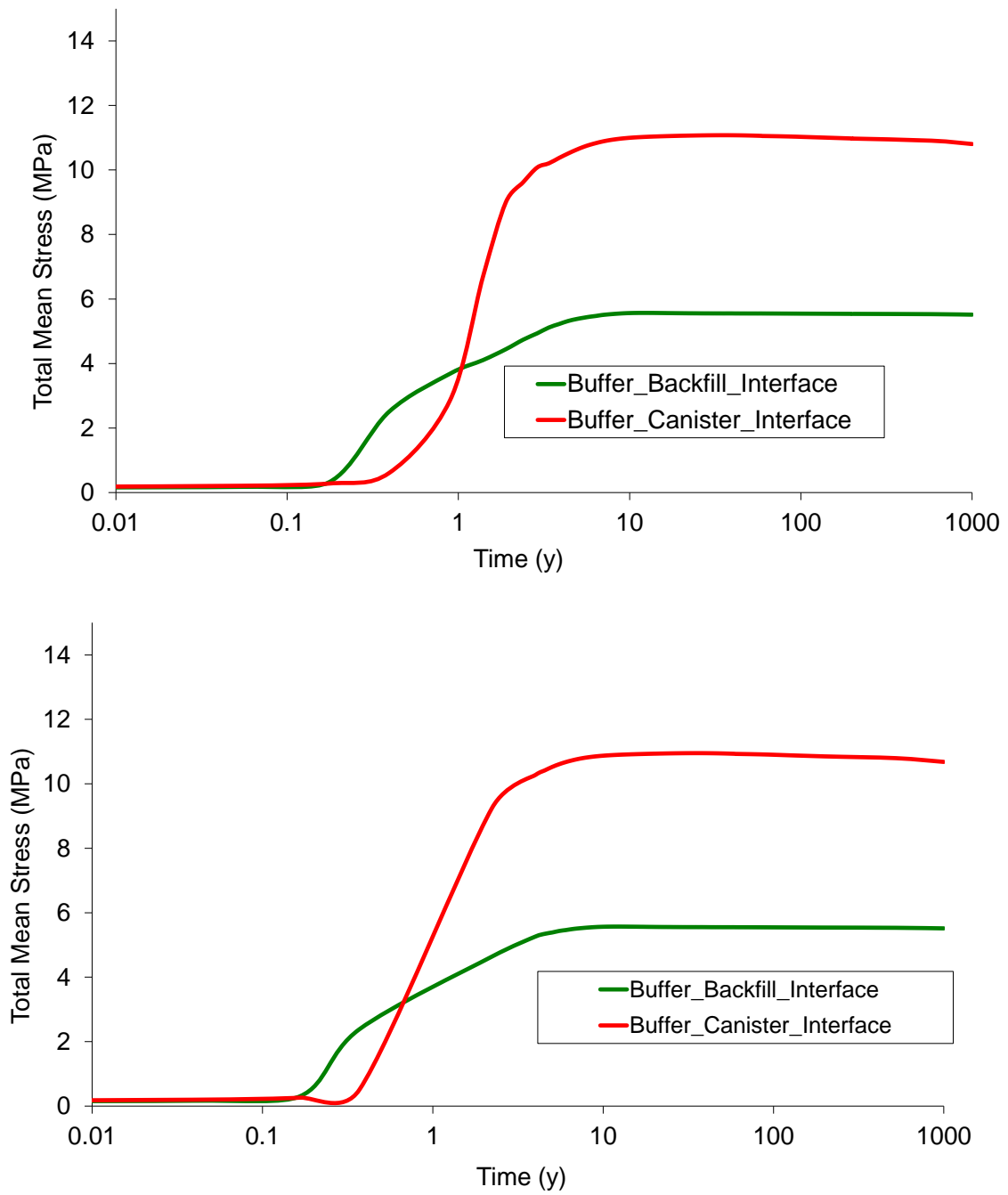


Figure 5-34. Evolution of total mean stress (Reference case above, Case C below)

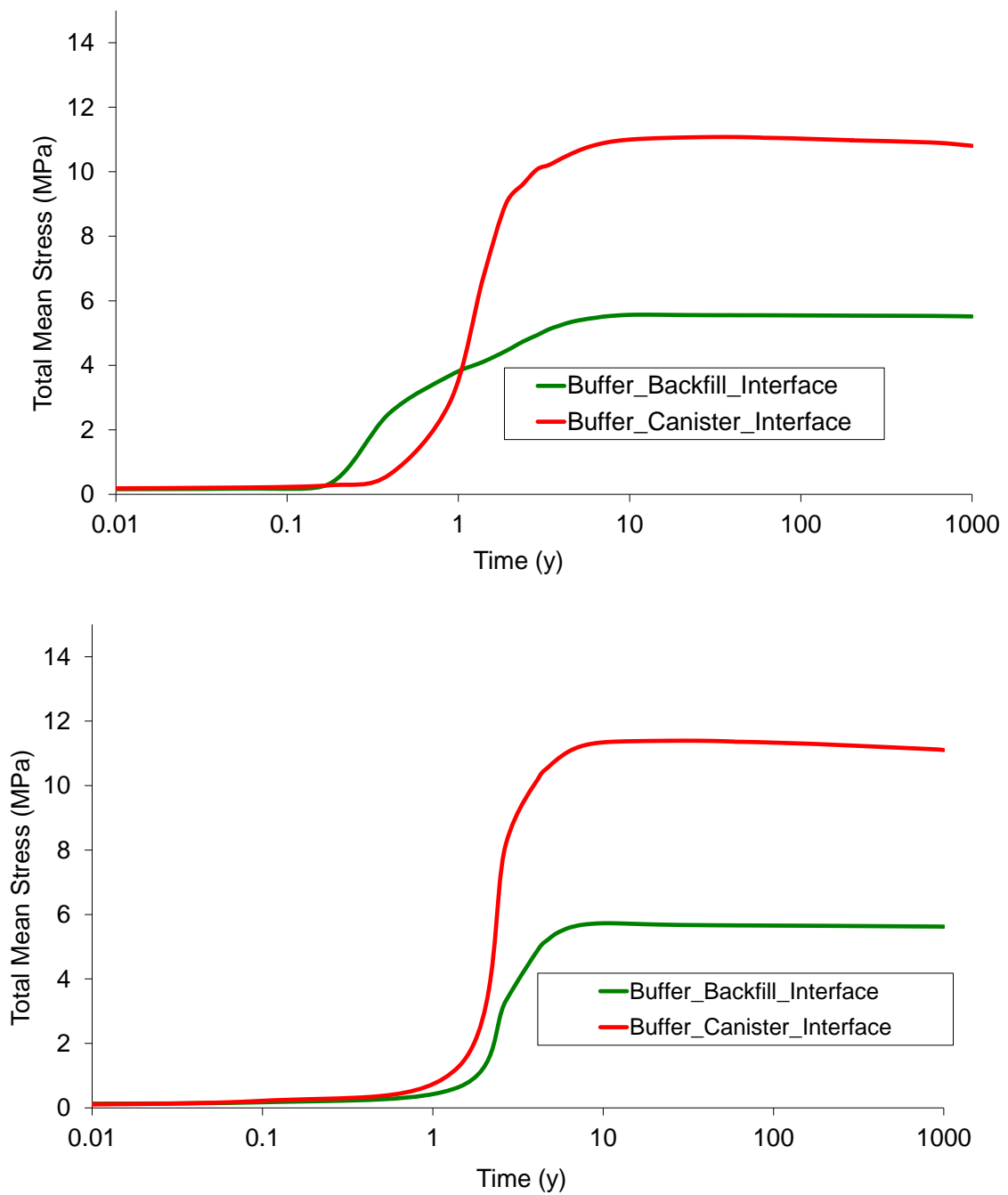


Figure 5-35. Evolution of total mean stress (Reference case above, Case D below)

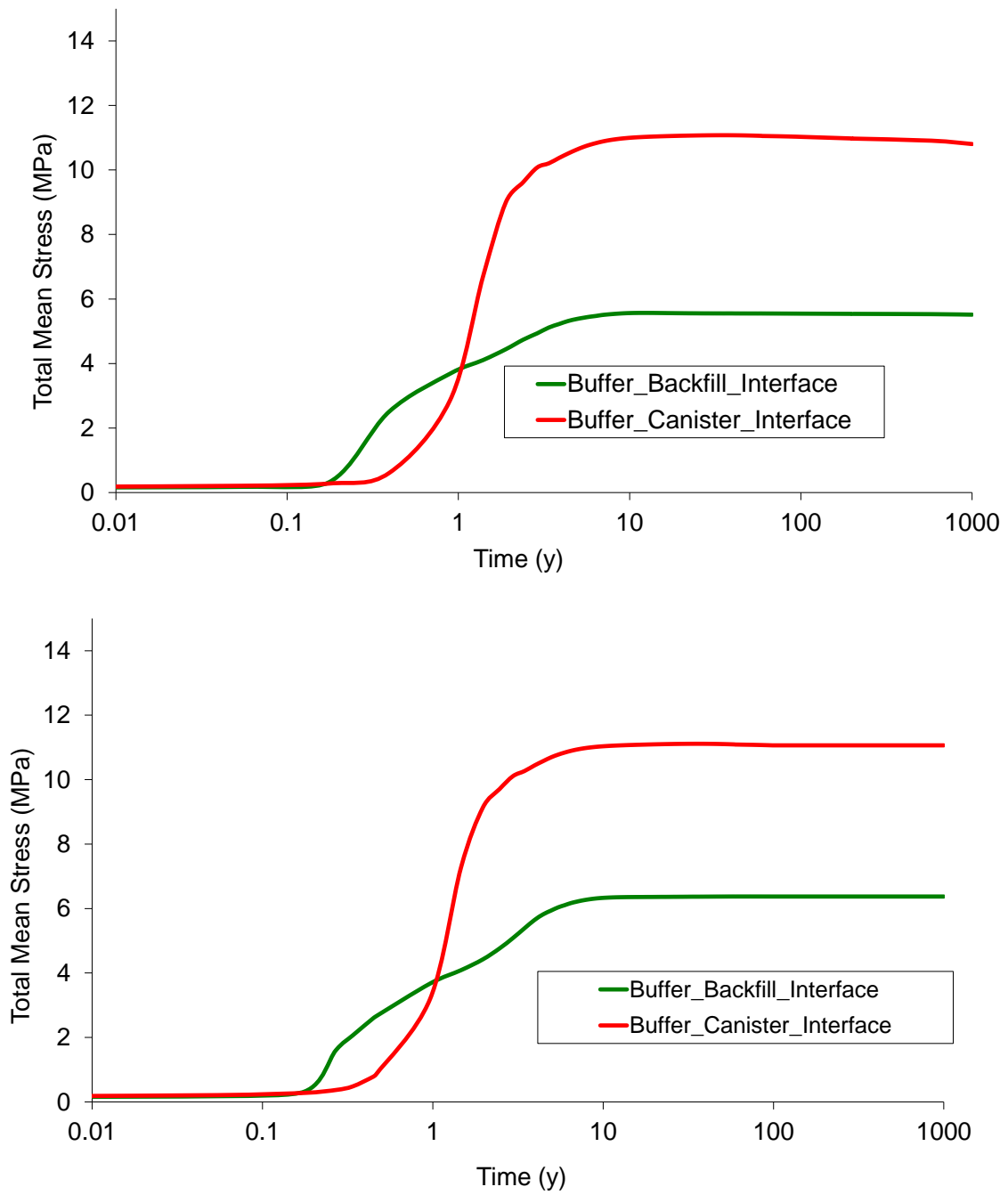


Figure 5-36. Evolution of total mean stress (Reference case above, Case E below)

5.3.4 Comparison of the evolution of effective mean stress

While some differences can be noted in the different cases as regards mean effective stress, it behaves in the same way in all of them as it is shown Figure 5-37 to Figure 5-41. It is known that the balance between stress and displacement in the buffer zone depends on the degree of saturation in the buffer and in the backfill. While changes in the permeability and vapour diffusivity have an important effect on saturation, but not on effective mean stress.

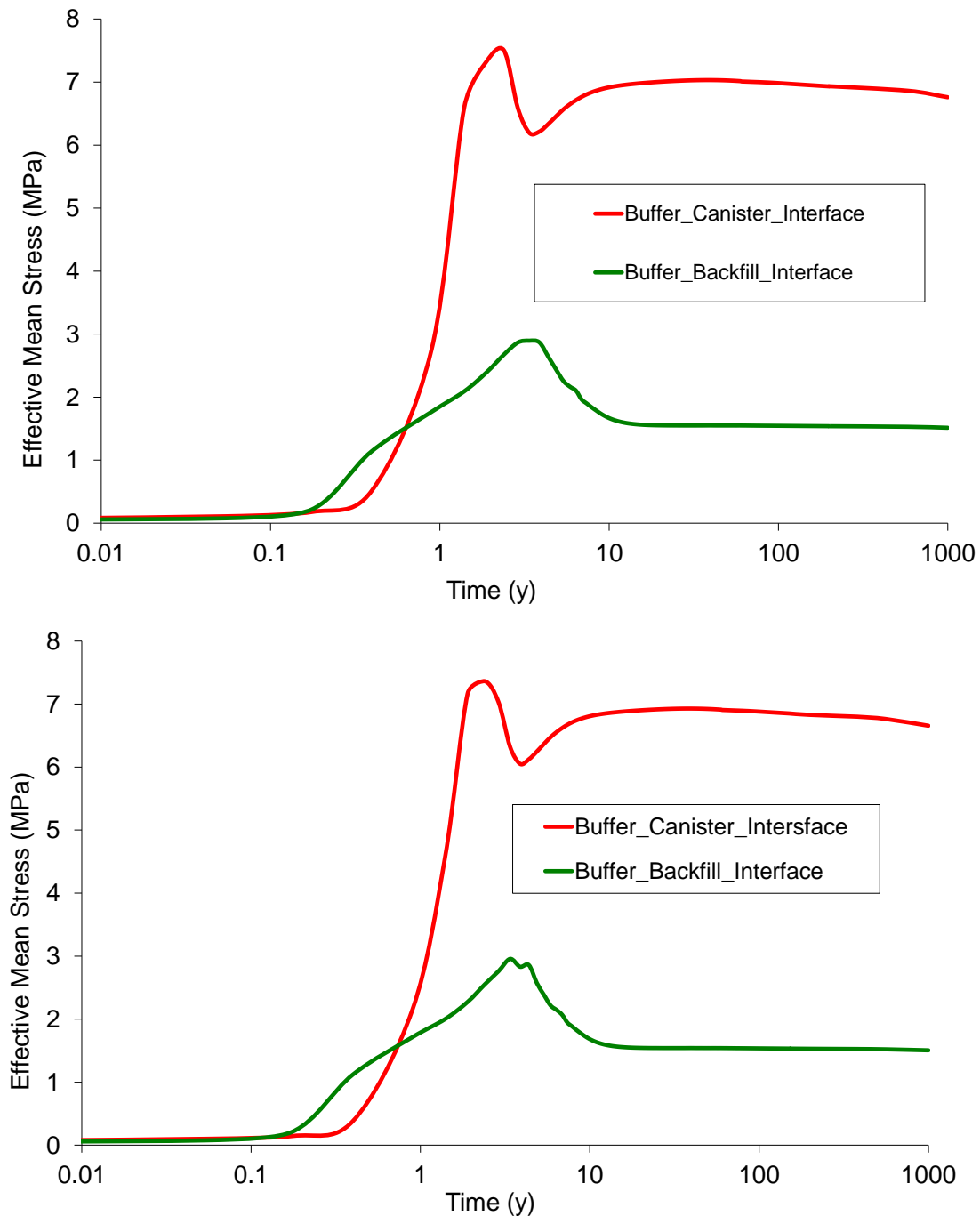


Figure 5-37. Evolution of mean effective stress (Reference case above, Case A below)

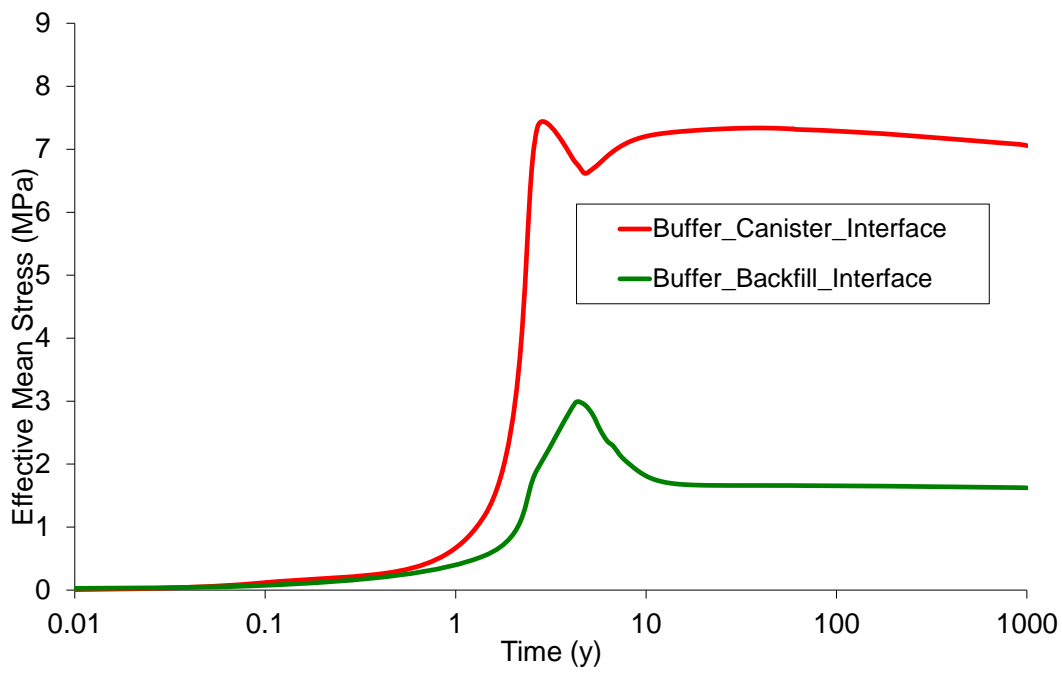
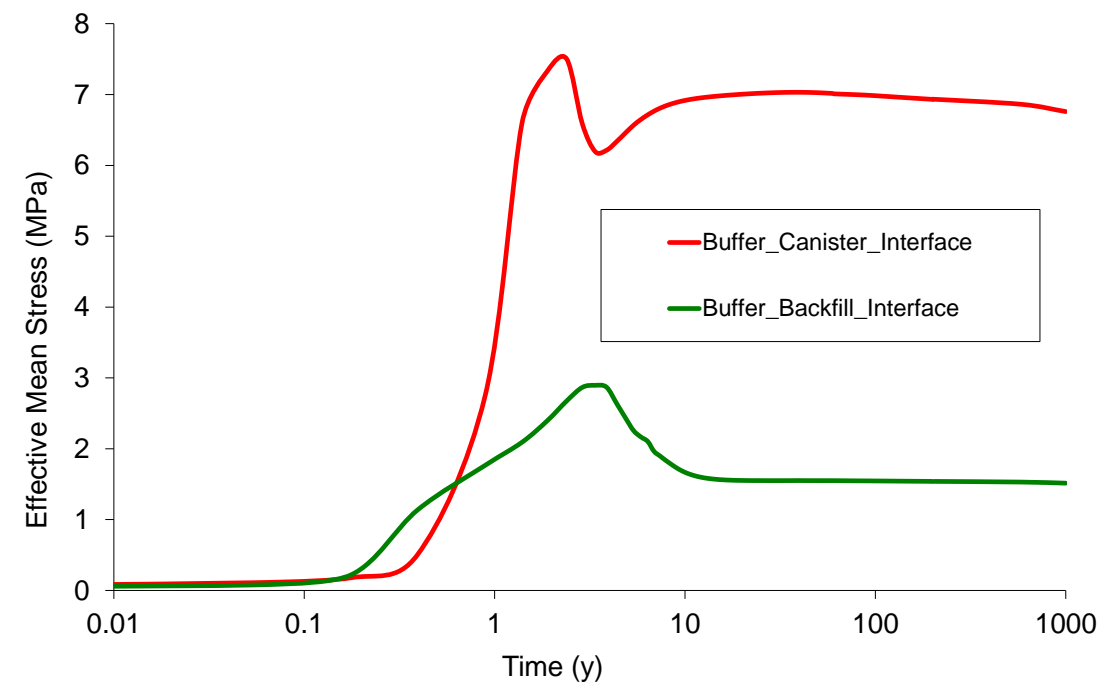


Figure 5-38. Evolution of mean effective stress (Reference case above, Case B below)

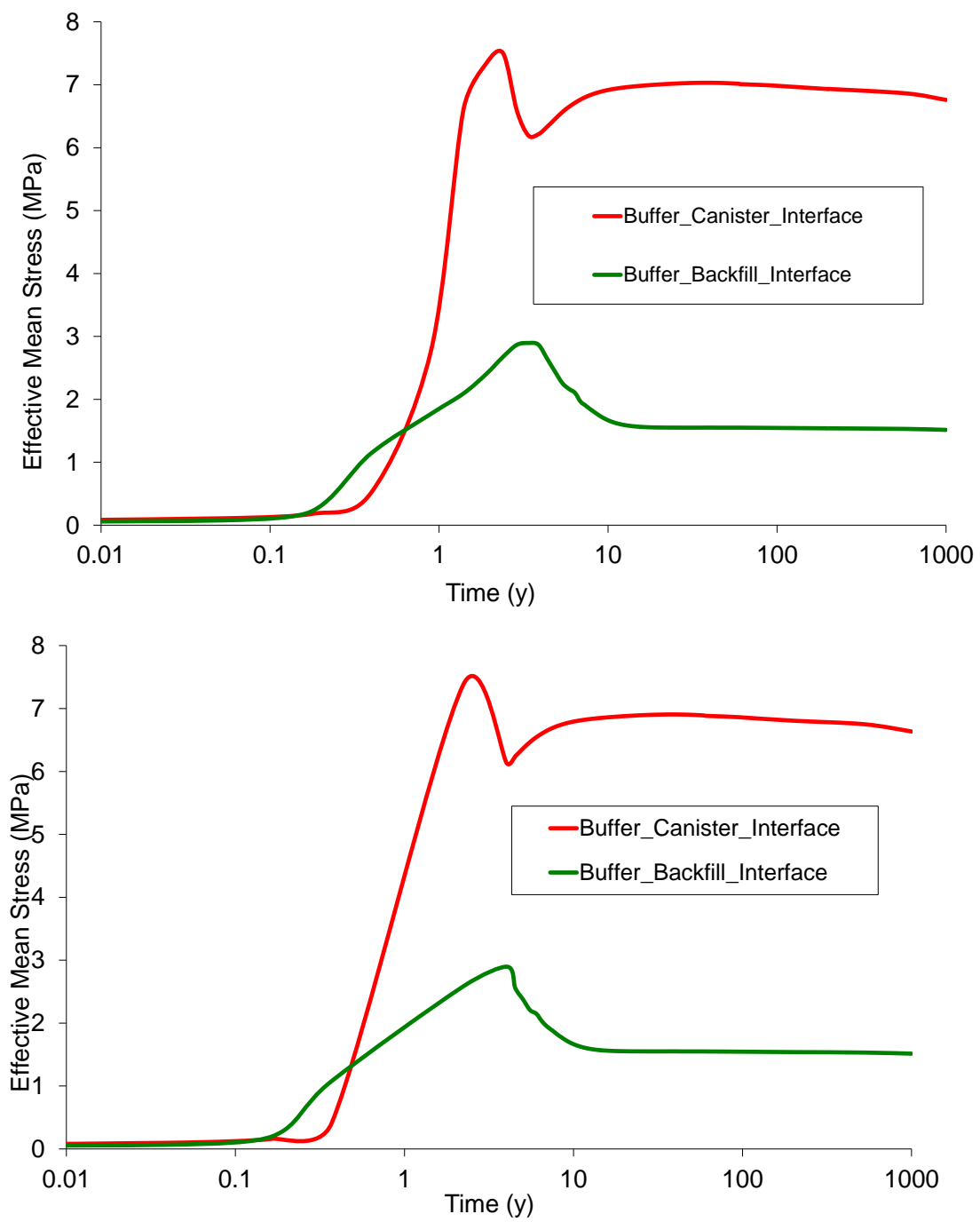


Figure 5-39. Evolution of mean effective stress (Reference case above, Case C below)

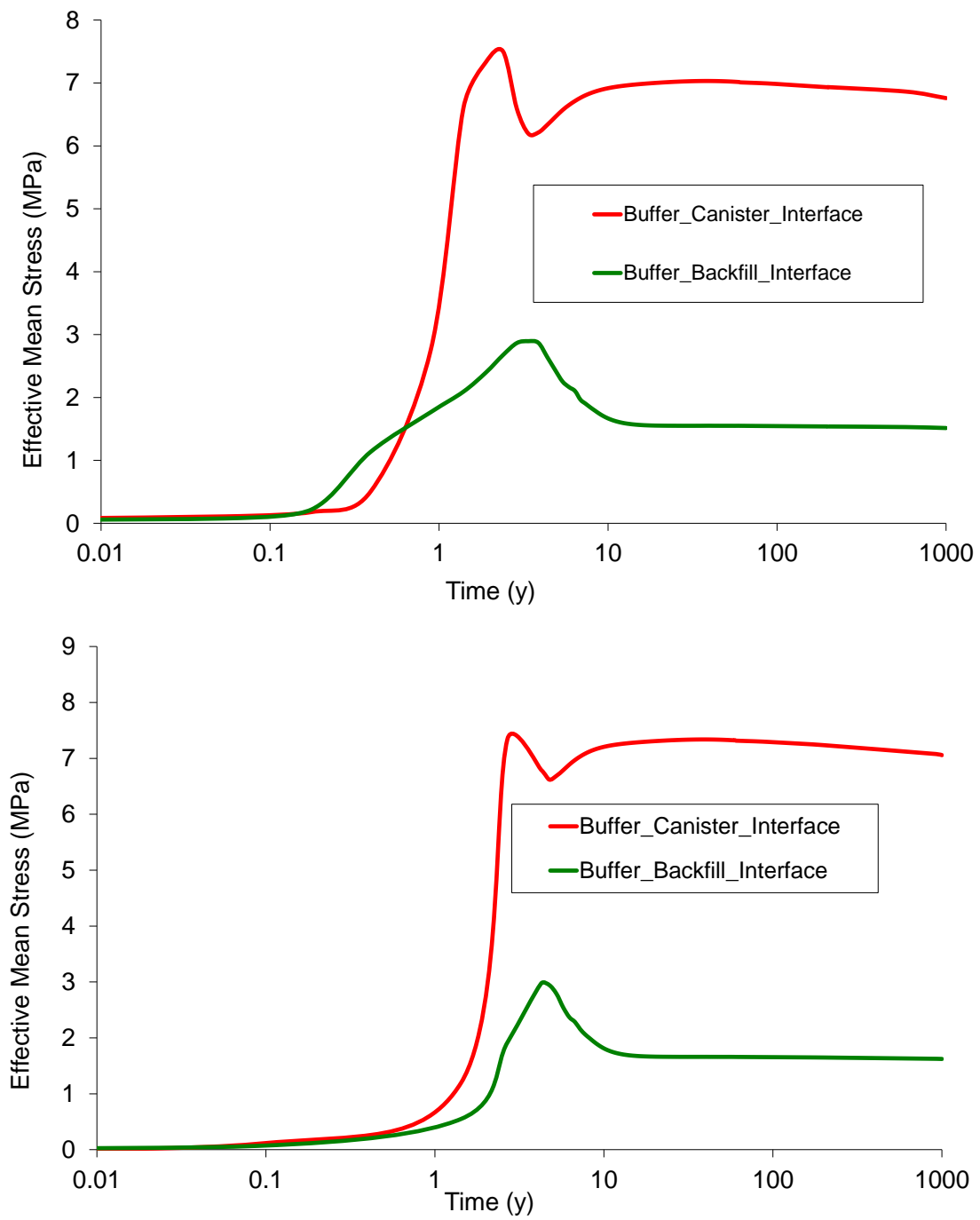


Figure 5-40. Evolution of mean effective stress (Reference case above, Case D below)

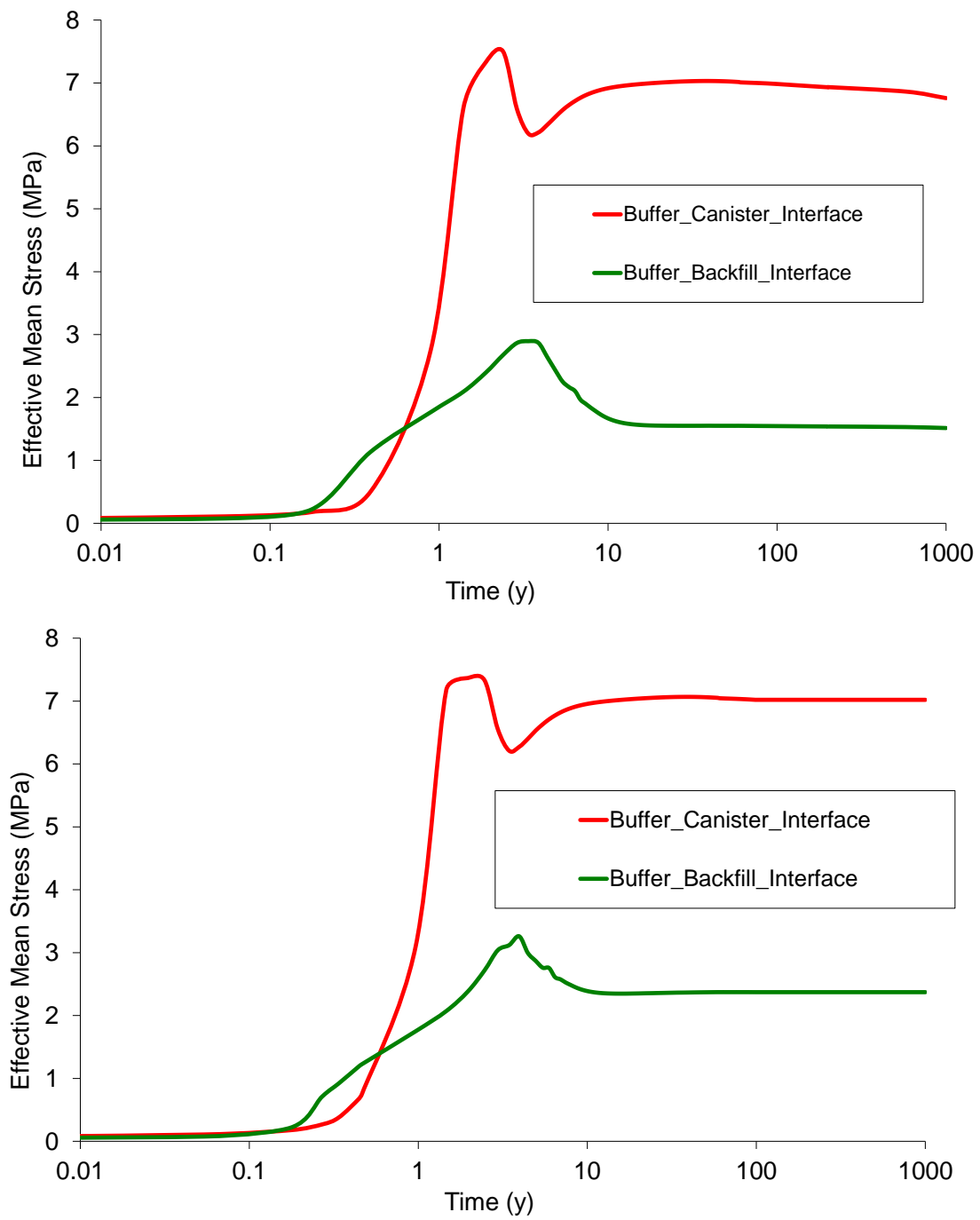


Figure 5-41. Evolution of mean effective stress (Reference case above, Case E below)

5.3.5 Comparison of the evolution of porosity

Permeability plays a significant role in total inflow into the deposition hole, and consequently affects the time required for the buffer to reach full saturation. Even though the behaviour of porosity is similar in all cases because the general processes are the same, the calculated values differ slightly as it is shown Figure 5-42 to Figure 5-46.

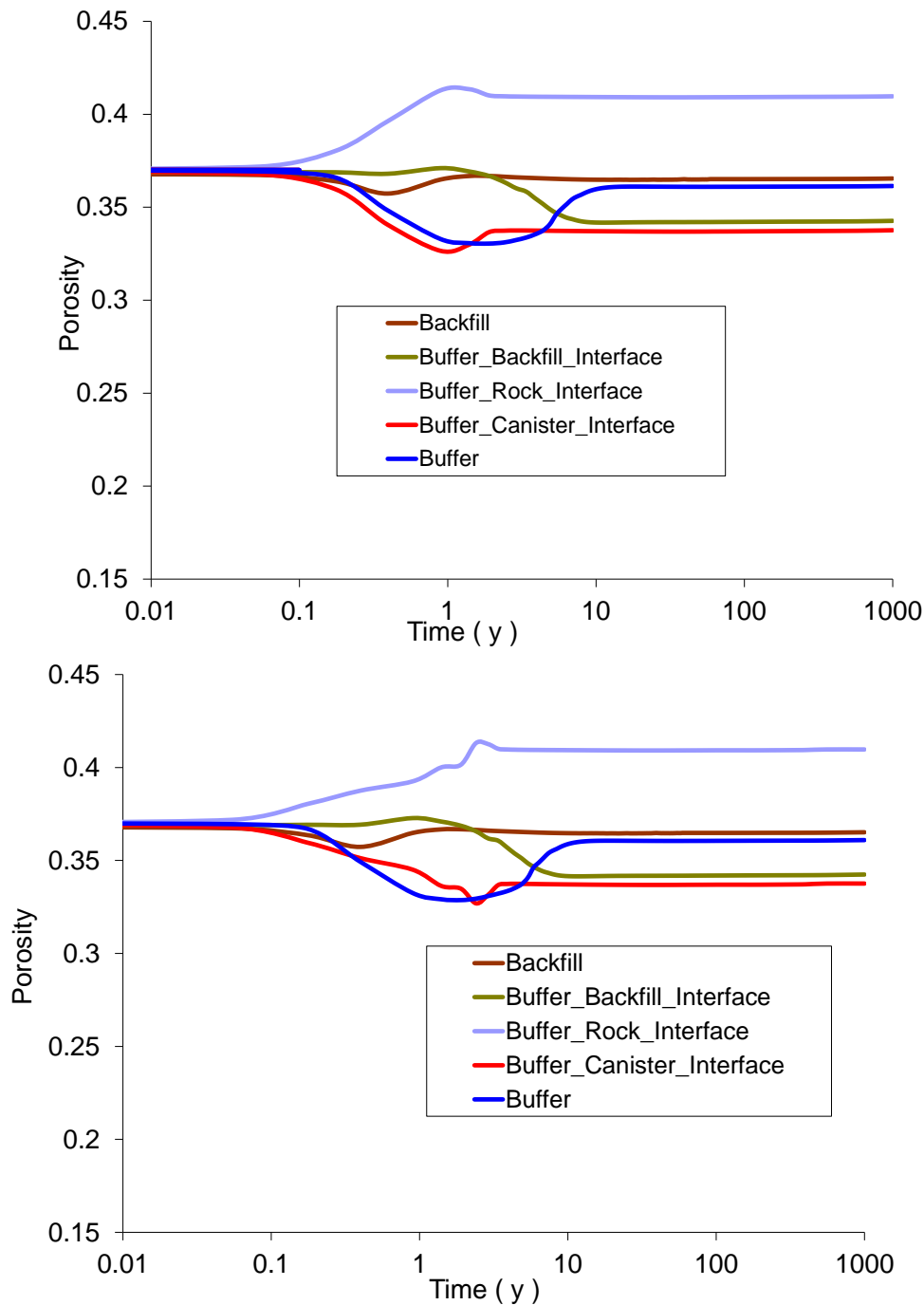


Figure 5-42. Evolution of porosity (Reference case above, Case A below)

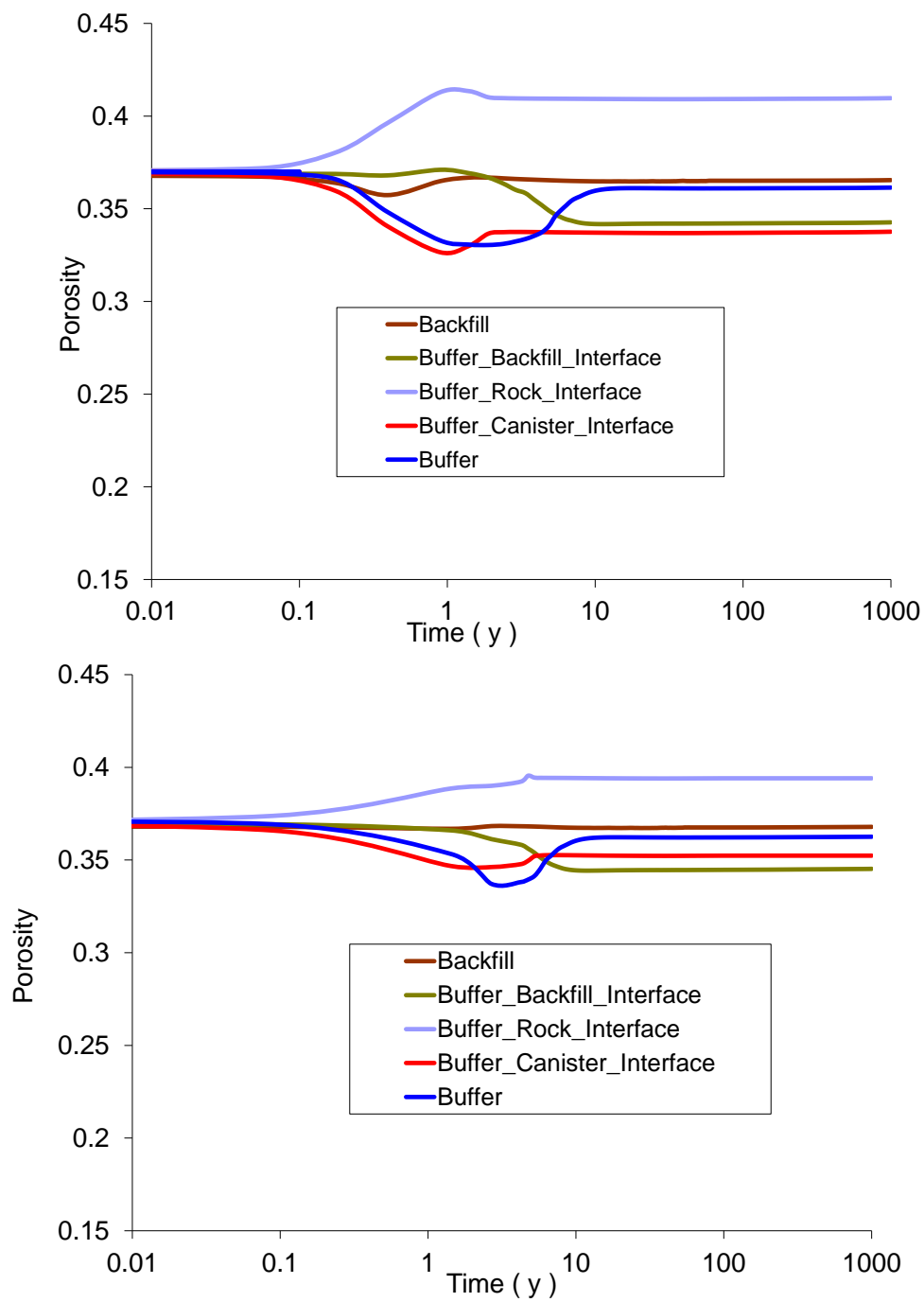


Figure 5-43. Evolution of Porosity (Reference case above, Case B below)

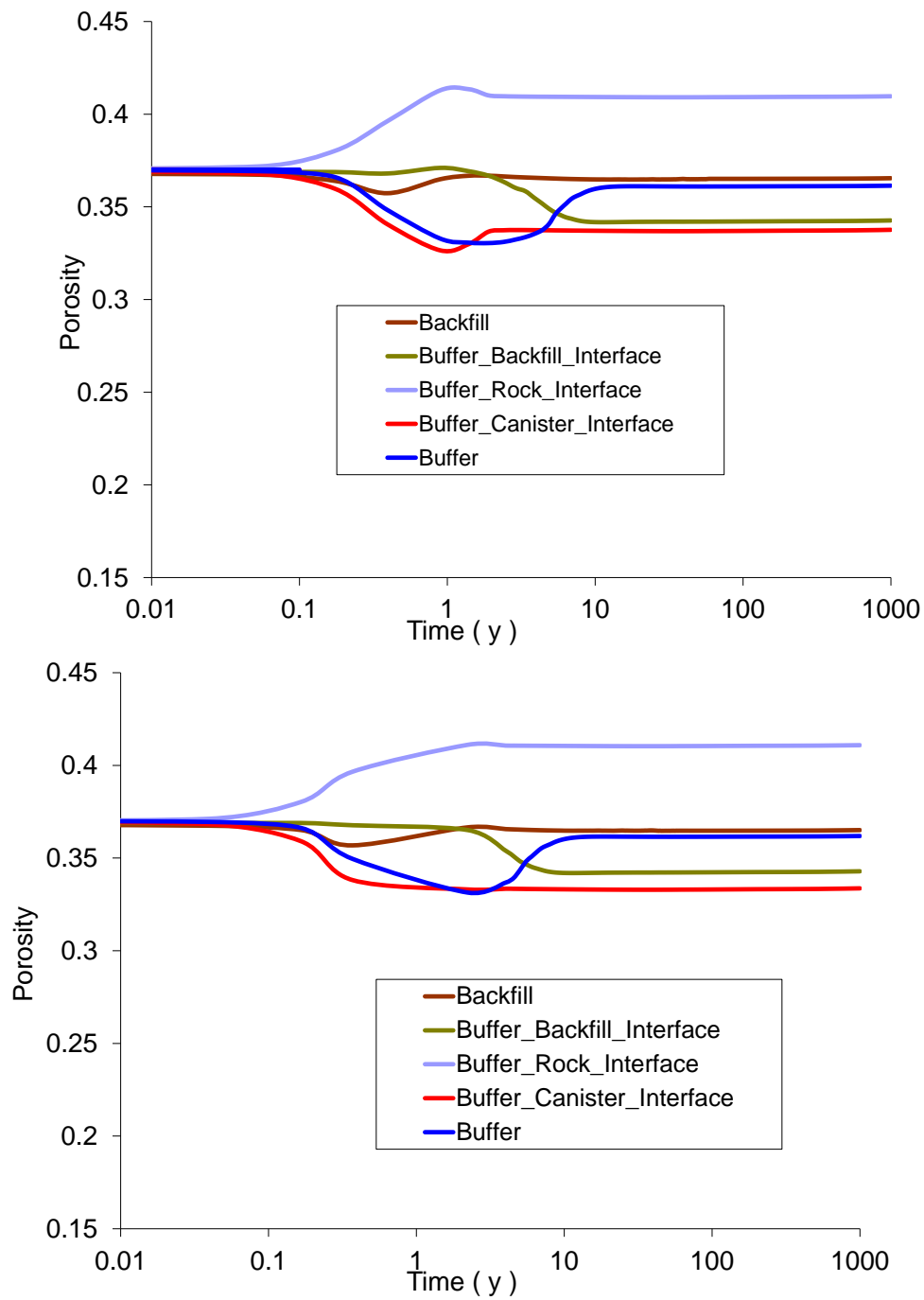


Figure 5-44. Evolution of porosity (Reference case above, Case C below)

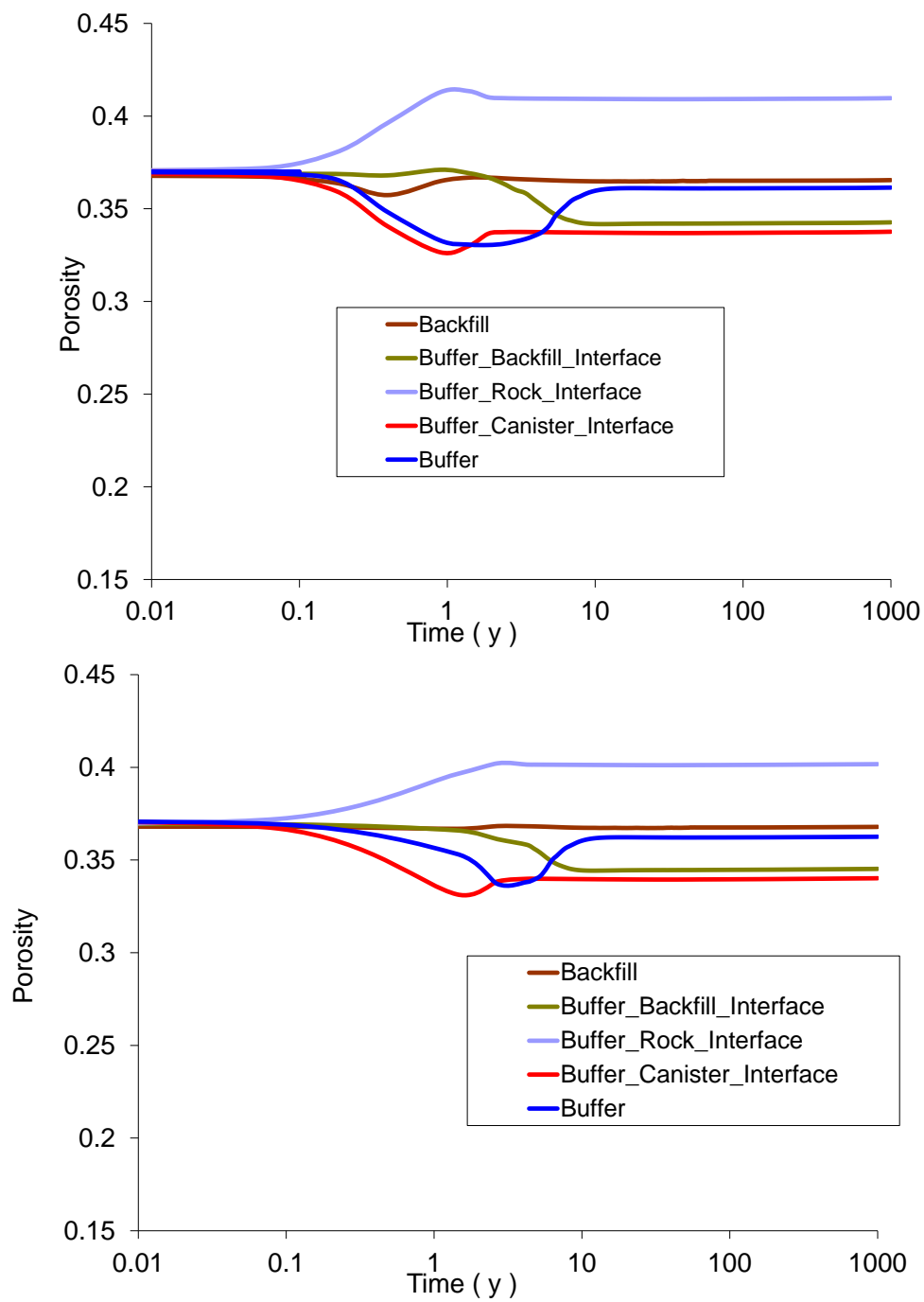


Figure 5-45. Evolution of porosity (Reference case above, Case D below)

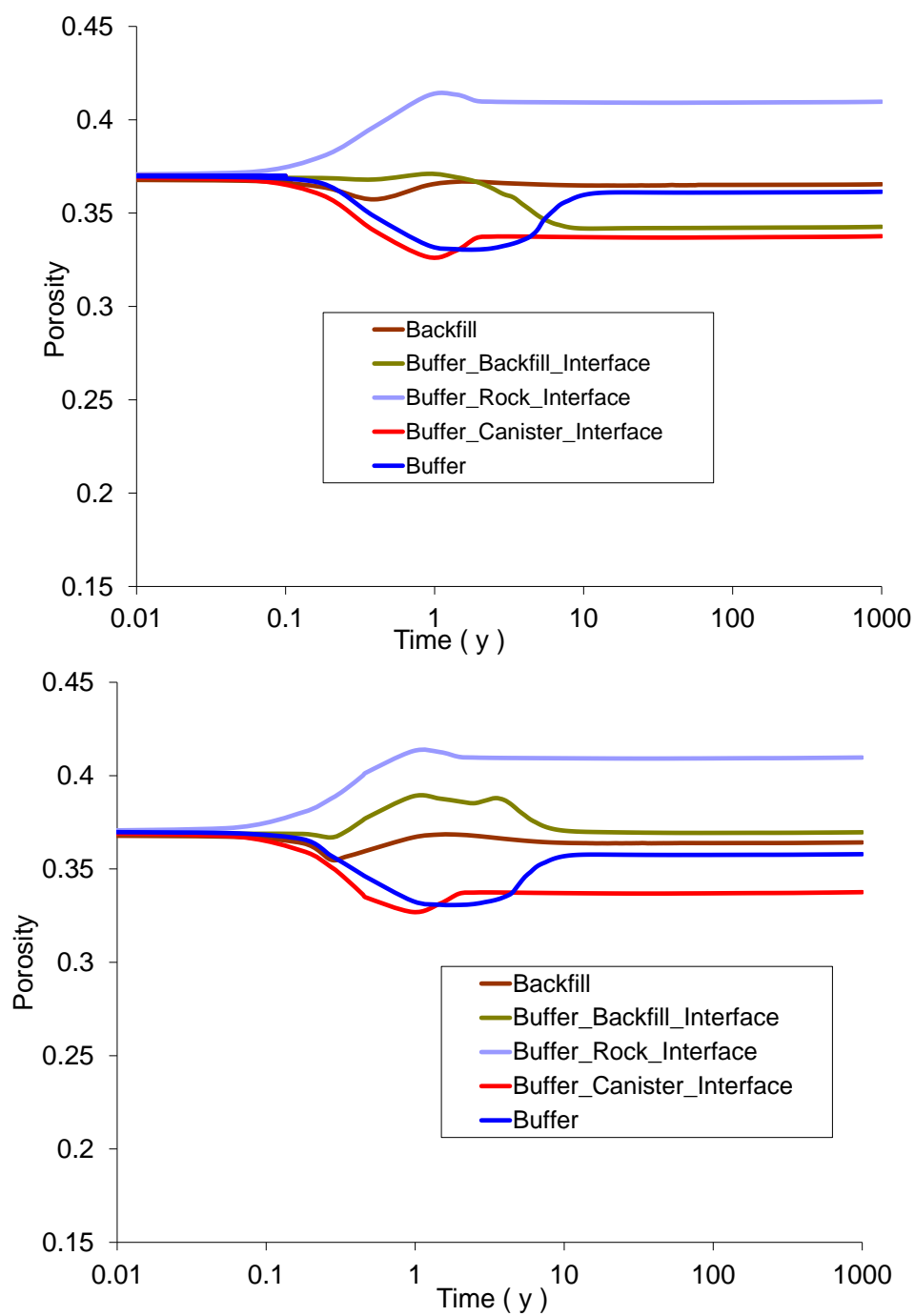


Figure 5-46. Evolution of porosity (Reference case above, Case E below)

5.3.6 Comparison of the evolution of the degree of saturation

As explained in the previous section, the time required to achieve full saturation is a fundamental part of the hydration problem. Intrinsic permeability is an important parameter. Figure 5-47 to Figure 5-51 show evolution of degree of saturation.

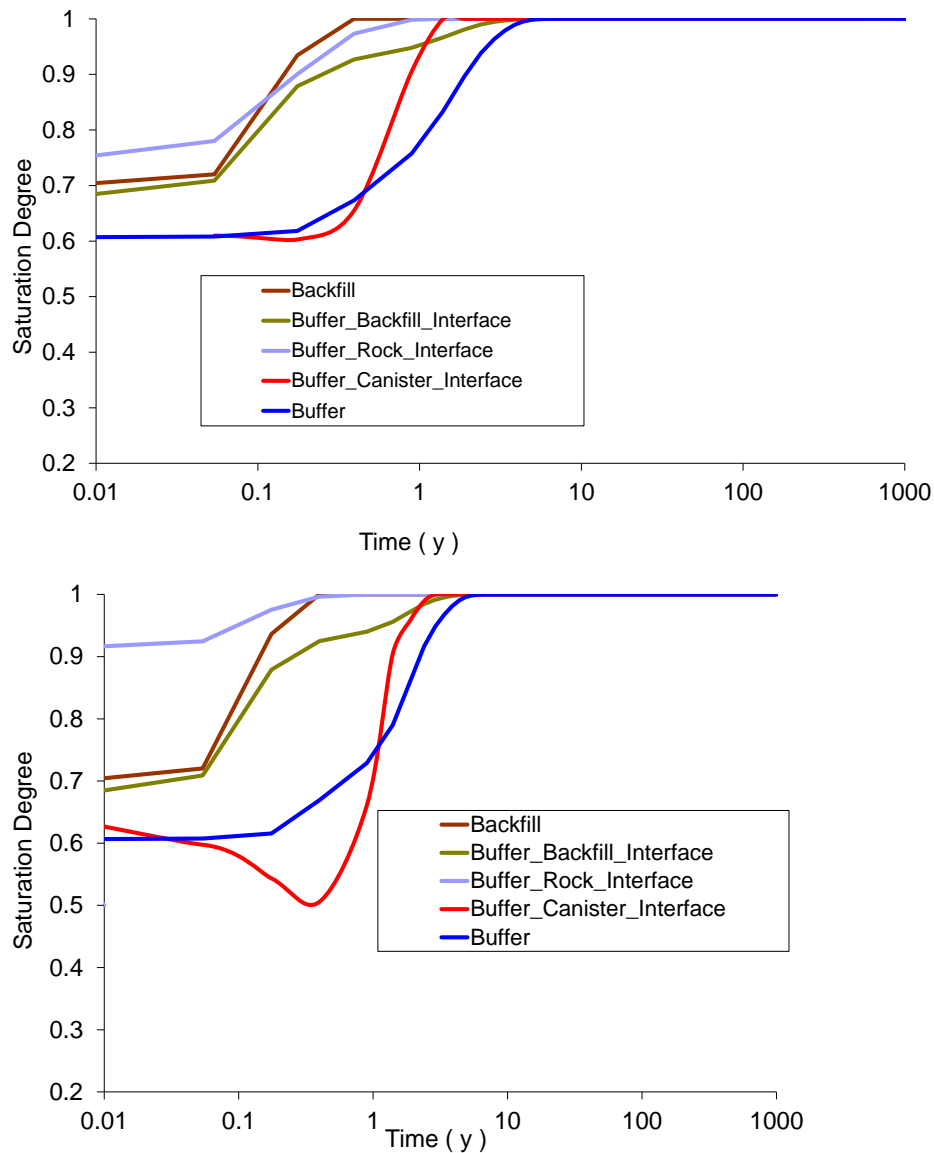


Figure 5-47. Evolution of the degree of saturation (Reference case above, Case A below)

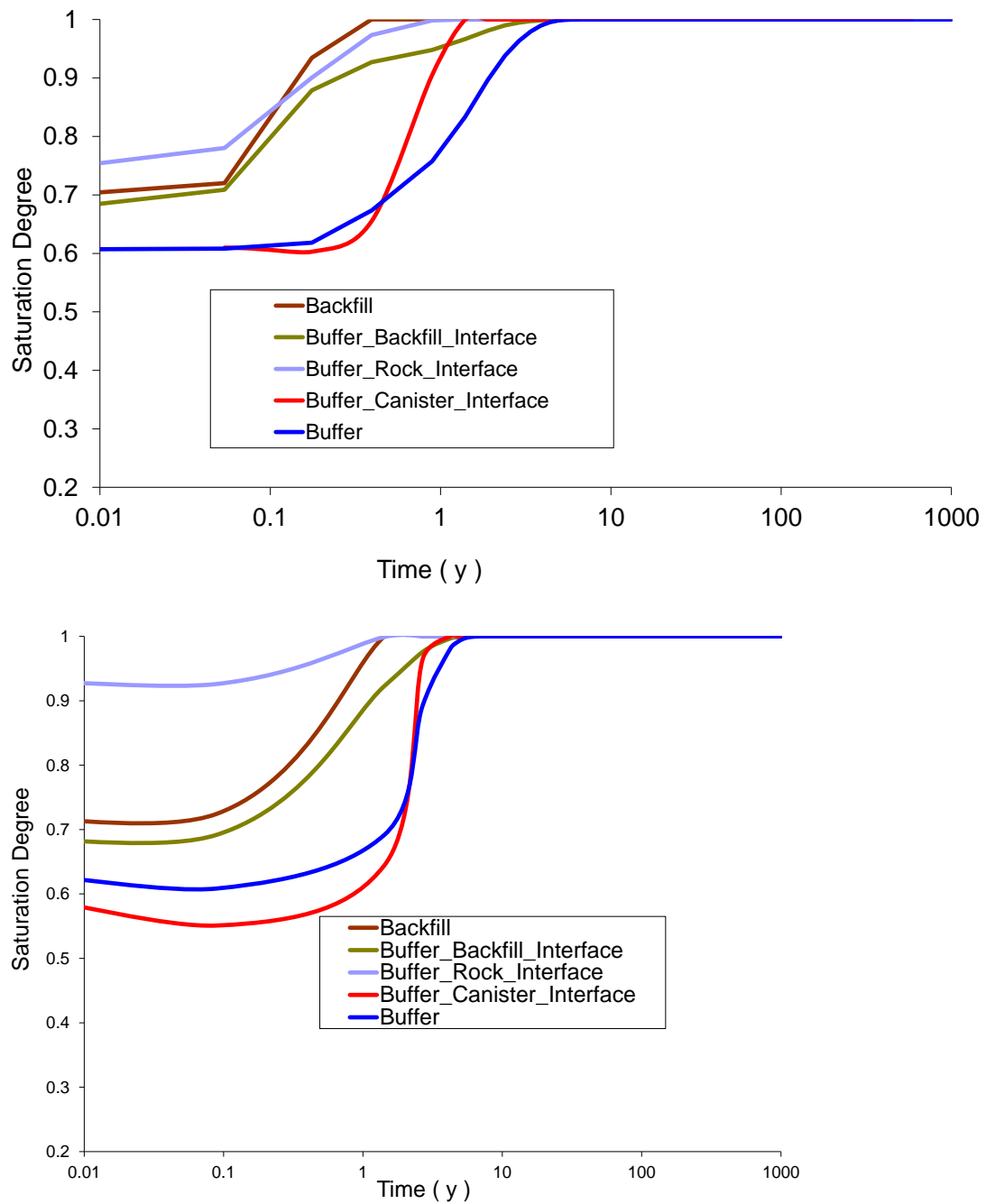


Figure 5-48. Evolution of the degree of saturation (Reference case above, Case B below)

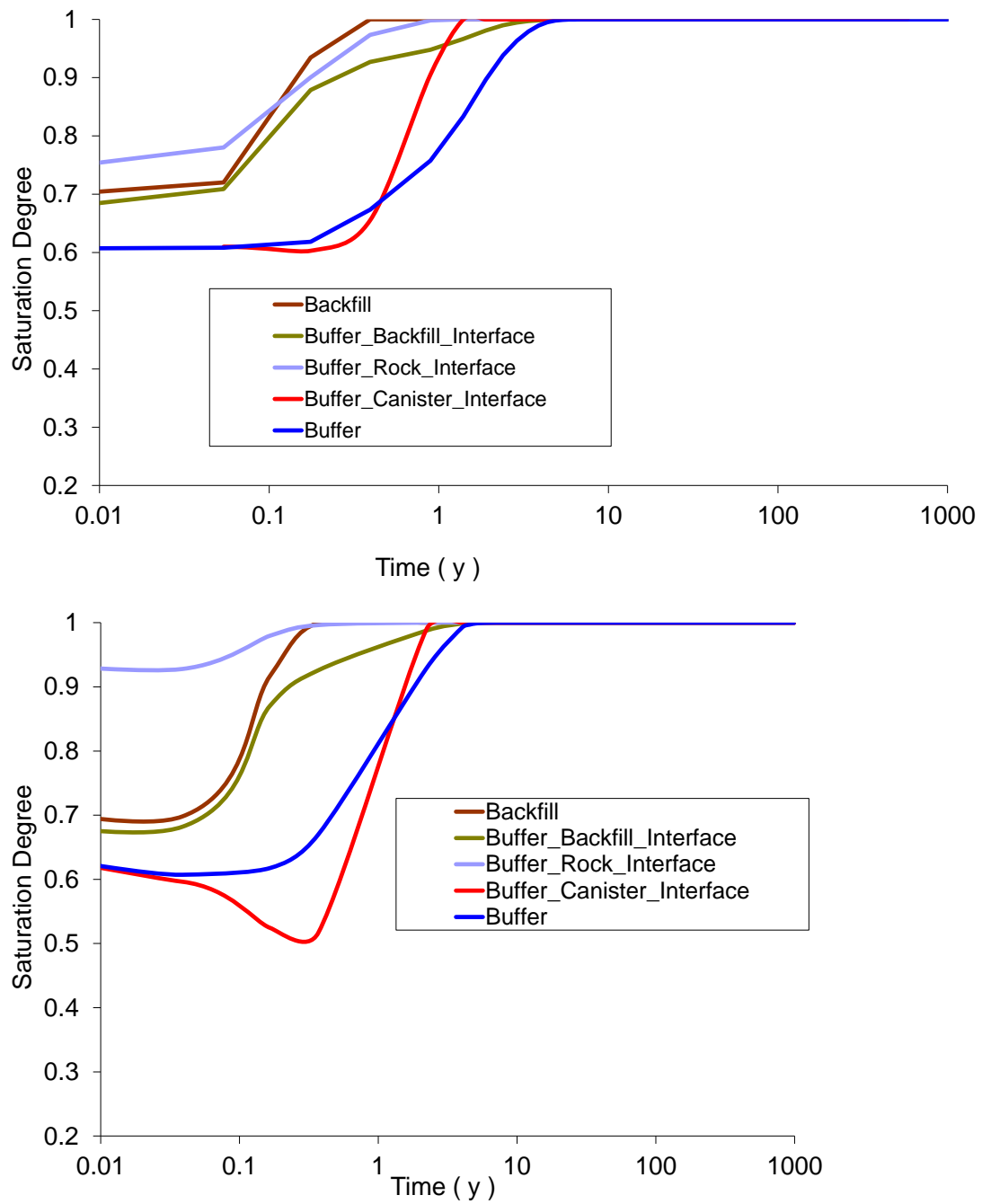


Figure 5-49. Evolution of the degree of saturation (Reference case above, Case C below)

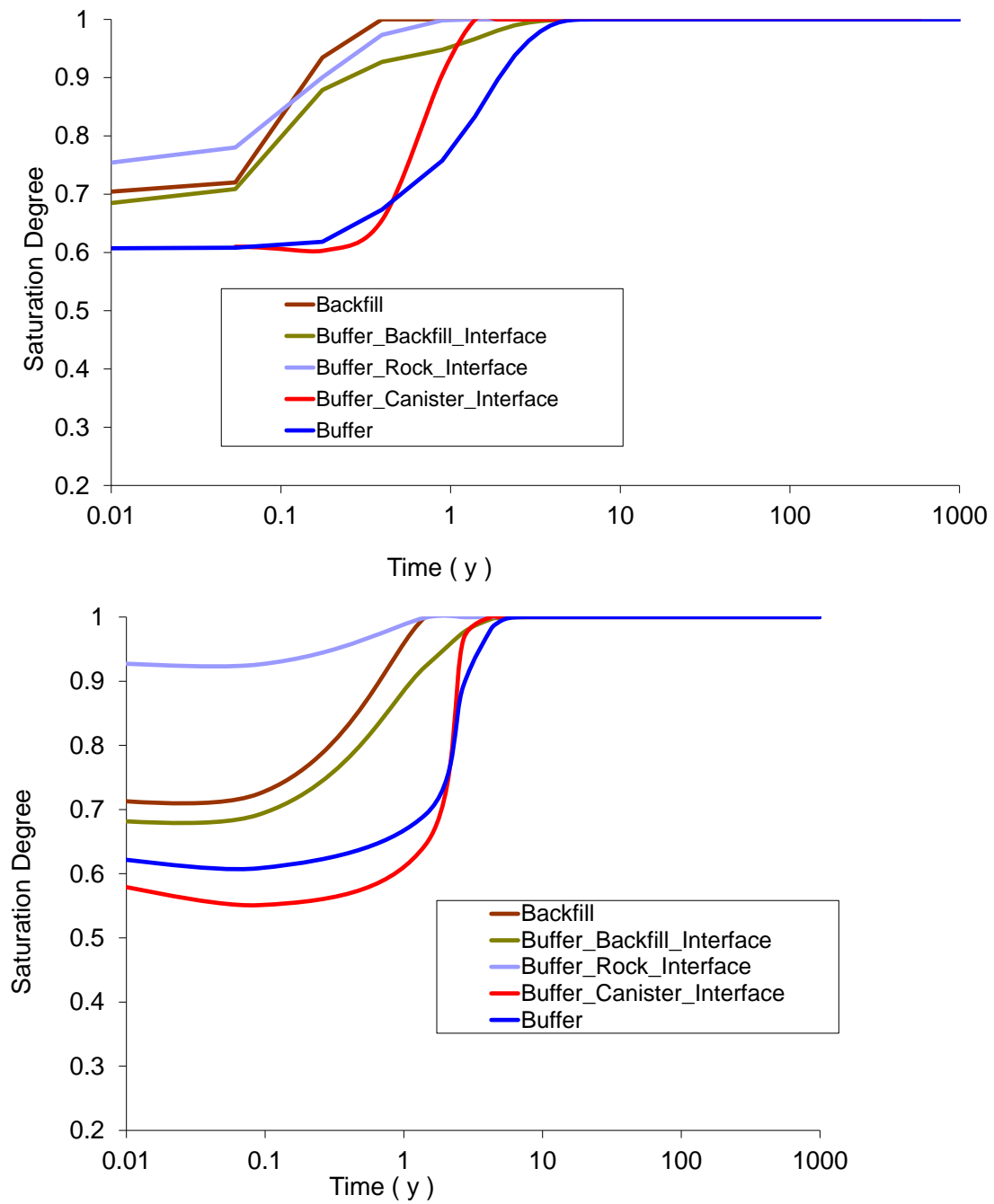


Figure 5-50. Evolution of the degree of saturation (Reference case above, Case D below)

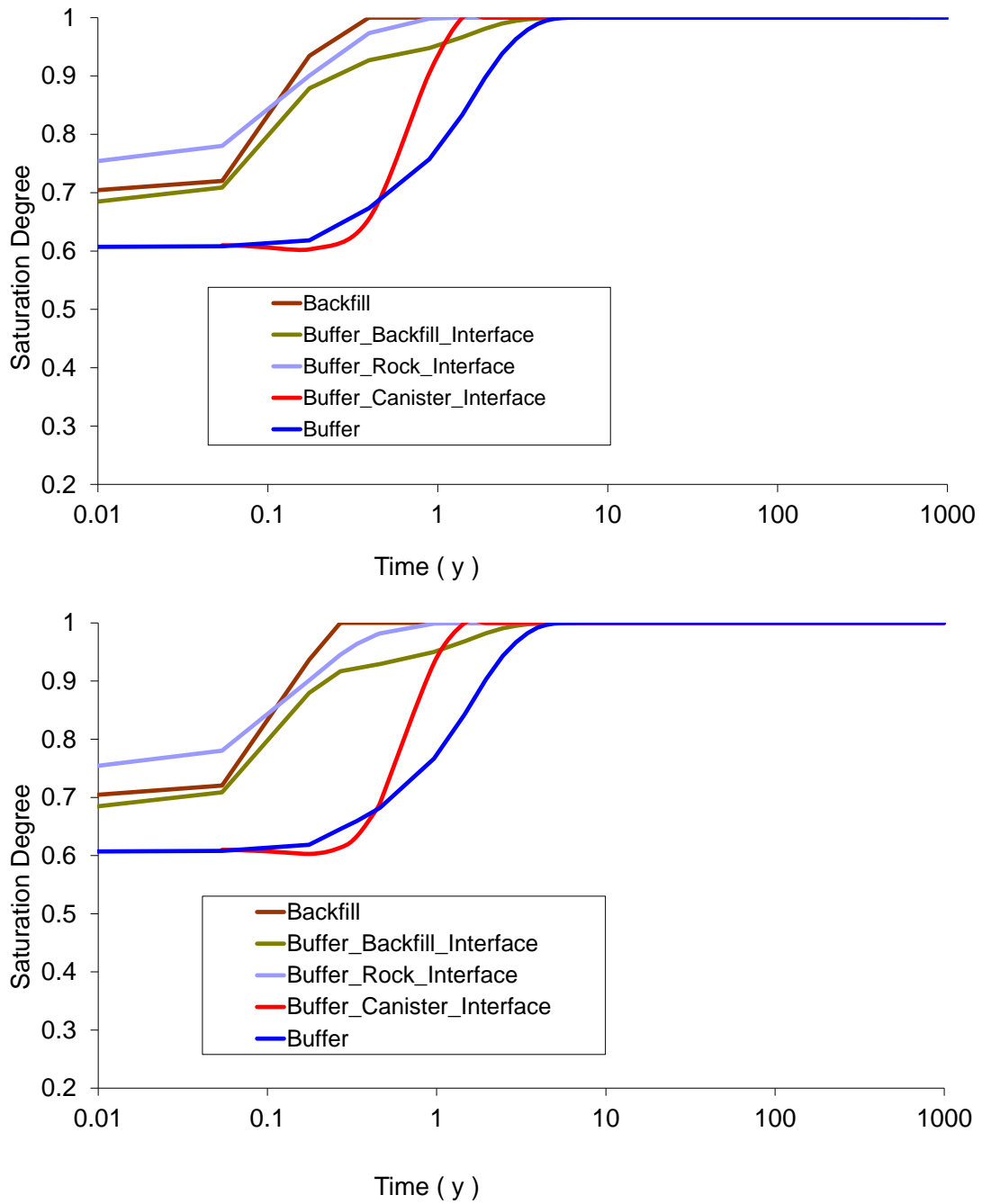


Figure 5-51. Evolution of the degree of saturation (Reference case and Case E)

Changing the permeability leads to different times for reaching full saturation. As explained in Section 3.2, even though the coefficient of tortuosity for molecular diffusion (τ) and power in the relative permeability law (λ) do not have a great influence on the time required for full saturation of the buffer, they affect the level of desaturation close to the canister.

5.3.7 Comparison of the evolution of axial effective stress

Figure 5-52 to Figure 5-57 show evolution of axial effective stress. It can be seen that there are no significant differences between the cases in terms of axial effective stress. Results for Case B and Case D are the most similar.

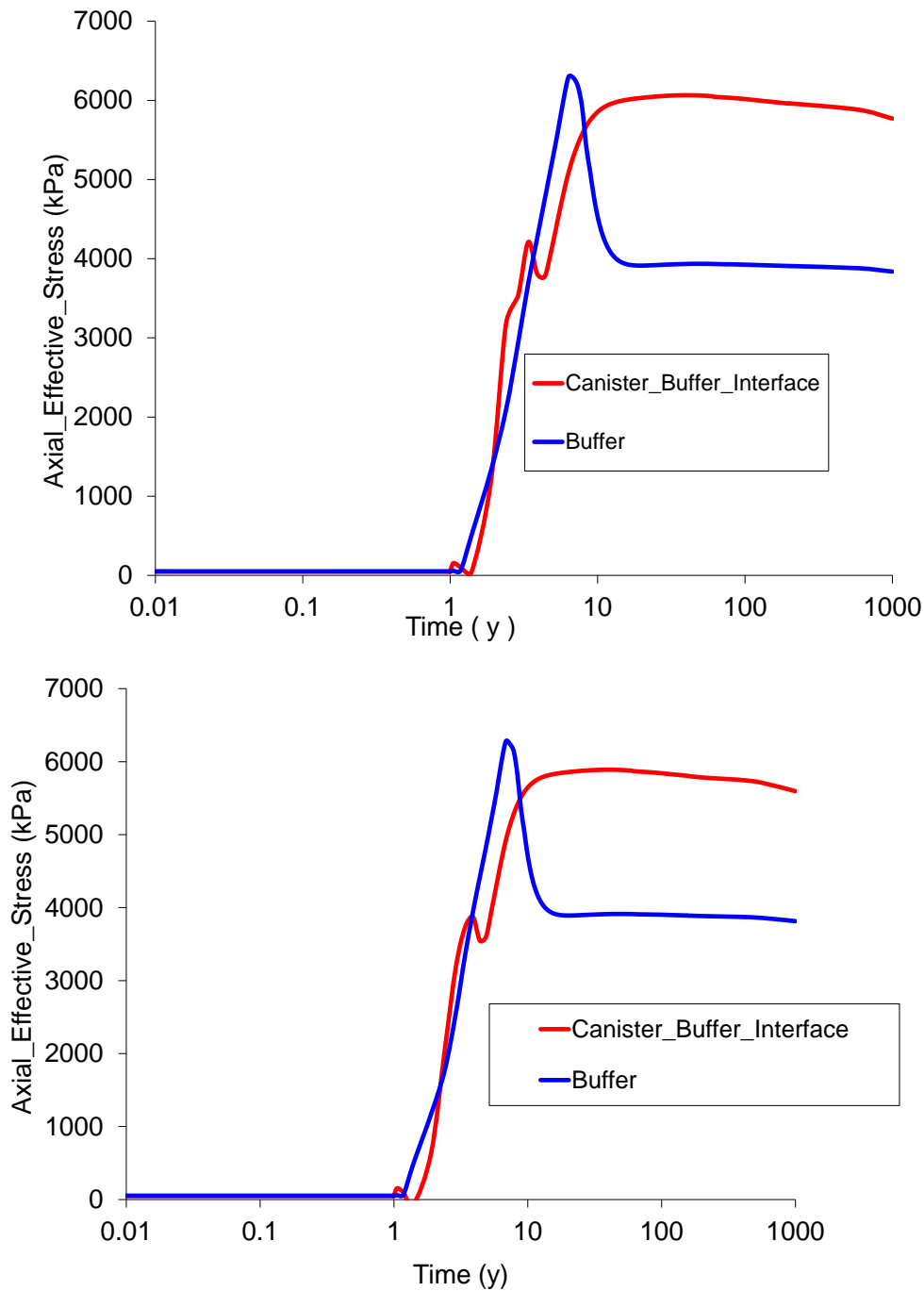


Figure 5-52. Evolution of axial effective stress (Reference case above, Case A below)

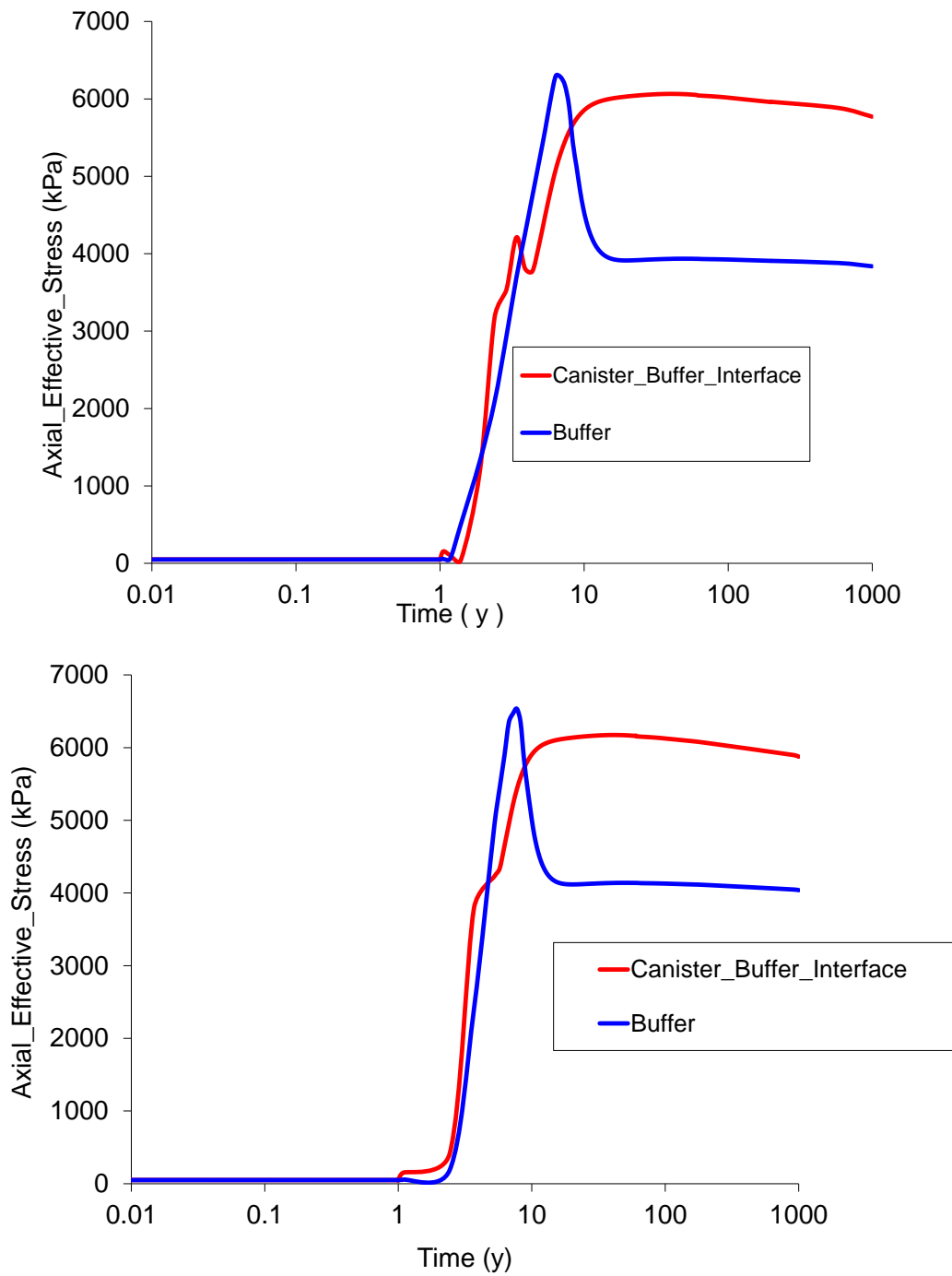


Figure 5-53. Evolution of axial effective stress (Reference case above, Case B below)

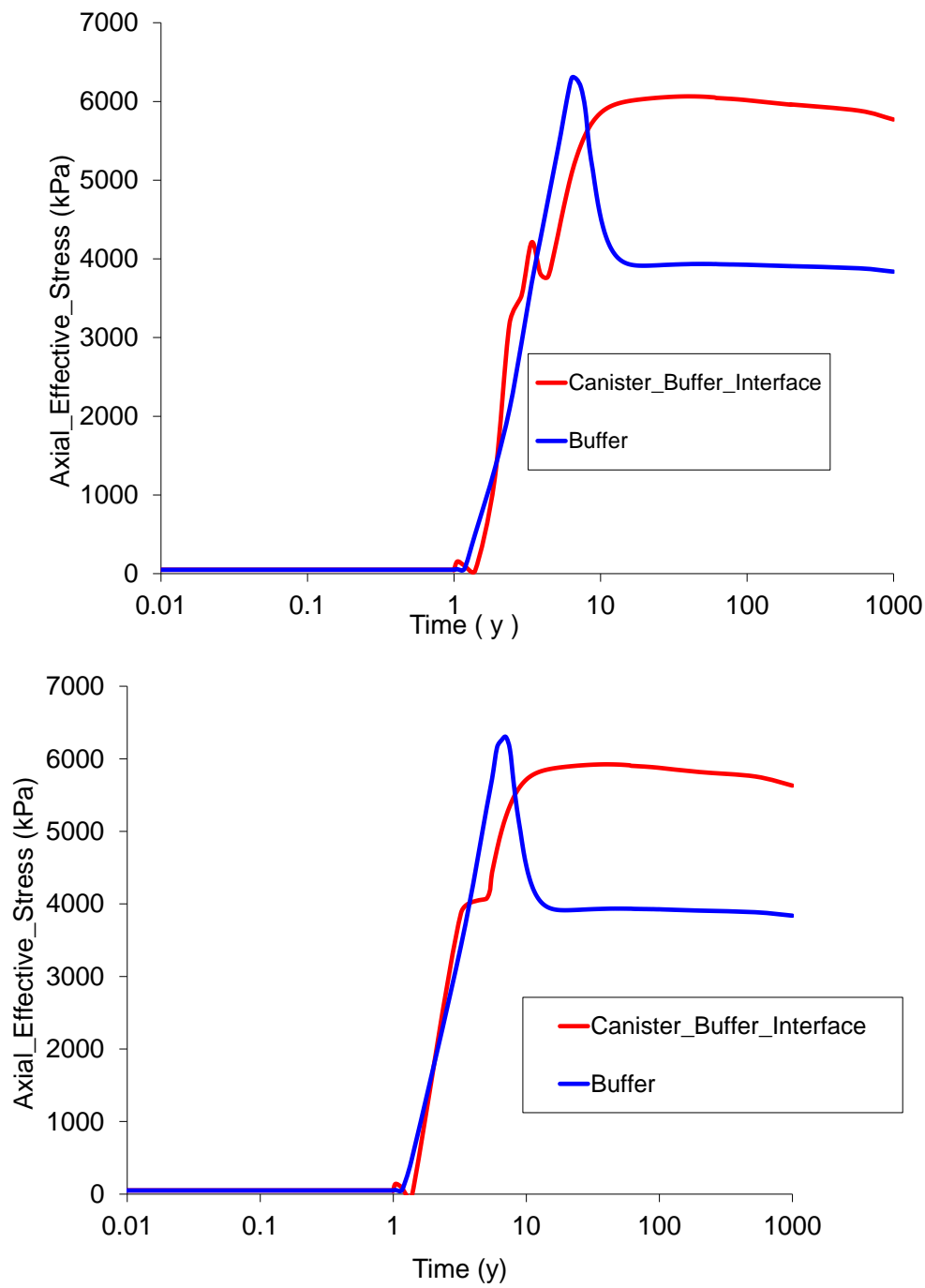


Figure 5-54. Evolution of axial effective stress (Reference case above, Case C below)

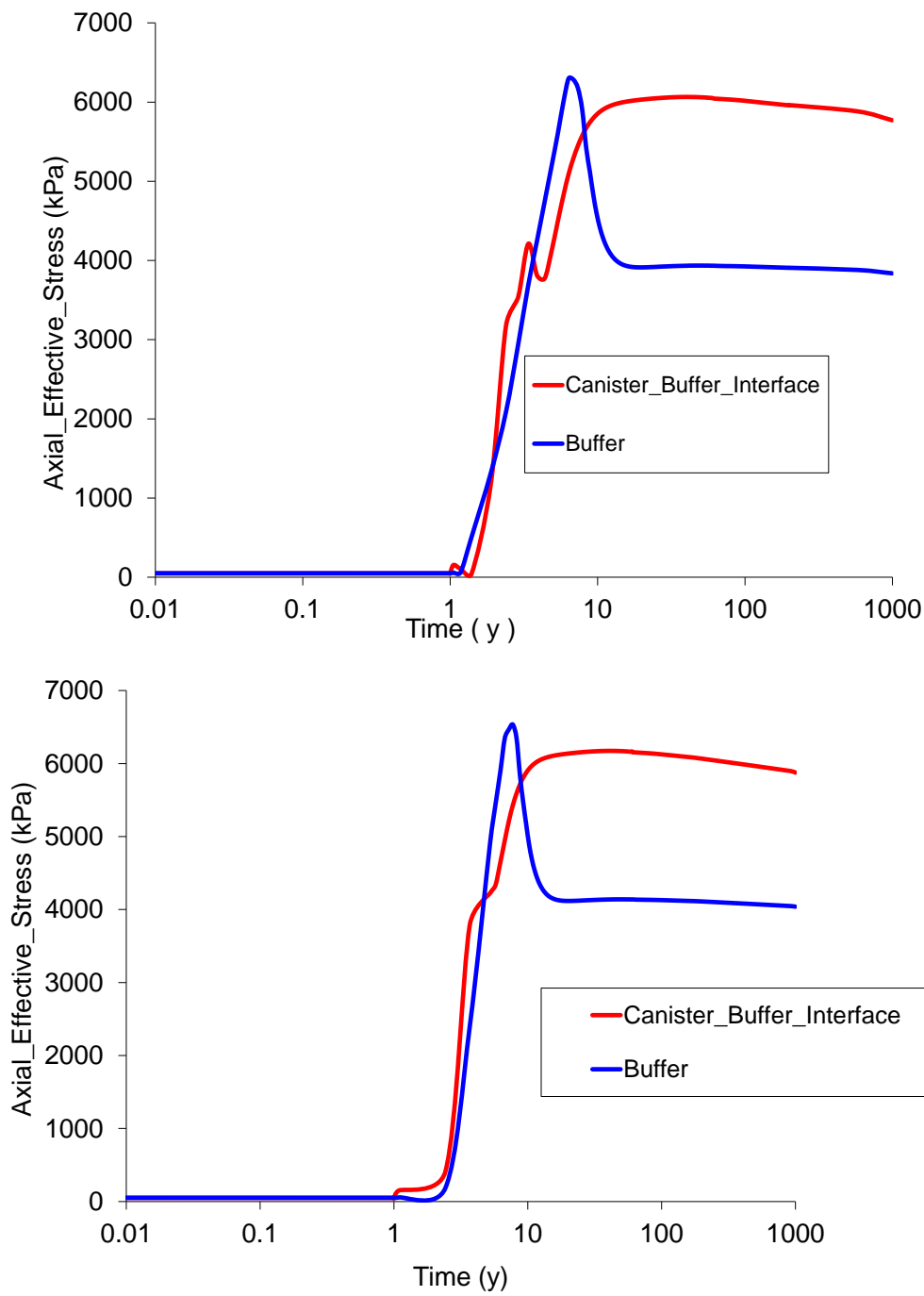


Figure 5-55. Evolution of axial effective stress (Reference case above, Case D below)

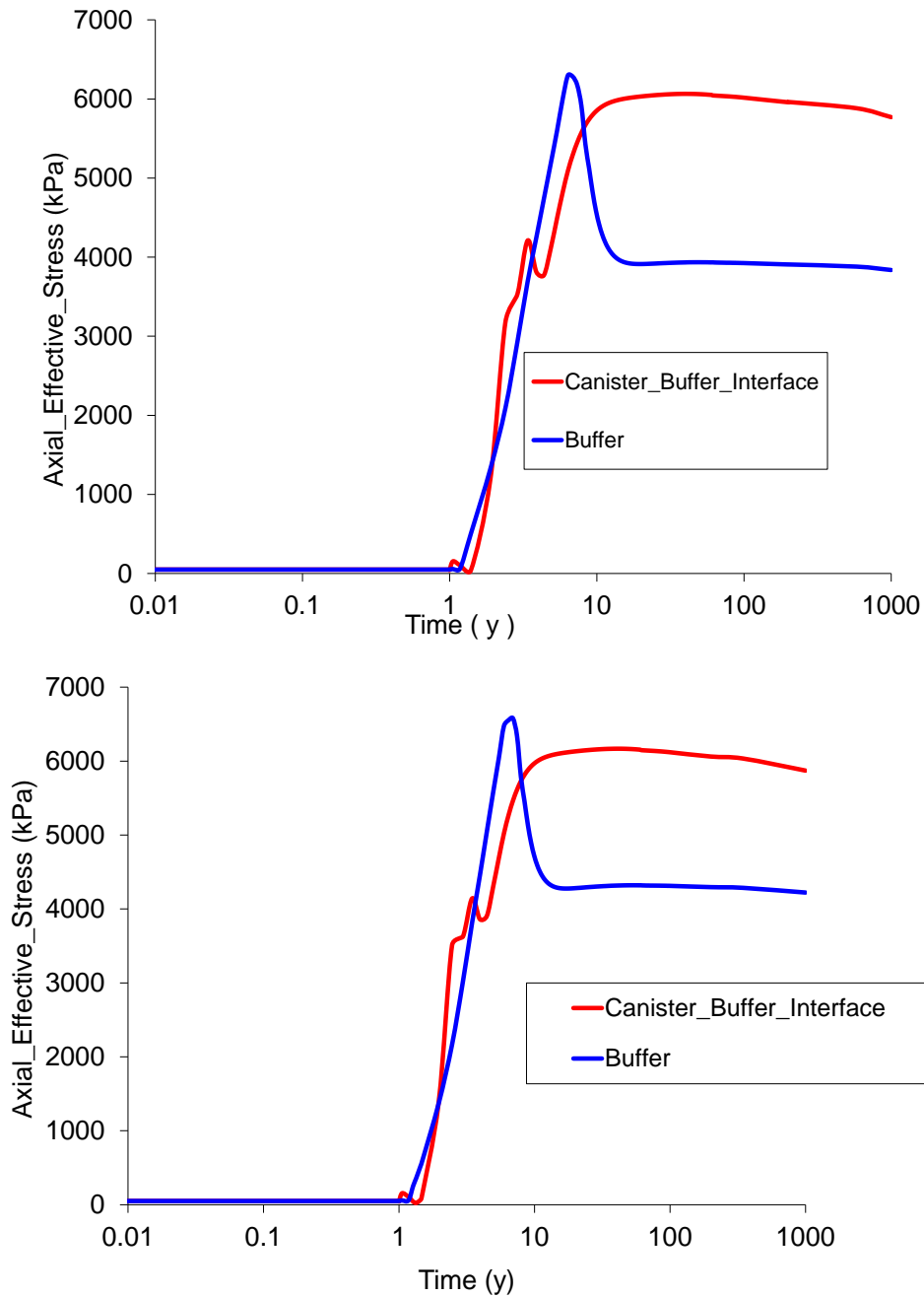


Figure 5-56. Evolution of axial effective stress (Reference case above, Case E below)

The excavation process is also simulated. As the figures show, there is no stress generation during the first year. After materials have been placed, stresses are generated and increase. When saturation is complete, axial effective stress starts decreasing at the buffer representative point and then becomes stable. At the canister-buffer interface, axial effective stress increases and then becomes stable after a period of time.

5.3.8 Comparison of the evolution of radial effective stress

Figure 5-57 to Figure 5-61 shows evolution of axial effective stress in five models.

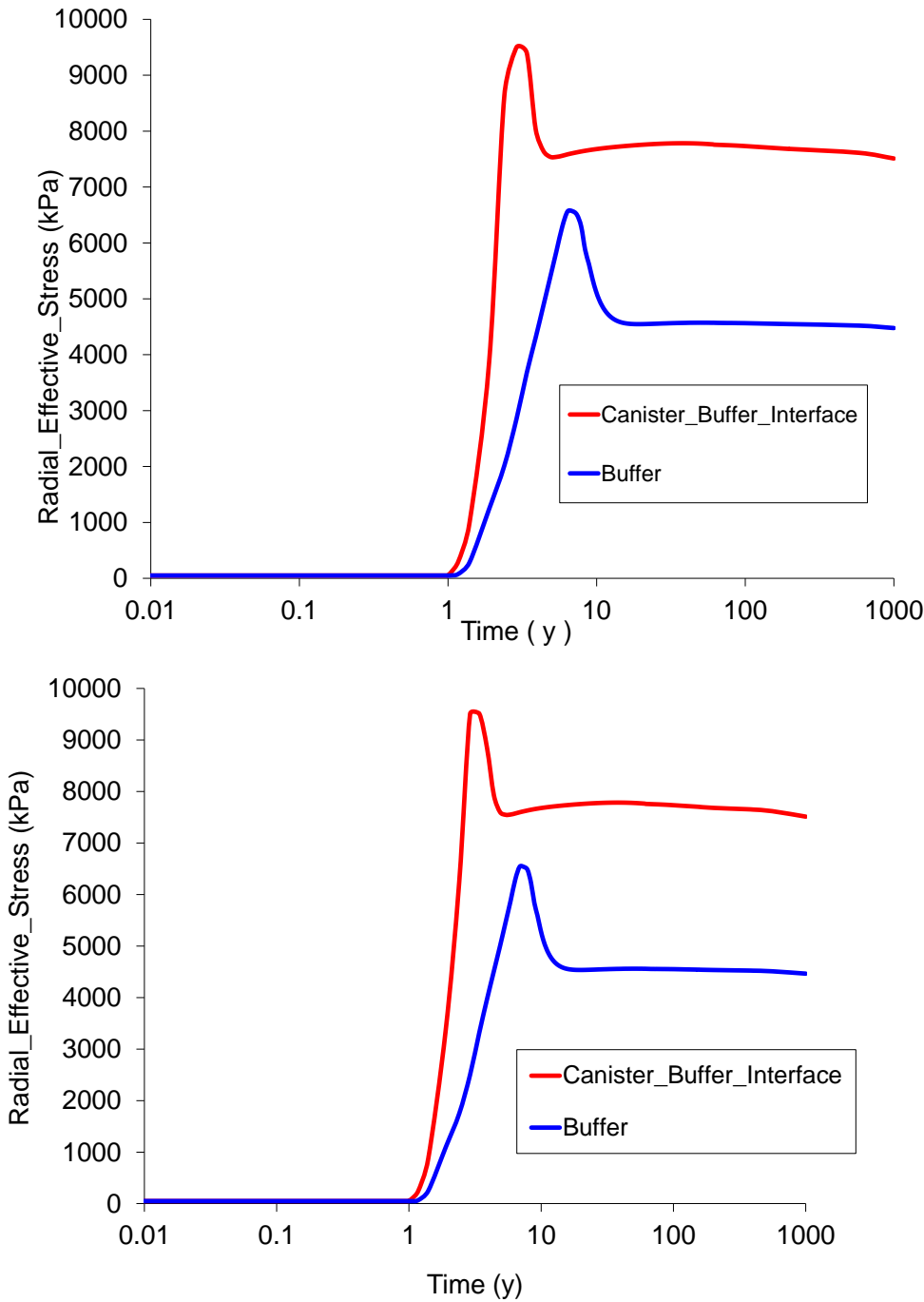


Figure 5-57. Evolution of radial effective stress (Reference case above, Case A below)

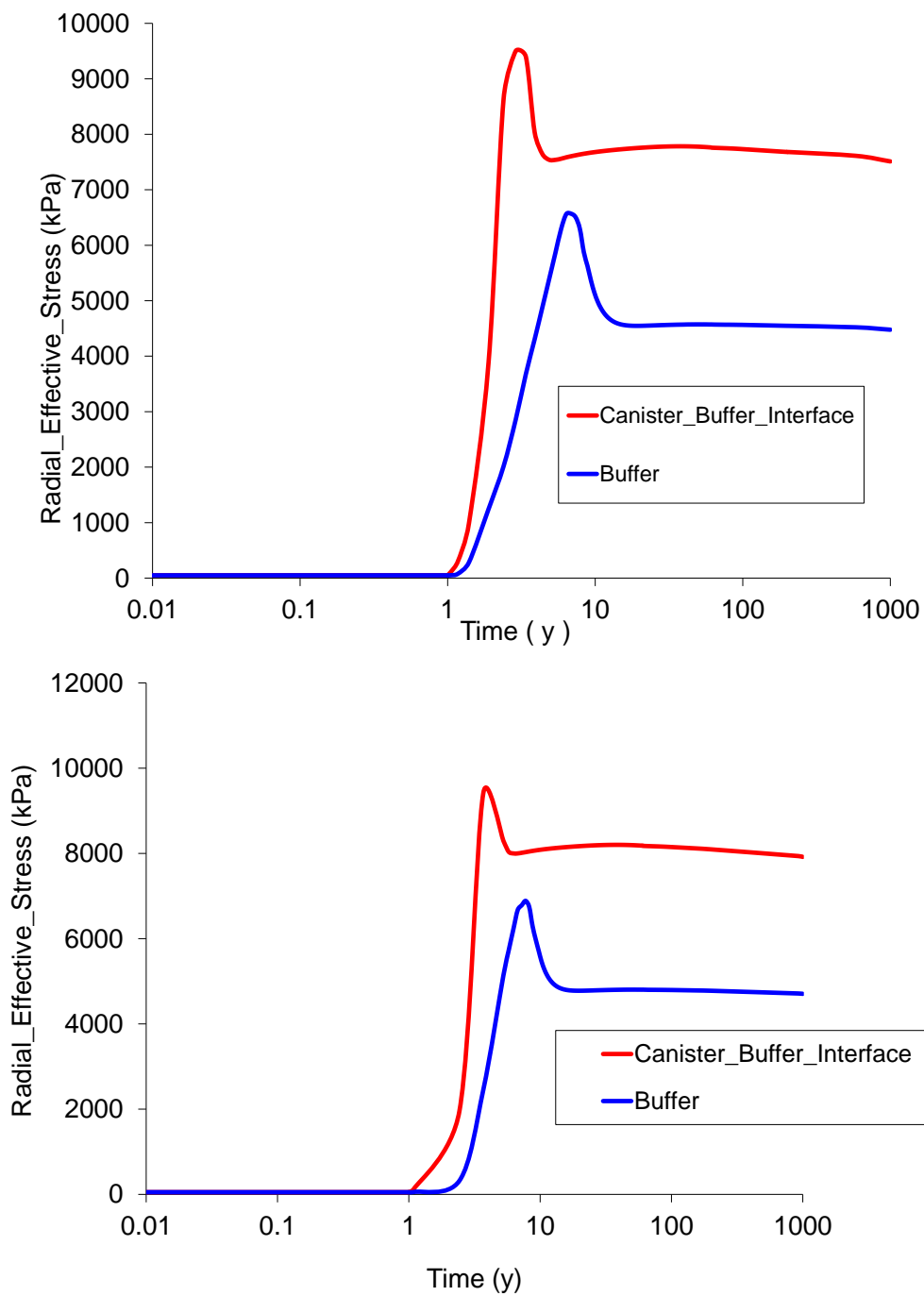


Figure 5-58. Evolution of radial effective stress (Reference case above, Case B below)

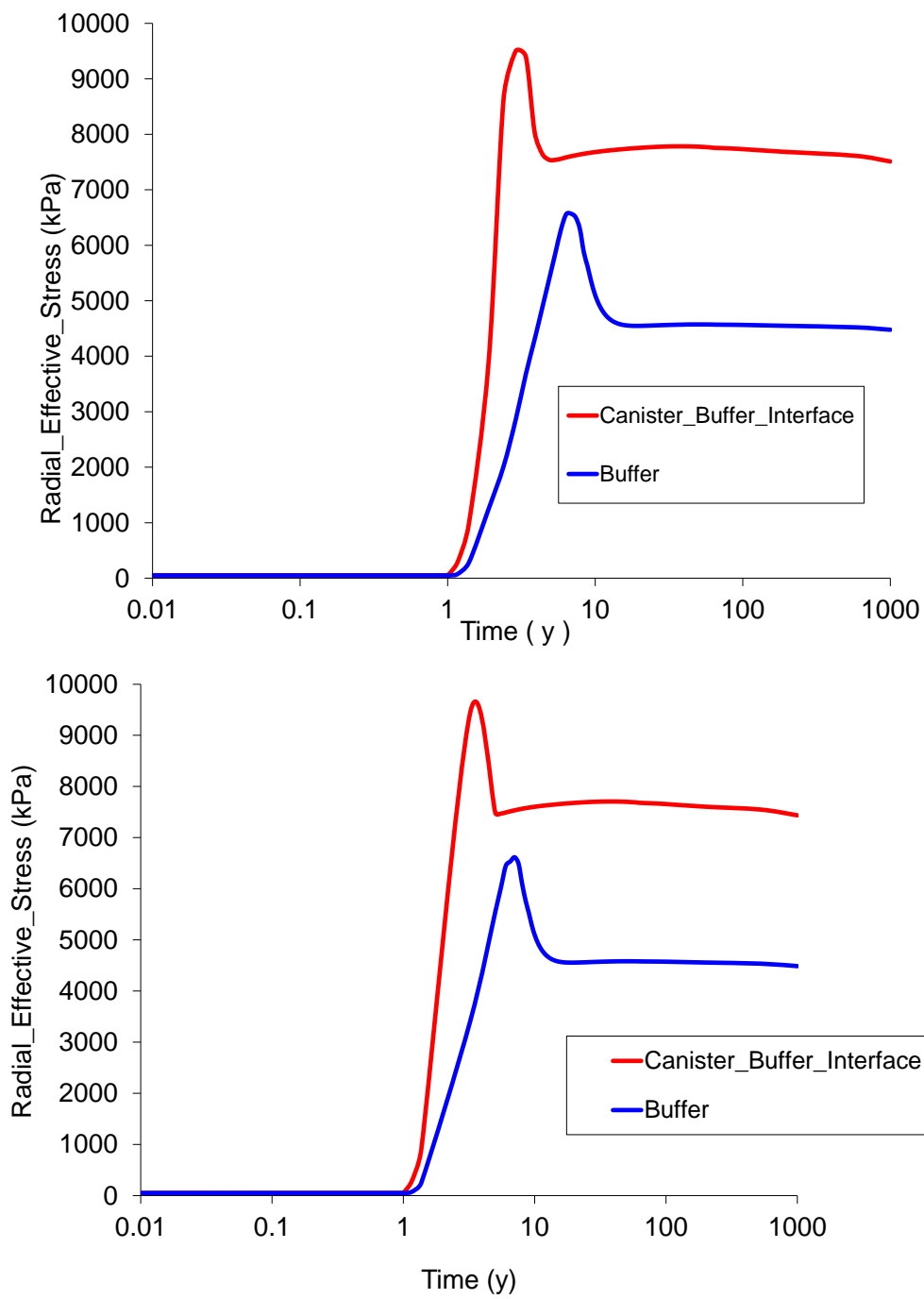


Figure 5-59. Evolution of radial effective stress (Reference case above, Case C below)

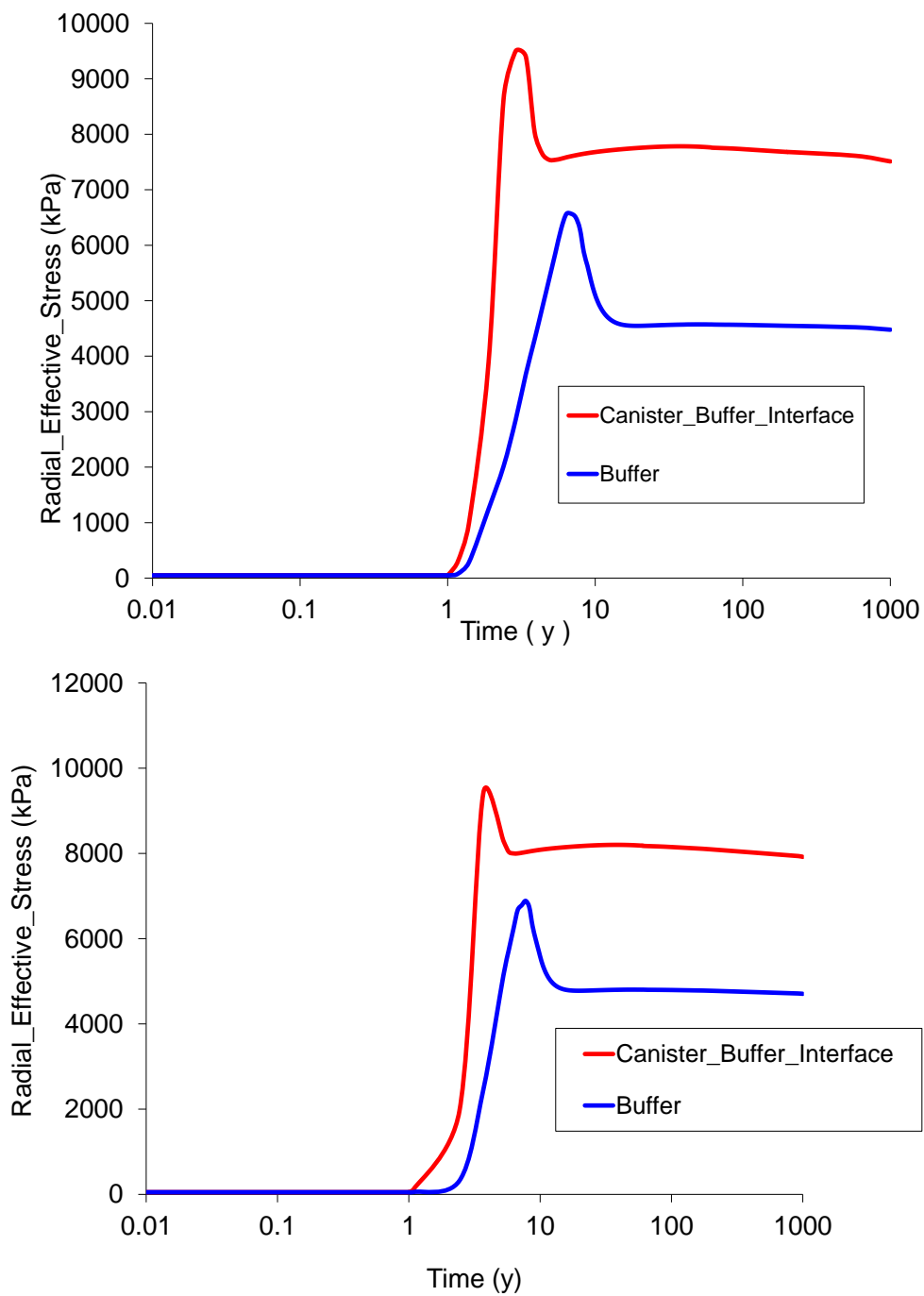


Figure 5-60. Evolution of radial effective stress (Reference case above, Case D below)

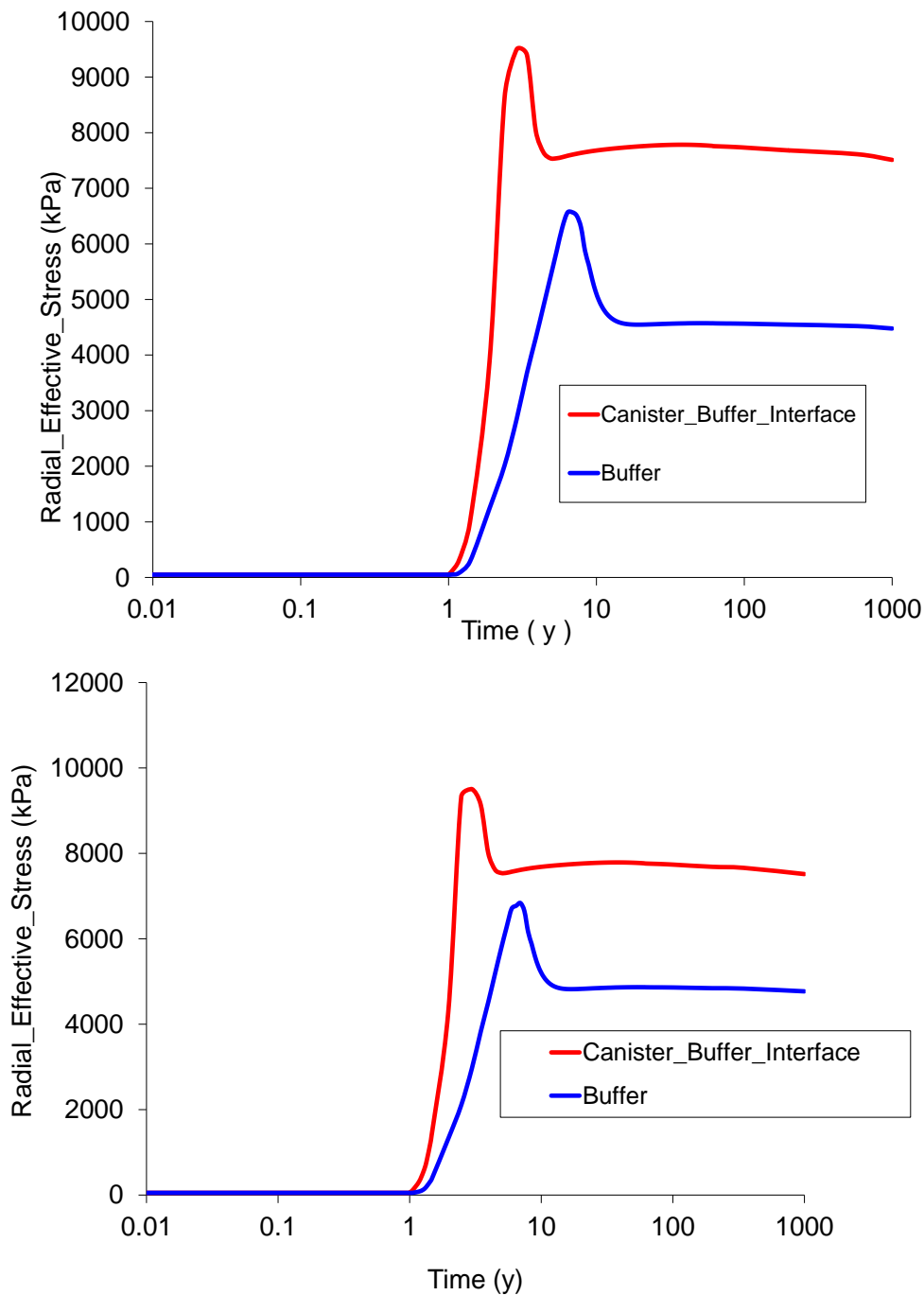


Figure 5-61. Evolution of radial effective stress (Reference case above, Case E below)

These figures also simulate the excavation process. The maximum values that stresses achieve in the buffer space are an important functional requirement of the repository. The figures in this section show that there are no significant differences between the five cases and the Reference case.

5.3.9 Comparison of the evolution of vertical displacements

Figure 5-62 to Figure 5-66 shows vertical displacement in two representative point in the five models.

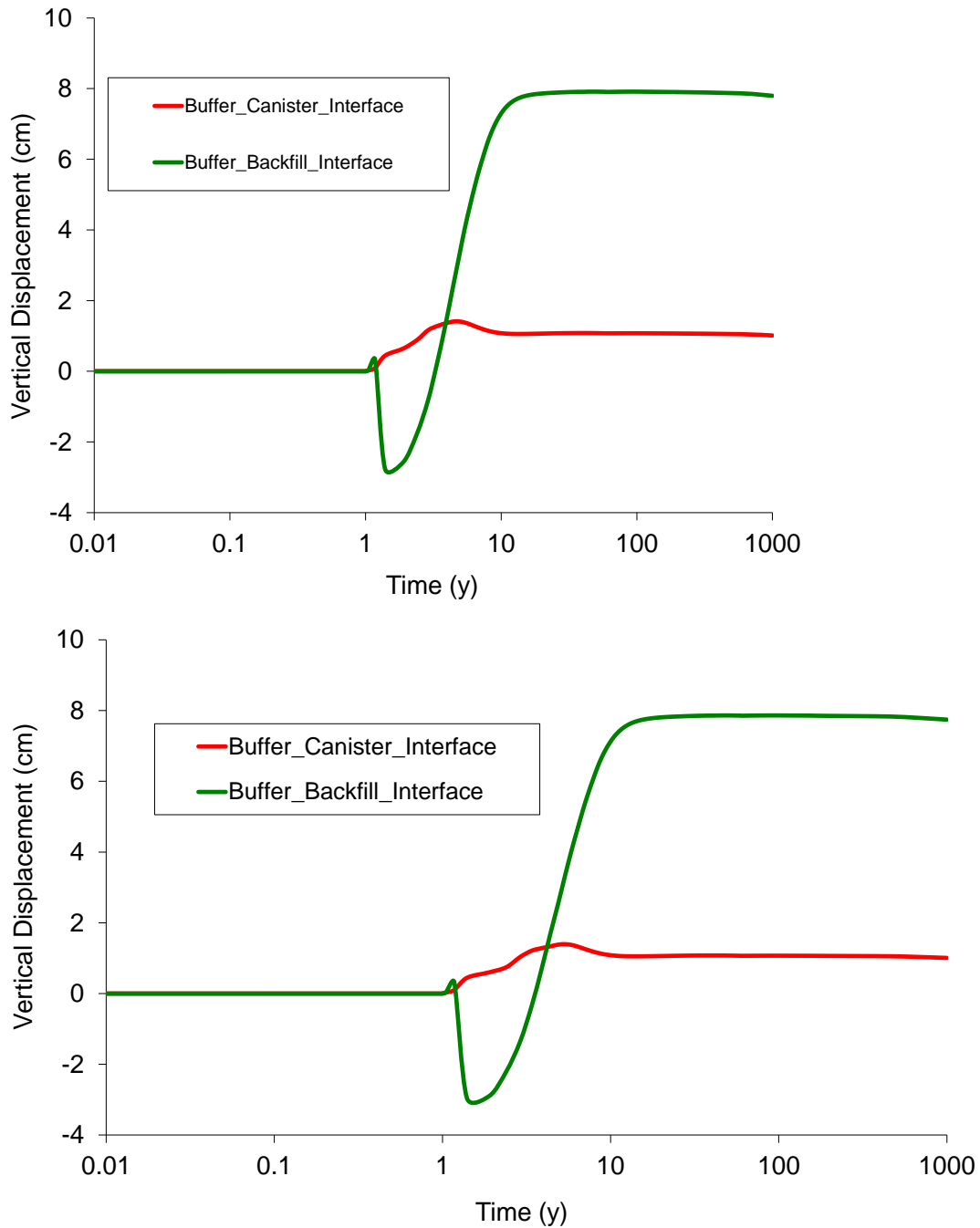


Figure 5-62. Evolution of vertical displacements (Reference case above, Case A below)

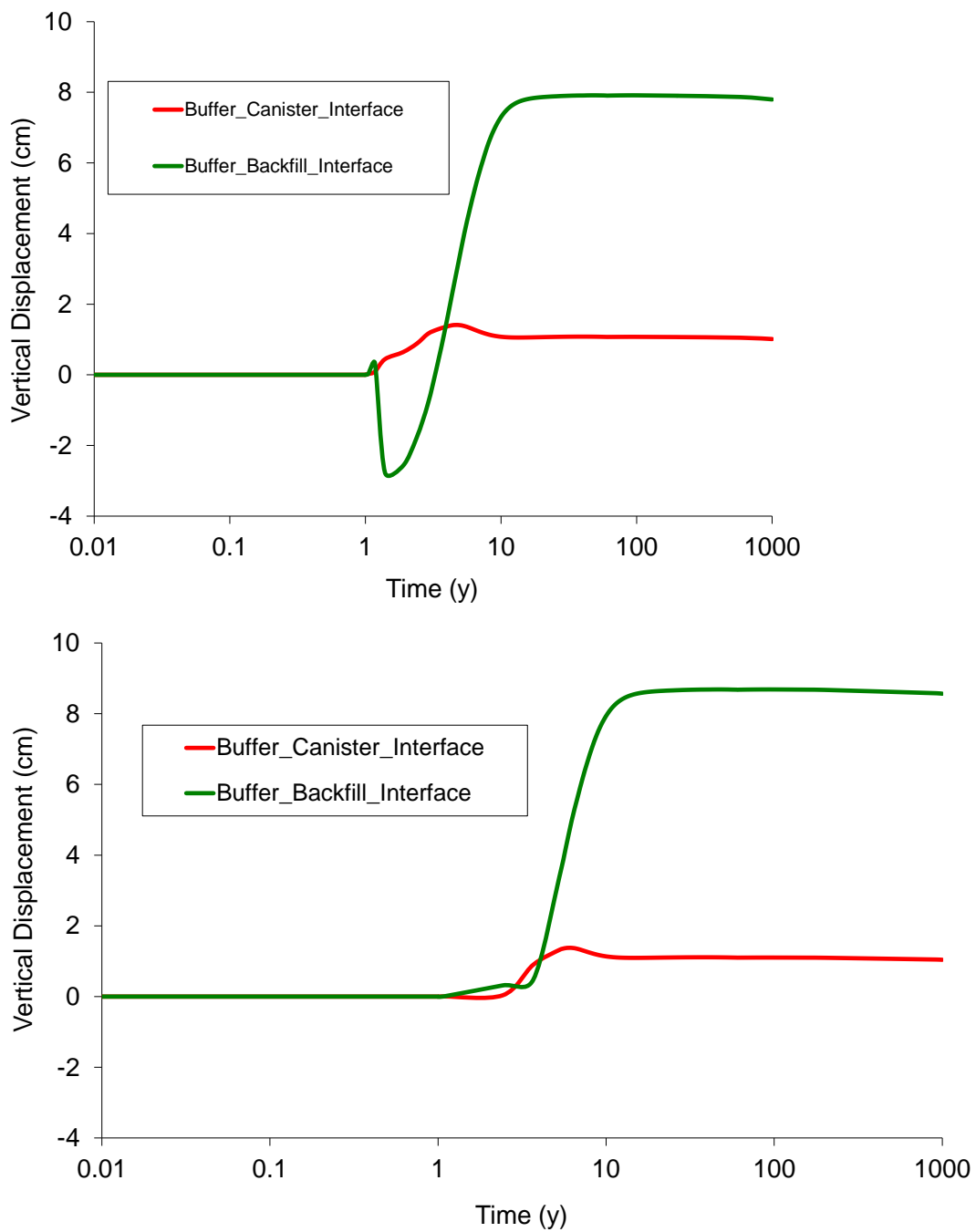


Figure 5-63. Evolution of vertical displacements (Reference case above, Case B below)

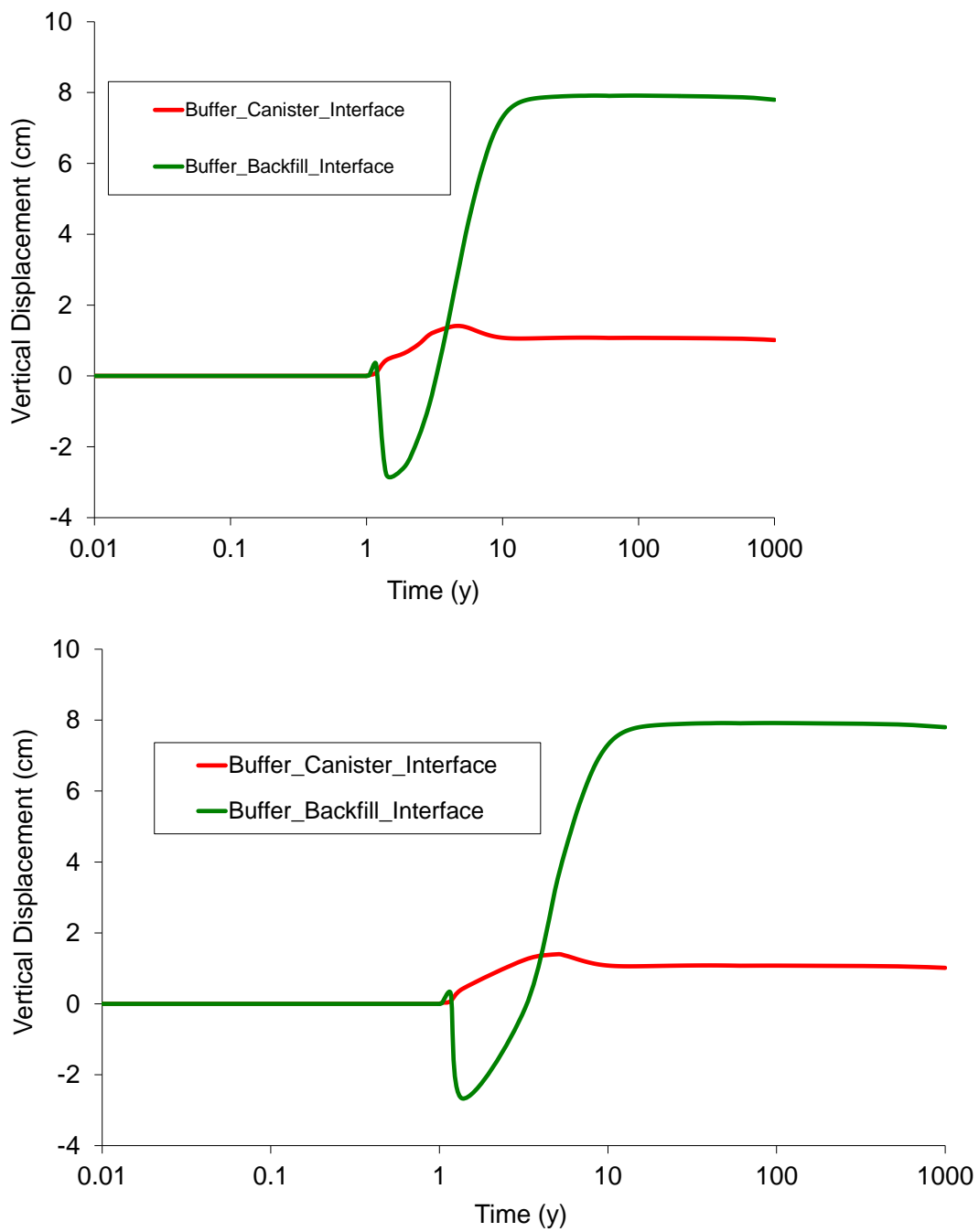


Figure 5-64. Evolution of vertical displacements (Reference case above, Case C below)

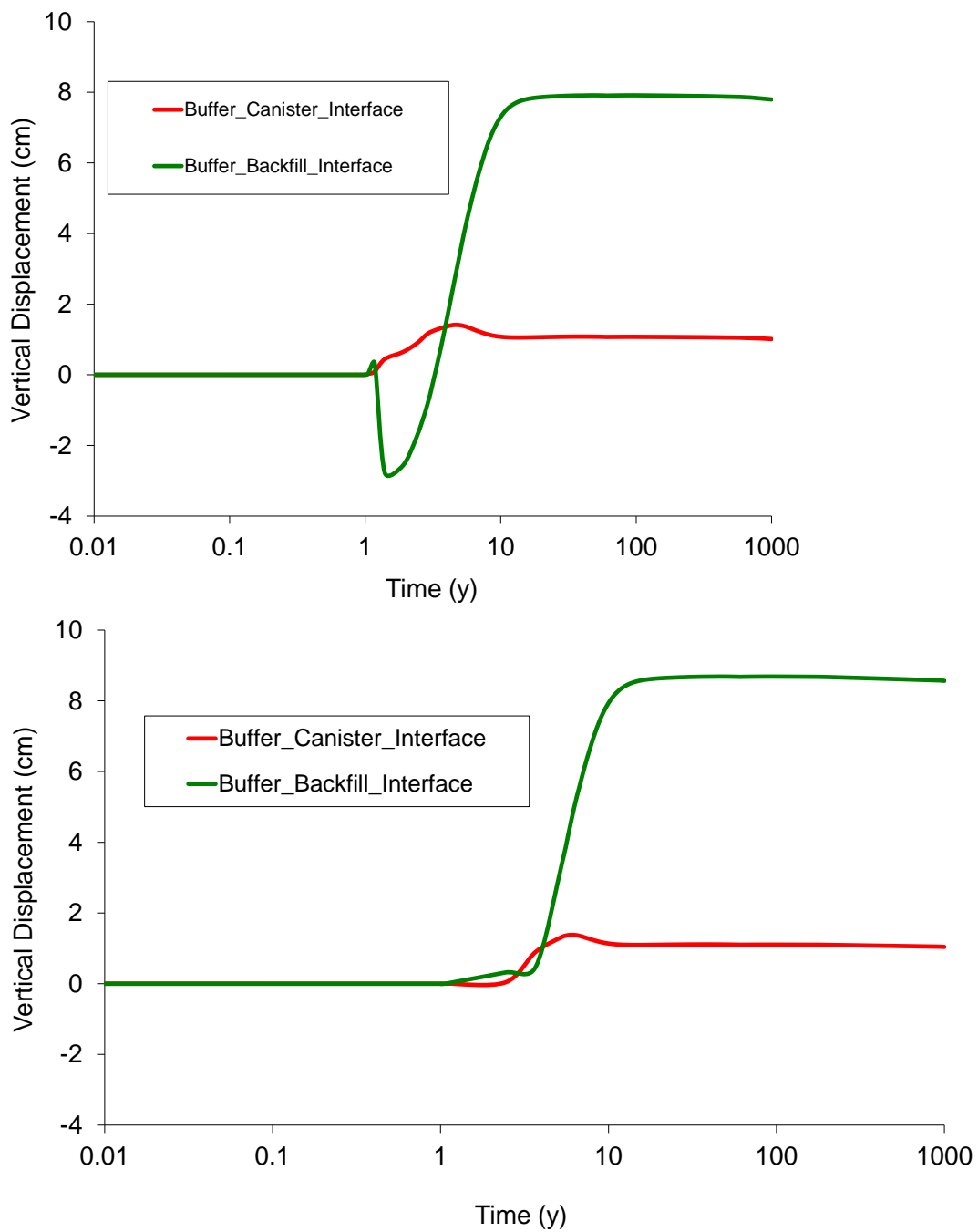


Figure 5-65. Evolution of vertical displacements (Reference case above, Case D below)

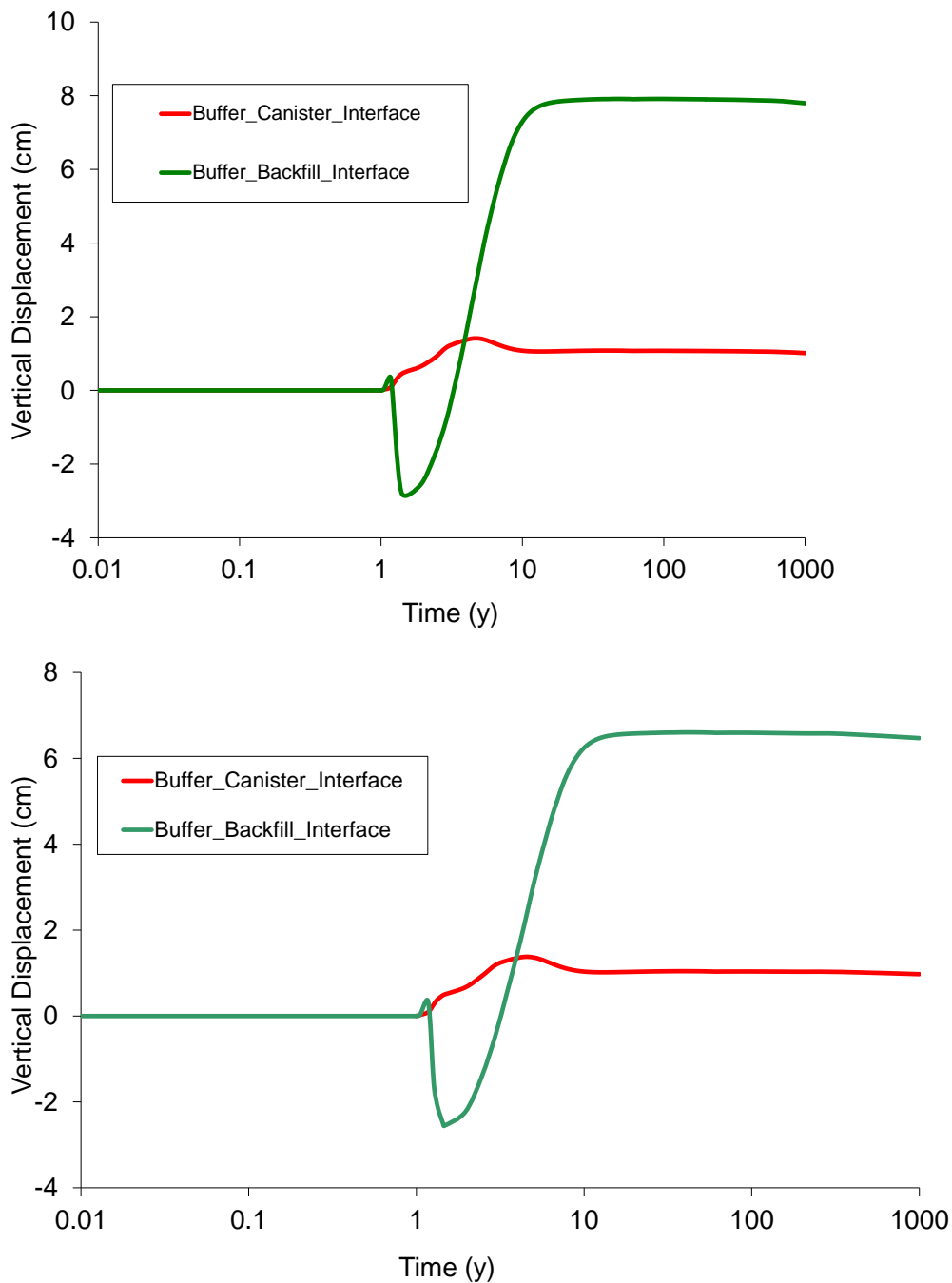


Figure 5-66. Evolution of vertical displacements (Reference case above, Case E below)

As they are a mechanical factor, vertical displacements deserve special attention. It is clear from the figures that Case B and Case D exhibit different behaviour. In both cases, the low intrinsic permeability of the rock affects the drying and swelling behaviour of the buffer material. In the other cases, the backfill initially moves down because it compresses the buffer, but starts moving upwards as soon as the buffer begins to swell.

5.4. Conclusions for THM modelling of deposition hole

Fundamental functional parameters of critical design parameters for a deposition tunnel of repository were investigated. The thermal calculations and the BBM parameters used in simulating THM evolution are explained in the previous chapters.

In connection with understanding the relative importance of intrinsic permeability, the power parameter in the relative permeability law [Eq. (5-2)], the tortuosity factor in the molecular diffusivity law [Eq. (5-4)] and pre-consolidation stress in the backfill were examined in the sensitivity analyses. Even though these parameters do not have a strong influence on the time required to achieve full saturation of the buffer, they do have some effect on liquid pressure, and thereby desaturation, close to the canister. It was seen that the maximum temperature achieved in the buffer is not affected by the fact that the buffer being unsaturated in its initial state.

The maximum canister temperature is reached 30 years after deposition. The maximum temperature of 80°C determined for the canister-buffer interface meets this design criterion for the canister.

The buffer space between the canister and the rock wall is fully saturated after 4-5 years. Heating results in variations in liquid pressure, and it decreases strongly near the canister. Evaporation of water occurs. When the heating process starts, evaporation induces a porosity reduction near the canister.

Total stress increase as the buffer hydrates. If pore pressure becomes positive, total stress increases accordingly. Effective stress also increases.

The density of the buffer around the canister depends on the stress-displacement balance at the buffer surface and is a functional requirement. Modelling results indicate that vertical displacements in the buffer-backfill interface will be in the range 7-8 cm. When the canister is first deposited, the buffer material will dry out because of heating and the buffer-backfill interface will move down. Once swelling begins, the buffer-backfill interface will start moving upwards.

In its initial stages, the POSIVA ONKALO Project concept envisages gaps between the canister and the buffer material, and between the buffer material and the rock wall. In

this chapter, the whole of the buffer was considered to be a homogeneous space and no account was taken of the effects of gaps or any initial lack of homogeneity. Additional simulations have been carried out in the subsequent chapter to examine these effects using a more detailed geometry in the vicinity of the canister.

6. GAP EFFECT ON THM ANALYSIS

This chapter of thesis describes the effect of the existence of an air-filled gap located between the canister and the bentonite buffer on the long term Thermo-Hydro-Mechanical (THM) behavior of the future nuclear waste repository in Olkiluoto.

The presence of the 10 mm air gap has some influence on the thermal, hydraulic and mechanical response of the deposition tunnel. The closure of the gap is controlled by the swelling deformation developed as the bentonite buffer saturates. Under unsaturated conditions, the buffer will not transfer heat efficiently and that may disturb heat dissipation and leads to somewhat higher canister temperature.

The water supply is affected by the permeability of the different elements and in particular by the permeability of the host rock formation. Hence, hydraulic conductivity of the rock also influences the gap closure time. A coupled Thermo-Hydro-Mechanical (THM) analysis of the deposition tunnel has been performed including the gap element. The finite element program Code_Bright is used to perform the modeling calculations. THM modeling of air gap element is performed in two stages. A sensitivity analysis has been performed in order to explore the effect of the permeability of the host rock.

6.1. Introduction

The repository will consist of a series of deposition holes in the bedrock. Bentonite buffer rings will surround the copper canisters containing spent fuel. As a protecting and isolating barrier between the waste canisters and the surrounding host rock, MX80 bentonite will be used as buffer material. Friedland clay is considered one of the best candidates to be used as drift backfill material to meet the long-term performance requirements set for backfilling of a disposal tunnel in the repository. Figure 3-2 shows a cross section of the spent nuclear final disposal facility. There are two alternative disposal conditions of the spent fuel. The first alternative envisages that the canisters will be disposed horizontally in the horizontal tunnels. The second alternative envisages the vertical emplacement of the canisters in boreholes excavated in horizontal tunnels.

The time required for reaching full saturation, maximum temperature reached in canister, deformations in the buffer-backfill interface and stress-deformation balance in this interaction were the main issues addressed of the Chapter V. In the previous chapters, it has been explained thermal calculations to identify appropriate boundary conditions and modeling laboratory experiments to calibrate material parameters for the buffer.

A fundamental issue in modeling was to determine relevant thermal boundary conditions so that the details of THM-behavior could be captured by defining proper near-field thermal boundaries. In the Chapter III, it has been shown that temperature on the considered close boundaries depends on initial canister power, fuel power decay characteristic and rock thermal properties. The thermal boundary conditions fixed at the THM modeling have been calculated solving the thermal problem for the entire repository with the numerical solution.

With regard to the hydraulic analyses, it has been shown in the Chapter V that the time required for full saturation is sensitive to vapor diffusion, hydraulic conductivity and water retention curve of the buffer and the hydraulic conductivity of the rock. A sensitivity study was a part of the first report to investigate the base case performance and its correspondence with realistic conditions.

The modeling process of buffer-backfill interface is an important part of tunnel backfill design. The calculations aimed to find out deformations in this interface whose behavior is important for the buffer swelling. In order to investigate the hydro-mechanical behavior of MX80 bentonite which is the buffer material, a series of laboratory tests have been started up by POSIVA and carried out at B+TECH laboratory. Two types of tests have been performed: oedometer tests and infiltration tests. These tests have been modeled using the finite element code Code_Bright for model calibrations. The Barcelona Basic Model (BBM) (Alonso et al., 1990) has been used to model the mechanical behavior of the material. Calibrations of these tests were given in the Chapter IV.

In this chapter, thermo-hydro-mechanical calculations are performed regarding the presence of a 10 mm air-filled gap between canister and the buffer ring according to reference design. The closure of the gap depends on the bentonite buffer saturation and expansion. If the saturation of buffer is delayed, the gap will not close and will disturb heat dissipation causing higher canister temperatures.

The main object of this work is to show the influence of the presence of the air-filled gap on the THM behavior of the engineered barrier. Several cases were considered in order to see the influence of the permeability of the rock on gap closure. The Base Case without gap is also included in order to make the comparison easier. The results presented here are the evolution of temperature, displacement, liquid pressure, liquid saturation and stresses.

6.2. Geometrical and Physical Properties of the Problem

The concept for storage considered in this study is based on parallel vertical boreholes excavated in horizontal tunnels. The canister placed in each borehole will be surrounded by MX80 bentonite buffer rings. According to the reference design, a 10 mm air-filled gap exists between the canister and the buffer rings. The hydro-mechanical behavior the Bentonite buffer is of great importance. In fact, the closure of the gap is controlled by the swelling deformation developed as the bentonite buffer saturates. The HM behavior of MX80 bentonite has been extensively investigated and the elasto-plastic properties of this material have been determined by calibration of the experimental tests (Table 6- 1).

Table 6-1. Parameters for elasto-plastic constitutive model (MX80 bentonite)

Parameters	Symbols	Units	Values
Poisson's ratio	ν (-)	-	0.35
Parameters for elastic volumetric compressibility against mean stress change	κ_{i0}	-	0.05
	α_i	-	-0.003
Parameters for elastic volumetric compressibility against suction change	κ_{s0}	-	0.25
	α_{sp}	-	-0.145
Elasto-plastic volumetric compressibility	$\lambda(0)$	-	0.15
Parameters to define LC yield curve	r	MPa ⁻¹	0.8
	β		0.02
Reference stress	p^c	MPa	0.01
Initial porosity	ϕ_0		0.375
Preconsolidations mean effective stress	P_o^*	MPa	0.75
Strength parameter	M	-	1.07

Friedland clay is envisaged as backfill material for the disposal tunnel. The Backfill material plays two main roles, to limit the upward movement of the strongly expansive

buffer in the deposition holes by having a low compressibility and to provide support to the roof and walls of the deposition tunnels by applying an effective pressure on them. According to current disposal option, 60-80% of the total volume of the deposition tunnel will be backfilled with pre-compacted blocks (Friedland clay) and the remaining space will be backfilled with bentonite pellets. Table 6-2 shows properties of the different materials.

Table 6-2. Material properties

Materials	Dry density (kg/m ³)	Porosity	Intrinsic permeability (m ²)
Bentonite Rings	1761	0.367	5.59x10 ⁻²¹
Bentonite discs	1701	0.388	5.59x10 ⁻²¹
Pellets	919	0.669	5.59x10 ⁻²¹
Backfill	1758	0.367	10 ⁻¹⁸

6.2.1 Gap Properties

The gap is modeled as a material with very high porosity and permeability (several orders of magnitude larger than the other materials) (Table 6-3). Intrinsic permeability is assumed to be a function of porosity. The following expression has been used:

$$k = k_o \frac{\phi^3}{(1-\phi)^2} \frac{(1-\phi_o)^2}{\phi_o^3} \quad (6-1)$$

ϕ_o : reference porosity

k_o : intrinsic permeability for matrix ϕ_o

For retention curve the van Genuchten model is used (Equation 2).

$$S_e = \frac{S_l - S_{rl}}{S_{ls} - S_{rl}} = \left(1 + \left(\frac{P_g - P_l}{P} \right)^{\frac{1}{1-\lambda}} \right)^{-\lambda} \quad (6-2)$$

$$P = P_o \frac{\sigma}{\sigma_o}$$

The dependence of the retention curve on density or porosity has been taken into account considering Equation 3.

$$P_o(\phi) = P_o \exp(a(\phi_o - \phi)) \quad (6-3)$$

A function with very low initial capillary pressure ($P_o = 0.001$ MPa) is considered for retention curve (Table 6-3). This implies that saturation takes place sharply as capillary pressure vanishes. For relative permeability the following function has been adopted:

$$k_{rl} = AS_e^\lambda \quad (6-4)$$

The mechanical response of the gap is achieved using two different stiffness values depending on the opening. When the gap is open, the elastic modulus is 1 MPa (i.e. very low stiffness). On the contrary when it is closed the elastic modulus is 1000 MPa (i.e. high stiffness) (Table 6- 3). In this way relative displacement of the air gap boundaries (nodes) stops when closure takes place because closure leads to stiffness increase.

Heat transfer across the gaps will take place by conduction, radiation and convection. For a gap with a thickness d , subjected to a temperature gradient (Figure 1), the radiant heat flux (q_r) can be calculated as follows:

$$q_r = \frac{e_1 \cdot e_2}{e_1 + e_2 - e_1 \cdot e_2} \sigma \cdot (T_1^4 - T_2^4) \quad (6-5)$$

Where e is surface emissivity, T_1 and T_2 are temperature on both sides of the gap and σ is Stefan-Bolzmans constant.

Table 6-3. Gap Parameters

Thermal parameters	
λ_{dry} (W/(mk)*)	0.045
λ_{sat} (W/(mk))	0.6
Hydraulic parameters	
k_0 intrinsic permeability (m^2)	10^{-16}
ϕ_o porosity (-)	0.8
λ Van Genuchten (-)	0.5
P_o	0.001
a Van Genuchten	10
Mechanical Properties **	
E_c (MPa)	1000
E_o (MPa)	1.0
ϵ_v limit (-)	0.95
ν (-)	0.3

*This effective conductivity is chosen according to SKB technical report TR - 03 – 09

** When gap is closed, linear elastic model is used with parameters of ν and E_c .

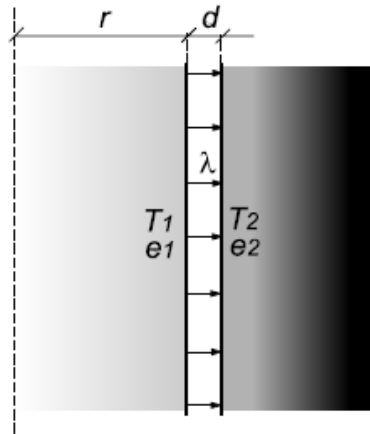


Figure 6.1. Heat transfer across the gap

For the conductive flux the Fourier law is used:

$$\mathbf{i}_c = -\lambda \nabla T \quad (6-6)$$

In this study the combined effects of conduction and radiation are included in conductive flux using an equivalent conductivity. Thermal conductivity changes with saturation between two extreme values. When the gap is full of gas, thermal conductivity of 0.045 W/mK (gas mixture of air and vapor) is considered while when it is full of water the value of 0.6 W/mK (water) is considered (Table 6-3).

6.3. Initial and Boundary Conditions

As mentioned previously, the closure of the gap is controlled by swelling deformations developed as the bentonite buffer saturates. Since permeability of the rock plays an important role on the saturation time of the backfill material and so on gap closing three cases have been analyzed (Table 6-4). For case A, permeability of the host rock is assumed to be one order of magnitude higher than for case B. Case C is similar to case B except for the air-filled gap which is not simulated here.

Table 6-4. Models for comparative study

Models	A	B	C
Rock Permeability	10^{-18} m^2	10^{-19} m^2	10^{-19} m^2
Initial pressure of barrier materials	-41 MPa	-41 MPa	-41 MPa
Gap Closing time (approx..)	2 years	4 years	No air gap

The analysis has been assumed under axis-symmetric conditions. Figure 6-1b shows the mechanical boundary conditions applied. An initial confining stress of 10.63 MPa has been considered for the host rock. This confining pressure has been used as boundary condition (applied on the horizontal upper boundary). The excavation process has also been simulated. The initial water pressure for all the material in the deposition hole is -41 MPa (Figure 6-1a). Initial porosities are shown in Figure 6-1d. The initial temperature is 10.5 °C throughout the domain modeled.

A fundamental issue in modeling was to determine relevant thermal boundary conditions so that the details of THM-behavior could be captured by defining proper near-field thermal boundaries. This was already discussed in Chapter II and implies that appropriate boundary conditions for thermal dissipation are considered for the top and bottom boundary conditions.

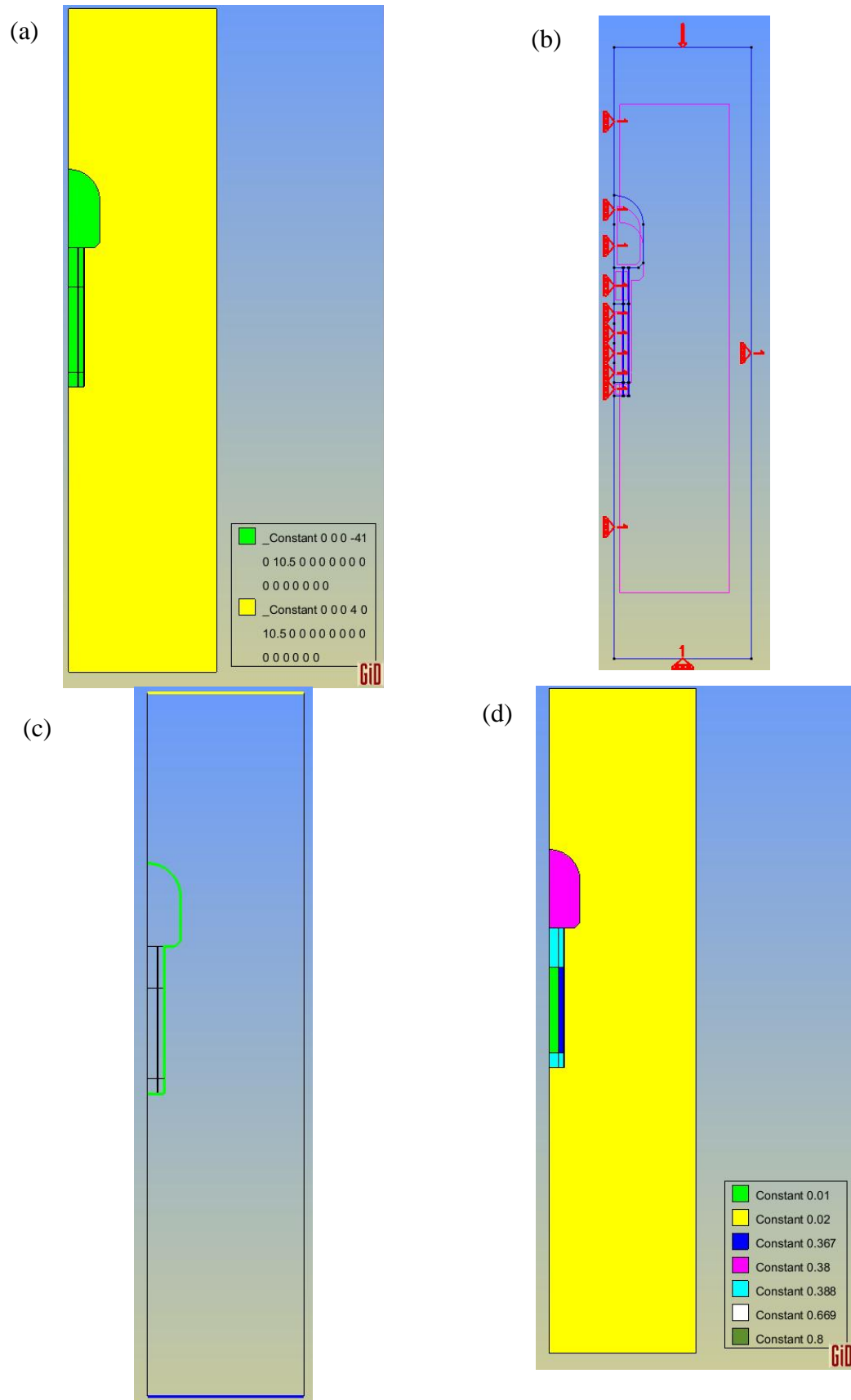


Figure 6-1. Initial and Boundary conditions. (a) Initial pressure and temperature, (b) mechanical boundary conditions, (c) prescribed pressure and (d) initial porosity

6.4. THM Analysis Including Gap Effect

In the analyses discussed in this chapter, i.e. cases A and B, a 10 mm gap has been considered between the bentonite-buffer and the canister. The properties of the gap have been described in section 6.1. This gap closes due to swelling of clay. The gap has been simulated by means of an air element, which is able to close completely as the bentonite swells. The presence of this air gap has effects on the thermal, hydraulic and mechanical behavior of buffer. Table 6-5 and Figure 6-2 show the different representative points considered for comparison of the results for the different cases.

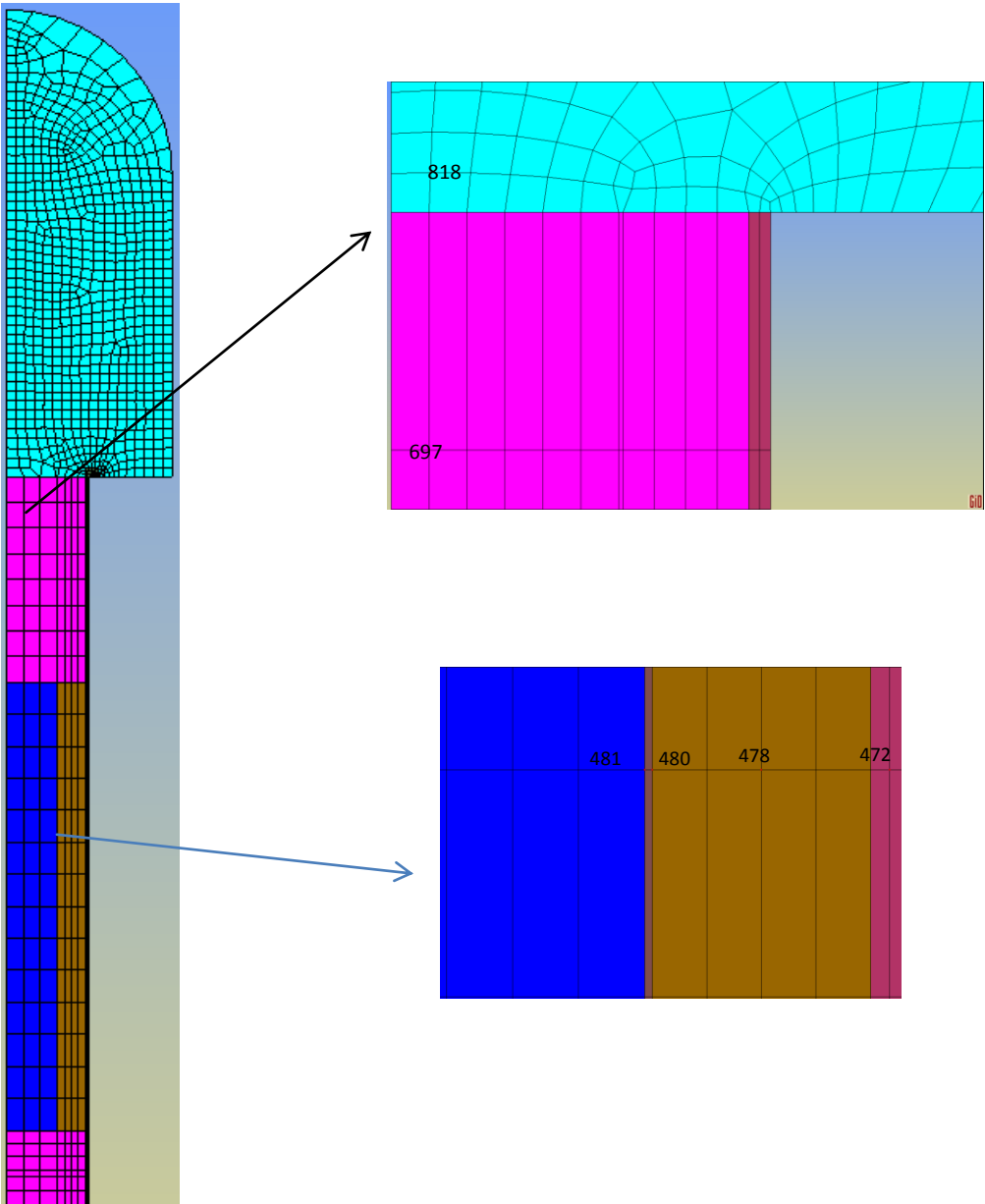


Figure 6-2. Details of the geometry and mesh and representative nodes for representation of results.

Table 6-5. Representative points for materials.

Materials	Point considered
Backfill	818
Bentonite disc	697
Gap canister side	481
Gap bentonite ring side	480
Bentonite ring	478
Pellets	472

6.4.1. Model A - Permeability of rock 10^{-18} m^2

The design criteria for the repository establish that the maximum allowed temperature for bentonite buffer is 90 °C. According to the model predictions of the model that is based on an adopted disposition of canisters, the maximum temperature is reached after about 30 years and it is about 80 °C.

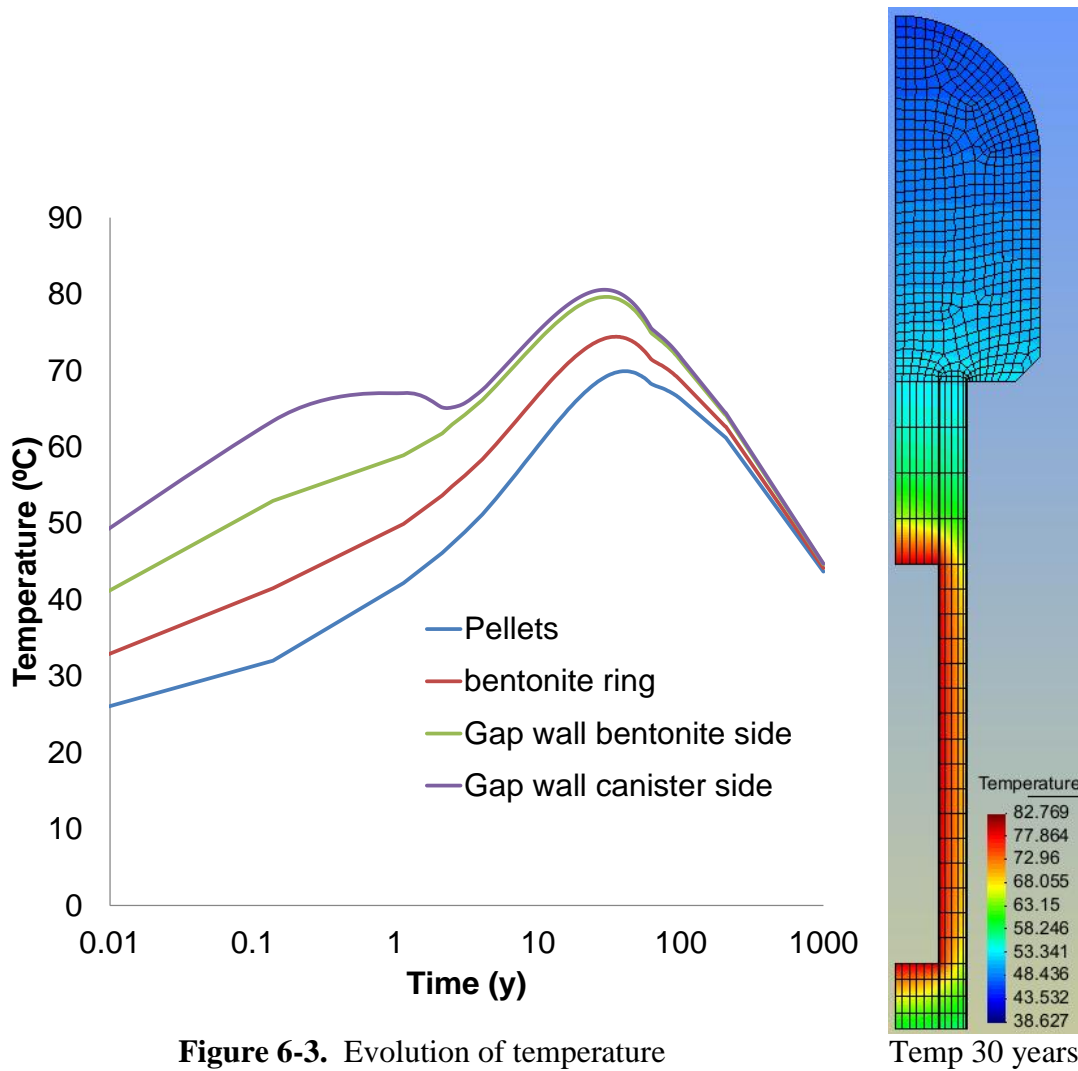


Figure 6-4 shows the effect on temperature of the existing air gap between the canister and the bentonite buffer. At both sides of the gap, temperature is not the same until a certain time. As the gap closes, its thermal conductivity increases. Actually, the contact between the two sides of the gas will produce in reality a high effective conduction (but this is not accounted by the model). Although the model does not account for the contact, it is observed that as the gap closes and saturates, the temperature differences vanish.

The insulating capacity of the gap produces an increment of the temperature in the canister at early times. Since the increment of temperature takes place before the temperature peak, the maximum temperature reached during all the calculation is practically not altered by the presence of the gap (a comparison of cases is carried out latter).

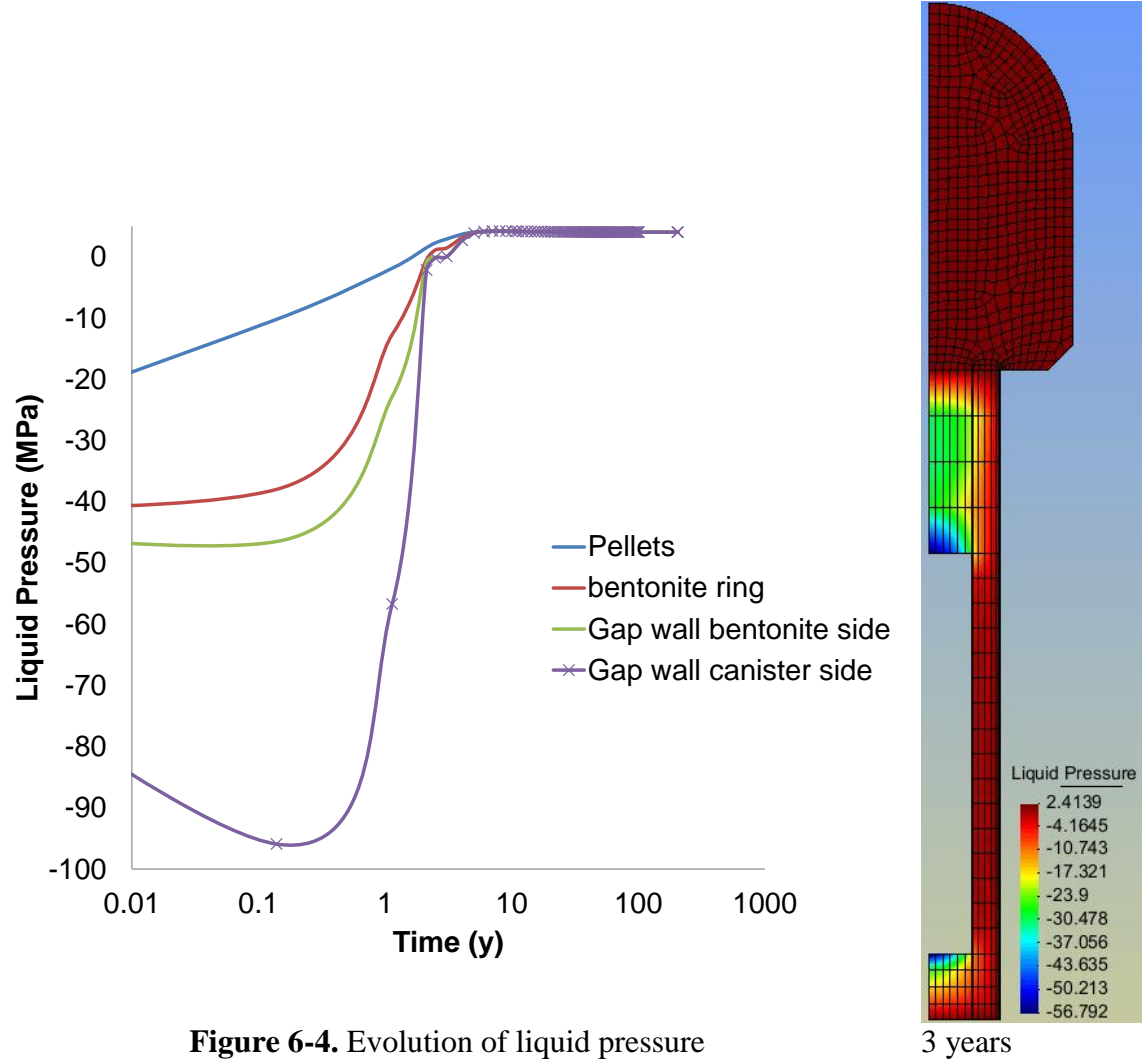


Figure 6-4 shows the evolution of liquid pressure at representative points of the disposal materials. High suction values (i.e. low water pressure) are observed close to the canister resulting from temperature increment induced by the heat generation through the canister. The temperature increase produces higher vapor content in the gas phase which leads to vapor diffusion from hotter to colder regions. In fact, the representative point for the air gap at the side of canister (it is a point on the canister) reaches a suction value of 95 MPa. The reached value highly depends not only on temperature but also on the rock hydraulic conductivity, and in general on the thermo-hydrological conditions.

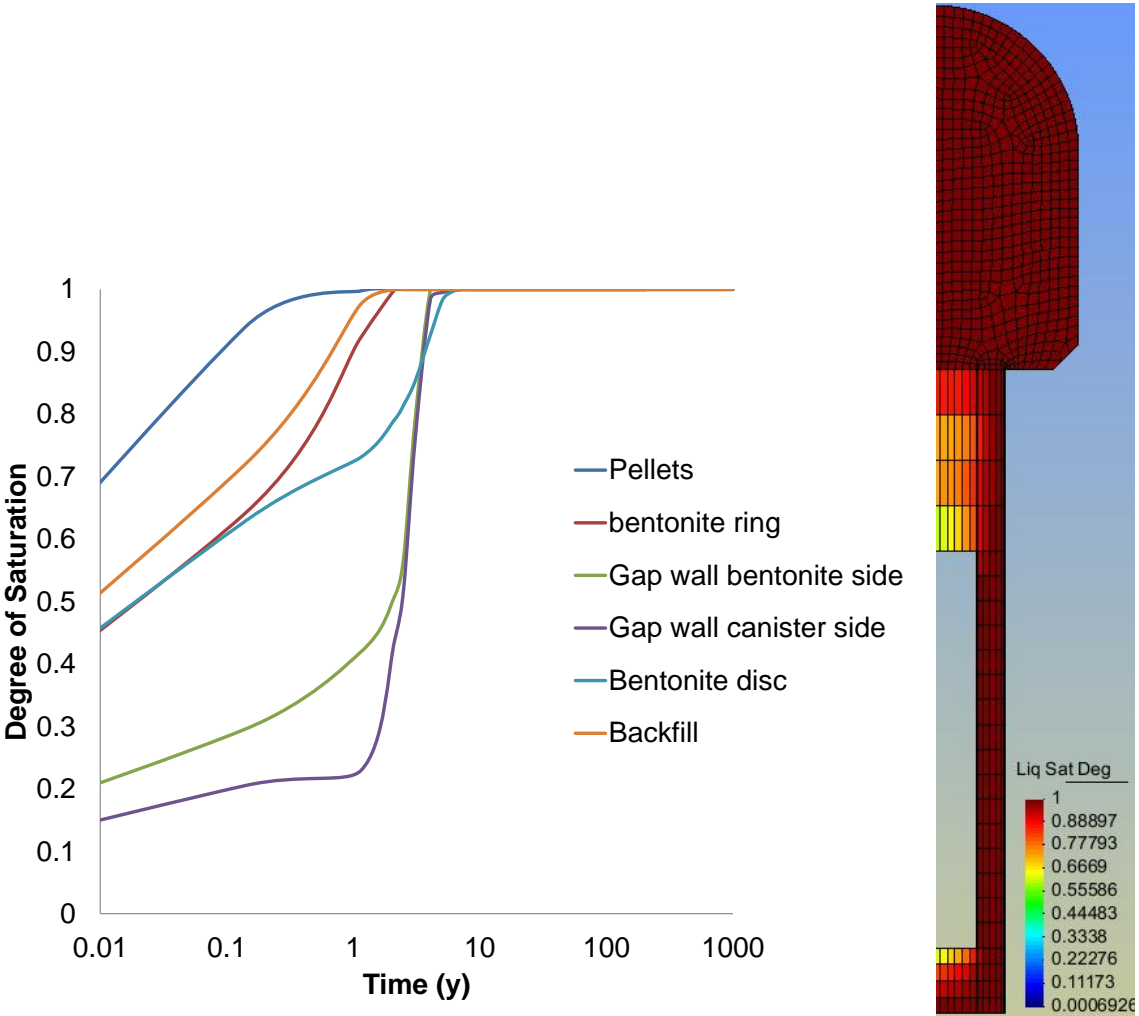


Figure 6-5. Evolution of degree of saturation 3 years

At early times large difference in liquid pressure is observed between the two sides of the air gap. After a certain time, when the gap reaches full saturated conditions (Figure 6-5), the two sides tend to have the same value of liquid pressure. Full saturation of all materials takes about 10 years (Figure 6-6). The strong heat generation from canister

causes the initial desaturation of bentonite buffer. The effect of air gap is considerable during the first year until the full saturation of the bentonite is achieved; because the gap permits lower water pressures to develop near the canister. This is due to the low capillarity capacity of the gap. So, water in the gap is not subjected to large capillary forces as it happens in the buffer, and therefore the water pressure decreases to very low values. In other words, the presence of the gap permits a much higher drying of the vicinity of the canister during heating. As the gap closes it also saturates.

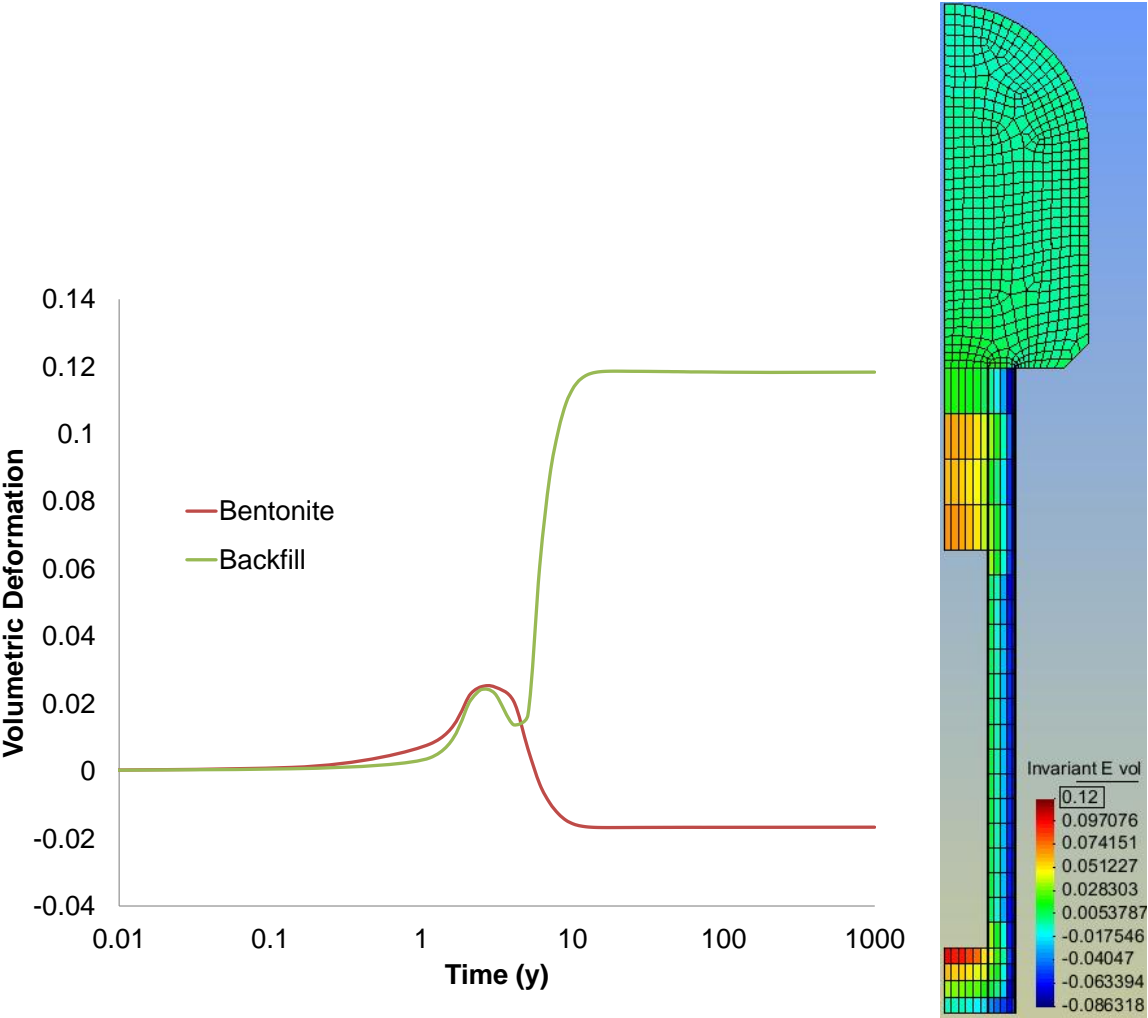


Figure 6-6. Evolution of volumetric deformation 10 years

Figure 6-6 shows the evolution of volumetric deformation in bentonite and backfill materials. It is noticed that due to its initial desaturation, the bentonite buffer experiences some compression. When water coming from the host rock reaches the buffer, the bentonite starts swelling. Swelling of the bentonite buffer results in compression of the backfill material (upward displacement). The maximum reached

deformation is equal to 0.12. One of the requirements for the backfill material is to have a low compressibility in order to limit the upward movement; otherwise the swelling of the bentonite could be excessive thus leading the compromising hydraulic properties.

Figure 6-7 shows the evolution of mean effective stress in the materials. Maximum effective stress reached in the bentonite buffer is equal to 9 MPa and tends to the swelling pressure of this material.

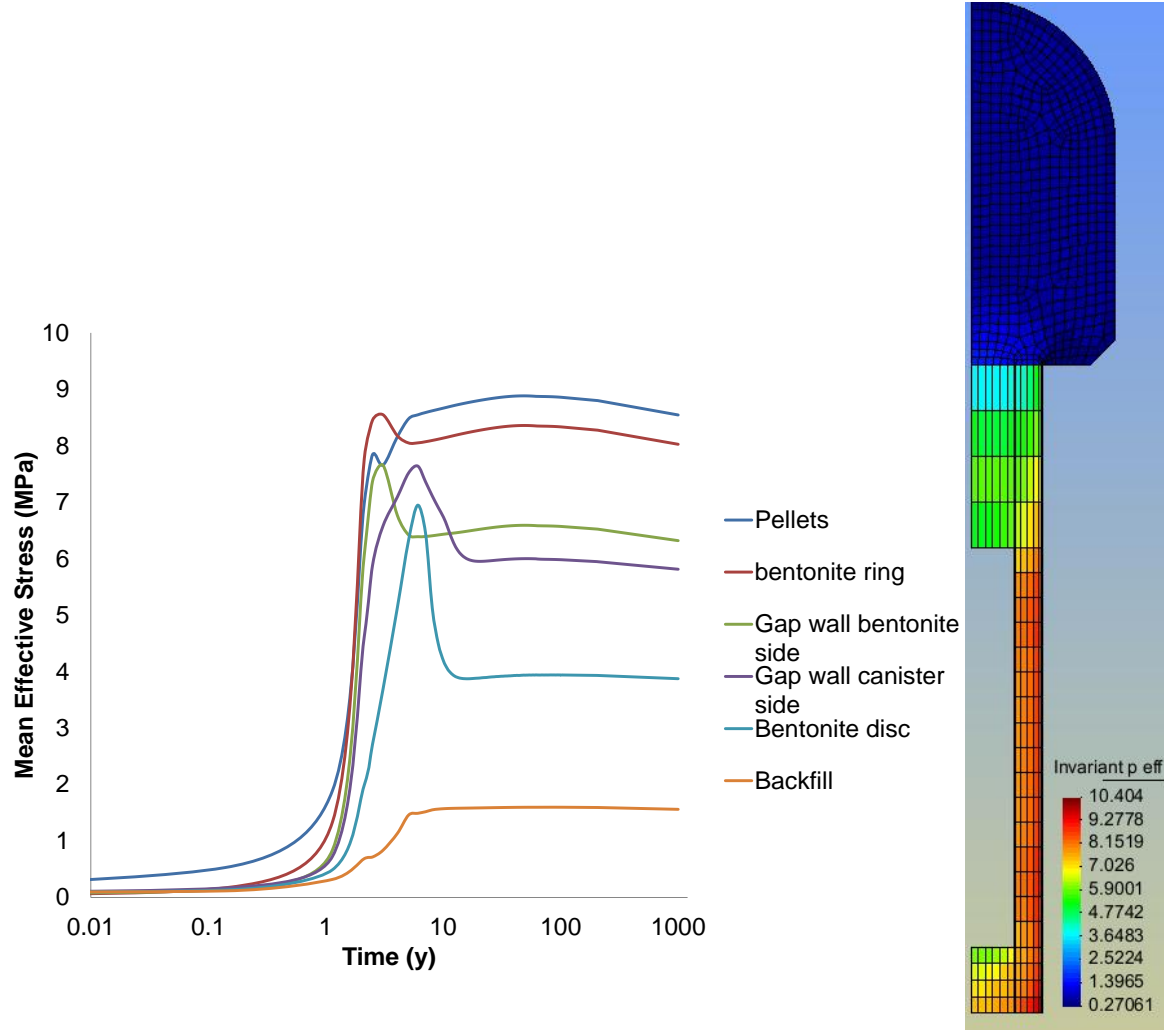


Figure 6-7. Evolution of mean effective stress 10 years

Some stress peaks are observed after saturation. This can be explained by the expansion induced by hydration at some point taking place while other still remain unsaturated and therefore stiff. After water redistribution, all zones tend to be more deformable thus leading to stress relaxation.

The presence of the 10 mm air gap has an effect on the thermal, hydraulic and mechanical response of the disposal site. This effect diminishes as the bentonite buffer saturates, expands and causes the closure of the gap.

Figure 6-8 and 6-9 show the evolution of the gap closure. In 4 years, horizontal displacement reaches a value of 10 mm and this implies that the gap can be considered totally closed. The closure time strongly depends on swelling of the buffer as it saturates. The kinetics of water supply will basically be controlled by the permeability of the host clay formation. Hence, hydraulic conductivity of rock has an important role to play on gap closure time.

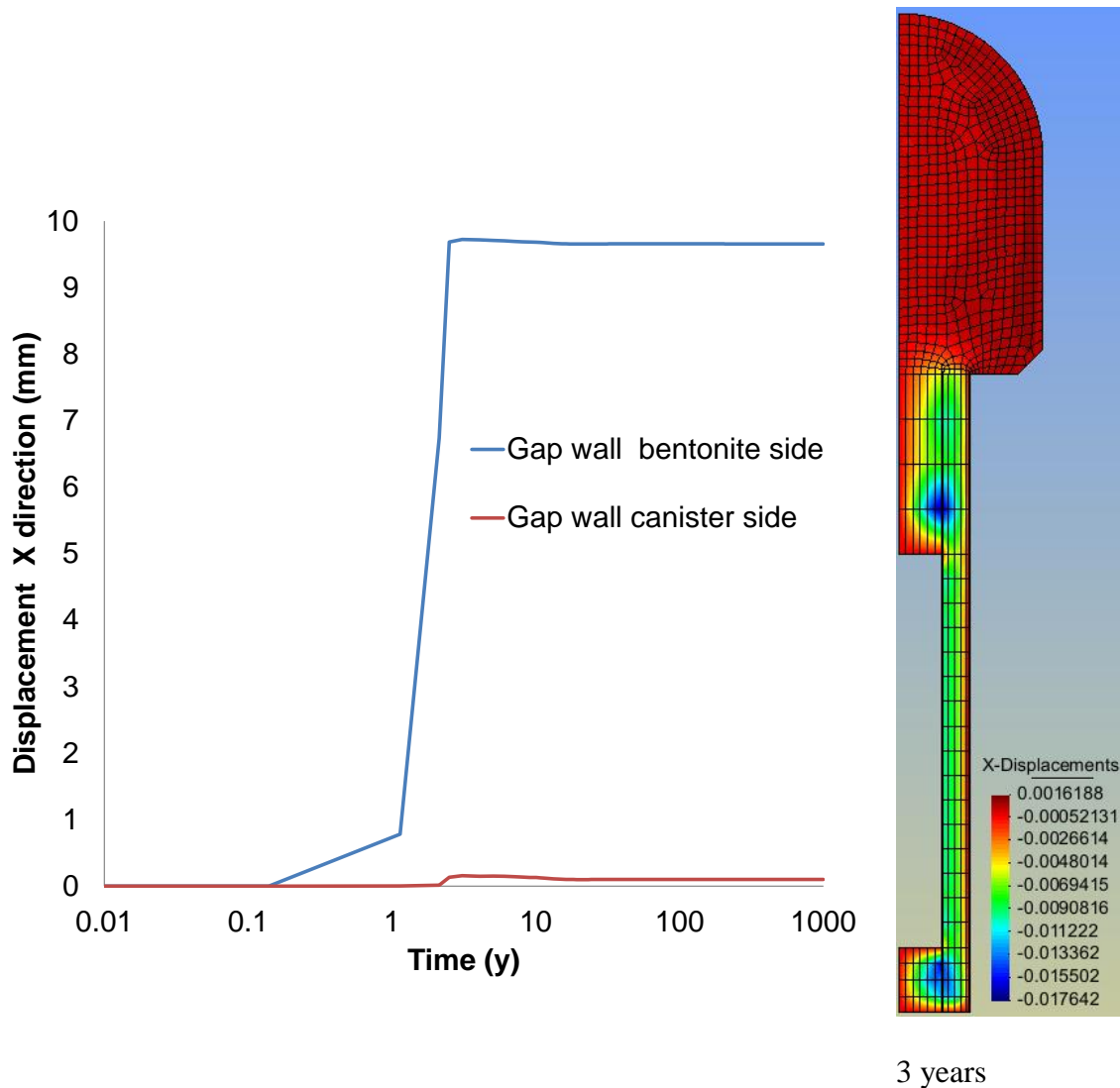


Figure 6-8. Horizontal displacements in the air gap element

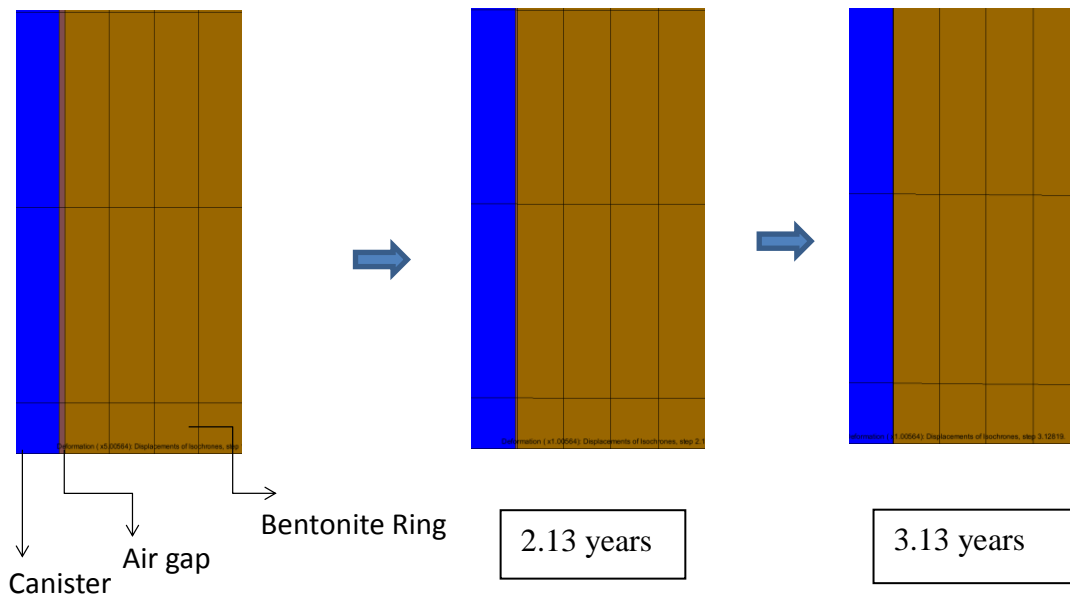


Figure 6-9. Illustration of gap closure. It is worth to remark that the amplification factor for displacement in this figure is equal to 1.

The model described in this section considers a host rock permeability of 10^{-18} m^2 . In the following section, the same case is considered but the permeability of the host rock is decreased by one order of magnitude. This must imply a slower saturation rate.

6.4.2. Model B - Permeability of rock 10^{-19} m^2

In this case, the rock hydraulic conductivity is reduced 10 times as compared with case A. The rest of conditions and materials parameters are kept same as Model A.

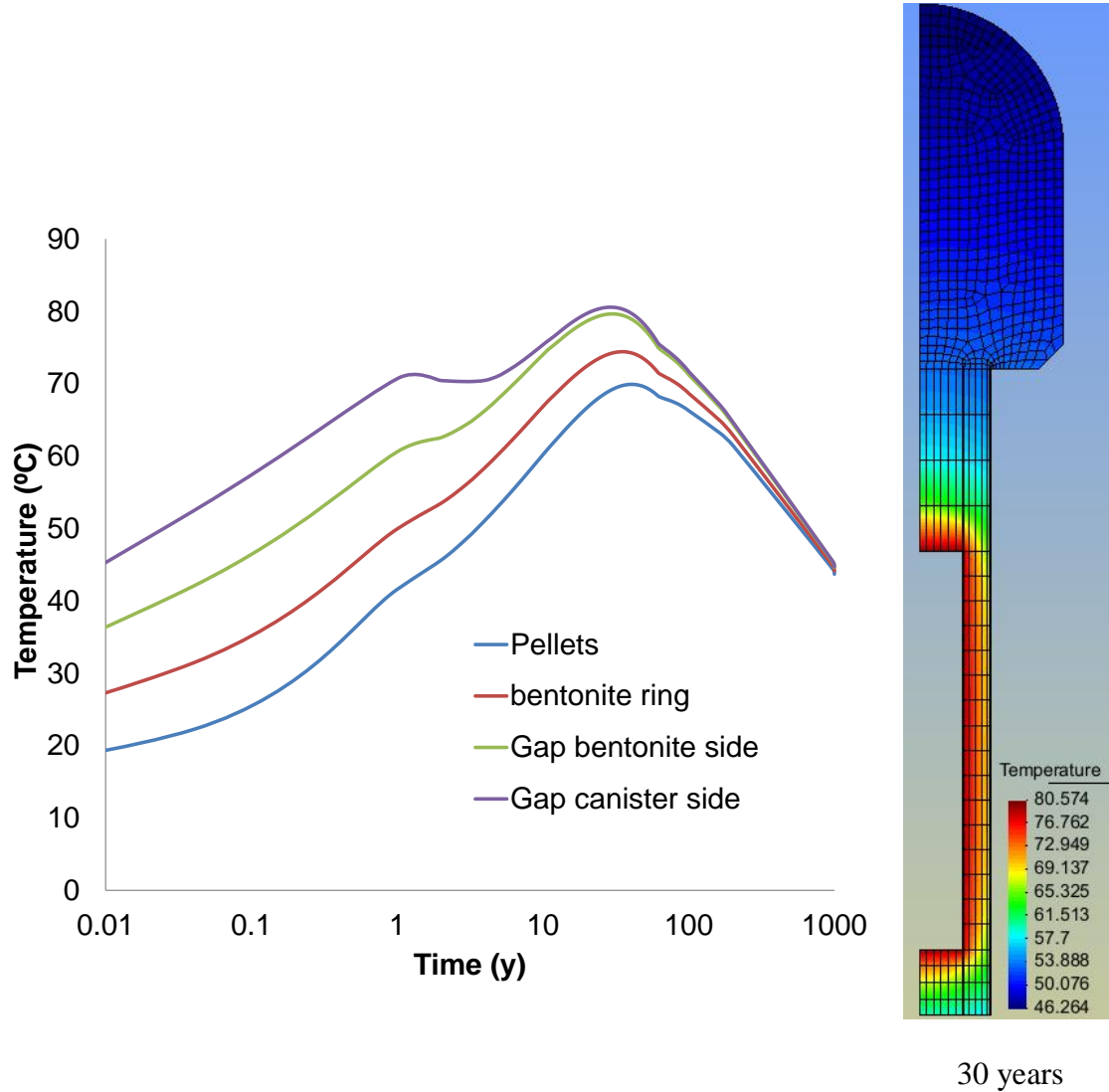


Figure 6-10. Evolution of temperature

Figure 6-10 shows the effect on temperature of the existing air gap between the canister and the bentonite buffer. The maximum temperature is reached in the buffer bentonite and it is less than 80 °C. No significant temperature variations are observed. This is normal as the thermal problem received small influence of the hydraulic one. The main couplings are heat advection and thermal properties varying with water content. Heat advection is small in this problem as the materials have, in general, low hydraulic conductivity. The thermal conductivity variations with water content may induce some

differences as the hydration process is delayed. However, thermal conductivity variations of a porous material with respect to water content are very moderate.

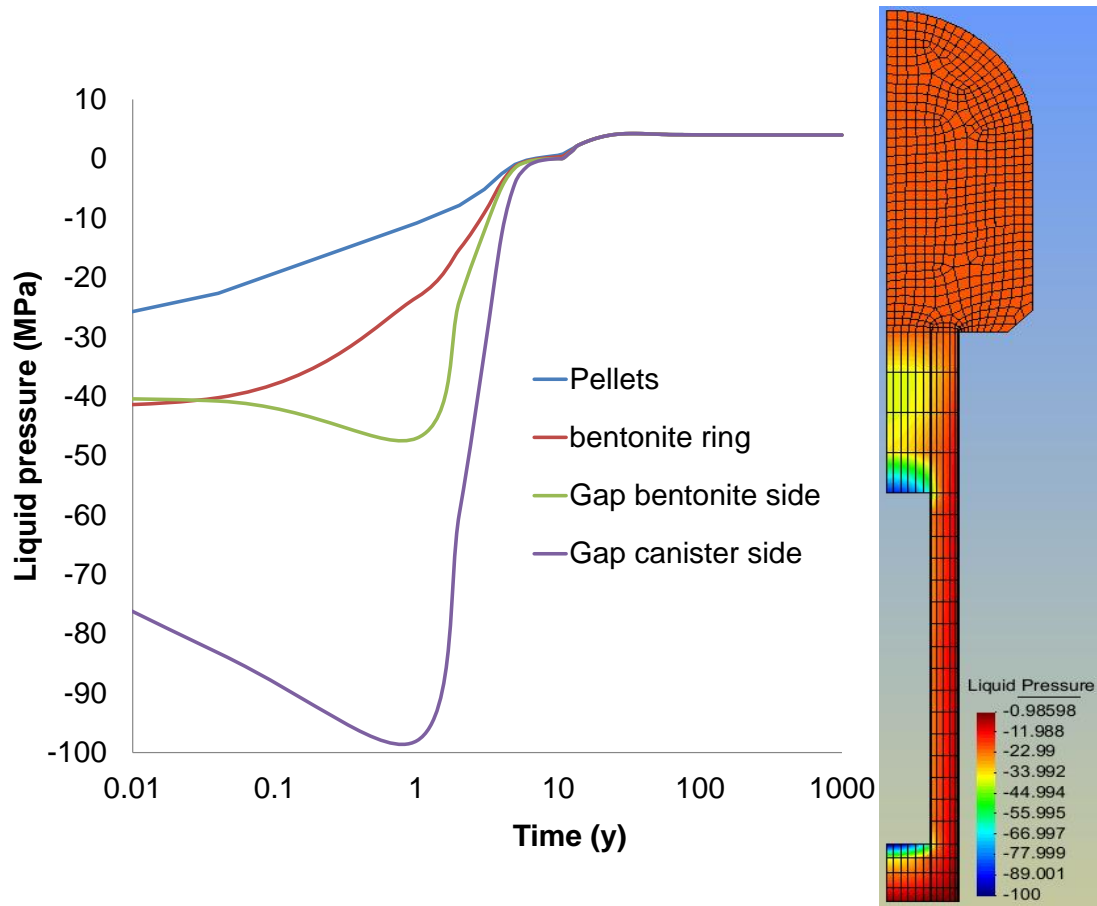


Figure 6-11. Evolution of liquid pressure

3 years

The evolution of liquid pressure at representative points of the disposal materials is shown in Figure 6-11. High suction values are observed close to the canister. Suction on the canister reaches a maximum value of about 100 MPa after 1 year of the deposition of the canister. At early times large difference in liquid pressure is observed between the two sides of the air gap. In fact, suction at the selected point of the gap element close to the bentonite ring is lower compared to other side close to the canister.

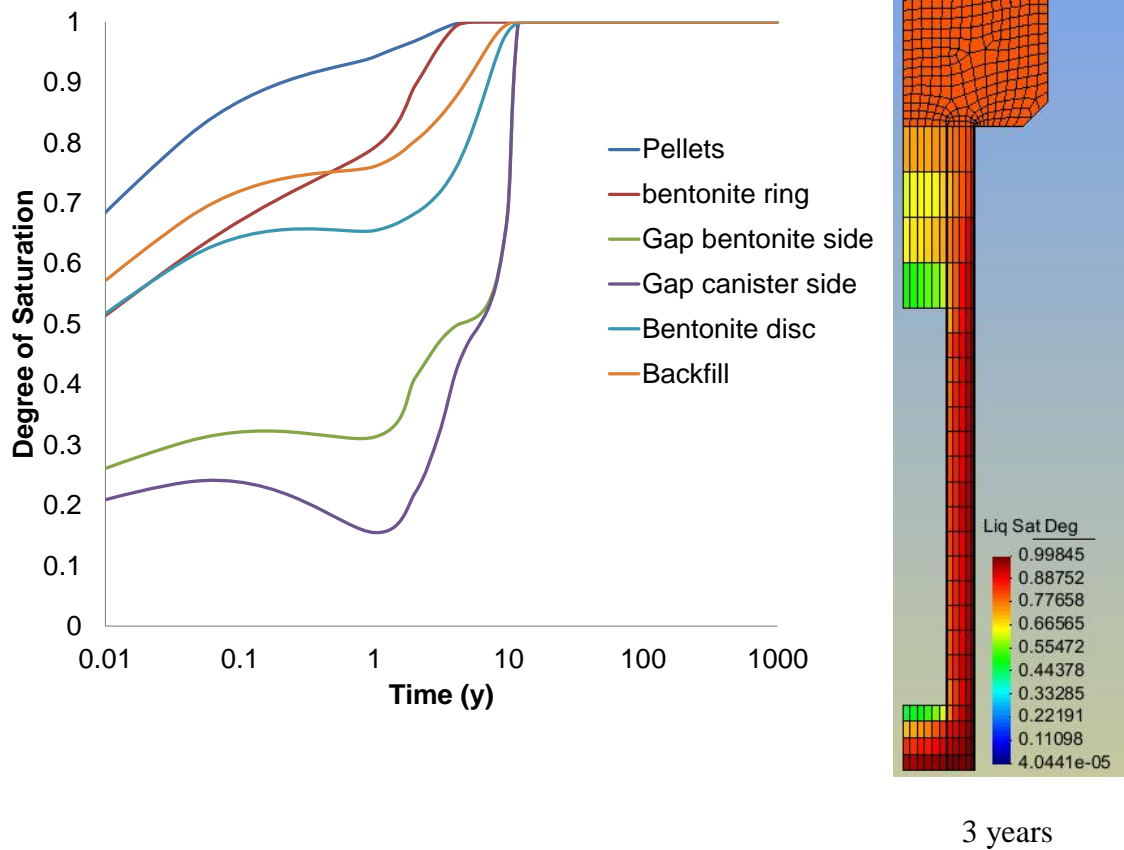


Figure 6-12. Evolution of degree of saturation

In this case B, as the rock is less permeable than in case A, the water supply from rock requires more time. Hence, saturation of bentonite is delayed (Figure 6-12). Saturation of the bentonite buffer causes the material to swell and as a result the backfill material compresses (Figure 6-13).

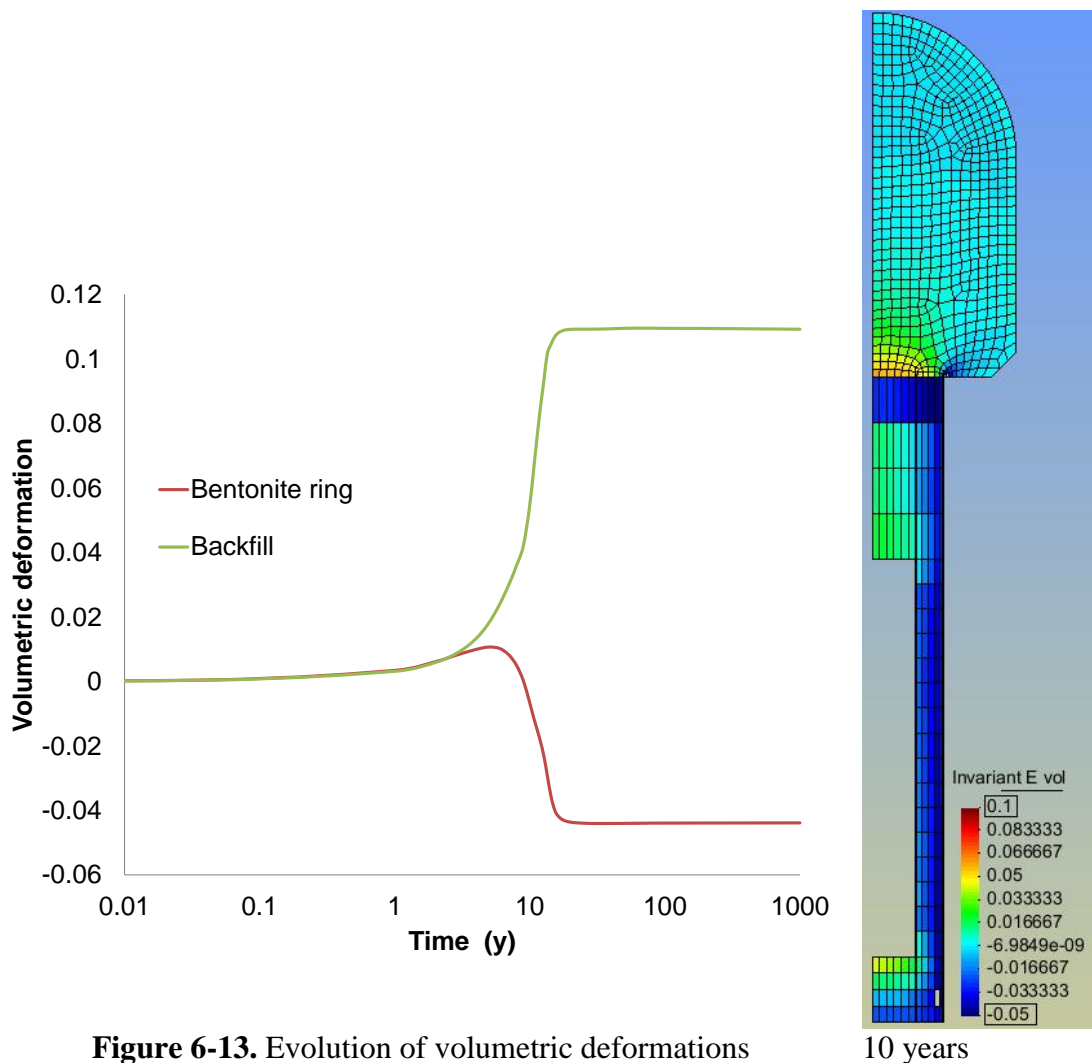


Figure 6-14 shows the evolution of mean effective stress in the materials. Maximum mean effective stresses reached in the bentonite ring are in the range of 9-10 MPa.

As for the previous case, the presence of the 10 mm air gap has an effect on the thermal, hydraulic and mechanical response of the disposal site. This effect diminishes as the bentonite buffer saturates, expands and causes the closure of the gap.

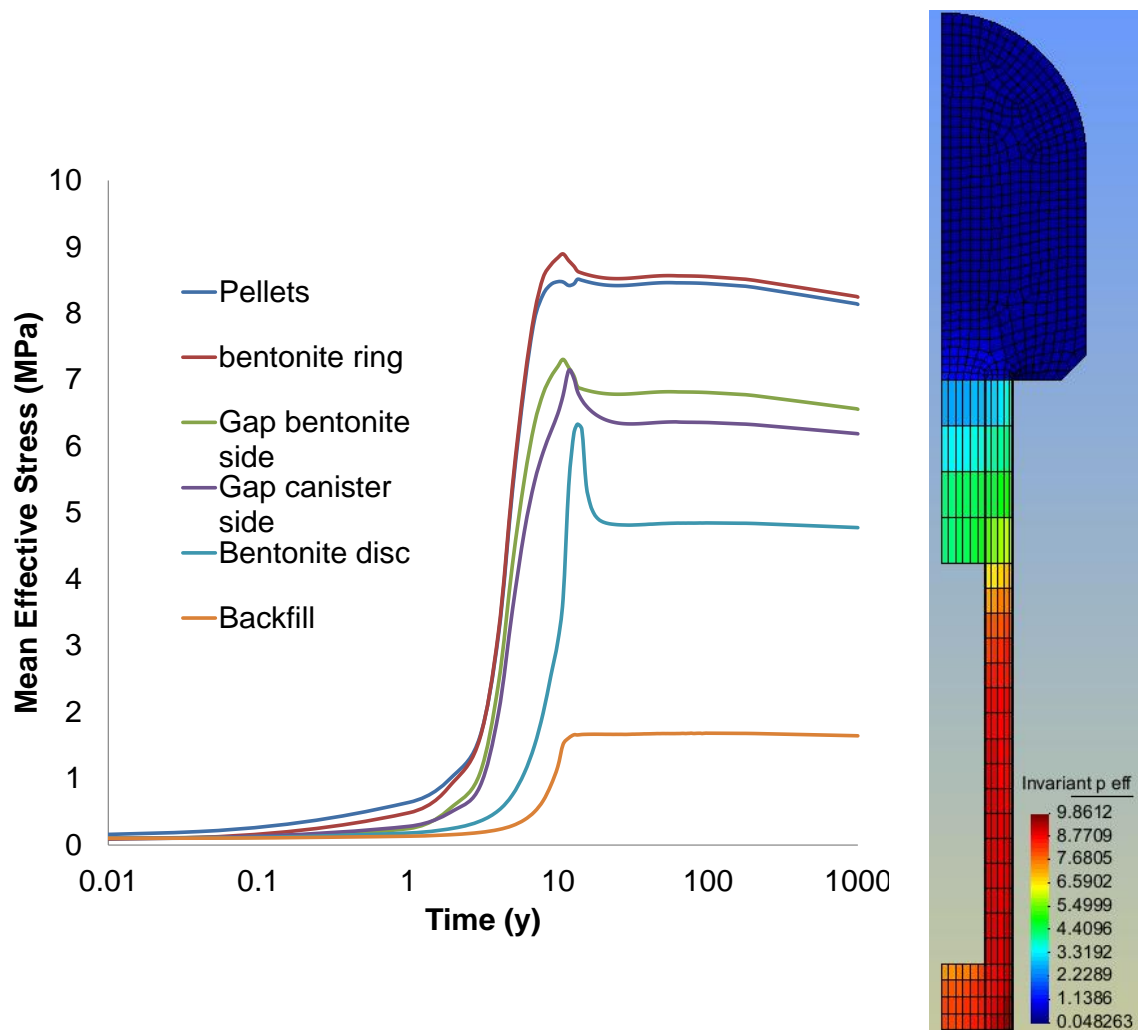


Figure 6-14. Evolution of mean effective stresses

10 years

Figures 6-15 and 6-16 show the evolution of the closure of the gap. It can be seen that the gap is totally closed after 5 years that is 1 year later than for the previous case (Model A). This is a direct consequence of the lower permeability of the host rock considered in this case.

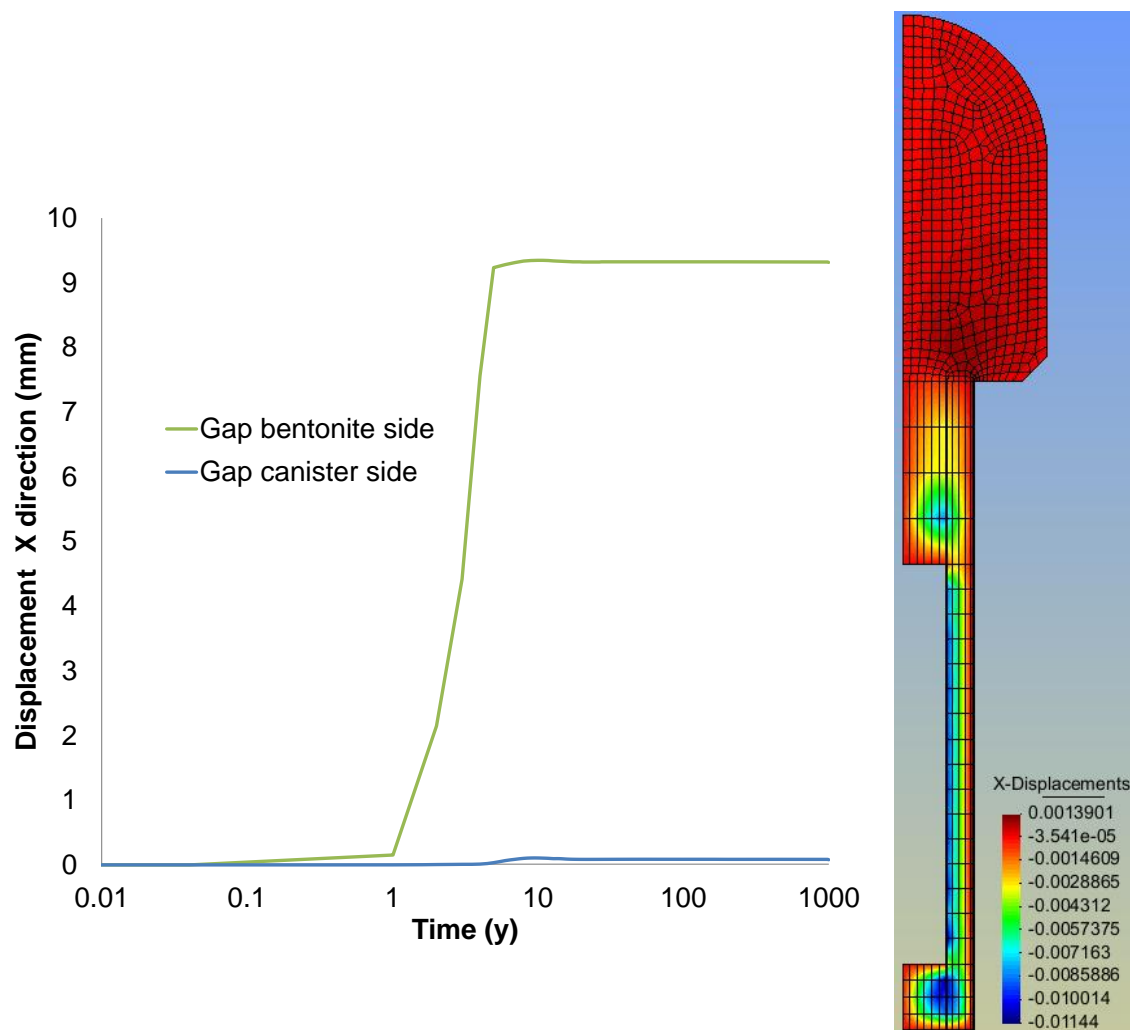


Figure 6-15. Evolution of horizontal displacements

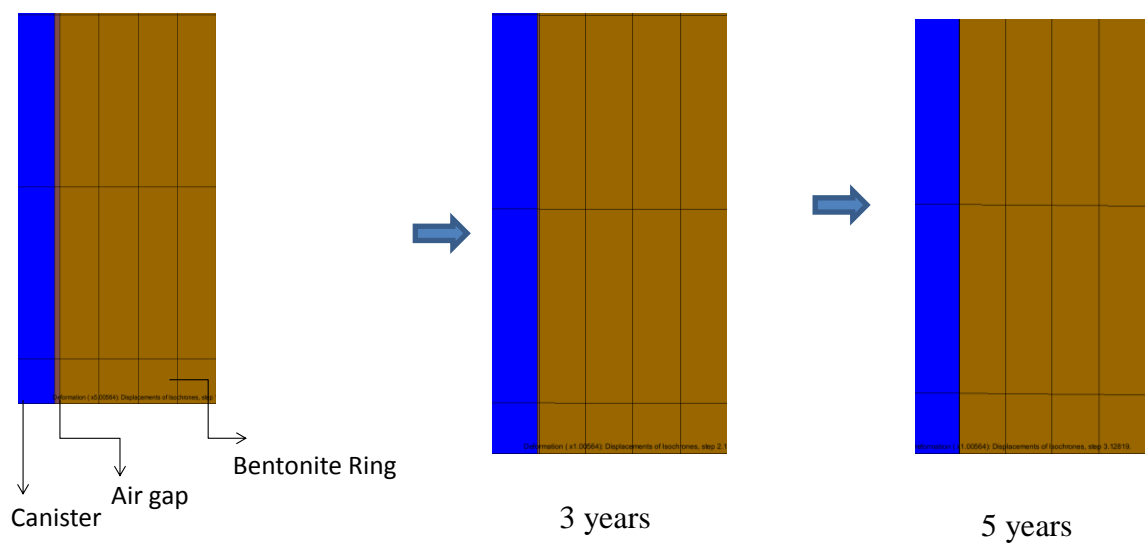


Figure 6-16. Simulation of gap closing

6.4.3. Model C Permeability of rock 10^{-19} m^2 (without gap)

It has been indicated in the preceding sections that the gap had an effect on the thermo-hydro-mechanical processes. In this section, quantification is done by calculation of Model C, which is equal to Model B except for the air gap which is not considered now. In practice, the gap elements have been changed in order to have the properties of the buffer.

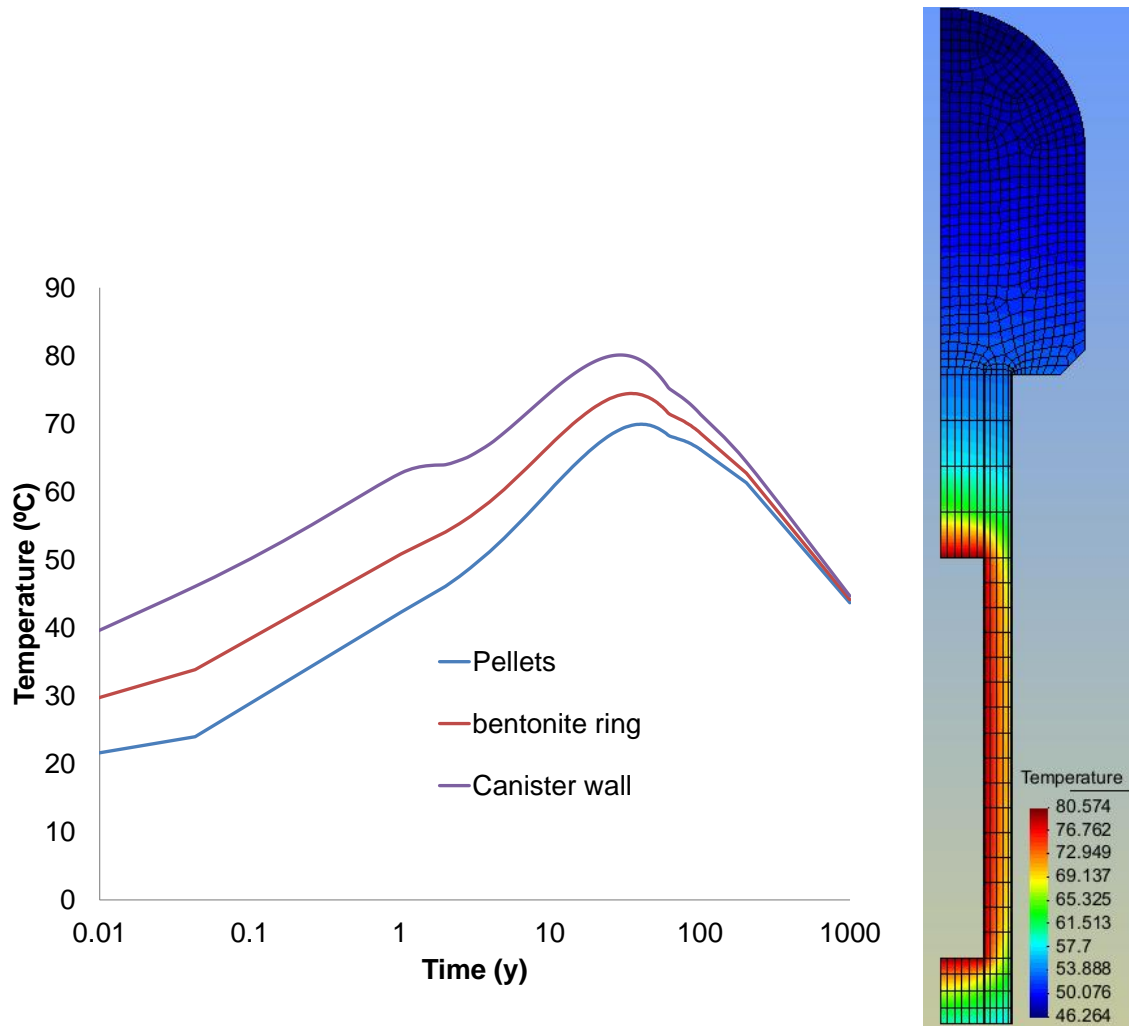
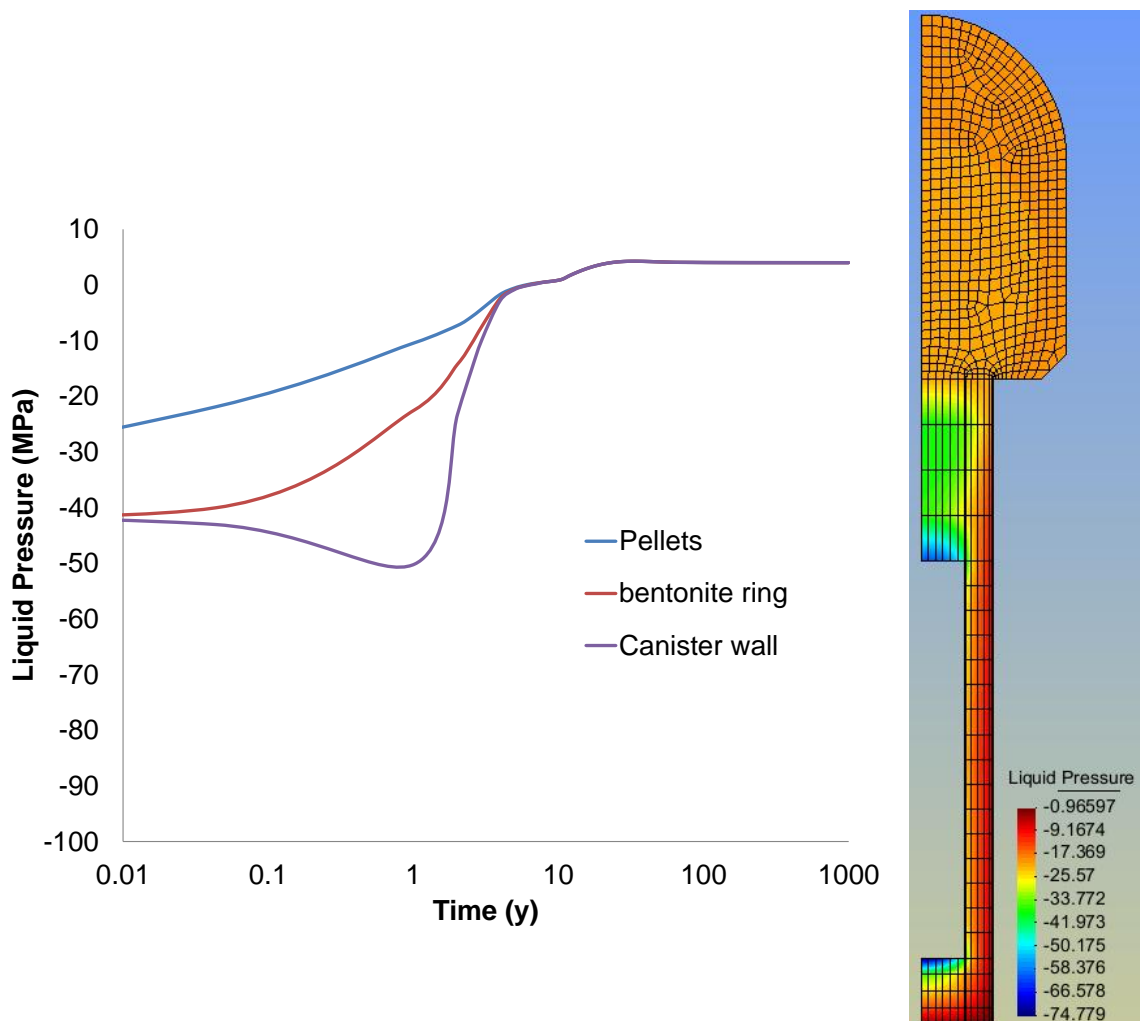


Figure 6-17. Evolution of temperature

30 years

Figure 6-17 shows the evolution of the temperature for the different materials. The maximum temperature in the bentonite buffer is reached after 30 years and is less than 80 °C. As there is no air gap, the selected points on both side of the gap element evolve in the same way. The temperature in the canister shows the effect of saturation of the buffer and the associated change in thermal conductivity. The water saturation of a

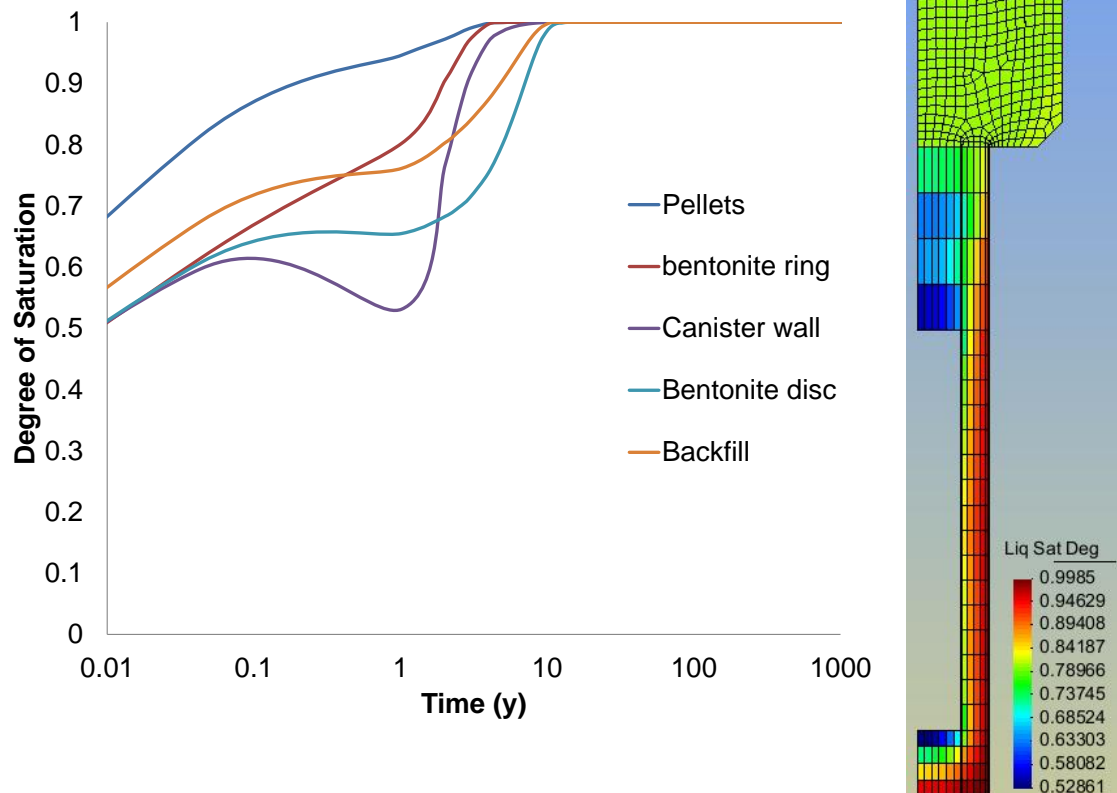
porous material implies an increase in thermal conductivity because the water is more conductive than the air.



3 years

Figure 6-18. Evolution of liquid pressure

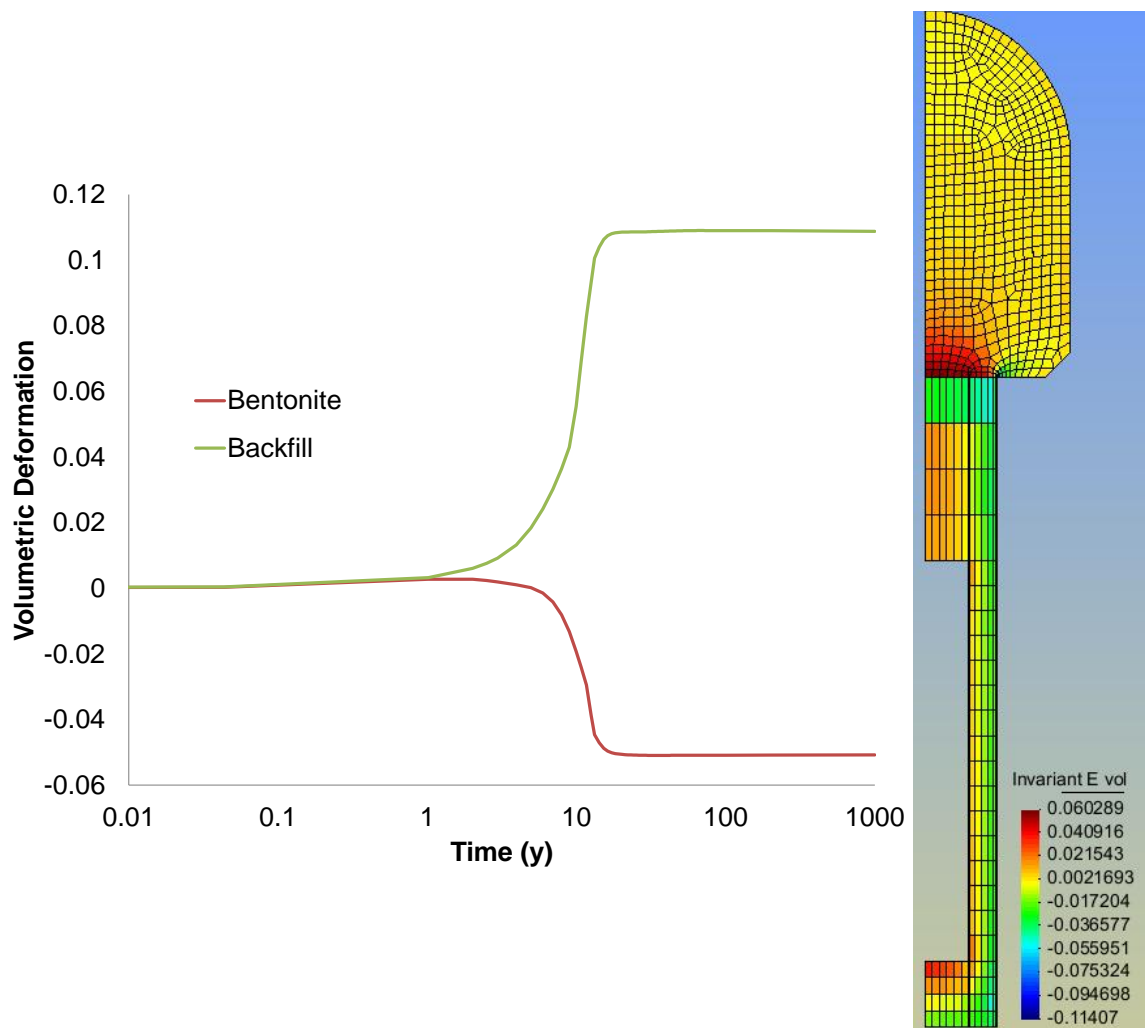
Figure 6-18 shows the evolution of the liquid pressure with time. Maximum suction is obtained close to the canister and reaches a value of 50 MPa. Although the desaturation of bentonite buffer takes place due to heat generation, there is no significant difference at the selected nodes on both sides of the gap element in comparison to Models A and B.



3 years

Figure 6-19. Evolution of degree of saturation

Strong heat generation causes to desaturation close to canister surface as it is depicted in Figure 6-19. Reaching to full saturation takes about 50 years. In Chapter 5, it has been discussed the parameters that have effect on degree of saturation. Hydraulic conductivity of rock is one of the most important parameter relating to saturation of bentonite buffer and backfill whereas effect of gap is not so important relatively.

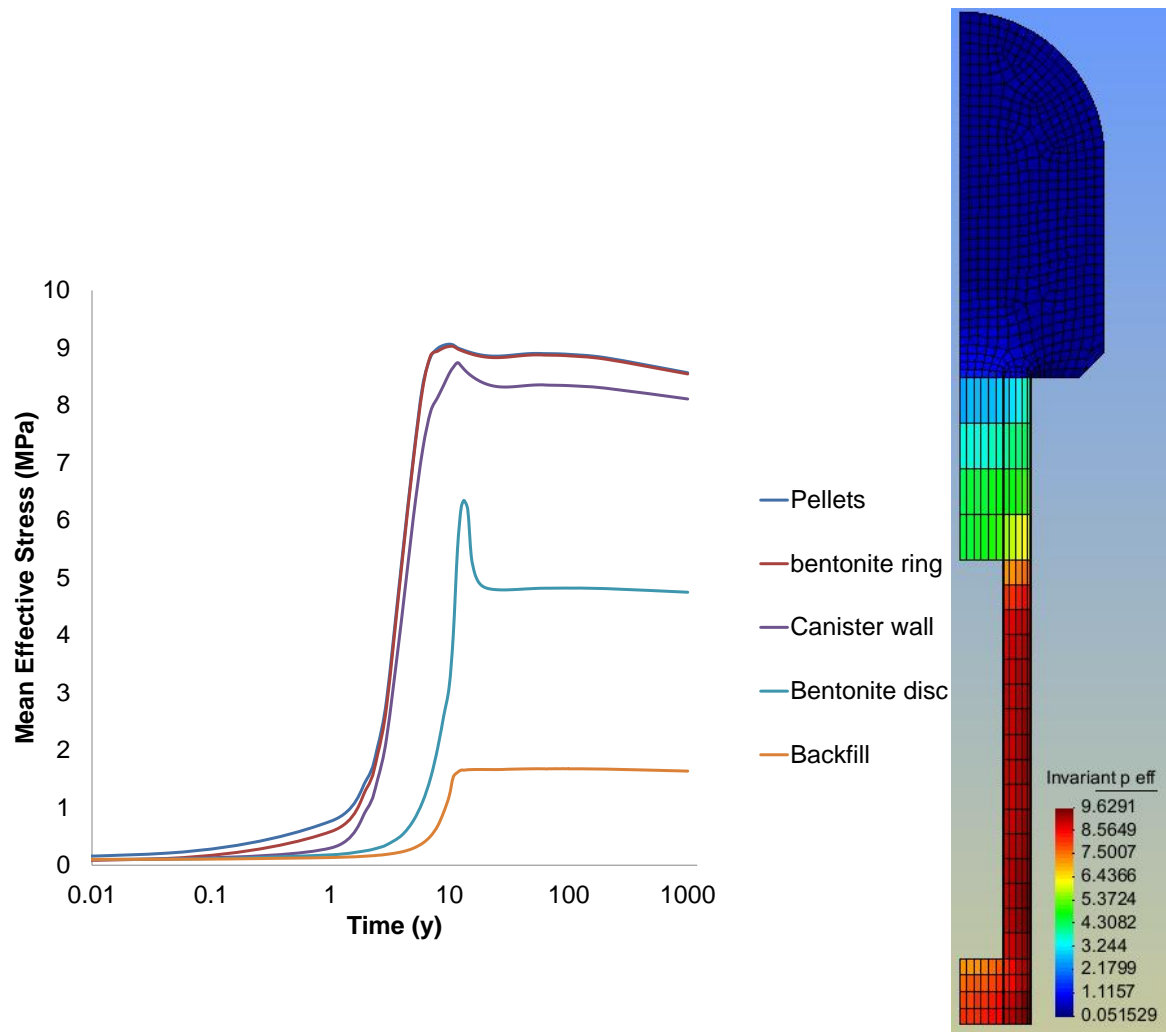


10 years

Figure 6-20. Evolution of volumetric deformations

As for the previous cases, saturation of the bentonite buffer causes the material to swell and as a result the backfill material compresses (Figure 6-20). In fact, no significant differences are observed in terms of volumetric deformations of the bentonite disc and the buffer between this model and the other two models that have air gap.

Figure 6-21 shows the evolution of mean effective stress in the materials. Maximum mean effective stresses reached after 10 years is around 9MPa.



10 years

Figure 6-21. Evolution of mean effective stresses

No change of the thickness of the gap element is observed (Figure 6-22)

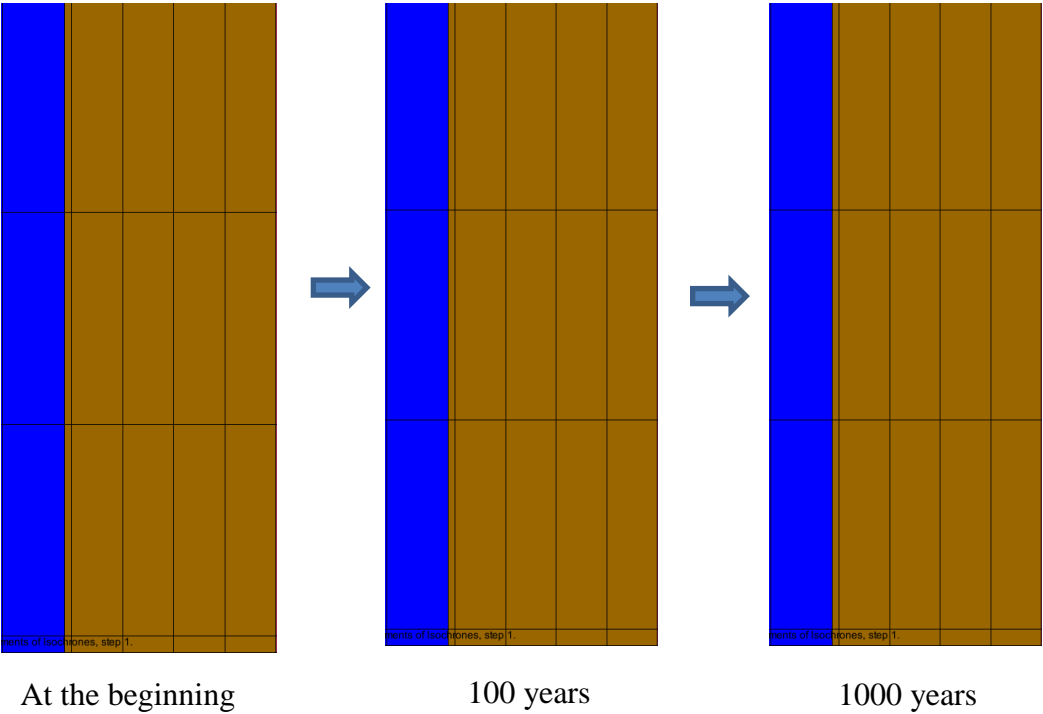


Figure 6-22. Simulation of planning gap element closure

6.4.4. Comparison of the results of 3 Models

In this section, comparison among the 3 cases presented is included. The permeability of the rock considered in the different models is included in Table 6- 6 together with the estimated time for gap closure.

Table 6-6. Models for comparative study

Models	A	B	C
Rock Permeability	10^{-18} m^2	10^{-19} m^2	10^{-19} m^2
Initial pressure of materials	-41 MPa	-41 MPa	-41 MPa
Gap Closing time (approx..)	2 years	4 years	No air gap

For the models A, B and C, the results are presented in Figures 6-23, 24 and 25.

The temperature evolution is not significantly different for the points in the buffer and pellets. However, the temperature in the canister shows a different response depending on the presence of the gap and the value of the rock permeability. The maximum temperature is not influenced but the evolution at short times is different due to the air gap.

Regarding water pressure, the most important differences occur near the canister. Permeability of the rock affects the time evolution of pressure, at least for the values of permeability considered here. The time is actually controlled by the combination of rock, buffer and backfill permeabilities. For higher permeabilities of the rock, the time control will be dominated by the lower permeability of the buffer.

Effective stress evolution is controlled by the evolution of water pressure. Therefore, the earlier hydration that takes place when the rock permeability is higher induces a faster effective stress development. However, the maximum effective stress is not significantly different, except for the different distribution of suction in the buffer and backfill which may induce a different strain and stress spatial and temporal variations.

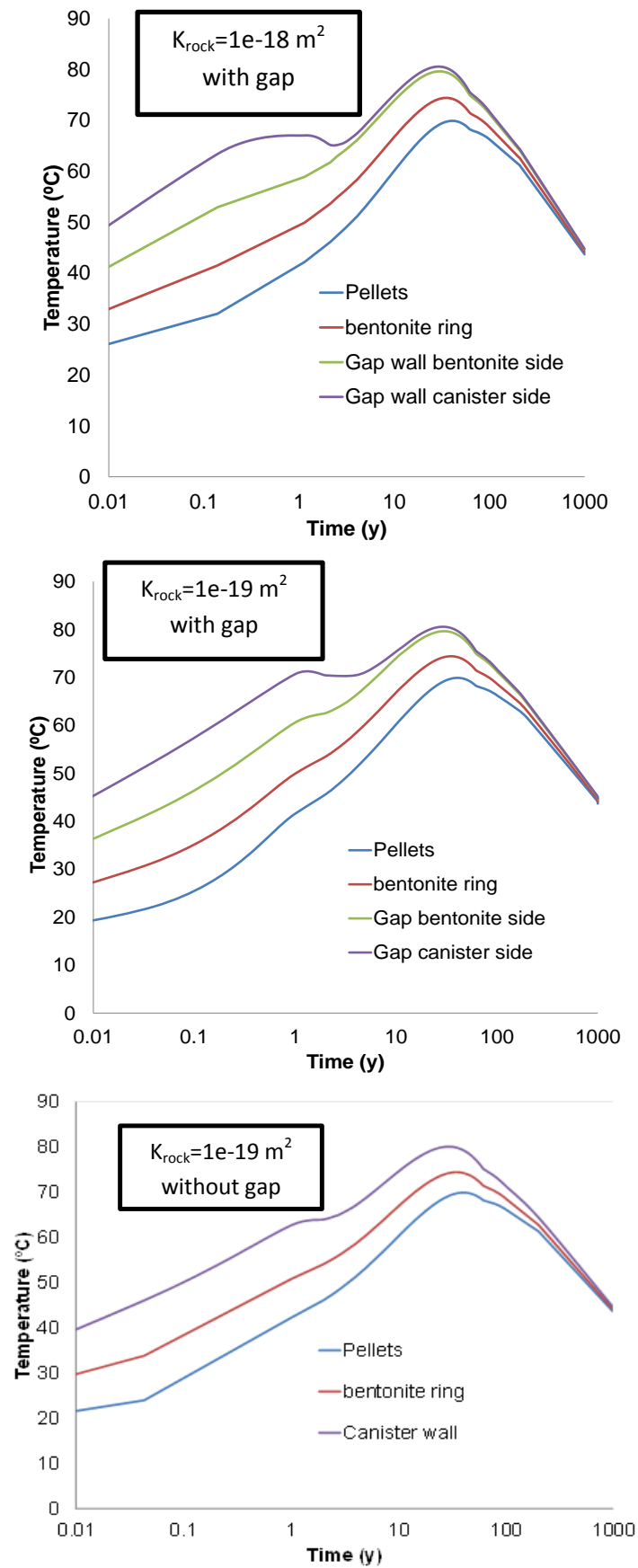


Figure 6-23. Comparison of models in term of temperature

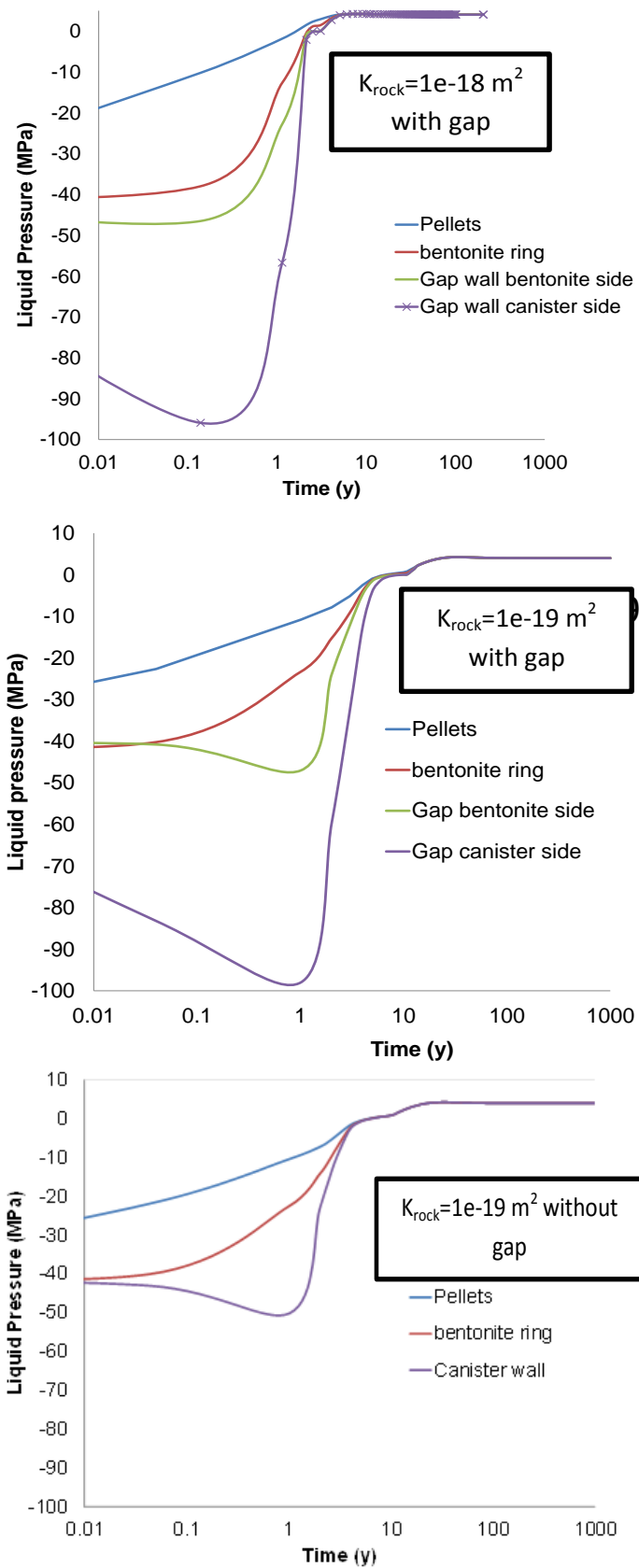


Figure 6-24. Comparison of models in term of liquid pressure.

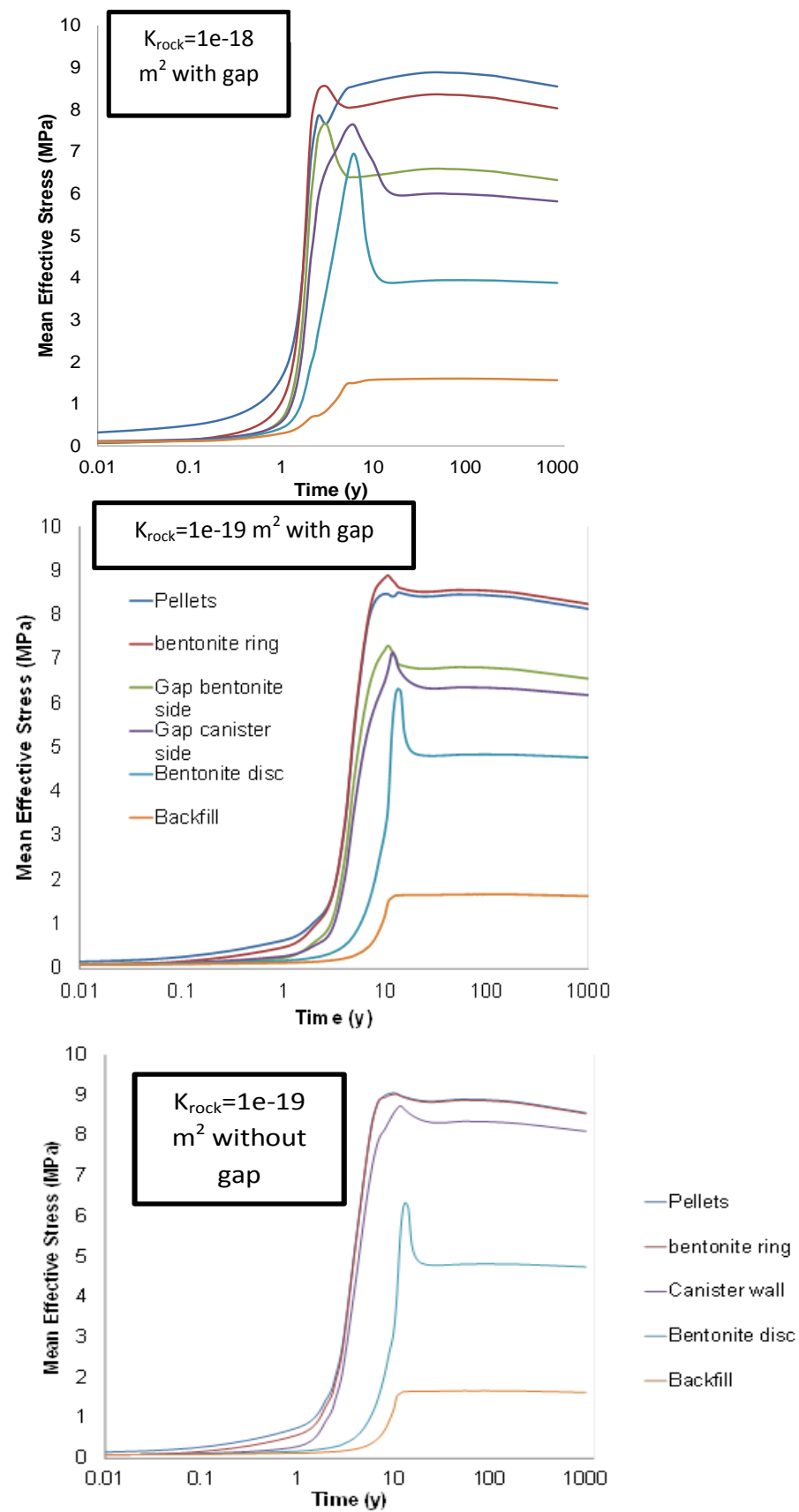


Figure 6-25. Comparison of models in term of mean effective stress

6.5. Model with Final Mesh and Geometry

In this section of the thesis, a coupled THM analysis of a deposition tunnel including the gap element has been performed considering an updated geometry and a more refined mesh (Figure 6-26). The same properties of the different material are used. Table 6-7 summarizes some basic properties of the bentonite buffer and the the backfill.

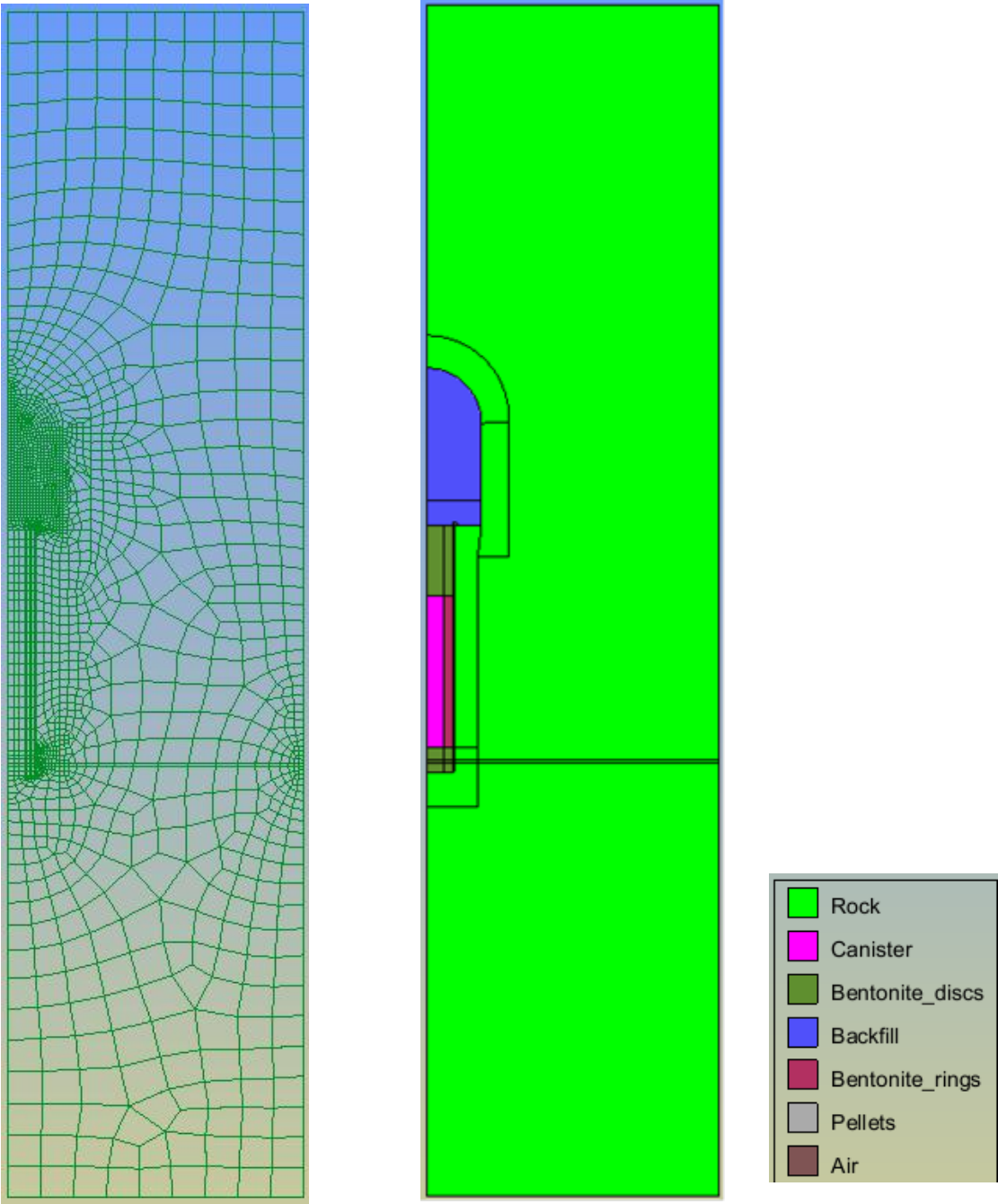


Figure 6.26. Mesh, geometry and materials of model

Table 6-7. Initial density and porosity of buffer and backfill

Materials	Solid density (kg/m ³)	Initial porosity	Initial dry density (kg/m ³)
Buffer bentonite	2779	0.388	1700
Backfill	2781	0.368	1757

Rock permeability is chosen as $1\text{e-}20\text{ m}^2$. In the analysis, it has been assumed axis-symmetric conditions. An initial suction of 5 MPa is imposed along the rock boundaries to simulate that after excavation, the drift and the deposition hole walls undergo certain drying. Table 6-8 and Figure 6-27 show the different representative points considered for comparison of the results.

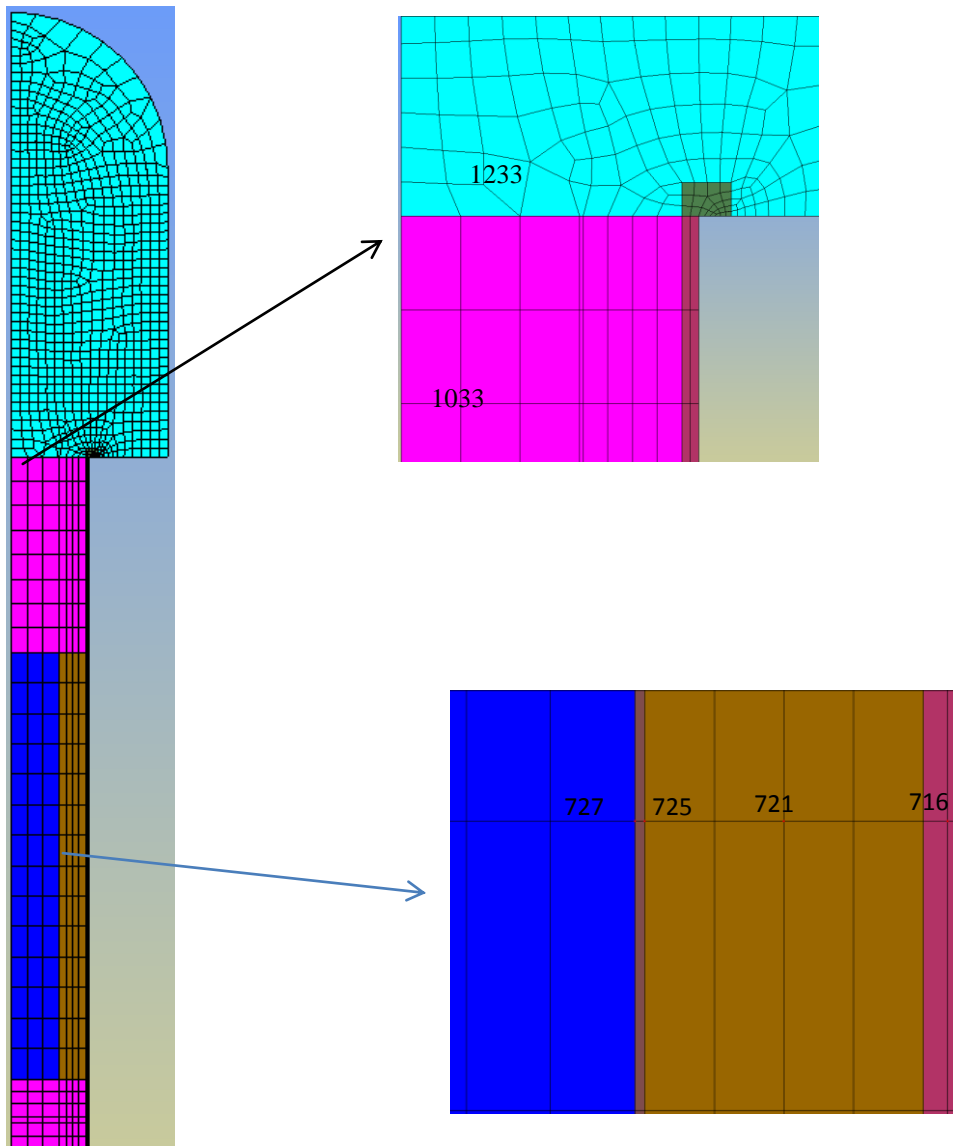


Figure 6.27 Representatives nodes for materials.

Table 6-8. Representative nodes for materials

Materials	Point considered
Backfill	1233
Bentonite disc	1033
Gap canister side	727
Gap bentonite ring side	725
Bentonite ring	721
Pellets	716

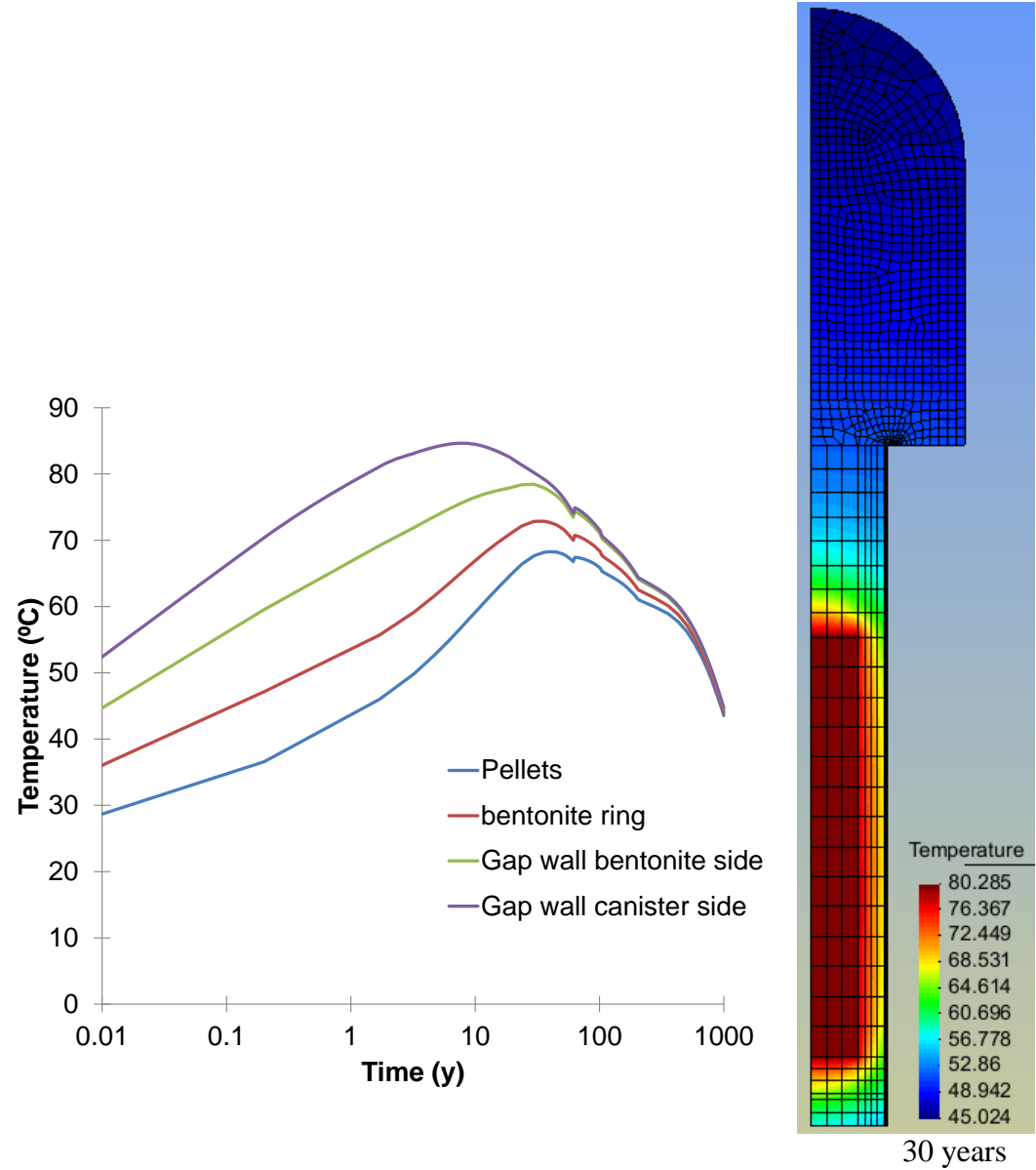


Figure 6-28.Evolution of temperature

Figure 6-28 shows the evolution of the temperature for the different materials. The Maximum temperature remains under 90 °C as in the preceding cases A, B and C. However, the increase of temperature due to the presence of the gap, takes place later because hydration evolves in a slower way. This implies that the maximum temperature increases somewhat, still remaining under the maximum design value of 90 °C.

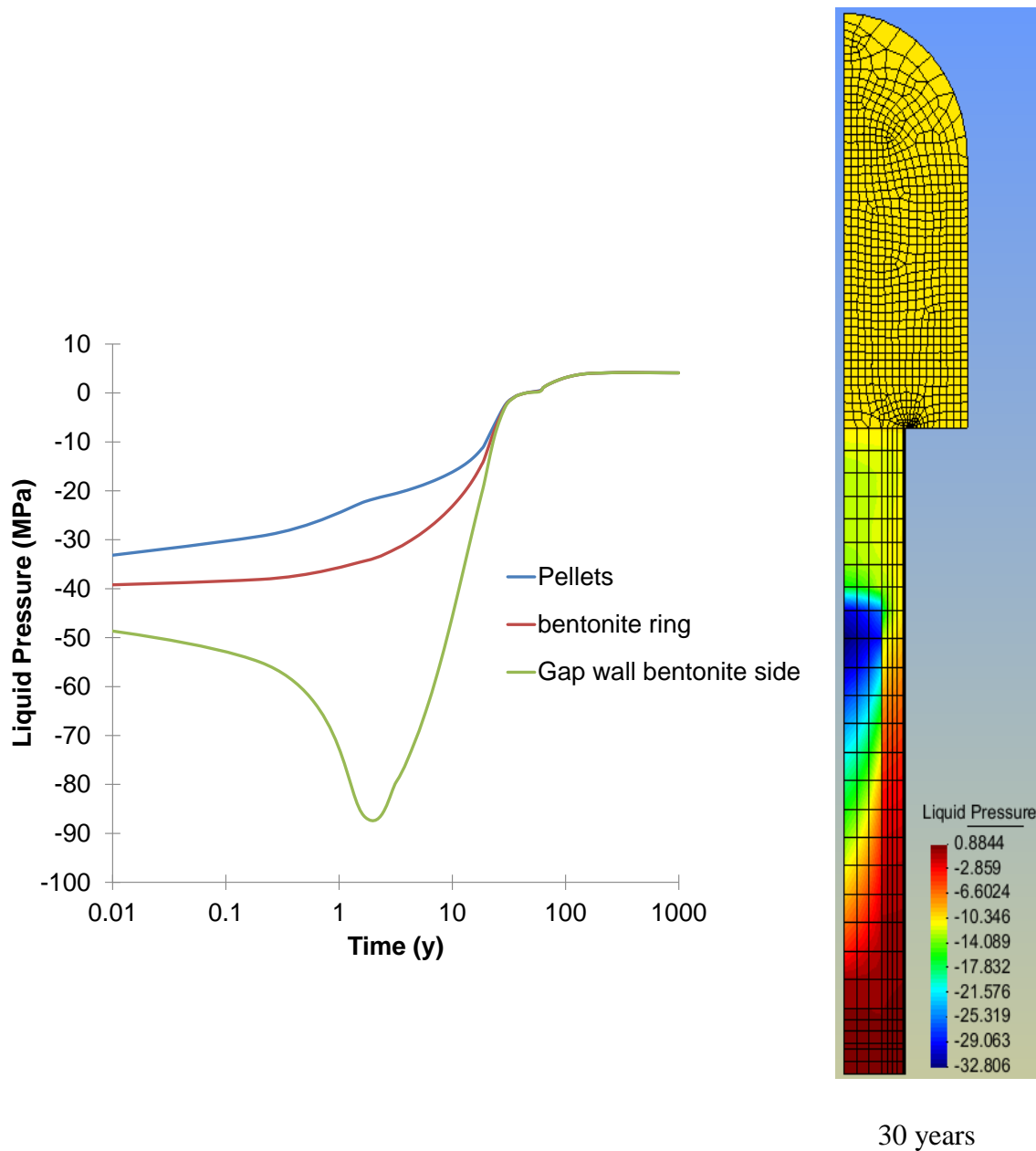


Figure 6-29. Evolution of liquid pressure

Figure 6-29 shows the evolution of the liquid pressure with time. Maximum suction is obtained close to the canister and reaches a value of 90 MPa. A big difference is observed at the selected nodes on both sides of the gap element.

The evolution of the dry density of both the backfill and the buffer are shown in Figure 31. The dry density requirement for the buffer is 1950 kg/m^3 according to working report 2088-88 “Finite Element Modeling of Deformation of Unsaturated Backfill Due to Swelling of the Buffer”. The plots show that dry density of buffer and backfill does not exceed this reference value.

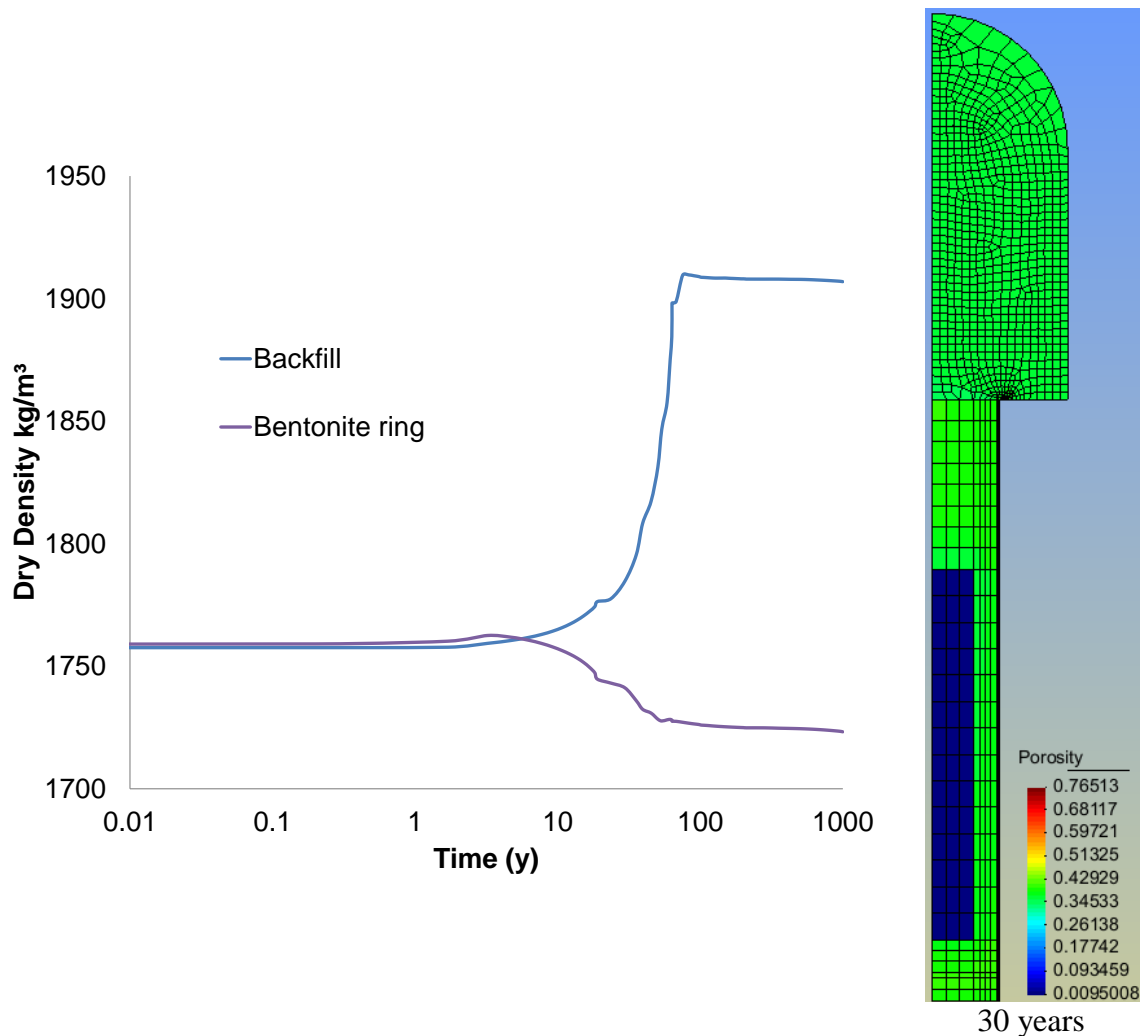
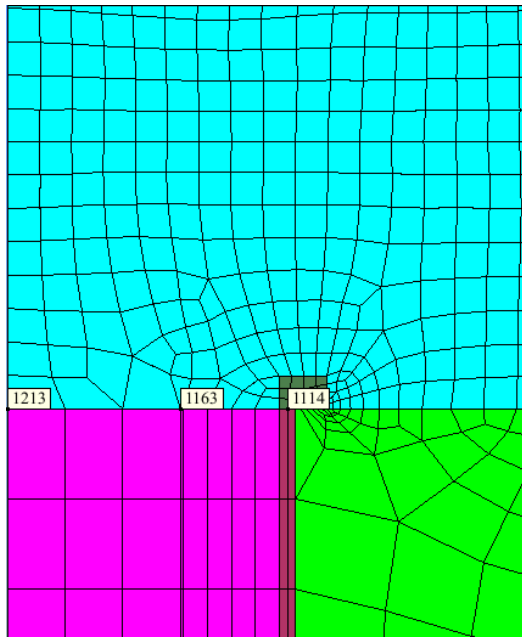
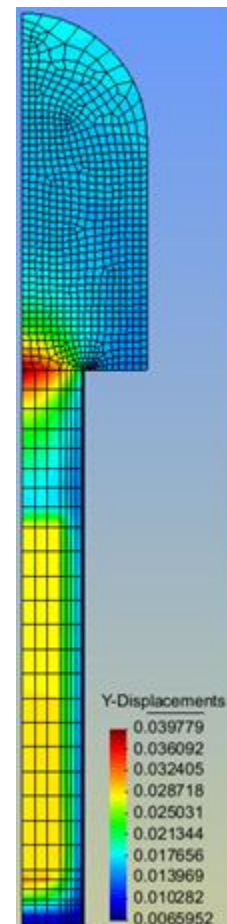
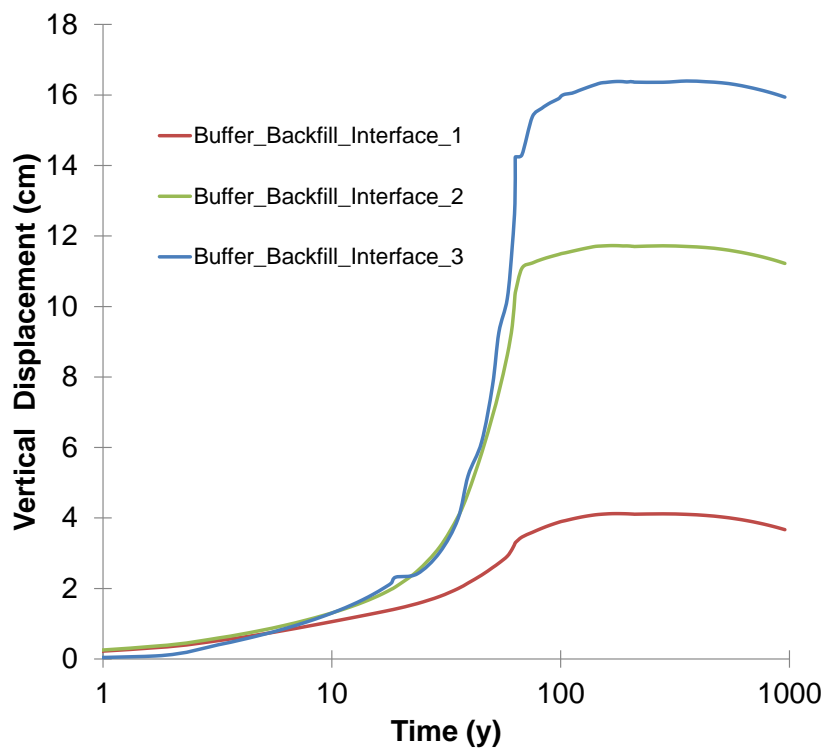


Figure 6-30. Evolution of dry density

As for the previous cases, saturation of the bentonite buffer causes the material to swell and as a result the backfill material compresses (Figure 6-30). Three points have been considered in the interface of the buffer and the backfill (Figure 6-31). A vertical displacement of 16 cm has been calculated at node 1213. Vertical displacements reduce in the direction of the arrow represented in the Figure 6-31.



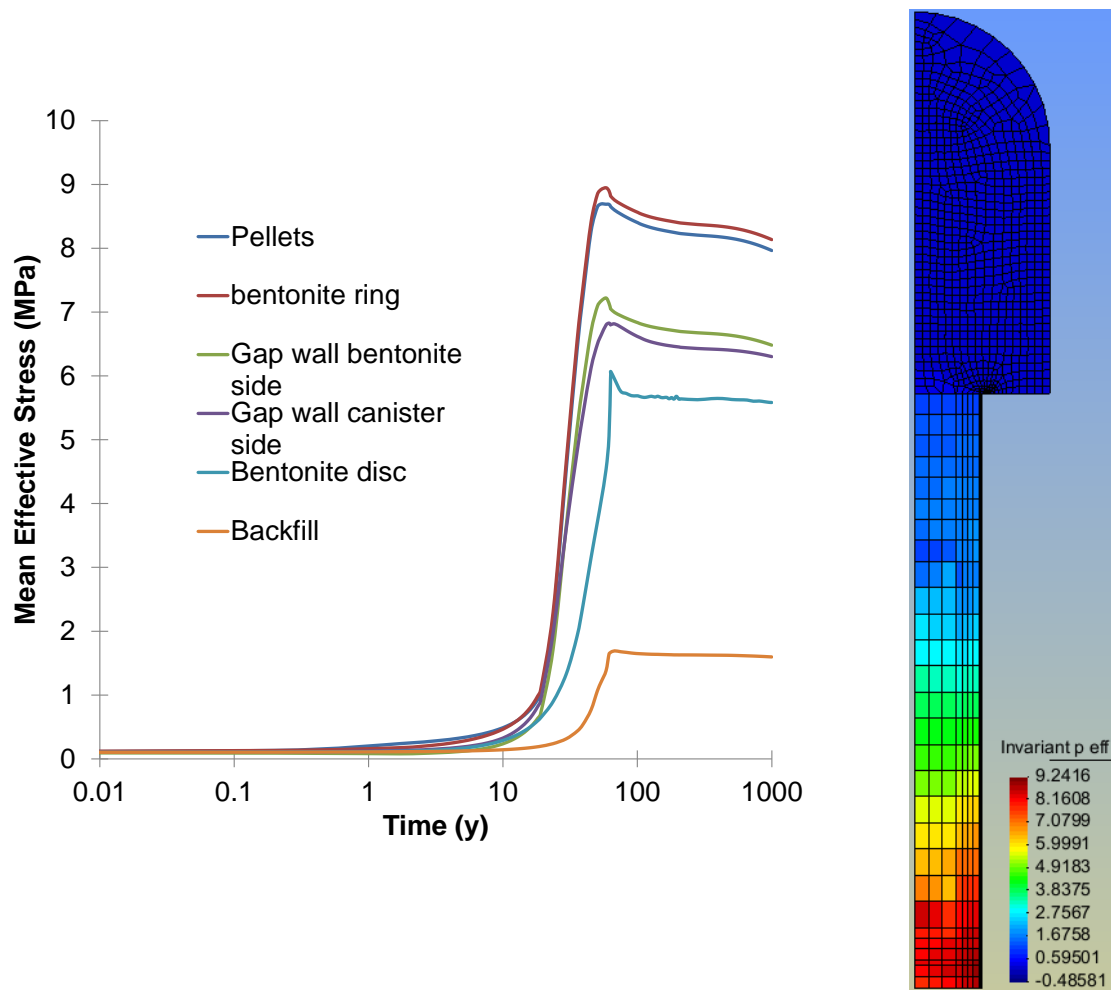
Node 1114 : Interface point 1
 Node 1163: Interface point 2
 Node 1213: Interface point 3



30 years

Figure 6-31. Evolution of vertical displacements

Figure 6-32 shows the evolution of mean effective stress at the selected points. A maximum mean effective stress reached is around 9.2MPa. Stresses increase during the hydration process and then remain stable as the material is fully saturated.



30 years

Figure 6-32. Evolution of mean effective stresses

Figure 6-33 shows desaturation of points close to canister. The effect of air gap can be seen as well. A sharp desaturation is observed at the point of the gap element close to the canister. In this case achieving full saturation of all buffer components takes about 50 years.

Figure 6-34 shows the evolution of the closure of the gap. It is observed that 20 years are needed for the gap to close totally. When the gap closes, horizontal displacements do not reduce anymore and effective horizontal stresses keep increasing after closure of the gap (Figure 6-35).

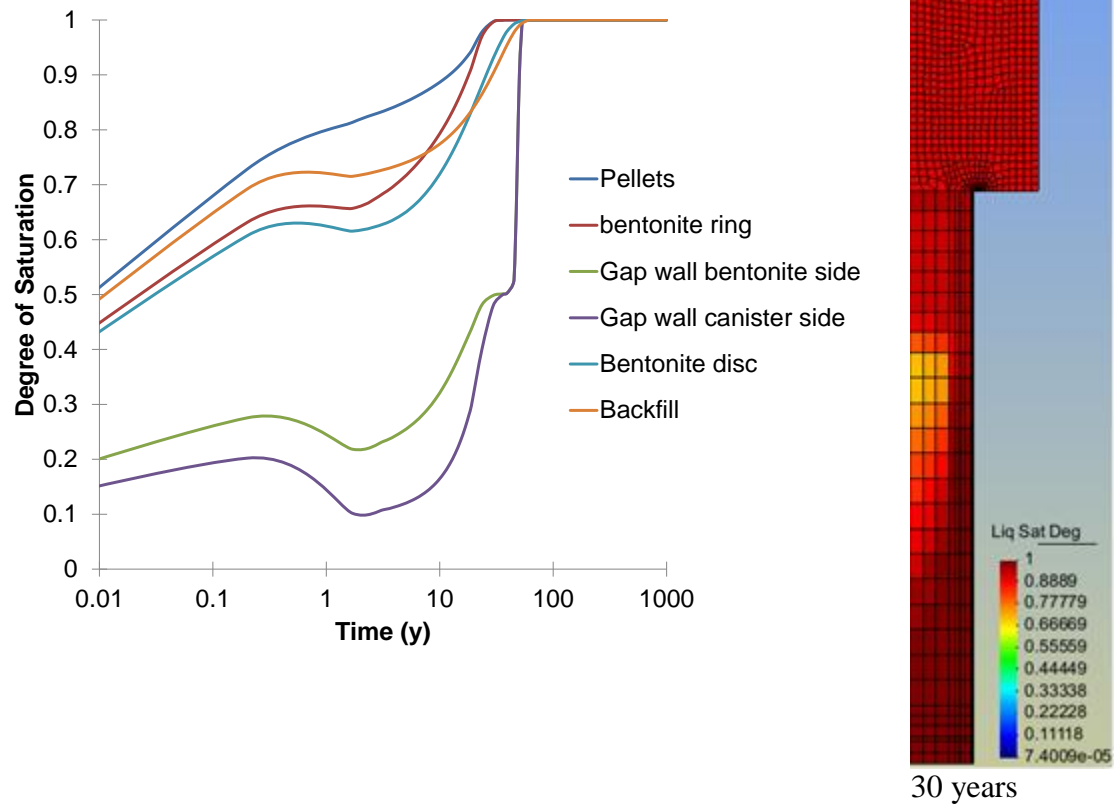


Figure 6-33. Evolution of degree of saturation

Desaturation of buffer takes place due to strong heating of canister. Time need to full saturation of buffer depends on water supply from the rock. As it has been discussed in previous sections, rock intrinsic permeability is a crucial parameter for the saturation of the buffer. Figure 6-33 demonstrates evolution of saturation degree of representative points considered for materials. It can be seen that

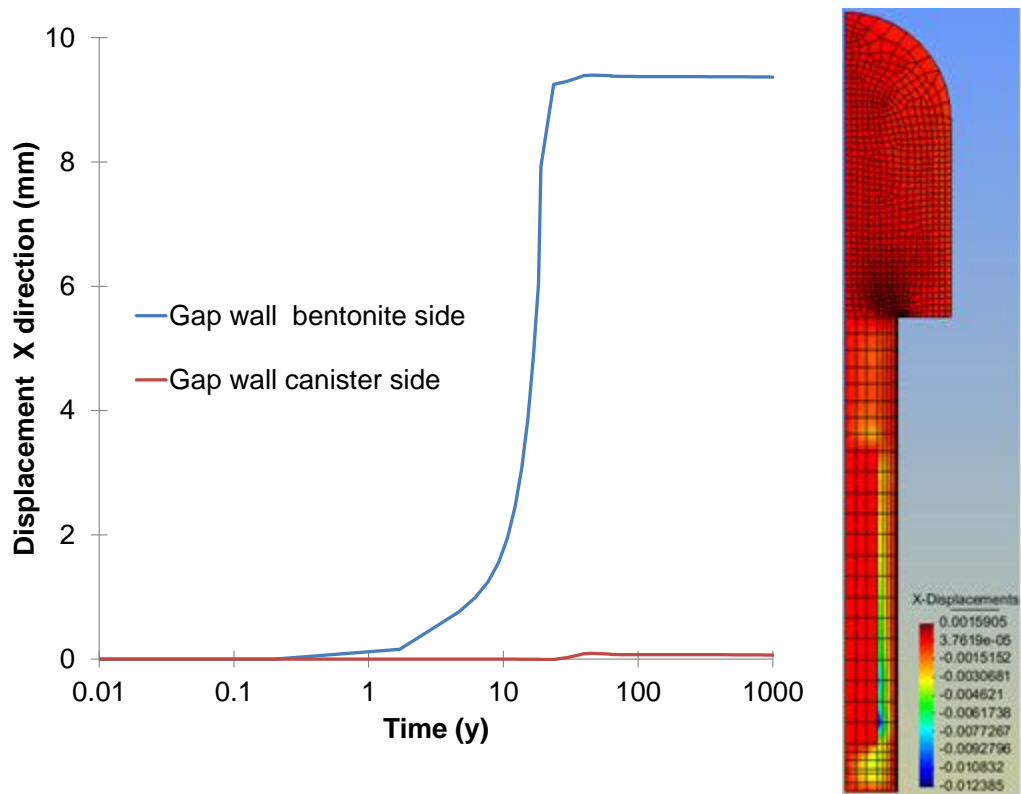


Figure 6-34. Horizontal displacements in the air gap element 30 years

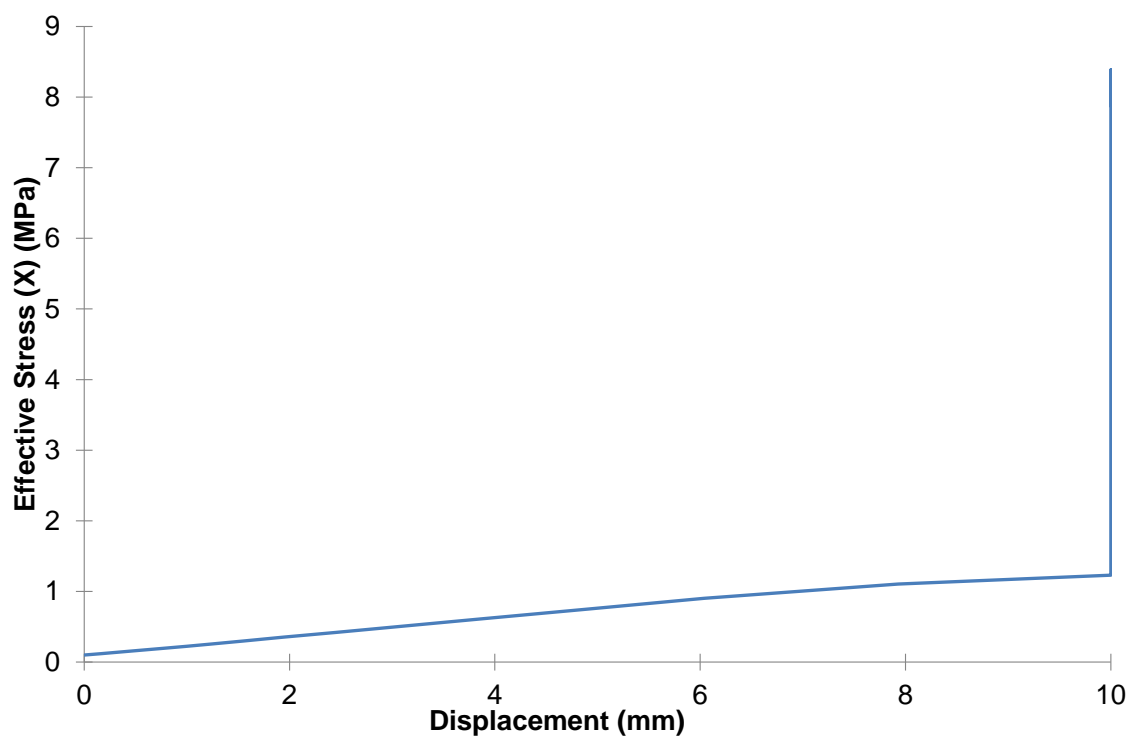


Figure 6-35. Horizontal effective stress – horizontal displacement relation in air gap.

The model results show that rock permeability has an effect on gap closing time. Gap closure can be demonstrated by the horizontal displacement achieved on the buffer wall touching to canister.

The maximum temperature does not reach 90 °C of maximum allowed design temperature in any of the cases presented.

Higher suction values close to buffer are observed for the models including air gap. The reason is that the gap has low retention capacity. This high suction does not imply significant changes on the evolution of pressures in the clay buffer and backfill as shown when the model with gap was compared with the model without gap. The evolution of stresses induced by swelling was similar as well. With regard to temperature, the gap induces an increment of the temperature in the canister.

It can be said that the presence of the gap does not affect significantly the buffer and backfill and only induces an increment of temperature of the canister smaller than 10 degrees.

Desaturation of buffer takes place induced by the heating but the effect of the gap on the desaturation of the buffer is not relevant because the total volume of the gap is small compared with the volume of the barrier. Therefore, even a large desaturation of gap is observed, it will re-saturate easily as its volume is small and the large suction developed induces an efficient gradient that attracts water. Closure reduces even more its volume and leads to negligible differences.

Total stress increases as the buffer hydrates. Effective stress also increases. As the buffer swells, buffer –backfill interface moves upwards. Total stress is the sum of the swelling pressure and the water pressure. For this reason, the total stress calculated is higher than the swelling pressure. Dry density of buffer and backfill is affected by the porosity changes. Swelling of these materials will cause to loss of dry density.

7. CONCLUSIONS

In this thesis THM (thermo-hydro-mechanical) modeling of a deposition tunnel in a under construction nuclear waste repository is presented.

Firstly thermal calculations have been carried out in order to set up appropriate thermal boundary conditions. Secondly, laboratory tests were modeled in order to determine the BBM parameters of buffer and backfill. Finally, THM calculations were performed considering different effects and geometries (for example air gap between canister and buffer).

Maximum temperature, time need to full saturation, homogenization and swelling pressure of bentonite buffer and displacements occurred at the interface of buffer and backfill are the main interest of the thesis.

Table 7.1 Evolution of important parameters

Analyzed parameters	Reached values
Maximum temperature in buffer	~ 82 °C
Time to reach full saturation of buffer	~ 50 years
Achieved maximum suction in buffer	85 MPa
Dry density of buffer	1700-1750 kg/m ³
Swelling pressure of buffer	6-9 MPa
Displacements at the interface of buffer-backfill	10 -16 cm

The most important results have been obtained in the thesis for buffer material (in the final geometry where buffer disc, buffer ring, backfill, pellet, rock and air-gap are considered as the components of deposition tunnel) is summarized in the Table 7.1.

These results are in the range of safety requirement for buffer which has been explained in the second chapter.

THM response of backfill, pellet, rock and air-gap has been presented in details.

However, laboratory tests for these materials have been going on and therefore a further study is to be performed to validate BBM parameters used for these materials.

Annex I. Description of basic THM formulation

A brief description of CODE_BRIGHT is included here. The reader may find more details in the references given below.

AI.1. General features of computer code

Name of code: CODE_BRIGHT

Method used: FEM

Dimensionality: 1D, 2D & 3D

Processes: Coupled THM

Previous application cases: CATSIUS CLAY, BAMBUS I and II, FEBEX I and II, RESEAL I and II, HE-B, EBS, NF-PRO, Prototype, TBT, DECOVALEX-III, THERESA

AI.2. Some features important to THM modeling of repositories

The code has options that allow to solve uncoupled or coupled problems, for instance, M, H, T, HM, TM, TH, and THM. The types of analyses can be 1D (uni-axial confined strain and axisymmetric), 2D (plane strain and axisymmetric) and fully 3D. The constitutive laws are defined by a set of parameters with alternative types of relations for different application cases.

The types of boundary conditions are:

- Mechanical problem: forces and displacement rate in any spatial direction.
- Hydraulic problem: mass flow rate of water and air prescribed and liquid/gas pressure prescribed.
- Thermal problem: heat flow rate prescribed and temperature prescribed.

The convergence criteria are defined by tolerances for absolute and relative error independent for each unknown, and tolerance for residual convergence of each problem (mechanical, hydraulic, etc.).

The output options include spatial distribution of variables at user defined time points, and time evolution of variables at user defined space points

AI.3. Mathematical representation of mechanical processes

AI.3.1 Equations of motion

The equation of equilibrium of stresses, the mass balance and the energy balance are:

$$\nabla \cdot \boldsymbol{\sigma} + \mathbf{b} = \mathbf{0}$$

$$\begin{aligned}
\frac{\partial}{\partial t}(\omega_l^w \rho_l S_l \phi + \omega_g^w \rho_g S_g \phi) + \nabla \cdot (\mathbf{j}_l^w + \mathbf{j}_g^w) &= f^w \\
\frac{\partial}{\partial t}(\omega_l^a \rho_l S_l \phi + \omega_g^a \rho_g S_g \phi) + \nabla \cdot (\mathbf{j}_l^a + \mathbf{j}_g^a) &= f^a \\
\frac{\partial}{\partial t}(E_s \rho_s (1-\phi) + E_l \rho_l S_l \phi + E_g \rho_g S_g \phi) + \nabla \cdot (\mathbf{i}_c + \mathbf{j}_{Es} + \mathbf{j}_{El} + \mathbf{j}_{Eg}) &= f^Q
\end{aligned} \tag{1}$$

Where:

ϕ : porosity	\mathbf{b} : body forces,
ρ : density	ω : mass fraction,
\mathbf{j} : total mass flux	$\omega \rho$: mass content per unit volume of phase,
\mathbf{i} : non-advective mass flux	E : specific internal energy
\mathbf{q} : advective flux	\mathbf{i}_c : conductive heat flux
\mathbf{u} : solid displacements	\mathbf{j}_E : energy fluxes due to mass motion
$\boldsymbol{\sigma}$: stress tensor	
S_l, S_g : degree of saturation of liquid and gas phases i.e., fraction of pore volume occupied by each phase.	
Superscripts w and a refer to water and air, respectively	
Subscripts s, l and g refer to solid, liquid and gas phase, respectively.	

(Note: **Bold** non italic symbols mean vector or tensor)

AI. 3.2 Mechanical Constitutive models

The viscoplasticity is assumed for bentonite as unsaturated soils based on Basic Barcelona Model, and linear elasticity behaviour is assumed for other materials.

The strain terms are defined as:

$$\begin{aligned}
\dot{\boldsymbol{\epsilon}} &= \dot{\boldsymbol{\epsilon}}^e + \dot{\boldsymbol{\epsilon}}^{VP}; \quad \dot{\boldsymbol{\epsilon}}^e = \dot{\boldsymbol{\epsilon}}^{stress} + \dot{\boldsymbol{\epsilon}}^{thermal} + \dot{\boldsymbol{\epsilon}}^{suction}; \quad \dot{\boldsymbol{\epsilon}}^{stress} \mathbf{D}^{-1} \dot{\boldsymbol{\sigma}} \\
\dot{\boldsymbol{\epsilon}}^{VP} &= \left[\Gamma \langle \phi(F) \rangle \frac{\partial G}{\partial \boldsymbol{\sigma}} \right] \text{ (Perzyna model)}
\end{aligned} \tag{2}$$

where $\boldsymbol{\epsilon}^e$ is the elastic strain tensor (with stress, temperature and suction terms), \mathbf{D} the elasticity tensor, $\dot{\boldsymbol{\epsilon}}^{vp}$ the viscoplastic strain rate tensor, Γ is the viscoplastic parameter, $\langle \phi(F) \rangle$ the plastic flow function, F is the yield surface, and G is the plastic potential function. $\langle \phi(F) \rangle = (F/F_0)^N$ F_0 is a reference stress to normalise F , N is a parameter of the model, and the Makulay brackets are used.

The model uses the effective stress and suction as state variables. Effectives stress is defines as: $\sigma' = \sigma - \max(P_g, P_l)$.

The thermal expansion of materials is considered. The parameters of the constitutive laws change with temperature and suction. The elastic terms in equation (2) related to temperature and suction are represented by a nonlinear function as in BBM.

Integration of (2) gives the stress increments as a function of the strain increments, temperature increments and suction increments.

The triaxial yield surface and plastic potential functions to be used in (2) are given by:

$$F(p, q, s) = q^2 - M^2 [p + p_s(s)] [p_o(s) - p] = 0 \quad (4)$$

$$G(p, q, s) = q^2 - \alpha M^2 [p + p_s(s)] [p_o(s) - p] = 0 \quad (5)$$

where p is the net average stress, q is the deviatoric stress, s is the matrix suction, M is the slope of critical state shear strength, α is the parameter that defines the non-associative of plastic potential (with $\alpha = 1.0$ indicating an associate flow rule), $p_s(s) = k_s s$, and k_s the material parameter that controls the increase in cohesion with suction, respectively. Parameter P_0 represents the loading-collapse curve (LC), is given by

$$p_o(s) = p^c \left(\frac{p_o^*}{p^c} \right)^{\frac{\lambda(0) - \kappa}{\lambda(s) - \kappa}} \quad (6)$$

where p^c is the reference stress of the loading-collapse curve, p_o^* is the initial yield mean net stress, and $\lambda(0) - \kappa$ is the virgin compressibility for saturated condition, with $\lambda(0)$ being the slope of the virgin elastic compressibility for saturated condition and κ the slope of the unload-reload line. The parameter $\lambda(s)$ is the volumetric compressibility index, written as

$$\lambda(s) = \lambda(0) [(1 - r) \exp(-\beta s) + r] \quad (7)$$

where r is the parameter that establishes the minimum value of the compressibility index for high values of suction, and β is the parameter that controls the rate of increase in stiffness with suction.

The hardening law is given as

$$dp_o^* = \frac{(1 + e)p_o^*}{\lambda(0) - \kappa} d\varepsilon_v^p \quad (8)$$

where e is the void ratio, and $d\varepsilon_v^p$ is the plastic volumetric strain increment.

AI-4. Mathematical representation of fluid flow processes.

The fluid flow is governed by Darcy's law, given as

$$\mathbf{q}_\alpha = -\frac{\mathbf{k}k_{r\alpha}}{\mu_\alpha}(\nabla P_\alpha - \rho_\alpha \mathbf{g}) \quad (9)$$

$$\mathbf{k} = \mathbf{k}_o \frac{\phi^3}{(1-\phi)^2} \frac{(1-\phi_o)^2}{\phi_o^3} \quad (10)$$

where \mathbf{q}_α is the flux vector along porous media, \mathbf{k} is the intrinsic permeability tensor at porosity ϕ , \mathbf{k}_o is the intrinsic permeability at porosity ϕ_o , $k_{r\alpha}$ is the phase relative permeability, $\mu_{r\alpha}$ is the viscosity of the fluid, P_α is the pressure of the fluid, and ρ_α is the density of the fluid. Gravity is represented by the vector \mathbf{g} . Parameters ϕ_o and ϕ are defined as before.

The fluid density changes with temperature and with pressure. The intrinsic permeability changes with porosity. The hydraulic conductivity is affected by fluid viscosity that changes with temperature. The density of water is calculated as: $\rho_\alpha = \rho_{\alpha 0} \exp(\beta(P_l - P_{l0}) + \alpha(T - T_0))$ where β is the fluid compressibility, α is a volumetric expansion coefficient; and the viscosity is calculated as:

$\mu_l = A \exp(B/(273.15 + T))$ $A=2.1 \times 10^{-2}$ MPa, $B=1808.5$ K⁻¹. For the gas phase, the ideal gases law is used.

Relative permeability is considered with the van Genuchten function or a power of degree of saturation: $k_{r\alpha} = \sqrt{S_l} \left(1 - (1 - S_l^{1/\lambda})^\lambda\right)^2$; $k_{r\alpha} = (S_l)^n$. A coupling of flow and deformations is achieved by Kozeny equation (10) and the thermal coupling is achieved considering the changes of fluid properties with temperature. However, primary couplings appear from balance equations.

Advection of water and air in gas and liquid phases is calculated by means Darcy's law. Non advective fluxes include diffusion and dispersion (see below),

AI.5. Mathematical representation of heat transfer processes.

The heat transfer process is governed by Fourier's law, given as the heat flux vector:

$$\mathbf{i}_c = -\lambda \nabla T \quad (11)$$

with

$$\lambda = \lambda_{sat} \sqrt{S_l} + \lambda_{dry} (1 - \sqrt{S_l}) \quad (12)$$

or

$$\lambda = (\lambda_{sat})^{S_l} (\lambda_{dry})^{1-S_l} \quad (13)$$

where \mathbf{i}_c is the conductive flux vector of heat, T is the temperature, λ is the thermal conductivity, λ_{sat} is the thermal conductivity of the water-saturated porous medium, λ_{dry} is the thermal conductivity of the dry porous medium, and S_l is the degree of saturation.

The heat is transport by liquid or gas flow and by vapour diffusion. The thermal conductivity is modified by liquid and gas flows that change the degree of saturation S_l in equation (12) and (13). The thermal conductivity changes with porosity that affects the saturation degree S_l as well.

Conduction is one of the heat transfer process considered in Equation (1), the other are advection due to mass movements.

AI.6. Some special features of the code

AI.6.1 Retention curve

For bentonite and rock interfaces, the hydraulic conductivity of the materials considered depends on their degree of saturation. The retention curve (Van Genuchten Model) is

$$S_e = \frac{S_l - S_{rl}}{S_{ls} - S_{rl}} = \left[1 + \left(\frac{P_g - P_l}{P} \right)^{1/(1-\lambda)} \right]^{-\lambda} \quad (14)$$

$$P = P_o \frac{\sigma(T)}{\sigma_o(T_o)} \quad (15)$$

where S_e is the degree of saturation of porous media, S_l is the degree of saturation of liquid, S_{rl} is the residual degree of saturation, S_{ls} is the maximum degree of saturation, P_g is the gas pressure, P_l is the liquid pressure, λ is the shape function coefficient for the retention curve, P_o is the pressure of air entrance at a reference temperature, and σ_o is the surface tension at a temperature at which P_o was measured. σ is the surface tension at a temperature T . (Pruess,1987).

AI.6.2 Molecular Diffusion

The molecular diffusion is governed by Fick's law

$$\mathbf{i}_\alpha^i = -(\phi \rho_\alpha S_\alpha D_\alpha^i \mathbf{I}) \nabla \omega_\alpha^i \quad (16)$$

where \mathbf{i}_α^i is the non-advective mass flux vector, ϕ is the porosity of porous media, ρ_α is the density of the phase α , S_α is the degree of saturation of the phase α , D_α^i is the diffusion coefficient, ω_α^i is the mass fraction⁽ⁱ⁾, respectively. \mathbf{I} is the identity tensor. The superindex i refers to species and the subindex α refers to phases.

The diffusion coefficient of vapour is given by

$$D_g^{vapor} = \tau D^v \left(\frac{(273.15 + T)^n}{P_g} \right) \quad (17)$$

where τ is the tortuosity and D^v is the coefficient of diffusion, where $D^v = 5.9 \times 10^{-6} \text{ m}^2/\text{s/K}^{-n}\text{Pa}$. The typical value for n is 2.3.

The diffusion coefficients of dissolved salt and air are given by

$$D_l^{air \text{ or } solute} = \tau D \exp \left(\frac{-Q}{R(273.15 + T)} \right) \quad (18)$$

where R is the ideal gas constant, $D = 1.1 \times 10^{-4} \text{ m}^2/\text{s}$, and $Q = 24530 \text{ J/mol}$ are model parameters.

For bentonite and rock interfaces, the vapour pressure depends on temperature, liquid and gas flow through suction changes (psychometric law).

Mass fractions and densities of the gas phase are calculated using ideal gases law. Vapour pressure as a function of temperature and suction is obtained as:

$$P_v(T, P_c) = P_v(T) \times F(P_c, T) \quad (19)$$

$$P_v(T) = 136075 \exp \left(\frac{5239.7}{273 + T} \right) \quad F(P_c, T) = \exp \left(\frac{P_c M_w}{R(273 + T) \rho_l} \right)$$

Where P_c capillary pressure, M_w (0.018 kg/mol) is the molar mass of water, T is the temperature absolute and R is the gas constant (8.31 J/mol/K).

AI. 6.3 Mechanical Dispersion.

The mechanical dispersion is governed by Fick's law, given by

$$\mathbf{i}_\alpha^i = -(\rho_\alpha \mathbf{D}_\alpha^i) \nabla \omega_\alpha^i \quad (20)$$

where \mathbf{i}_α^i is the non-advective mass flux vector, with superindex i refers to species and the subindex α refers to phase, ρ_α is the density of phase α , \mathbf{D}_α^i is the mechanical dispersion tensor and ω_α^i is the mass fraction, respectively.

Note that diffusion and dispersion have similar mathematical form (based on Fick's law) and can be added up together in a single nonadvective flux vector (Eq 16 and 20).

References

- Alonso, E.E., A. Gens and A. Josa (1990). A constitutive model for partially saturated soils. *Géotechnique*, 40(3), 405-430.
- David Dixon, Atomic Energy of Canada Limited. Review of the Properties and Uses of Bentonite as a Buffer and Backfill Material.
- David Savage Andrew Lind Randolph C Arthur May 1999SKI Report 99:9. Design report of the canister for nuclear fuel disposal
- Erika Holt, Jutta Peura 2011. Buffer Component Manufacturing by Uniaxial Compression Method– Small Scale. Posiva Working Report 2011-42.
- Esther Jonsson, Svensk Kärnbränslehantering AB, February 2011. Harald Hökmark. October 2003. Hydration of the bentonite buffer in a KBS-3 repository.
- Heikki Raiko VTT Energy .Jukka-Pekka Sale Hökmark, H, Falth, B. (2003). Thermal dimensioning of the deep repository. Influence of canister spacing, canister power, rock thermal properties and near field design on the maximum canister surface temperature. SKB Report R-08-30. Stockholm
- Ikonen, K. (2003). Thermal Analysis of Spent Nuclear Fuel Repository. Posiva Working report 2003-04. Eurajoki.
- Ikonen, K. (2005). Thermal Analysis of Repository for Spent EPR-type fuel. Posiva Working report 2005-06. Eurajoki.
- Johanna Hansen, Posiva Oy, Kari Ikonen. June 2003. Thermal Analyses of Spent Nuclear Fuel Repository
- Lars Erik Johannesson, Ulf Nilsson 2006. Deep repository – engineered barrier systems. Geotechnical behaviour of candidate backfill materials. Laboratory tests and calculations for determining performance of the backfill. Clay Technology AB. SKB technical report. R-06-73.
- Leena Korkiala-Tanttu. April 2009. Finite Element Modelling of Deformation of Unsaturated Backfill Due to Swelling of the Buffer. Posiva Working Report 2008-88.
- Leena Nolvi POSIVA 2009-03 Manufacture of Disposal Canisters December 2009
- M.V. Villar, 1999. Investigation of the behaviour of bentonite by means of suction-controlled oedometer tests. *Engineering Geology* 54 (1999) 67–73.

- M.V. Villar, 2005. Infiltration tests on a granite/bentonite mixture: Influence of water salinity. *Applied Clay Science* 31 (2006) 96– 109.
- Mattias Åkesson, Lennart Börgesson, Ola Kristensson Clay Technology AB. March 2010. SR-Site Data report THM modelling of buffer, backfill and other system components. Technical Report TR-10-44.
- O. Kristensson, M. Åkesson 2008. Mechanical modeling of MX-80 – Quick tools for BBM parameter analysis. *Physics and Chemistry of the Earth* 33 (2008) S508–S515.
- Ola Karnland, Torbjörn Sandén, Lars-Erik Johannesson Clay Technology AB. Trygve E Eriksen, Mats Jansson, Susanna Wold Royal Institute of Technology. Karsten Pedersen, Mehrdad Motamedi Göteborg University. Bo Rosborg Studsvik Material AB. 2000. Long term test of buffer material Final report on the pilot parcels. SKB technical report. TR-00-22.
- Olivella, S., Gens, A., Carrera, J., Alonso, E.E., (1996). Numerical formulation for a simulator (CODE-BRIGHT) for the coupled analysis of saline media. *Eng. Comput.* 1: 87– 112
- Olivella, S., J. Carrera, A. Gens & E.E. Alonso (1994) Nonisothermal multiphase flow of brine and gas through saline media. *Transport in Porous Media*, 15: 271-293.
- Paula Keto. March 2004. Natural Clays as Backfilling Materials in Different Backfilling Concepts. Working Report 2003-79.
- POSIVA 2008-03 Horizontal Deposition of Canisters for Spent Nuclear Fuel
- POSIVA 2009-01 Olkiluoto Site Description 2008 Part 1 April 2009 Posiva Oy
- POSIVA 2011-03 Effects of Bedrock Fractures on Radionuclide Transport near a Vertical Deposition Hole for Spent Nuclear Fuel December 2011
- POSIVA Working Report 2003-79 Natural Clays as Backfilling Materials in Different Backfilling Concepts
- Pusch Roland The buffer and Backfill Handbook, Part 3: Models for calculation of processes and behaviour. SKB Technical Report TR-03-07.
- SKI Report 99:9 Review of the Properties and Uses of Bentonite as a Buffer and Backfill Material Summary of the KBS-3H Project 2004 – 2007 December 2008

Technical Report TR-10-47 Buffer, backfill and closure process report for the safety assessment SR-Site Svensk Kärnbränslehantering AB Torbjörn Sandén, Clay Technology AB

Veli Matti Pulkkanen, Henrik Nordman Posiva Oy. Olkiluoto Site Description 2008
Part 2. POSIVA 2009-01